

*Morphometrics of submarine channels:*

*Variation between channel types and around bends*

Franziska Anna Palm

Submitted in accordance with the requirements for the degree of  
Doctor of Philosophy

The University of Leeds  
School of Earth and Environment

April 2022

The candidate confirms that the work submitted is her own, except where work which has formed part of jointly-authored publications has been included. The contribution of the candidate and the other authors to this work has been explicitly indicated below. The candidate confirms that appropriate credit has been given within the thesis where reference has been made to the work of others.

The work in Chapter 4 of the thesis has appeared in publication as follows:

Palm, F.A., Peakall, J., Hodgson, D.M., Marsset, T., Silva Jacinto, R., Dennielou, B., Babonneau, N. and Wright, T.J., 2021, Width variation around submarine channel bends: Implications for sedimentation and channel evolution. In: *Marine Geology*, v. 437, p. 106504.

As the primary author, I was responsible for data collection, processing, collation and interpretation, and writing of the manuscript. The contribution of the other authors was limited to discussion of the data and editorial suggestions.

This copy has been supplied on the understanding that it is copyright material and that no quotation from the thesis may be published without proper acknowledgement.

The right of Franziska Anna Palm to be identified as Author of this work has been asserted by her in accordance with the Copyright, Designs and Patents Act 1988.

*For*  
*Wilfride "Fidi" Oellerich*  
*(1919-2011)*

# Acknowledgements

Many people have helped me either academically or privately to complete this PhD thesis. As a true submarine channel thesis, I dance for you to swing music till the sunrise and do not sweep the floor in the morning.

First of all, I would like to thank my supervisors Dave Hodgson and Jeff Peakall for giving me the opportunity to conduct a PhD in the first place. Thank you for your guidance, support and scientific feedback. I am especially grateful to Jeff Peakall for sharing his vast knowledge and enthusiasm about submarine channels, for his encouragement, and to help me to develop as a scientist. This PhD would not exist without the access of dataset. A special thanks goes to Andrea Ortiz-Karpf for giving me access to the Magdalena dataset and to Ifremer in Brest for providing access to the Congo and Amazon dataset. I am grateful to Ricardo Silva Jacinto for inviting me to Brest to analyse the data sets. Thank you, Ricardo, for your support, scientific discussions and welcome me in Brest. Here, I am especially grateful for scientific discussions and support from Tania Marsset, Bernard Dennielou and Nathalie Babonneau. This PhD was sponsored by the Leeds University Anniversary Research Scholarships (LARS).

Thank you to my Bangor Crew: Ben Strachan, Clara Alvarez-Rodriguez, Mathias Biber, and Ilka Illers. Even so, we live far away from each other, we manage to meet up and I always have the feeling we have never been apart for long with discussions about geology, biology, life and absolute nonsense during our meetings. Thank you to Lydia Siegmüller, for our long-lasting friendship. Even so, submarine channels are far away from your expertise, our catch-ups are always a nice diversion and your support towards me is much appreciated.

A special thanks goes to my family, especially my parents, Peter and Elke Palm. Thank you for the lifelong support, being it emotionally, when I needed an open ear, or financially. You let me grow freely to become the person I am today. I am also massively grateful for the support of Giorgio Taverna. Thank you for your love and calm attitude in times I wanted to give it all up. We continued playing the tennis match. My last thanks but not least important goes to Adam Taverna. Thank you for your curiosity, love and making me a more organised person.

# Abstract

Submarine channels are common sediment pathways along the sea floor globally. Single-thread submarine channels in the modern can be classified depending on the environmental setting as: submarine-fan, slope, axial, isolated deep ocean, confined slope, and non-margin ocean channels, yet all have been considered morphologically similar. Bend migration for aggradational single-thread submarine channels is dominantly controlled by bend expansion with very limited downstream migration. However, paradoxically, laboratory experiments and numerical simulations predict that submarine channels exhibit a downstream bend migration similar to rivers. In rivers, the importance of bend morphology, especially channel width, on bend migration is known. Here, the morphometrics of submarine channels in different environmental settings, and the morphology around submarine channel bends, are investigated.

A detailed analysis of 177 bends from 11 submarine channels, composed of 3 channel types, has been undertaken. For each bend, 13 cross-sections were measured, and width analysed at different heights from the channel bed to the channel banks. Additional cross-sections from a range of channel types have been extracted from the literature, and integrated with the new data to assess the morphometric variation with channel type.

The main outcomes of this study are: 1) Submarine channels types are distinguishable based on their morphometry with for example submarine-fan, slope, and non-margin ocean channels having a similar aspect ratio to rivers, and axial and isolated deep-ocean channels having a greater aspect ratio than rivers, 2) Contradictions of bend migration between laboratory experiments or numerical simulations, and observations, can be explained by width variation around bends, 3) Width variation around bends is variable between channel types with submarine-fan channels having a wider width at bend apices, whereas isolated deep-ocean channels exhibit a constant channel width around bends. 4) Width variation around bends may be controlled by allogenic controls such as flow magnitude and bank resistance.

# Table of Contents

<b>Acknowledgements</b> .....	<b>iv</b>
<b>Abstract</b> .....	<b>v</b>
<b>Table of Contents</b> .....	<b>vi</b>
<b>List of Tables</b> .....	<b>x</b>
<b>List of Figures</b> .....	<b>xii</b>
<b>Chapter 1 Thesis rationale</b> .....	<b>30</b>
1.1 Thesis background .....	30
1.2 Thesis aims .....	31
1.3 Thesis outline .....	34
<b>Chapter 2 Current understanding of submarine channel bend dynamics: flow processes, sedimentation morphometrics and channel evolution</b> .....	<b>38</b>
2.1 Morphology and environmental setting of submarine channels.....	39
2.2 Channel evolution in submarine channels.....	50
2.3 Evolution of river bends.....	55
2.4 Morphometrics of submarine channels .....	62
2.4.1 Geometry of submarine channels .....	62
2.4.2 Geometry around submarine channel bends .....	65
2.5 Flow processes from channel development to bend scale .....	68
2.5.1 Flows that generate a submarine channel .....	68
2.5.2 Flows around bends.....	72
a) Rivers.....	72
b) Submarine Channels.....	76
2.6 Sedimentation processes around bends in submarine channels.....	79
2.7 Conclusions.....	86
<b>Chapter 3 Morphometric variation as a function of submarine channel type: implications for hydraulic properties</b> .....	<b>88</b>
3.1 Chapter Summary .....	88
3.1 Introduction .....	89
3.2 Definition and classification of submarine channels .....	93
3.3 Dataset and Methodology .....	96
3.3.1 Analysis of channel parameters .....	106
3.3.2 River dataset.....	113

3.3.3	Statistical analysis.....	115
3.4	Results .....	117
3.4.1	Comparison between channels within a channel type.....	118
3.4.2	Comparison between channel types .....	124
3.4.3	Comparison of morphometric parameters between submarine channel types and rivers.....	129
3.4.4	Application to a wider dataset .....	131
3.5	Discussion.....	140
3.5.1	Aspect ratios of submarine channel types.....	141
3.5.2	“Bankfull condition” for submarine channels .....	143
3.6	Conclusions.....	145
<b>Chapter 4</b>	<b>Width variation around submarine channel bends: Implications for sedimentation and channel evolution.....</b>	<b>147</b>
4.1	Chapter Summary .....	147
4.2	Introduction .....	148
4.3	Width variations around river bends.....	152
4.4	Geological setting and study area .....	154
4.5	Dataset and methodology .....	156
4.5.1	Methodology for cross-section measurement around bends .....	158
4.5.2	Channel width measurements: definitions and methodology.....	164
4.5.3	Error analysis .....	167
4.6	Characteristics of studied channel reaches.....	171
4.7	Results .....	174
4.7.1	Variation of channel width around bends in individual channel reaches.....	174
4.7.2	Summary of width variations around bends in individual channels.....	182
4.7.3	Width variation between channel base and channel banks .....	186
4.7.4	Channel width variation as a function of sinuosity.....	188
4.7.5	Channel width variation as a function of radius of curvature .....	191
4.7.6	Overall trend of channel width variation around bends .....	192
4.8	Discussion.....	195
4.8.1	Comparison of submarine channel bends to river bends ..	195
4.8.2	Sedimentation at channel bends.....	198

4.8.3	Bank pull or bar push? .....	200
4.8.4	Control on width of submarine channel bends .....	202
4.9	Conclusions.....	205
<b>Chapter 5</b>	<b>Width variation around submarine channel bends for different channel types: implications for bend migration.....</b>	<b>206</b>
5.1	Chapter summary.....	206
5.2	Introduction .....	207
5.3	Methodology.....	209
5.4	Results .....	225
5.4.1	Total width around bends.....	225
5.4.2	Ratio between outer and inner bend width.....	228
5.4.3	Width variation between channel base and channel banks .....	231
5.4.4	Apex-inflection width ratio as a function of sinuosity .....	233
5.4.5	Overall trend of width around bends .....	234
5.4.6	Comparison between upstream and downstream channel section .....	237
5.5	Discussion.....	244
5.6	Conclusions.....	249
<b>Chapter 6</b>	<b>Discussion: Processes and morphology of submarine channels for different channel types, and implications for bend migration.....</b>	<b>251</b>
6.1	Why is it important to distinguish submarine channels? .....	251
6.2	Comparison of the morphometrics between submarine channels and rivers .....	252
6.3	Behaviour of the downstream (primary) directed flow in submarine channels .....	256
6.4	Hydraulic power-law scaling relationships.....	258
6.5	Influence of the flow on the morphometrics of channels .....	258
6.6	Equilibrium channel morphometrics .....	260
6.7	Evolution of channel types .....	263
6.8	Processes around bends .....	264
6.8.1	Why is it important to study the width around bends? .....	264
6.8.2	Summary of width variation around bends for different channel types.....	265
6.8.3	Bend evolution .....	273
6.8.4	Behaviour of flow around bends.....	274
6.8.5	Bend migration.....	283



6.9	Conclusions.....	292
<b>Chapter 7</b>	<b>Thesis summary.....</b>	<b>294</b>
7.1	Is channel width constant around submarine channel bends? How does width vary around a bend in submarine channels? ..	294
7.2	Are there morphometric variations between different types of submarine channels and how do the morphometrics of different types compare to rivers? .....	295
7.3	What can the width variation around bends tell us about the flow and sediment processes and hence the evolution of submarine channel bends? .....	296
7.4	Recommendations for future research .....	297
	<b>List of References .....</b>	<b>299</b>
	<b>Appendix A: Methodology guide for measuring the width and depth of cross-sections around bends .....</b>	<b>327</b>
	<b>Appendix B: References used for the literature-based channel dataset in Section 3.4.4.....</b>	<b>330</b>
	<b>Appendix C: Width measurement results for Chapter 4 .....</b>	<b>335</b>

# List of Tables

<b>Table 3.1</b> Summary of analysed channel sections.....	97
<b>Table 3.2</b> Methodology from each reference source.....	114
<b>Table 3.3</b> Submarine channel dataset. ....	133
<b>Table 4.1</b> Summary of the vertical error for height, for each channel system.....	170
<b>Table 4.2</b> Characteristics of each studied channel reach.....	172
<b>Table 4.3</b> Results of two-sample Student's t-test between bend apex and bend inflection widths, for a range of different width measurements, for the four channel reaches. The null hypothesis was that the apex-width was not larger than the inflection region width. The table reports p-values, or probability values, that identify whether a statistically significant relationship exist between two sample groups. A p-value of <0.05 identifies a statistical significance between two sample groups with a 95% confidence interval, and rejects the null hypothesis and thus confirms the alternative hypothesis. The alternative hypothesis is that bend apex width is greater than bend inflection width. 'None' represents no significant relationship.....	185
<b>Table 5.1</b> Total number of cross-sections measurements, and subdivided by non-complex, and complex topography.....	221
<b>Table 5.2</b> Summary of different methodologies for comparing width variations around bends between submarine channels and rivers....	236
<b>Table 5.3</b> Statistical results of the two-sampled t-test for submarine-fan channels and isolated deep-ocean channels. Calculation of a significant difference, between mean-apex and mean-inflection region for submarine-fan and isolated deep-ocean channels.....	237
<b>Table 5.4</b> Results of two-sample t-test between apex-region and inflection region with for all channel heights. The null hypotheses ( $H_0$ ) was that apex-region width and inflection-region width were equal. The null hypothesis was tested for each channel. ....	240
<b>Table 5.5</b> Summary of different methodologies for comparing width variations around bends between submarine channels and rivers....	246
<b>Table 6.1</b> Characteristics of the main studied channel types and their comparison to rivers.....	252
<b>Table 6.2</b> Comparison of width, depth and aspect ratio between rivers, submarine fan, isolated deep-ocean and axial channels.....	254
<b>Table 6.3</b> Percentage of bends being wider.....	271
<b>Table 6.4</b> Percentage of average width that bend apices are wider than inflections. ....	273

**Table 6.5** Results of cross-section shape analysis for submarine-fan channels (orange) and isolated deep-ocean channels (blue). A value of  $1 > b \geq 0$  represents a convex-upward shaped cross-section, a value of  $b = 1$  represents a “V”-shaped cross-section, a value of  $2 \geq b > 1$  represents a “U” or parabolic-shaped cross-section and a value of  $b > 2$  represents a box-shaped cross-section. Cross-sectional shape did not change substantially between points and regions. Note the channel bed width was not considered in this analysis. .... 292

# List of Figures

- Figure 1.1** The PhD thesis (Morphometrics of submarine channels) can be divided into two sections (“between channel types” and “around bends”). Chapter 2 is a literature review. Chapter 3 only considers the section “between channel types”. Chapter 4 considers only the morphometrics around bends for channels on the Congo Fan. Chapter 5 and Chapter 6 deals with both sections. For Chapters 3-5, the research question, which are answered in the chapters and the used dataset are mentioned. For Chapter 6, a summary of the main points discussed in the chapter is given. .... 37
- Figure 2.1** Bend evolution is controlled by an interaction of flow processes, sedimentation and channel morphometrics. .... 38
- Figure 2.2** Comparison of channel cross-sections. Cross-section are from: A) Congo Channel (Babonneau *et al.*, 2004), B) Bounty Channel (Carter and Carter, 1996), C) Amazon Channel (Flood and Damuth, 1987), D) Bengal Channel (Schwenk *et al.*, 2003), E) Indus Channel (Mishra *et al.*, 2016), F) Lofoten Channel (Ó Cofaigh *et al.*, 2006), G) Cascadia Channel (Griggs and Kulm, 1973), H) NAMOC, Northwest Atlantic Mid-Ocean Channel (Klaucke *et al.*, 1998b), I) Tanzania Channel (Bourget *et al.*, 2008), J) Surveyor Channel (Ness and Kulm, 1973), K) Toyama Channel (Nakajima *et al.*, 1998), L) Brunei Channel (Straub *et al.*, 2012), M) LUCIA Channel (Maier *et al.*, 2012), and N) Hikurangi Channel (Lewis and Pantin, 2002). Grey box present the area of the channel belt. External levees are adjacent to the channel belt (see Figure 2.3 for definition). .... 39
- Figure 2.3** Different processes responsible for forming terraces (Hansen *et al.*, 2015). .... 40
- Figure 2.4** Characteristics of submarine channels in cross-section: A) Depositional characteristics are dominant levees and an aggradational channel bed. B) Erosional characteristics are weak levees and an erosional/incised channel bed. C) Depositional-erosional characteristics are a mix of depositional and erosional characteristics. Adapted from Clark and Pickering (1996b). .... 42
- Figure 2.5** Planform of submarine channels can be composed of either a A) single channel, e.g. Hikurangi Channel, modified from Lewis *et al.* (1998) or B) a network of submarine channels, e.g. Congo Channel from Picot *et al.* (2016). .... 44
- Figure 2.6** Classification of a meander and a bend. A meander is considered as a trough and a peak loop, whereas a bend is considered from inflection point to inflection point with an apex point in between. Modified from Leopold and Wolman (1960). .... 45
- Figure 2.7** Classification of submarine channels. Modified from Peakall and Sumner (2015). .... 48

- Figure 2.8** Schematic diagram of deposition and erosion, as a function of Coriolis forces, within a submarine channel architecture at three latitudes for traction dominated (A-C) and suspension fallout dominated (D-F) flows. From: Cossu *et al.* (2015). ..... 50
- Figure 2.9** Schematic model showing the contrasting evolution between rivers and aggradational submarine channels. Bend growth from an initially straight channel (central black line) is shown in both cases. Rivers undergo regular lateral (swing) and downstream (sweep) bend migration forming tabular, sheetlike bodies referred to as channel belts. In contrast, aggradational submarine channels undergo bend increase with no significant downstream bend migration, forming a ribbon geometry (Peakall *et al.*, 2000b)..... 51
- Figure 2.10** Bend development in a subsurface example from the uppermost (~40 m) of a 120 m ( $\pm 20$  m) aggradational submarine channel stack that infills the upper fan valley on the west African margin. Successive position of the channel thalweg is shown; thalweg width is ~60 m, channel width is ~400 m. *Note:* Poor seismic resolution at bend 10. From Peakall *et al.* (2000a)..... 52
- Figure 2.11** Submarine channel evolution is controlled by a lateral bend expansion (Stage 1), followed by a zone of bypass and vertical aggradation (Stage 2) and ends with sediment filling of the channels, where the channel gets abandoned (Stage 3). From Peakall *et al.*, 2000b..... 53
- Figure 2.12** Three types of channel width are identified from the Brice (1975) classification of single-thread alluvial rivers: A) Equiwidth channels with a constant width between inflections and apexes, B) Wider-at-bends channels are wider at bend apexes than at bend inflections and C) Irregular-width channels are wider at bend inflections and bend apexes. Classification is also divided on the dominant sedimentation style (modified from Zolezzi *et al.*, 2012)..... 57
- Figure 2.13** A) Satellite images of a river reach with variable width of the Rio Beni (Bolivien Amazon. B) Variation of channel width along the reach. Small letters (a, b, c...) refer to inflection points,  $W^*$  to longitudinal channel width variation and  $s^*$  refer to a curvilinear arclength, channel centreline (modified Luchi *et al.*, 2011). ..... 58
- Figure 2.14** A) Spatial distribution of the hydrodynamic (solid line) and morphologically active width (dashed line) along a meandering reach from the River Bollin. Letters I1, I2 and I3 refer to inflection regions and letters B1, B2, and B3 refer to apex region). B) Sketch of a cross-section at a point bar (Modified from Luchi *et al.*, 2012)..... 61
- Figure 2.15** Channel width vs. depth. Data from Clark and Pickering (1996a), Konsoer *et al.* (2013), and Cullis *et al.* (2019)..... 64
- Figure 2.16** Comparison of different submarine channels in the downstream direction. Curves are redrawn from Hesse *et al.* (1980), Babonneau *et al.* (2002), Pirmez and Imran (2003), Bourget *et al.* (2008) and Fournier (2016). A: Channel depth from channel bed to mean levee crest. B: Channel width between levee crest. Modified from Fierens *et al.* (2019). ..... 64

<b>Figure 2.17</b> A lower channel relief compared to the channel banks at the inner bend suggests width variation with height above the bend. Modified from Babonneau <i>et al.</i> (2010). .....	65
<b>Figure 2.18</b> Observations of a shallow marine channel showing the locations of erosion and deposition. From Conway <i>et al.</i> (2012). .....	66
<b>Figure 2.19</b> A) Location of cross-sections. Cross-sections 1-4 are upstream of the bend apex and cross-sections 6-9 are downstream of the bend apex. Asymmetry is the ratio between the distance to the thalweg from the inner bend margin ( $D_i$ ) and the channel width ( $w$ ). B) Density probability plots of channel asymmetry upstream and downstream of the bend apex from the LUCIA Chica channel. Modified from Reimchen <i>et al.</i> (2016). .....	67
<b>Figure 2.20</b> Terminology of flow types for submarine sediment density flows as a function of sediment concentration based on percentage by volume (Modified from Mulder and Alexander, 2001). .....	69
<b>Figure 2.21</b> Characteristics of flow transformation from hyper-concentrated density flow to turbidity flows. From Mulder and Alexander (2001). .....	69
<b>Figure 2.22</b> Characteristics of flows within submarine channels (from Hansen <i>et al.</i> , 2015). .....	71
<b>Figure 2.23</b> A) Schematic view of flow components from the primary flow component (high velocity core, green) and secondary flow component (near-bed flow component, red and surface flow component, orange) Modified from Kasvi <i>et al.</i> (2015) and Lagasse <i>et al.</i> , 2004 based on Thompson (1986). B) Schematic view of the generalised flow components in a meander. Downstream primary flow (open parabolas with arrows) and lateral secondary flow (closely lined area) components of velocity as vectors and surface stream lines (From Leopold and Wolman, 1960). .....	74
<b>Figure 2.24</b> Secondary flow at bend apex in rivers showing outward shoaling flow across point bar and outer bank cell (modified from Lagasse <i>et al.</i> , 2004 based on Markham and Thorne, 1992). .....	75
<b>Figure 2.25</b> Secondary flow component in a natural river bend. From: Dietrich and Smith (1983). .....	75
<b>Figure 2.26</b> Simplified flow structure model for A) clockwise or river-like in rivers and B) anticlockwise or river-reversed secondary flow for submarine channels at bend apexes. High velocity core (HVC) is situated close to the outer bend for rivers and HVC is similarly situated near the outer bend for an anti-clockwise (river reversed) flow structure or near the inner bend for a clockwise flow structure (river-normal) in submarine channels. Modified from Peakall and Sumner (2015) and Kasvi <i>et al.</i> (2015). .....	77
<b>Figure 2.27</b> Lateral velocity and density fields at three bend apexes for confined flows with a 0.15-m-wide channel (left panel) and 0.30-m-wide channel (right panel). Curvature is constant. From Ezz and Imran (2014). .....	79

<b>Figure 2.28</b> Processes around submarine channel bends. Modified from Peakall and Sumner, 2015.....	80
<b>Figure 2.29</b> Characteristics of oblique accretion deposits with A) point bar and B) without a point bar. Point bars develop from traction-dominated sedimentation and Oblique accretion deposition develop from suspension-dominated sedimentation. Modified from Page <i>et al.</i> (2003).....	82
<b>Figure 2.30</b> Comparison of scroll bars in A) submarine channels (Abreu <i>et al.</i> , 2003) and B) rivers (Page <i>et al.</i> , 2003). ....	83
<b>Figure 2.31</b> Time slices from the Amazon Channel (Lower Channel Levee System) with reflection cross-sections around bends. Outer-bank bars (OBB) are observed at sections W-T. Green arrows indicate north. From Nakajima <i>et al.</i> (2009). ....	84
<b>Figure 2.32</b> Process of bend cut-off in submarine channels. Adapted from Babonneau <i>et al.</i> (2004). ....	86
<b>Figure 3.1</b> Cumulative distribution of channel aspect ratio (W/D). Three submarine channel datasets (Pirmez and Imran, 2003; Konsoer <i>et al.</i> , 2013; Jobe <i>et al.</i> , 2016) are compared to three river datasets (Jerolmack and Mohrig, 2007; Wilkerson and Parker, 2011; Jobe <i>et al.</i> , 2016). Modified from Jobe <i>et al.</i> (2016).....	91
<b>Figure 3.2</b> Classification of submarine channels. Channel types are submarine-fan, slope, axial, non-margin ocean and isolated deep-ocean channels. Modified from Peakall and Sumner (2015). ....	96
<b>Figure 3.3</b> Location and tectonic setting of the Magdalena Channel. A) The channel is located in the Caribbean Sea, offshore Colombia, where the Caribbean Plate converges with the South American Plate (Map data: Esri). B) The Magdalena Fan (Fan extent: Idárraga-García <i>et al.</i> , 2019) is between the Southern (SSBF) and Northern Sinu Folt Belt (NSBF). The channel is part of a complex channel system (channel fragments from Kolla and Buffler (1984) and Ercilla <i>et al.</i> (2002)) and situated at the upper fan on the Southern Sinu Folt Belt (SSBF). C) Top surface of a 3D seismic survey with a horizontal resolution of approximately 15 m. In total, the channel section consists of 17 bends and a total of 217 cross-sections. DTM produced from seafloor horizon from a 3-D seismic survey – © Equión Energía Limited, Ecopetrol S.A. and Petrobras.....	98
<b>Figure 3.4</b> Location of the Bryant Channel. A) The channel is located in the Gulf of Mexico (Map data: Esri, Basemap from BOEM). B) Bathymetric map of the north-western Gulf of Mexico showing the location of the Bryant canyon and fan with the position of the low stand Mississippi River and delta position (Suter and Berryhill, 1985). Fan outline and canyon location from Lee <i>et al.</i> (1996) and Twichell <i>et al.</i> (2000). C) Location of Bryant Channel section with 133 cross-sections. DTM data from Law of the Sea U.S. UNCLOS Bathymetry Project.....	100

- Figure 3.5** Tectonic setting and channel locations from Surveyor, Baranof and Horizon Channel. A) The channels are situated in the Gulf of Alaska. B) Tectonic and channel extent derived from: Reece *et al* (2011, 2013); Walton *et al.* (2014); and Zhang and Gulick (2019). Fan extensions from Walton *et al.* (2014). C) Location of Surveyor Channel with 73 cross-sections and D) Location of Baranof with 85 cross-sections and Horizon Channel with 97 cross-sections. Map data: Esri, Basemap. DTM data from Law of the Sea U.S. UNCLOS Bathymetry Project. .... 103
- Figure 3.6** Location of the studied Mariana Channels on the West Mariana Ridge. Map data: Esri, Basemap. DTM data from Law of the Sea U.S. UNCLOS Bathymetry Project..... 105
- Figure 3.7** Three approaches for extracting channel width and height from a cross-section, a non-complex (Case A), and complex topography (Case B, C) in submarine channels. The approach adopted depends on the position of the cross-section in relation to the channel bank: A) Cross-section measured from channel bank to channel bank; B) Cross-section measured from channel bank to terrace; or, C) Cross-section measured from failed channel bank to terrace. Examples are shown from the Magdalena Channel..... 109
- Figure 3.8** Examples of cross-sectional shape (U/V index) and related b-values obtained through the General Power Law program: a) convex-upward shaped form,  $0 \leq b < 1$  (Example from Vidal Channel; Embley *et al.*, 1970); b) 'V'-shaped form,  $b=1$ ; c) 'U'-shaped form,  $1 < b \leq 2$  (Example from Brunei Channel; Straub *et al.*, 2012); d) box-shaped form,  $b > 2$  (Example from Tanzania Channel; Bourget *et al.*, 2008). .... 112
- Figure 3.9** Representation of a random dataset (range: -4.0 to 4.0) with a normal distribution. Mean and median are at 0. a) Box and whisker plot, b) Histogram plot with a histogram interval of 0.5, c) Cumulative distribution, and d) Kernel density estimation. For the box and whisker plot: the plot within each box indicates the median value, "+" indicates the mean, box ends are the 25<sup>th</sup> and 75<sup>th</sup> percentiles, whiskers represent 99.3 % in a normal distribution, and x indicates outliers. Data produced in MatLabR2016a. .... 117
- Figure 3.10** Submarine-fan channel (Magdalena Channel: black cross, Bryant Channel: blue dot): (A) Longitudinal depth profile (Channel central line). (B) Channel width. (D) Channel height, (E) Cross-sectional shape with division at 1 and 2. Values of shape refer to: shape < 1 convex-upward shaped form, shape = 1 "V"-shaped form, shape < 1 and shape  $\leq 2$  "U"- or parabolic-shaped form, shape > 2 box-shaped form. .... 119



- Figure 3.11** Isolated deep-ocean channel (Baranof Channel: blue circle, Surveyor Channel: black cross, Horizon Channel: red point) measurements: (A) Longitudinal depth profile (Channel central line). (B) Channel width. (D) Channel height, (E) Cross-sectional shape with division at 1 and 2. Values of shape refer to: shape < 1 convex-upward shaped form, shape = 1 “V”-shaped form, shape < 1 and shape ≤ 2 “U”- or parabolic-shaped form, shape > 2 box-shaped form. .... 121
- Figure 3.12** Non-margin ocean channel (Mariana Channel A: red point, Mariana Channel B: blue circle, Mariana Channel C: black cross) measurements: (A) Longitudinal depth profile (Channel central line). (B) Channel width. (D) Channel height, (E) Cross-sectional shape with division at 1 and 2. Values of shape refer to: shape < 1 convex-upward shaped form, shape = 1 “V”-shaped form, shape < 1 and shape ≤ 2 “U”- or parabolic-shaped form, shape > 2 box-shaped form. .... 123
- Figure 3.13** Plots of normalised down-stream distance as a function of A) Width, B) Height and C) Aspect ratio and channel types. .... 125
- Figure 3.14** Box and whisker plots of channel bed width (m) for studied channel sections (Magdalena, Bryant, Horizon, Baranof, Surveyor, and Mariana). Box indicates 25<sup>th</sup> and 75<sup>th</sup> percentiles, “+” indicates the mean, “-“ within the box indicates the median, whiskers indicate 99.3 % in a normal distribution and x indicate outliers. Mean for each category is shown. .... 126
- Figure 3.15** Box and whisker plots of area (km<sup>2</sup>) for studied channel sections (Magdalena, Bryant, Horizon, Baranof, Surveyor, and Mariana). The area was either calculated as A)  $Area_{bed} = WB + W^2 \times H$  or B)  $Area_{simple} = W * H^2$ , where  $W_{Bed}$  is the channel bed width,  $W$  is the mean channel width and  $H$  is the mean channel height. Box indicates 25<sup>th</sup> and 75<sup>th</sup> percentiles, “+” indicates the mean, “-“ within the box indicates the median, whiskers indicate 99.3 % in a normal distribution and x indicate outliers. Mean for each category is shown. .... 128
- Figure 3.16** Box and whisker plots of width, depth and width/depth ratio for 5 submarine channel sections and river data (Leeder, 1973; Van den Berg, 1995; Jerolmack and Mohrig, 2007; Whittaker, 2007; Wohl and David, 2008; Yanites *et al.*, 2010; Wilkerson and Parker, 2011). The line within each box indicates the median value, “+” indicate the mean, box ends are the 25<sup>th</sup> and 75<sup>th</sup> percentiles, whiskers represent 99.3 % in a normal distribution, and “x” indicated outliers. Mean for each category is written. .... 130
- Figure 3.17** World map showing the locations of 23 submarine channels used for the compiled dataset from four submarine channel types: Isolated deep-ocean (▲), Submarine-fan (■), Slope (▲), and Axial channels (◆). .... 132

- Figure 3.18** Cumulative distribution of A and B) width (m), C and D) height (m), and E and F) aspect ratio. Figures A, C and E are composed of the compiled dataset from the literature only and rivers. Figures B, D and F are compiled dataset, rivers and studied channel types from the study herein. River datasets are from bedrock and alluvial rivers (Leeder, 1973; Van den Berg, 1995; Jerolmack and Mohrig, 2007; Whittaker, 2007; Wohl and David, 2008; Yanites *et al.*, 2010; Wilkerson and Parker, 2011); blue solid line), submarine channel types from compiled dataset are: submarine-fan (orange solid), slope (brown solid), axial (red solid) and isolated deep-ocean (dark blue solid). Studied channel types from the study herein are: submarine-fan (Magdalena, orange dashed; Bryant Channel, green dashed), non-margin (Mariana, pale pink dashed), and isolated deep-ocean (Surveyor, Baranof, Horizon; dark blue dashed). ..... 136
- Figure 3.19** Kernel density estimation (blue) and histogram with a bin interval of 0.2 (orange) of the cross-sectional area for A) submarine-fan, B) Slope, C) Axial and D) isolated deep-ocean channels. Data from the compiled dataset from the literature. .... 137
- Figure 3.20** Kernel density estimation (blue) and histogram with a bin interval of 0.01 (submarine-fan: A, B, C) and 0.2 (isolated deep-ocean: D, E) data (orange) of the cross-sectional area as a comparison between submarine-fan and isolated deep-ocean channel from the compiled dataset (A, D) and this study with Magdalena (B) and Bryant (C) and Surveyor, Horizon and Baranof compiled (D). ..... 138
- Figure 3.21** Kernel density estimation (blue) and histogram with an interval of 0.5 (orange) of the cross-sectional shape for the compiled dataset. .... 139
- Figure 3.22** Kernel density estimation (blue) and histogram with an interval of 0.2 (orange) of the cross-sectional shape as a comparison between Submarine-fan and isolated deep-ocean channel from the compiled dataset (A, C) and this study (B, D). ..... 140
- Figure 3.23** Comparison of the literature-based dataset from this study to three submarine channel datasets (Pirmez and Imran, 2003; Konsoer *et al.*, 2013; Jobe *et al.*, 2016) and river datasets (bedrock and alluvial; Leeder, 1973; Van den Berg, 1995; Jerolmack and Mohrig, 2007; Whittaker, 2007; Wohl and David, 2008; Yanites *et al.*, 2010; Wilkerson and Parker, 2011). ..... 142

**Figure 4.1** Schematic diagram of in-channel morphology as a function of bend position and curvature for A) an experimental submarine channel with a constant width, adapted from Peakall et al. (2007) and Amos et al. (2010); and B) a river channel with greater width at the bend apex relative to the inflections, adapted from Trush et al. (2000) and Rossi (2012). Positions of maximum erosion (black stripes) and aggradation (orange area) are shown. Purple dotted lines represent apex cross-section and green dashed lines represent inflection cross-sections. Note that the areas of enhanced aggradation and erosion are located further downstream relative to the apex in the submarine channel than in the river case. .... 151

**Figure 4.2** A) Location of the Congo Submarine Fan and Congo basin. B) Bathymetry map of the Congo Submarine Fan with its individual fans (Northern, Southern and Axial Fan). The study area is situated on the Axial Fan, the youngest individual fan of the Congo Submarine Fan. The studied channel reaches are part of the Northern (Ax52), Central (Ax12) and Southern Channels (Ax02, Ax14). Channel Ax52 is currently active. The canyon head is the starting point for channel length measurements and is 77 km upstream, as measured by along channel distance, from the point of origin used by Babonneau et al. (2002). Grey diamonds represent positions of recorded activity; data obtained from Khripounoff *et al.* (2003), Vangriesheim *et al.* (2009) and Azpiroz-Zabala *et al.* (2017a). Studied channel reaches are shown as white boxes. Outline of fans, location of channels and relative age of channels are based on Picot *et al.* (2019). .... 156

**Figure 4.3** Methodology for measuring: A) sinuosity, and B) width variation around bends. A) Sinuosity was measured per channel and per bend. B) Methodology for measuring cross-sections around a bend. Flow is from right to left. Thirteen cross-sections per bend were measured perpendicular to the channel base centreline (dashed line): at the up-stream inflection (1ui, white circle), at the down-stream inflection (13di, white circle), at bend apex (7a, grey square) and 5 cross-sections between the bend apex and up-stream (2u, 3u, 4u, 5u, 6u), and 5 between the bend apex and the down-stream inflection point (8d, 9d, 10d, 11d, 12d). Cross-sections were divided into an inflection region (blue dashed ellipses) and an apex region (red solid ellipse). .... 159

**Figure 4.4** Methodology for cross-section measurements in submarine channel bends. A) Bathymetric map showing an example of a channel reach with the channel base centreline, channel bank crestlines, bend trajectory lines, and the points on the centreline (yellow dots) where cross-sections would be taken from (see Figure 4.3 for details of the cross-sections themselves). For simplicity only 4 channel cross-sections are shown; lines B-B' to E-E'. The grey lines join the centreline points (yellow dots) at equivalent downstream and upstream positions around the bend (e.g., points 6u and 8d, see Figure 4.3). Trajectory lines are connected along the mid-points of these grey lines. B-E) Examples of width and height measurements from channel cross-sections. At each perpendicular cross-section width and height were measured as followed: channel width was measured at the channel base ( $W_0$ ), at the channel banks ( $W_{Outer}$ ,  $W_{Inner}$ ), and at height intervals of 10 m between the channel base and channel banks; channel heights were measured between the channel base ( $H_0=0$  m) and channel banks ( $H_{Outer}$ ,  $H_{Inner}$ ). B) Simple cross-section close to bend inflection, showing an inner bend without a clear crestal position; crestal position and height are estimated from the planform map of the crestline on part A. C) Simple cross-section close to the bend apex. D) Complex cross-section at the bend apex, where the bank to bank section at the height of the crestline, crosses the channel twice as a result of a lower elevation of the inner bend. Here, atypically, there is no intersection of the cross-section with the trajectory line (red dotted line). In this case the measured inner bend position is the position of the maximum elevation of the inner bank along the cross-section (position b1). The estimated channel height at the inner bend is measured up to the intersection of the trajectory line (red dotted line) with the bank crest (w1). E) Complex cross-section close to the bend inflection, showing multiple crossings of the channel. The intersection of the cross-section with the trajectory line (c1) is used to identify the inner bend position, and therefore identify the true width (see text for details). The estimated channel height at the inner bend (w2) is calculated as in D. DTM produced by IFREMER Géosciences Marines – ©IFREMER. .... 163

**Figure 4.5** Absolute error distribution around a point on a DTM grid. A) Planform view of a DTM grid, showing the distribution of distances (errors) around a point; the length of the maximum absolute error is shown with a red line. B) The probability density function of absolute errors around a DTM point; generated from choosing randomly selected points in the unit square and calculating the distance to the centre. The mean absolute value is 0.38 of the cell size (Weisstien, 2021), thus 0.54 of the maximum absolute error..... 168

**Figure 4.6** Slope map with identified terraces and bend apices shown for each studied channel reach. (A) Ax02-channel. (B) Ax12-channel. (C) Ax14-channel. (D) Ax52-channel. Flow direction is from right to left. .... 173

- Figure 4.7** Bank-top channel width at individual cross-sections (brown dashed-pointed line), at mean bank inflection points (blue dotted line), at bank apex point per bend (red solid line), and % wider at apex point, against downstream distance (km) and bend number for individual channel reaches A) Ax02, B) Ax12, C) Ax14 and D) Ax52. Flow direction is from right to left. .... 175
- Figure 4.8** Box and whisker plots of the bank-top channel width between apex point (7a, red solid line) and inflection points (1ui, 13di, blue dotted line) for A) Ax02, B) Ax12, C) Ax14 and D) Ax52. Data include the widths as measured at the height of the inner and outer banks. Box indicates 25th and 75th percentiles, “red diamond” indicates the mean, “-” within the box indicates the median, whiskers indicate 99.3% in a normal distribution and “x” indicate outliers. Mean  $\pm$  standard error of the mean, standard deviation (std. dev.) and the number of measurements (n) are shown for each position..... 176
- Figure 4.9** Box and whisker plots of the comparative depth-avg. channel width between apex point (7a, red solid line) and inflection points (1ui, 13di, blue dotted line) for A) Ax02, B) Ax12, C) Ax14 and D) Ax52. Data include an equal number of measurements per cross-section for each bend and exclude the bank-top channel width. Box indicates 25th and 75th percentiles, “red diamond” indicates the mean, “-” within the box indicates the median, whiskers indicate 99.3% in a normal distribution, and “x” indicate outliers. Mean  $\pm$  percentage error of the mean, standard deviation (std. dev.) and the number of measurements (n) are shown for each position. .... 177
- Figure 4.10** Box and whisker plots of the depth-averaged channel width between apex point (7a, red solid line) and inflection points (1ui, 13di, blue dotted line) for A) Ax02, B) Ax12, C) Ax14 and D) Ax52. Data include the widths as measured at the height of the inner and outer banks. Box indicates 25th and 75th percentiles, “red diamond” indicates the mean, “-” within the box indicates the median, whiskers indicate 99.3% in a normal distribution and “x” indicate outliers. Mean  $\pm$  standard error of the mean, standard deviation (std. dev.) and the number of measurements (n) are shown for each position. .... 178
- Figure 4.11** Box and whisker plots of the bank-top channel width between apex (4u-10d, red solid line) and inflection (1ui-3u, 11d-13di, blue dotted line) regions for A) Ax02, B) Ax12, C) Ax14 and D) Ax52. Data include the widths as measured at the height of the inner and outer banks. Box indicates 25th and 75th percentiles, “red diamond” indicates the mean, “-” within the box indicates the median, whiskers indicate 99.3% in a normal distribution and “x” indicate outliers. Mean  $\pm$  standard error of the mean, standard deviation (std. dev.) and the number of measurements (n) for each region are shown..... 180

- Figure 4.12** Box and whisker plots of the comparative depth-avg. channel width between apex (4u-10d, red solid line) and inflection (1ui-3u, 11d-13di, blue dotted line) regions for A) Ax02, B) Ax12, C) Ax14 and D) Ax52. Data include an equal number of measurements per cross-section for each bend and exclude the bank-top channel width. Box indicates 25th and 75th percentiles, “red diamond” indicates the mean, “-” within the box indicates the median, whiskers indicate 99.3% in a normal distribution and “x” indicate outliers. Mean  $\pm$  percentage error of the mean, standard deviation (std. dev.) and the number of measurements (n) for each region are shown..... 181
- Figure 4.13** Box and whisker plots of the depth-averaged channel width between the apex (4u-10d, red solid line) and inflection (1ui-3u, 11d-13di, blue dotted line) regions for A) Ax02, B) Ax12, C) Ax14 and D) Ax52. Data include the widths as measured at the height of the inner and outer banks. Box indicates 25th and 75th percentiles, “red diamond” indicates the mean, “-” within the box indicates the median, whiskers indicate 99.3% in a normal distribution and “x” indicate outliers. Mean  $\pm$  standard error of the mean, standard deviation (std. dev.) and the number of measurements (n) for each region are shown..... 182
- Figure 4.14** Bar charts showing the percentage width increase at bend apices compared to the inflection points (symbol: dots), or between apex and inflection regions (symbol: vertical lines), for different measures of channel width. The different width measures are depth-avg. width (symbol: white box), comparative depth-avg. width (symbol: black box) or the bank-top channel width (symbol: grey box). The inactive channels are Ax02, Ax12 and Ax14 and the active channel is Ax52. All results are statistically significant ( $p < 0.05$ ) other than both depth-averaged measures for Ax14, and the depth-averaged region data for Ax52 (see Table 4.3)..... 184
- Figure 4.15** Depth-averaged width with normalised height at A) apex point (red dashed line) and inflection points (blue dotted line), and B) apex (red dashed line) and inflection region (blue dotted line) for all channel reaches (Ax02, Ax12, Ax14, and Ax52). The normalised height was calculated using the maximum height of each cross-section. Width measurements were calculated by taking the intersection of the normalised height at 0.1 increments with the extracted cross-section profile. Afterwards the data were averaged. Each data-point corresponds to the average of all bends of a reach. .... 186
- Figure 4.16** Percentage width increase at the apex with normalised height, at A) apex point, and B) apex region, for all channel reaches (Ax02, Ax12, Ax14, and Ax52). The normalised height was calculated using the maximum height of each cross-section. .... 187

- Figure 4.17** Bar charts showing the apex-inflection width ratio for A) bends classified as straight ( $1 \leq P \leq 1.2$ ), B) low sinuosity bends ( $1.2 < P < 1.5$ ), and C) high sinuosity bends ( $P \geq 1.5$ ). Sinuosity was obtained for each bend and corresponds to the ratio between bend length and inflection length (see Figure 4.3A). A second way to assess the relationship between sinuosity and variations in width around channel bends, is to plot mean apex width at regions, against mean inflection width at regions, as a function of sinuosity classes (Figure 4.18). The linear regression varied little between bends classified as straight, low sinuosity, and high sinuosity, suggesting that there is little if any relationship between sinuosity and a wider apex region width (Figure 4.18). No difference is seen between different channel reaches. .... 189
- Figure 4.18** Mean apex region width versus mean inflection region width for A) bends classified as straight ( $1 \leq P \leq 1.2$ ), B) low sinuosity bends ( $1.2 < P < 1.5$ ), and C) high sinuosity bends ( $P \geq 1.5$ ). The following channels were used: Ax02 (19 bends, circle), Ax12 (27 bends, cross), Ax14 (13 bends, square) and Ax52 (49 bends, diamond). Each point represents one bend and contains measurements from the depth-averaged channel width. Sinuosity was obtained for each bend and corresponds to the ratio between bend length and inflection length (see Figure 4.3A)..... 190
- Figure 4.19** Relationship between the percentage bank-top channel width increase at the bend apex point relative to inflection points, and the ratio of radius of curvature to bank-top channel width, is shown for A) Ax02 (19 bends), B) Inactive channel reach Ax12 (27 bends), C) Inactive channel reach Ax14 (13 bends) and D) Active channel reach Ax52 (49 bends). Each point represents one bend. The radius of curvature was measured for each bend using the curve-fitting method (Brice, 1973, 1974) along the channel base centreline. The channel width is the bank-top channel width of the 13 cross-sections along the bend..... 191
- Figure 4.20** A) Mean apex-region width versus mean inflection region width. Each point represents one bend and contains measurements of the depth-averaged channel width. The mean width for a bend was obtained from six cross sections for mean inflection-region and seven cross-sections for mean apex region width. A high correlation (blue dashed line,  $R^2=0.85$ ) is shown. The active channel reach is Ax52 (49 bends, diamond). Inactive channel reaches are Ax02 (19 bends, circle), Ax12 (27 bends, cross) and Ax14 (50 m resolution, 13 bends, square). B) Mean apex region width versus mean inflection region width for bends with terraces present or not. Bends with a terrace (cross) had an  $R^2$  of 0.83 and bends with no terrace (circle) had an  $R^2$  of 0.81. Black dotted line represents an equal mean inflection region and apex region width..... 194

- Figure 4.21** Mean apex region width versus mean inflection region width. Each point represents one bend and is based on depth-averaged measurements. Blue dashed line represents the linear regression and black dotted line represents equal mean apex and inflection region width. A) Active channel reach Ax52 (49 bends), B) Inactive channel reach Ax02 (19 bends), C) Inactive channel reach Ax12 (27 bends), and D) Inactive channel reach Ax14 (13 bends)..... 194
- Figure 4.22** Summary diagram of submarine channels illustrating that they are wider at bend apices compared to inflections. Purple dotted line represents apex cross-section and green dashed lines represent inflection cross-sections. Postulated positions of maximum erosion (white area) and aggradation (black area) are shown. This schematic diagram also suggests that point bars and zones of outer bank erosion are located more symmetrically around the bend apex, rather than prominently downstream of the bend apex; for channels without significant external tectonic or topographic influence. .... 200
- Figure 4.23** Relationship between climate, progradation/retrogradation, and channel bend width variations. Aspects modified from Caley *et al.* (2011) and Picot *et al.* (2016, 2019). Channel bend width variations are based on depth-averaged width measurements from the apex point and inflection points. .... 204
- Figure 5.1** Location of submarine-fan channels: 1.1) Amazon, 1.2) Magdalena, and 1.3) Bryant Channel. 1.1) Fan extension for A) Amazon Fan (extension from Damuth and Flood, 1984) with channel segments (blue) and black (canyon). 1.1a) Middle fan channel section with 20 bends analysed and 1.1b) Lower fan section with 20 bends analysed..... 214
- Figure 5.2** Tectonic setting and channel locations from Surveyor, Baranof and Horizon Channel. A) The channels are situated in the Gulf of Alaska. B) Tectonic and channel extension derived from: Reece *et al.* (2011, 2013); Walton *et al.* (Walton *et al.*, 2014); Zhang and Gulick (2019). Fan extensions from Walton *et al.* (2014). C) Location of Surveyor Channel with 6 bends. D) Location of Horizon and Baranof Channel with 7 bends each. .... 215
- Figure 5.3** A, B) Channels locating along the West Mariana Ridge. C, D) Location of the studied Mariana Channels on the West Mariana Ridge with 4 bends..... 216



- Figure 5.4** Methodology of (A) bend analysis and (B) cross-section analysis. A) Methodology for cross-section measurements around a bend. Flow is from left to right. 13 cross-sections per bend were measured perpendicular to the channel bed centreline: at the up-stream inflection (1ui), at the down-stream inflection (13di), at the bend apex (7a) and 5 cross-sections between the bend apex and up-stream (2u, 3u, 4u, 5u, 6u) and equally down-stream inflection points (8d, 9d, 10d, 11d, 12d). Cross-sections were divided into an inflection region (orange ellipse: 1ui, 2u, 3u, 11d, 12d, 13di) and an apex region (yellow ellipse: 4u, 5u, 6u, 7a, 8d, 9d, 10d). B) At each cross-section channel width and height were measured at the channel bed and at vertical intervals of 10 m away from the channel bed up to the top of the channel banks. Additionally, width was measured at each position, and separately the outer and inner bank widths were measured to either side of the bed centreline position. .... 219
- Figure 5.5** Three approaches for extracting channel width and height from a cross-section for the case of a non-complex (Case A) and complex topography (Case C) in submarine channels. The approach adopted depends on the position of the cross-section in relation to the channel bank: A) Cross-section measured from channel bank to channel bank; B) Cross-section measured from channel bank to terrace; or, C) Cross-section measured from failed channel bank to terrace. Examples are shown from the Magdalena channel. .... 222
- Figure 5.6** Box and whisker plot of total channel width from each cross-section (averaged channel width from channel bed to channel banks) for A) Submarine-fan, B) Isolated deep-ocean channels, C) Bryant Channel, and D) Non-margin ocean channels. Grey boxes represent inflection region (1ui-3u, 11d-13di) and the white box represents the apex region (4u-10d). Box indicates 25th and 75th percentiles, “red diamond” indicates the mean, “-“ within the box indicates the median, whiskers indicate 99.3% in a normal distribution and “x” indicates outliers. .... 228
- Figure 5.7** Box and whisker plots of the ratio between outer and inner bank width from each cross-section for A) Submarine-fan, B) Isolated deep-ocean channels, C) Bryant Channel, and D) Non-margin ocean channels. Grey boxes represent the inflection region (1ui-3u, 11d-13di) and the white box represents the apex region (4u-10d). Box indicates 25<sup>th</sup> and 75<sup>th</sup> percentiles, “red diamond” indicates the mean, “-“ within the box indicates the median, whiskers indicate 99.3% in a normal distribution and “x” indicates outliers. .... 231
- Figure 5.8** Pie chart of the percentage of bends being wider at bend apex, wider at inflection width or equal with height for all channels. Height is normalised..... 232

- Figure 5.9** Apex-inflection width ratio distribution based on sinuosity for A) submarine-fan, and B) Isolated deep-ocean channels for straight bends ( $1 \leq P \leq 1.2$ ), low sinuosity bends ( $1.2 < P < 1.5$ ), and high sinuosity bends ( $P \geq 1.5$ )..... 233
- Figure 5.10** Comparison between mean apex-region and mean inflection-region width for different channel types (A): submarine-fan channel (blue circles, 69 bends), isolated deep-ocean channel (black crosses, 20 bends), and non-margin ocean channels (green squares, 4 bends), and zoomed graphs for B) submarine-fan channels and C) isolated deep-ocean channels. B) High correlation (blue dashed line,  $R^2=0.91$ ) between mean apex-region and mean inflection-region width for submarine-fan channels. Channels were: Amazon channel (blue crosses), Magdalena channel (black squares) and Bryant (red diamonds). C) High correlation (blue dashed line,  $R^2=0.88$ ) between mean apex-region and mean inflection-region width for isolated deep-ocean channels. Channels were: Surveyor Channel (blue circles), Horizon Channel (black crosses) and Baranof Channel (red squares). For all figures: Each point represents one bend. The mean width for a bend was obtained from six cross-sections for mean inflection-region and seven cross-sections for mean apex-region width. At each cross-section all channel width measurements from channel bed to channel banks were included. .... 235
- Figure 5.11** Comparison between mean apex-region and mean inflection-region width for mid (blue cross) and lower fan section (black circle). Each point represents one bend. The mean width for a bend was obtained from six cross-sections for mean inflection-region and seven cross-sections for mean apex-region width. At each cross-sections all channel width measurements from channel bed to channels banks were included. .... 239
- Figure 5.12** Box and whisker plot of total width from each cross-section for A) Mid Amazon Fan and B) Lower Amazon Fan. Grey box represents inflection region (1ui-3u, 11d-13di) and white box represents apex region (4u-10d). Box indicates 25<sup>th</sup> and 75<sup>th</sup> percentiles, “red diamond” indicates the mean, “-“ within the box indicates the median, whiskers indicate 99.3 % in a normal distribution and “x” indicates outliers. .... 241
- Figure 5.13** Box and whisker plot of ratio between outer and inner bank width from each cross-section for A) Mid Amazon Fan and B) Lower Amazon Fan. Grey box represents inflection region (1ui-3u, 11d-13di) and white box represents apex region (4u-10d). Box indicates 25<sup>th</sup> and 75<sup>th</sup> percentiles, “red diamond” indicates the mean, “-“ within the box indicates the median, whiskers indicate 99.3 % in a normal distribution and “x” indicates outliers. .... 242
- Figure 5.14** Pie chart of percentage of bends being wider at bend apex (light grey), wider at inflection width (white) or equal (dark grey) with height for all channels. Height is normalised with 0 is equal to channel bed and 1 to channel banks..... 243

- Figure 6.1** Aspect ratios of different submarine channel types and rivers. Both river and submarine channel widths and depths range between 10:1 and 100:1. Data are composed for rivers (Leeder, 1973; Van den Berg, 1995; Jerolmack and Mohrig, 2007; Whittaker, 2007; Wohl and David, 2008; Yanites *et al.*, 2010; Wilkerson and Parker, 2011) submarine-fan channels (literature-based and studied), isolated deep-ocean channels (literature-based and studied) and axial channels (literature-based). ..... 253
- Figure 6.2** Comparison of channel width between A) submarine fan and isolated deep-ocean channels, B) different submarine fan channels, and C) different isolated deep-ocean channels in the downstream direction. Data are from this study: Bryant, Magdalena, Surveyor, Horizon and Baranof Channel; and from the literature: NAMOC (Hesse *et al.*, 1987), Hikurangi Channel (Lewis, 1994), Tanzania Channel (Bourget *et al.*, 2008), Amazon Channel (Pirmez and Flood, 1995) and Congo Channel (Babonneau *et al.*, 2002). Distance is based on downstream distance away from the canyon head. .... 254
- Figure 6.3** Comparison of channel depth between A) submarine fan and isolated deep-ocean channels, B) different submarine fan channels, and C) different isolated deep-ocean channels in the downstream direction. Data are from this study: Bryant, Magdalena, Surveyor, Horizon and Baranof Channel; and from the literature: NAMOC (Hesse *et al.*, 1987), Hikurangi Channel (Lewis, 1994), Tanzania Channel (Bourget *et al.*, 2008), Amazon Channel (Pirmez and Flood, 1995) and Congo Channel (Babonneau *et al.*, 2002). Distance is based on downstream distance away from the canyon head. .... 255
- Figure 6.4** Generalised profiles of A) velocity and B) density for rivers (green dashed line) and submarine channels (black solid line). Maximum velocity ( $U_{max}$ ) in rivers is at the top of the flow and in submarine channels is near the bottom of the flow. Density is relative constant throughout the flow in rivers (shown here schematically, albeit actual profiles will be a function of the Rouse number, related to the sediment grain-size within the flow) but varies to a greater degree in submarine channels with the maximum density close to the bottom. Height of flow in rivers is from the channel bed to the air/water surface (maximum tens of metres for large rivers and a few metres for most rivers). Height of flow for submarine channels is harder to define as it is from the channel bed to the height of the dilute sedimentation/ambient water position (probably a few tens of metres to hundreds of metres depending on the flow). Flow height for submarine channels is usual defined between the channel bed and the banks of the channel. .... 257

- Figure 6.5** Thickness of turbidity flow changes the type of erosion and deposition. Type A thickness of flow is lower than the channel banks, hence no levee formation. Type B: thickness of flow is higher than the channel banks, hence levee formation. Adapted from Piper and Normark (1983)..... 257
- Figure 6.6** Channel width is established earlier than channel depth. Channel width is relative constant between Interval B and G, but channel depth increases between Interval B and G. Example is from the NAMOC (Adapeted from Klaucke *et al.*, 1998b). ..... 261
- Figure 6.7** Variations of cross-sections for an aggradational and erosional flow for submarine fan and isolated deep-ocean channels. Arrows indicate the locations where aggradation, erosion or lateral widening occur. Modified from Kneller (2003). ..... 262
- Figure 6.8** Bar chart showing the percentage width increase at apices compared to bend inflections (symbol: dots), or at apex compared to inflections regions (symbol: vertical lines) at different width measurements (depth-avg. width (symbol: white box) or bank-top channel width (symbol: grey box)) for all studied submarine-fan channels..... 267
- Figure 6.9** Bar chart showing the percentage width increase at apices compared to bend inflections (symbol: dots), or at apex compared to inflections regions (symbol: vertical lines) at different width measurements (depth-avg. width (symbol: white box) or bank-top channel width (symbol: grey box)) for isolated deep-ocean channels in the Gulf of Alaska..... 269
- Figure 6.10** Comparison of flow processes around bends for A) rivers and B) submarine channels. HVC moves from an inner bend position at the bend entrance to an outer bend position at the bend exit. At the bend entrance (cross-section 1) maximum centrifugal force is near the bed in submarine channels and near the top in rivers. Superelevation starts to occur. At the bend apex (cross-section 2), superelevation is greater in submarine channels than in rivers, due to dominant radial fluid fluxes, which leads to outer-directed basal flow in submarine channels with HVC is situated at the outer bend position. Past the bend apex (cross-section 3) as the high velocity core shifts inward in submarine channels, the pressure gradient force towards the inner bend starts to be dominant near the bed and the secondary flow cell is directed towards the inner bend near the bed. Adapted from Leopold and Wolman (1960), Kasvi *et al.* (2015) and Peakall and Sumner (2015)..... 278

- Figure 6.11** Snapshot of the secondary flow at the bend apex for A) Rivers, B) Submarine channels with two flow cells stacked on top of each other, and C) Submarine channels with a reversed secondary flow cell. A) In rivers, centrifugal force is dominated at the top of the flow due to the maximum flow velocity near the top of the flow. The pressure gradient force is dominated near the channel bed due to a reduction of the centrifugal force. Radial fluid fluxes are not important as density stratification is in general small in rivers. B) Submarine channels with two flow cells stacked on top of each other occur when just considering the velocity and not the radial fluid flux due to the density stratification. Coriolis Force is dominated where the maximum flow velocity occur and pressure gradient force with an inward-directed flow exceeds the centrifugal force near the channel bed and on top of the flow. Hence two cells stacked on top of each other are created. C) A “basal-outward” flow direction in submarine channels is created by considering the radial fluid flux due to the density stratification giving rise to the superelevation. The combination of the radial fluid flux and the centrifugal force exceeds the pressure gradient force near the channel bed, hence only one basal-outward directed flow cell is created. For further explanation see Dorrell *et al.* (2013) and Peakall and Sumner (2015). Note: The height of the secondary flow cells is not for scale. .... 279
- Figure 6.12** Comparison of the radius of curvature near the channel bed. The radius of curvature for “V”-shaped cross-section ( $r_1$ ) is smaller than for the “U”-shaped cross-section. .... 282
- Figure 6.13** Comparison of the flow field with a constant and wider-at-bend apex width. At the bend entrance (Cross-section 1), centrifugal force and radial fluid flux is dominated near the bottom. The secondary flow cell increases due to increase of the radial fluid flux hence superelevation towards the bend apex. At the bend apex (cross section 2), outer-directed bed flow is dominated due to an increase in the radial fluid flux hence superelevation, but is reduced in wider-width cross-section relative to constant-width cross-section. At the bend exit (cross-section 3), the pressure gradient force is maintained for longer around the bend and therefore near the bed is dominant, relative to the centrifugal force, in wider-at-apex width than at constant width channels, hence this causes a quicker switch of the secondary flow cell. .... 285
- Figure 6.14** Bend processes are either controlled by bar push, inner bend deposition, or bank pull, outer bend erosion..... 286

# Chapter 1 Thesis rationale

---

## 1.1 Thesis background

Submarine channels are common natural sediment pathways along the ocean sea floor all around the world, thereby building complex networks, which can be similar in size to rivers (Menard, 1955; Johnson *et al.*, 1971; Lewis, 1994; Wynn *et al.*, 2007; Pickering and Hiscott, 2015). Even though submarine channels are referred to as “rivers of the ocean”, submarine channels are not an identical twin of rivers since there are a number of key differences in the fluid dynamics of submarine channels and rivers (see Peakall and Sumner, 2015). Firstly, the maximum downstream flow velocity is commonly near the channel bed in submarine channels rather than near the top of the flow as in rivers (Hampton, 1972; Kneller and Buckee, 2000; Hansen *et al.*, 2015). Secondly, many flows within submarine channels consistently entrain fluid from the surrounding flow rather than having a sharp boundary between the flow and the surrounding ambient fluid as in rivers where air is the ambient fluid (Corney *et al.*, 2006; Piper and Normark, 2009). Thirdly, submarine channels may experience a variety of secondary flow circulation patterns at channel bends, from outer-directed near bed flow, to inner-directed near bed flow as in rivers (Keevil *et al.*, 2007; Sumner *et al.*, 2014). Such variation in the fluid dynamics compared to rivers may lead to different sedimentation patterns and hence evolutionary processes within submarine channels.

Our knowledge of submarine channels is primarily based on observations from bathymetric data (e.g. Flood and Damuth, 1987; Klaucke and Hesse, 1996; Babonneau *et al.*, 2002), seismic subsurface studies (e.g. Klaucke *et al.*, 1998a; Kolla *et al.*, 2001; Fonnesu, 2003; Schwenk *et al.*, 2005), laboratory experiments (e.g., Peakall *et al.*, 2007; Straub *et al.*, 2008; Amos *et al.*, 2010), numerical models (Sylvester *et al.*, 2011) and outcrop

studies (e.g., Kane and Hodgson, 2011; Pyles *et al.*, 2012; Hubbard *et al.*, 2014). However, laboratory experiments and numerical models have dominated our understanding of flow and sedimentation processes within submarine channels (Peakall and Sumner, 2015). Since, in particular, flow measurements within submarine channels beyond the continental rise are rare (Khripounoff *et al.*, 2003; Vangriesheim *et al.*, 2009) and the majority of flow properties for submarine channels have been primarily derived from turbidity currents observed in other settings, including canyons (Xu *et al.*, 2002; Paull *et al.*, 2013), fjords (Conway *et al.*, 2012; Hughes Clarke, 2016; Gales *et al.*, 2018), and from estimated flow properties of sediment gravity flows derived from deposits and flow timelines (Stevenson *et al.*, 2013, 2018). Our knowledge of flow and sedimentation processes can be improved by conducting detailed analyses of the morphometrics of submarine channels (Konsoer *et al.*, 2013; Shumaker *et al.*, 2018). In particular, a detailed morphometric analysis around bends would help improve the understanding of sedimentation and particular evolutionary processes.

## 1.2 Thesis aims

The aim of the research is to understand the nature of morphometrics in submarine channels, and whether there are variations in morphology around submarine channel bends. The influence of channel morphometrics on flow and sedimentation within submarine channels is then considered. In particular, the following key research questions are posed:

**Question 1:** *Are there morphometric variations between different types of submarine channels and how do the morphometrics of different types compare to rivers?*

**Question 2:** *Is channel width constant around submarine channel bends? How does width vary around a bend in submarine channels?*

**Question 3.** *What can the width variation around bends tell us about the flow and sediment processes and hence the evolution of submarine channel bends?*

---

**Question 1:** *Are there morphometric variations between different types of submarine channels and how do the morphometrics of different types compare to rivers?*

**Rationale:** Submarine channels are typically classified as one group when considering a large dataset of submarine channels (Clark and Pickering, 1996a; Konsoer *et al.*, 2013; Foreman *et al.*, 2015; Jobe *et al.*, 2016; Shumaker *et al.*, 2018; Cullis *et al.*, 2019). However, contradictions arise when comparing, for example, the aspect ratio to rivers. The aspect ratio of submarine channels to rivers can be, depending on the study, smaller, similar or greater (Flood and Damuth, 1987; Clark *et al.*, 1992; Peakall *et al.*, 2000a; Konsoer *et al.*, 2013; Jobe *et al.*, 2016).

Submarine channels have been identified from cross-sectional analysis to have either erosional or aggradational characteristics (Mutti and Normark, 1987; Clark and Pickering, 1996b). However, cross-sectional characteristic can vary locally, can change over time, or submarine channels can have a mix with both characteristics. Hence, distinguishing submarine channels through a cross-sectional analysis in this manner may be very subjective. However, submarine channels have also been recognised to occur in a range of environmental settings (Schweller and Kulm, 1977; Carter, 1988; Klaucke *et al.*, 1998a; Peakall and Sumner, 2015). Channels can be classified depending on the environmental setting as submarine-fan, as slope, as axial, as isolated-deep ocean, as confined slope and as non-margin ocean channels (Peakall and Sumner, 2015). Although distinguishing submarine channels based on the environmental setting has been made, channel types have not been assessed based on their morphometrics for different environmental settings.



**Question 2:** *Is channel width constant around submarine channel bends? How does width vary around a bend in submarine channels?*

**Rationale:** Width around bends in rivers is controlled by deposition and erosion of the inner and outer banks (Nanson and Hickin, 1983; Parker *et al.*, 2011; Eke *et al.*, 2014a, 2014b). In rivers, it is known that bend migration is either controlled by a faster eroding outer bank (bank pull), or a faster depositing inner bank (bar push; Eke *et al.*, 2014a, b; Van de Lageweg *et al.*, 2014). Hence, an understanding of width variation around bends may explain whether submarine channel bends migrate via bank pull or bar push. Additionally, understanding the width variation around bends has an influence on the flow and sedimentation processes since these are non-linear related to the morphometrics around bends. However, width around bends has been kept constant in laboratory experiments and numerical models of submarine channels since it is not known if, and how, the channel width varies with curvature (Imran *et al.*, 1999, 2007; Das, 2004; Kassem and Imran, 2004; Peakall *et al.*, 2007; Islam and Imran, 2008; Amos *et al.*, 2010; Straub *et al.*, 2011; Janocko *et al.*, 2013). Some studies observed a variation of the geometry around bends (Nakajima *et al.*, 2009; Babonneau *et al.*, 2010; Conway *et al.*, 2012; Reimchen *et al.*, 2016), but a detailed analysis of width around bends has not been conducted.

**Question 3.** *What can the width variation around bends tell us about the flow and sediment processes and hence the evolution of submarine channel bends?*

**Rationale:** Laboratory experiments and numerical models of submarine channels predict that channels exhibit a downstream migration similar to rivers (Keevil *et al.*, 2007; Peakall *et al.*, 2007; Straub *et al.*, 2008; Amos *et al.*, 2010; Darby and Peakall, 2012; Janocko *et al.*, 2013; Cossu *et al.*, 2015), with the exception of Sylvester *et al.* (2011). By contrast, observations of aggradational submarine channels at passive margins suggest that channel bends undergo bend expansion but very limited downstream migration, whereas simultaneously aggrading, in marked contrast to rivers (Peakall *et al.*, 2000a,b; Deptuck *et al.*, 2007; Sylvester *et al.*, 2011; Jobe *et al.*, 2016). When

single-thread modern submarine channels on the sea-floor experience downstream bend migration it is often less than 2-3 times the channel width (Wynn *et al.*, 2007). However, exceptions exist such as the Bengal Channel (Schwenk *et al.*, 2003). Here, channel migration occur within a 15-20 km wide corridor with no avulsion, which is 10 times the channel width (channel width max. 1.6 km). Additionally, downstream bend migration has been observed to increase during the early development stage of submarine channels (Sylvester *et al.*, 2011; Kolla *et al.*, 2012), in salt-tectonic controlled settings (Covault *et al.*, 2020), in confined slope channels (Deptuck *et al.*, 2003, 2007; Posamentier, 2003; Kolla *et al.*, 2012), and for erosionally-controlled submarine channels (Abreu *et al.*, 2003). Although such variations in environmental setting and active tectonic deformation may explain observations between different systems, they cannot explain the contradiction between laboratory experiments and numerical simulations that predict significant downstream bend migration and observations from single-thread aggradational submarine channels on passive margins of bend expansion with very limited downstream translation. This suggests that an important aspect is missing to explain the observed contradictions. In rivers, the importance of width around bends for channel migration has been examined (Parker *et al.*, 2011; Eke *et al.*, 2014a, b; Van de Lageweg *et al.*, 2014). However, such connections between bend migration and channel width variation with curvature have not been conducted for submarine channels.

### 1.3 Thesis outline

This thesis is composed of a literature review and three independent research chapters (Chapter 3-Chapter 5), followed by a discussion (Chapter 6) and a summary that addresses each research question outlined in section 1.1 (Chapter 7, Figure 1.1). In Chapters 3, 4 and 5, bathymetric data were analysed through a Digital Elevation Model (DEM). A digital elevation model

(DEM) is a geospatial dataset, which contains information of elevations sampled on a regularly spaced rectangular grid.

**Chapter 2:** *Submarine channel bend dynamics: flow processes, sedimentation morphometrics and channel evolution.* This chapter is a literature review and describes the following aspects: the morphology and environmental setting of submarine channels, the bend evolution of submarine channels; and a description of the morphometrics, sedimentation and flow processes around submarine channel bends. Additionally, the processes around bends in terms of channel evolution are compared to rivers.

**Chapter 3:** *Morphometric variation as a function of submarine channel type: implications for hydraulic properties.* This chapter analyses downstream morphometrics of 8 submarine channels from 3 channel types, followed by a literature-based dataset analysis with 23 channels from 4 channel types with a comparison of the morphometrics to rivers and previous studies.

**Chapter 4:** *Width variation around bends of active and inactive submarine-fan channels: implications for sedimentation and channel evolution.* This chapter analyses width variation around bends from one active and three inactive channels on the Axial Congo Fan, with a focus to explain the contradiction observed in channel evolution between laboratory experiments and numerical simulations, and observations from modern submarine channels.

**Chapter 5:** *Width Variation around Submarine Channel Bends for different channel types: Implications for bend migration.* This chapter analyses width variation around bends for 3 channel types and links the observations to identify if variation in terms of width around bends exists between different channel types.

**Chapter 6:** *Discussion.* This chapter summarise and discusses the three previous chapters.

**Chapter 7:** *Conclusion.* This chapter answers the three research questions and incorporates these novel observations and enhanced understanding with the main findings from the literature in Chapter 2.

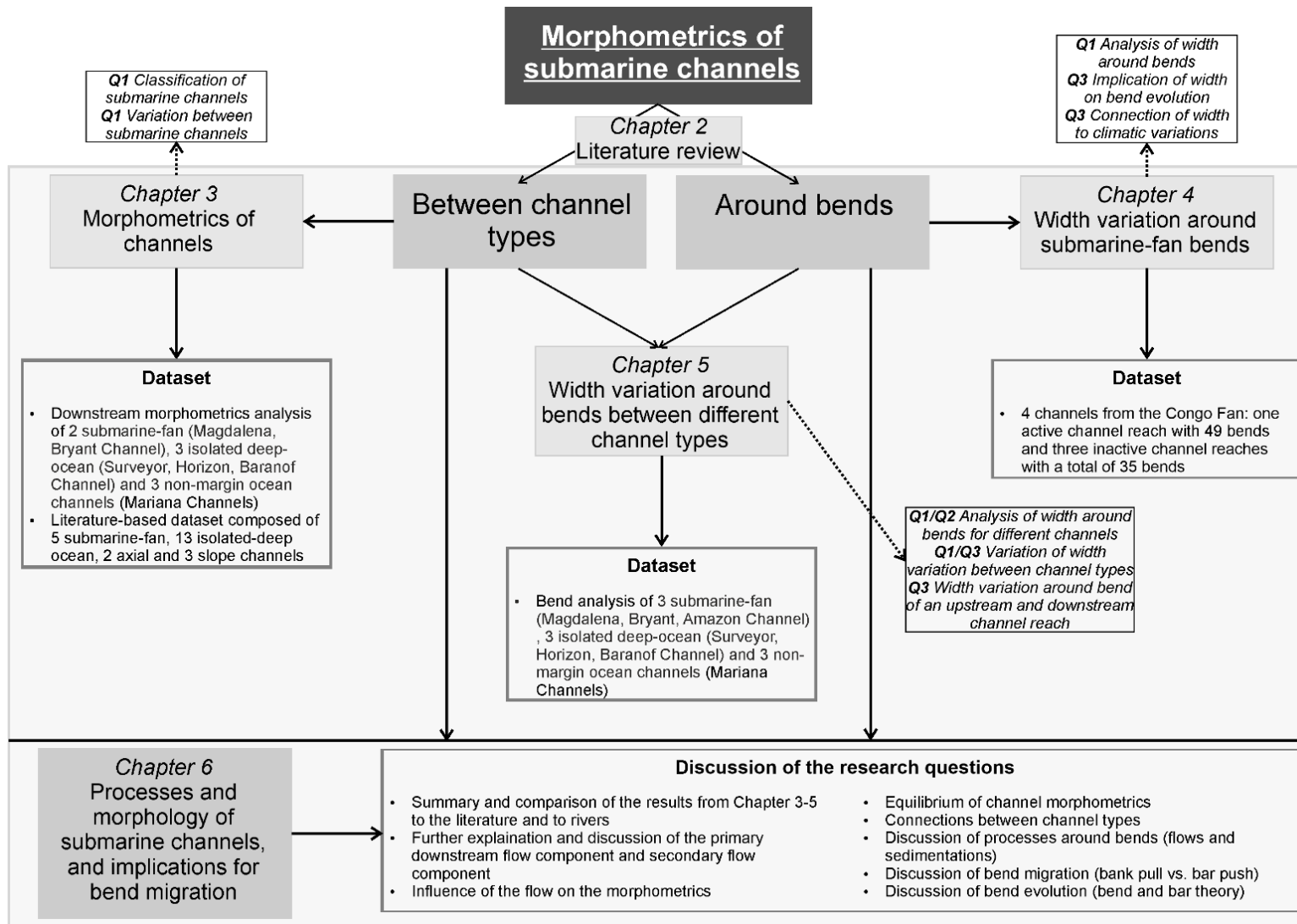


**Figure 1.1** The PhD thesis (Morphometrics of submarine channels) can be divided into two sections (“between channel types” and “around bends”). Chapter 2 is a literature review. Chapter 3 only considers the section “between channel types”. Chapter 4 considers only the morphometrics around bends for channels on the Congo Fan. Chapter 5 and Chapter 6 deals with both sections. For Chapters 3-5, the research question, which are answered in the chapters and the used dataset are mentioned. For Chapter 6, a summary of the main points discussed in the chapter is given.

## Chapter 2 Current understanding of submarine channel bend dynamics: flow processes, sedimentation morphometrics and channel evolution

---

This chapter focus on the processes around submarine channel bends, and their control on the evolution of submarine channels. Comparison is made with river bend dynamics which have been the object of detailed study. Channel evolution is ultimately controlled by an interaction of flow processes, sedimentation and the morphology of the channel (Figure 2.1).

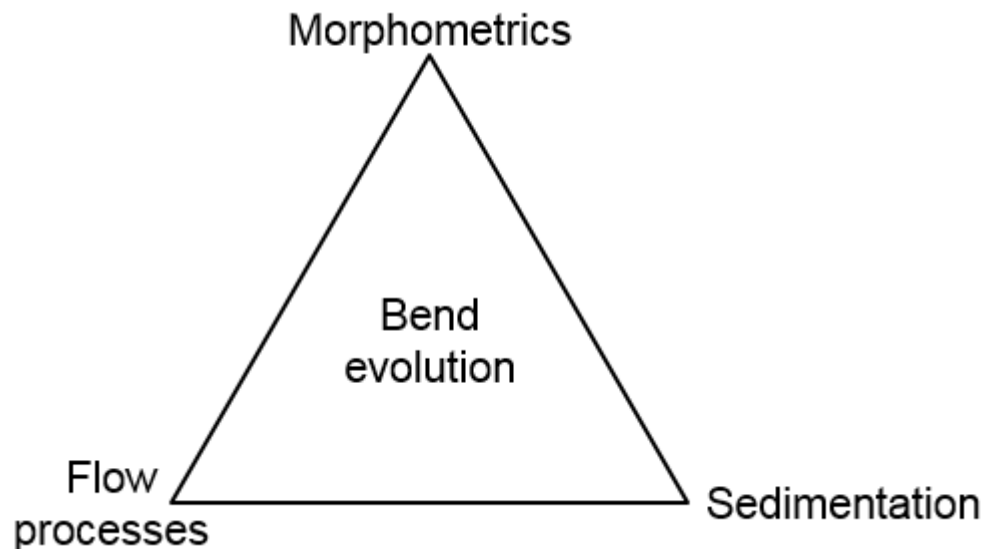


**Figure 2.1** Bend evolution is controlled by an interaction of flow processes, sedimentation and channel morphometrics.

---

## 2.1 Morphology and environmental setting of submarine channels

### *Cross-sectional characteristics*

Submarine channels in cross-section can occur in a wide range of shapes and sizes (Figure 2.2) and may be associated with channel levees in many cases. Levees, also referred to as external levees, are positive depositional relief features adjacent to the channel, which are built by overspill processes (see Kane and Hodgson, 2011; Nakajima and Kneller, 2013; Hansen *et al.*, 2015). Additionally, submarine channels can exhibit topographically flat surfaces within the channel banks, which are called “terraces”. Terraces are formed by multiple processes, such as incision, bend cut-off, inner bend deposition, or margin failure (Figure 2.3; Babonneau *et al.*, 2004; Hansen *et al.*, 2015).

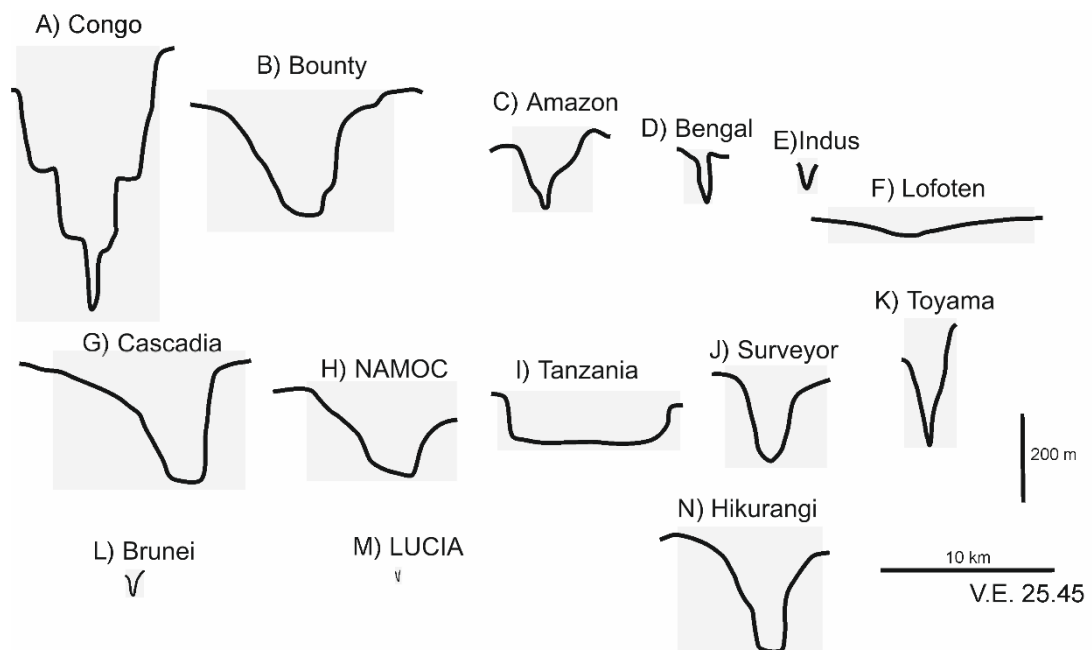
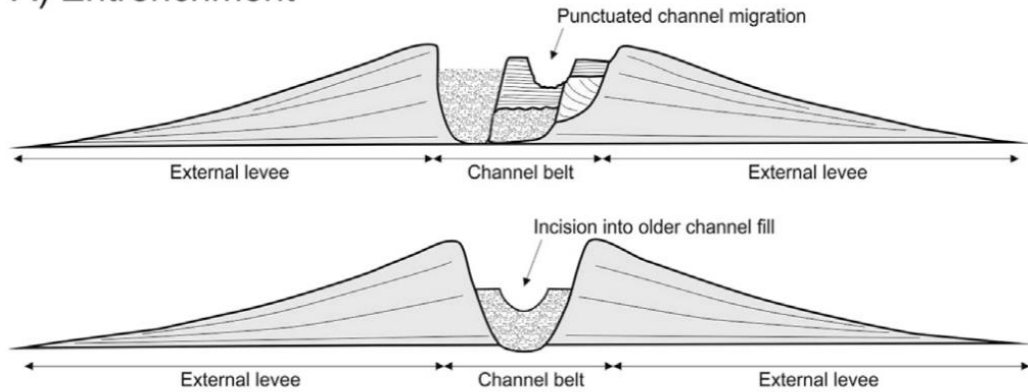


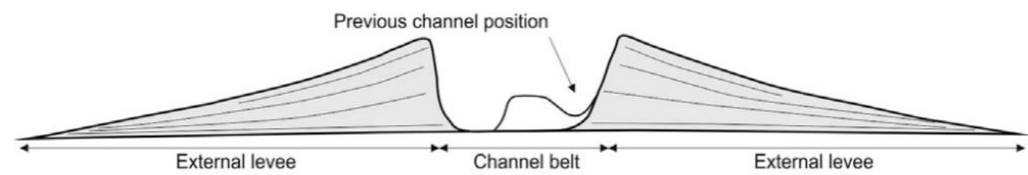
**Figure 2.2** Comparison of channel cross-sections. Cross-section are from: A) Congo Channel (Babonneau *et al.*, 2004), B) Bounty Channel (Carter and Carter, 1996), C) Amazon Channel (Flood and Damuth, 1987), D) Bengal Channel (Schwenk *et al.*, 2003), E) Indus Channel (Mishra *et al.*, 2016), F) Lofoten Channel (Ó Cofaigh *et al.*, 2006), G) Cascadia Channel (Griggs and Kulm, 1973), H) NAMOC, Northwest Atlantic Mid-

Ocean Channel (Klaucke *et al.*, 1998a), I) Tanzania Channel (Bourget *et al.*, 2008), J) Surveyor Channel (Ness and Kulm, 1973), K) Toyama Channel (Nakajima *et al.*, 1998), L) Brunei Channel (Straub *et al.*, 2012), M) LUCIA Channel (Maier *et al.*, 2012), and N) Hikurangi Channel (Lewis and Pantin, 2002). Grey box present the area of the channel belt. External levees are adjacent to the channel belt (see Figure 2.3 for definition).

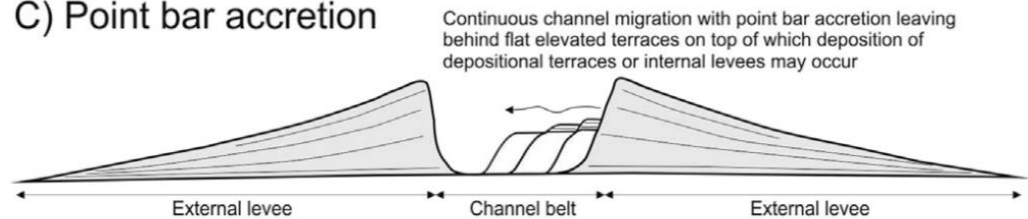
### A) Entrenchment



### B) Meander bend cut-off by entrenchment



### C) Point bar accretion



### D) Margin failure

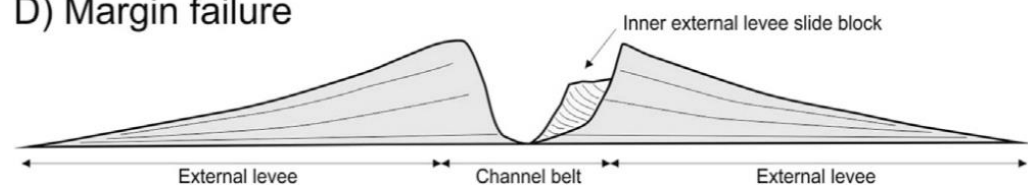


**Figure 2.3** Different processes responsible for forming terraces (Hansen *et al.*, 2015).



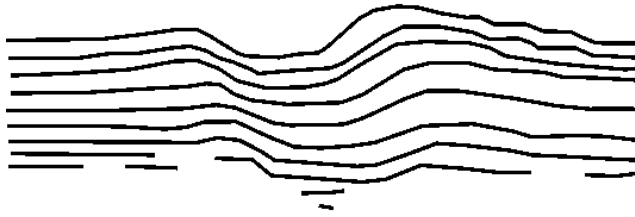
### *Erosional and aggradational characteristics*

In cross-section, submarine channels can be sub-divided based on erosional or aggradational characteristics, into: a) depositional, b) erosional or c) depositional-erosional types (Figure 2.4; Mutti and Normark, 1987; Clark and Pickering, 1996b). The following characteristics are identified for each type:

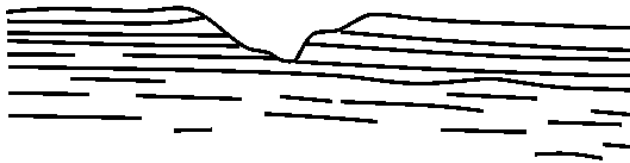
- a) Depositional channels are characterised by prominent levees and an aggradational channel bed. An aggradational channel bed is composed of sediment deposition at the channel bed, which results in vertical aggradation over time (Flood *et al.*, 1991).
- b) Erosional channels are characterised by flat banks or minor channel levees and an incising channel bed and channel entrenchment. Erosional-depositional channels have characteristics of both depositional and erosional channels. They are characterised by levees, but the channel floor is erosional, and is typically incised into the surrounding seafloor.

The classification is complicated to follow in practise as most submarine channels show depositional and erosional elements, and change sedimentation style spatially and temporally. A channel often changes from erosional to depositional characteristics, or a depositional channel may become incised over time, e.g. Congo Channel (Babonneau *et al.*, 2002). Hence most submarine channels exhibit evidence of both characteristics.

## A) Depositional



## B) Erosional



## C) Depositional-Erosional

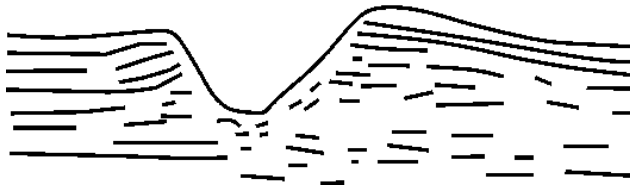


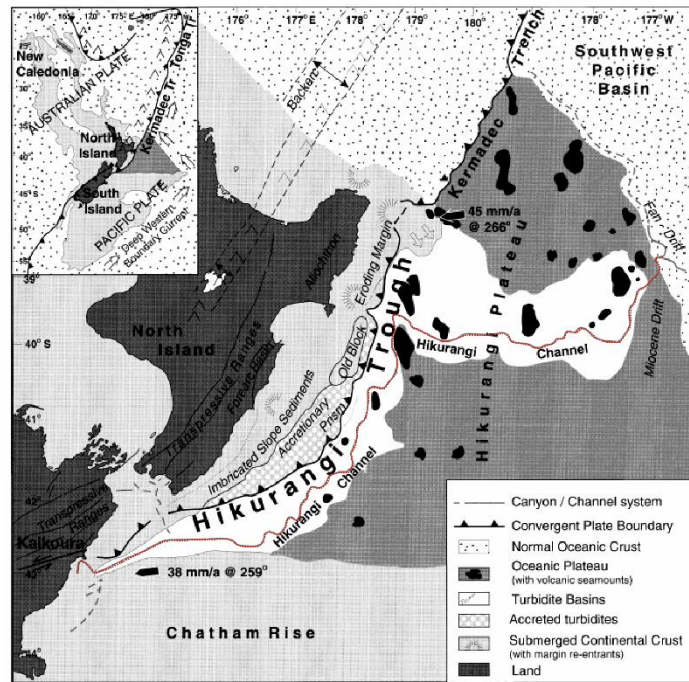
**Figure 2.4** Characteristics of submarine channels in cross-section: A) Depositional characteristics are dominant levees and an aggradational channel bed. B) Erosional characteristics are weak levees and an erosional/incised channel bed. C) Depositional-erosional characteristics are a mix of depositional and erosional characteristics. Adapted from Clark and Pickering (1996b).

### *Planform characteristics*

Submarine channels can either occur as a single main channel or as a complex network of submarine channels (Figure 2.5), but in both cases the majority of underwater channels have a sinuous channel pattern rather than a braided channel pattern (Wynn *et al.*, 2007; Foreman *et al.*, 2015). Even so braided patterns may be formed at similar flow aspect ratios in rivers and submarine channels (Foreman *et al.*, 2015). However, a greater flow depth in submarine channels compared to rivers (Konsoer *et al.*, 2013; Shumaker *et*

*al.*, 2018), typically prevents the formation of braided submarine channels (Foreman *et al.*, 2015). Hence, a “true” braided submarine channel system has not been discovered. The Orionoco deep-sea fan, which was once described as a “true” braided system (Belderson *et al.*, 1984), turned out with a higher resolution to be a complex network of sinuous and braided channel (Ercilla *et al.*, 1998). A channel is divided based on the curvature of the centreline into inflection and apex points, whereby inflections represent points of minimum curvature and apices represent points of maximum curvature. Measurements of river channels are either conducted on a bend or on a meander belt. A bend is classified from inflection point to inflection point with one bend apex, so either as a trough or a peak loop, whereas a meander belt is classified as two consecutive bends with a trough and a peak loop (Figure 2.6; Leopold and Wolman, 1960; Richards, 1982).

A) Single channel



B) Complex network of channels with one active channel at a time

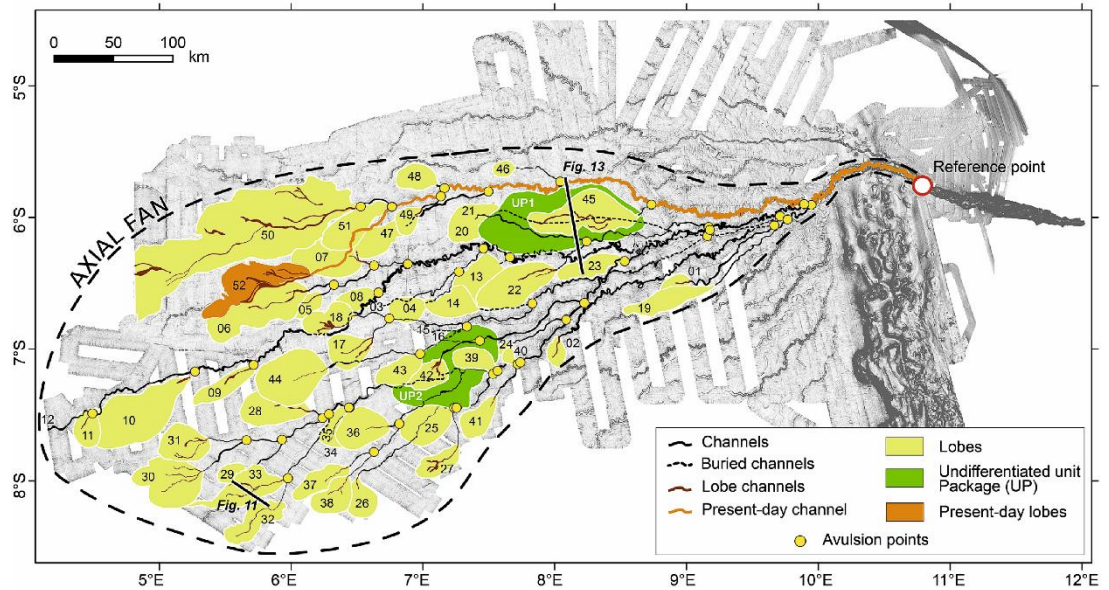


**Figure 2.5** Planform of submarine channels can be composed of either a A) single channel, e.g. Hikurangi Channel, modified from Lewis *et al.* (1998) or B) a network of submarine channels, e.g. Congo Channel from Picot *et al.* (2016).

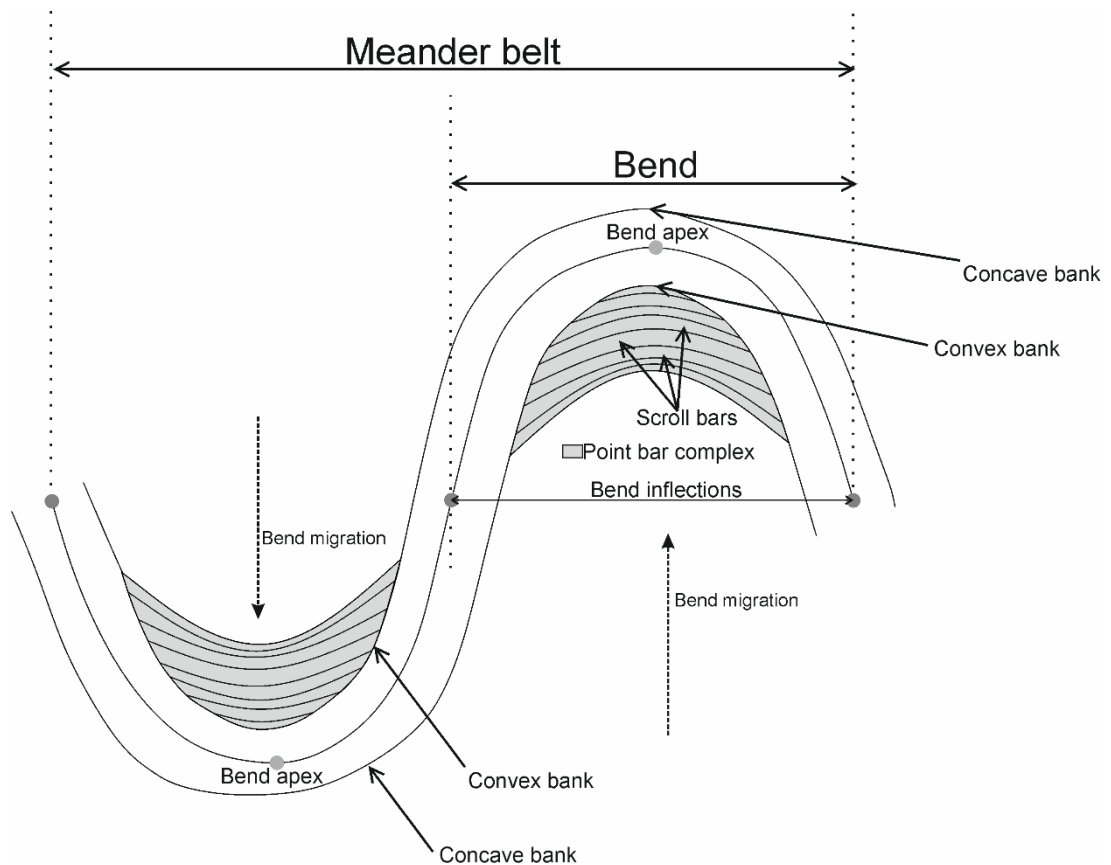


**Figure 2.6** Classification of a meander and a bend. A meander is considered as a trough and a peak loop, whereas a bend is considered from inflection point to inflection point with an apex point in between. Modified from Leopold and Wolman (1960).

### *Environmental settings of submarine channels*

Submarine channels occur in a range of environmental settings from the continental shelf (Kostaschuk *et al.*, 1992; Conway *et al.*, 2012; Dowdeswell and Vásquez, 2013; Gales *et al.*, 2018) and beyond the shelf break all the way down to the abyssal plains (Menard, 1955; Lewis, 1994; Wynn *et al.*, 2007; Pickering and Hiscott, 2015). Wynn *et al.* (2007) made a division for deep-water channels, which occur on the continental slope and rise beyond the shelf edge (frequently between 1 and 4 km, Wynn *et al.*, 2007).

Channels on the continental shelf, such as fjords (Conway *et al.*, 2012; Dowdeswell and Vásquez, 2013; Gales *et al.*, 2018) or delta fronts (Kostaschuk *et al.*, 1992), occur at a maximum water depth of 1000 m and

commonly have a small channel size with a maximum channel depth of 50 m with the majority having a channel depth of 20 m or less (Conway *et al.*, 2012; Gales *et al.*, 2018; Pope *et al.*, 2019). Similar features, such as erosional and depositional characteristics around channel bends and channels banks are observed (Conway *et al.*, 2012; Gales *et al.*, 2018) to submarine channels in deeper settings. Hence submarine channels in shallow water settings are a useful laboratory to study flows and sedimentary processes of turbidity currents, but it is not known how similar these processes are for submarine channels beyond the shelf break, as only a few flow measurements exist from submarine channels beyond the shelf break (e.g., Vangriesheim *et al.*, 2009).

Submarine channels beyond the shelf break can be distinctively divided into six geomorphological types (Figure 2.7; Peakall and Sumner, 2015): “arteries and veins” of submarine fans, here called a) submarine fan channels, b) slope channels c) isolated-deep ocean channels, d) non-margin ocean channels, e) axial channels and f) confined slope channels.

- a) Submarine fan channels build a complex network of channels on a submarine fan, are situated between the continental rise and the abyssal plains, and represent the largest sediment accumulations on earth (Curry *et al.*, 2003). Submarine fans can be classified based on their feeder systems into point source or multiple sources and their sediment characteristics, into mud, sand or gravel-dominated fans (Reading and Richards, 1994; Richards *et al.*, 1998). The developed channel pattern of straight, sinuous, and braided will change depending on the fan system. Sinuous channels are especially observed for mud to mud/sand fans and braided channels are identified for sand to gravel fans (Reading and Richards, 1994). Submarine-fan channels are commonly linked to large rivers. Examples of submarine-fan channels are the Amazon Channel (Damuth and Flood, 1984); Bengal Channel (Curry *et al.*, 2003), Indus Channel (Kenyon *et al.*, 1995), Congo Channel (Picot *et al.*, 2016) and Navy Channel (Piper and Normark, 1983).

- b) Isolated deep-ocean channels are basement controlled and develop in the early stage of ocean basin formation and act as a sediment pathway between submarine fans/canyons and abyssal plains with a single sediment system (Carter, 1988). These channels remain active for as long as subsidence at the terminus exceeds sediment deposition (Carter, 1988), hence they are commonly amongst the longest and the longest-lived channel systems on Earth. For example, the Bounty Channel is over 800 km long and over 50 million years old (Carter and Carter, 1996).
- c) Slope channels occur along the slope and include examples such as the Fuji and Einstein Channel (Sylvester *et al.*, 2012); the Brunei Channel (Straub *et al.*, 2012), and the Lucia Chica Channel (Maier *et al.*, 2013).
- d) Non-margin submarine channels occur in settings far from any terrestrial sediment source, such as volcanic arc-ridges or seamounts (Gardner, 2010).
- e) Axial channels occur along axial trenches between two convergent plates (Schweller and Kulm, 1977; Thornburg and Kulm, 1987; Pickering *et al.*, 2013).
- f) Confined slope channels are confined within canyons and valleys. These channels fill up over time after the initial formation of a master erosional surface, and build a complex network of channels within a confined setting (Deptuck *et al.*, 2003; Mayall *et al.*, 2006). The master erosional surface is typically much larger than the scale of the infilling channels, in contrast to the other submarine channel types, hence the processes controlling the confined slope channels may be different compared to the other submarine channel types.

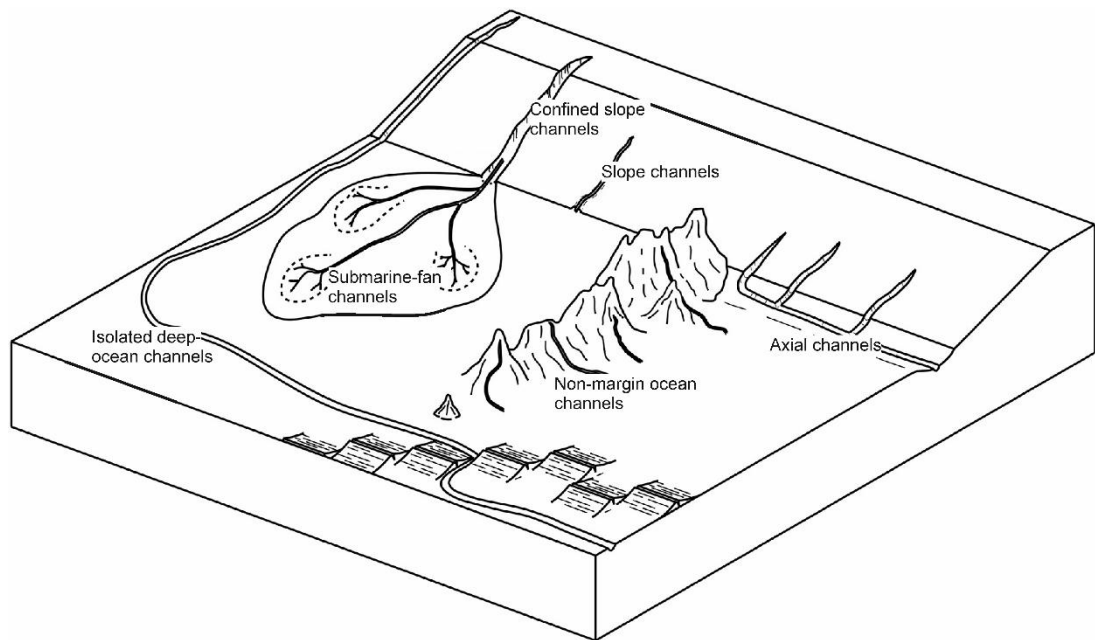


**Figure 2.7** Classification of submarine channels. Modified from Peakall and Sumner (2015).

### *Effect of Coriolis*

Sinuuous pathways are a common feature observed for submarine channels (e.g., Damuth *et al.*, 1988; Lewis and Pantin, 2002; Babonneau *et al.*, 2010). The degree of sinuosity varies on scales from a few bends, to the whole channel length pathway. Clark *et al.* (1992) demonstrated from a dataset of 16 different channel systems that sinuosity correlates with slope, similar to rivers. The relationship is that as channel slope (or fan gradient) decreases, sinuosity increases to a peak sinuosity value before decreasing. The peak sinuosity value was unique and different for each channel system with high sinuous system reaching peak sinuosity on a lower slope than low sinuous system reaching peak sinuosity on a steeper slope. Hence, from this slope-sinuosity relationship, two end members were identified: low-gradient high-sinuosity channels and high-gradient low-sinuosity channels. For an individual system, sinuosity increases with decreasing slope to a maximum sinuosity at approximately the mid-fan position and decreases afterwards again with further decreasing slope (Clark *et al.*, 1992). Even though sinuosity is influenced by the slope, a relationship between sinuosity and latitude was also



found, which has not been identified for rivers (Peakall *et al.*, 2012, 2013). In general, high-sinuosity channels are associated with low latitudes and low-sinuosity channels are associated with high latitudes. Such a sinuosity-latitude relationship has in part, for large channels, been associated with the Coriolis force (Peakall *et al.*, 2012; Cossu and Wells, 2013; Cossu *et al.*, 2015).

The effect of Coriolis on sedimentation around bends has been tested experimentally (Figure 2.8; Cossu and Wells, 2013; Wells and Cossu, 2013; Cossu *et al.*, 2015). For traction-dominated flows, Coriolis forces are reduced at low latitudes, and centrifugal forces dominate and give rise to inner-bank deposition, which lead to sinuous channel pathways at low latitudes near the equator. By contrast, at high latitudes, Coriolis forces shift the downstream velocity core to the right-hand side in the Northern Hemisphere and left-hand side in the Southern Hemisphere, hence deposition of traction dominated sediment occurs on the other side of the channel, on the left hand side in the Northern Hemisphere and right hand side in the Southern Hemisphere. In consequence, the sinuosity of channels in high latitudes reduces.

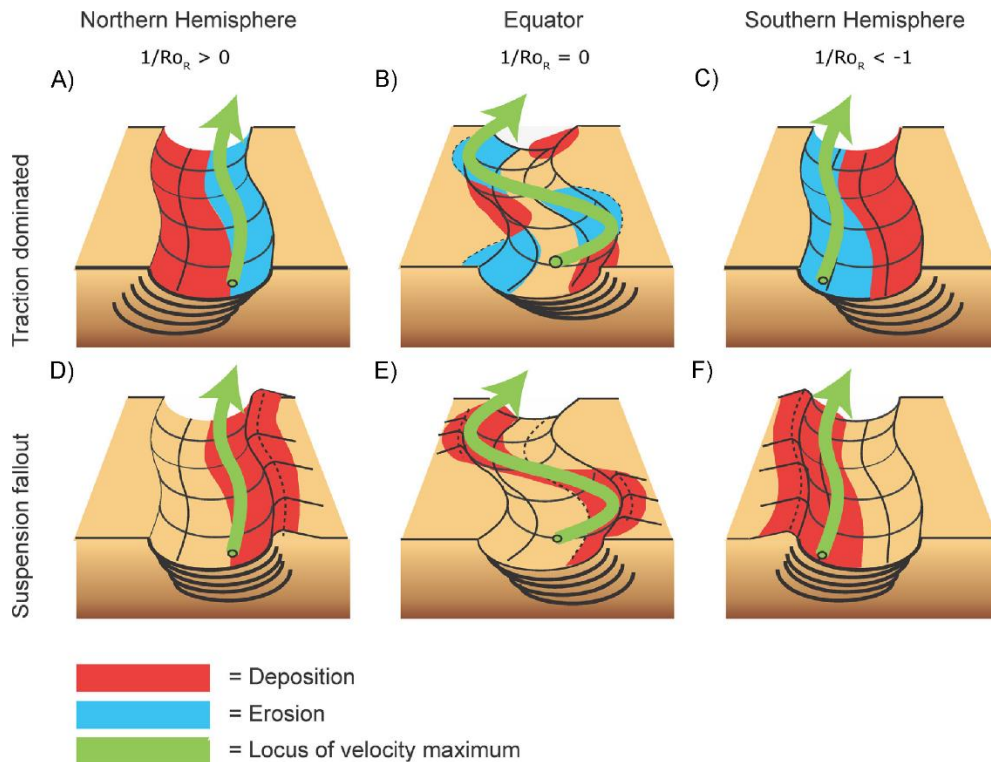


**Figure 2.8** Schematic diagram of deposition and erosion, as a function of Coriolis forces, within a submarine channel architecture at three latitudes for traction dominated (A-C) and suspension fallout dominated (D-F) flows. From: Cossu *et al.* (2015).

## 2.2 Channel evolution in submarine channels

Channel evolution is controlled by the combination of lateral or horizontal bend expansion, and translation or downstream bend migration (Allen, 1982). Additionally, in aggradational and erosional submarine channels, the process of vertical aggradation or incision at the channel bed becomes important. Alluvial rivers are typically dominated by lateral expansion and downstream bend migration with limited vertical aggradation (Figure 2.9; Peakall *et al.*, 2000a, b; Hooke, 2004; Ghazi and Mountney, 2009). By contrast, observations of submarine channels (Figure 2.10; Einstein Channel on the Mississippi Fan and the Amazon Channel) suggest that many submarine channels on passive margins are dominated by initial bend expansion (swing) and then exhibit little to no downstream bend migration (sweep) as the

channel position remains relatively fixed over time and is dominated by vertical aggradation (Figure 2.9; Peakall *et al.*, 2000a, b; Deptuck *et al.*, 2007; Wynn *et al.*, 2007; Sylvester *et al.*, 2011; Jobe *et al.*, 2016).

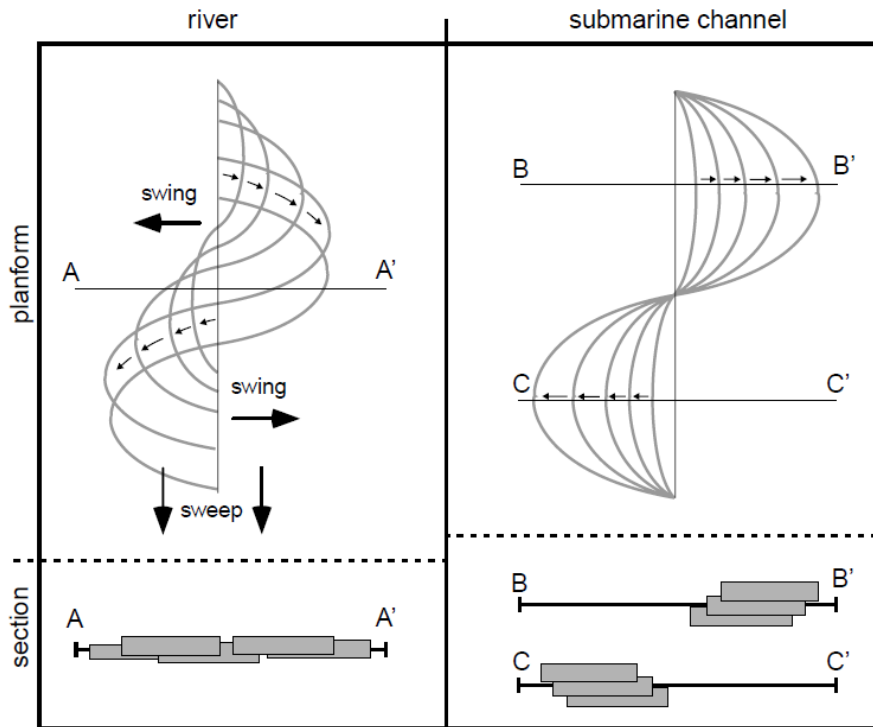


**Figure 2.9** Schematic model showing the contrasting evolution between rivers and aggradational submarine channels. Bend growth from an initially straight channel (central black line) is shown in both cases. Rivers undergo regular lateral (swing) and downstream (sweep) bend migration forming tabular, sheetlike bodies referred to as channel belts. In contrast, aggradational submarine channels undergo bend increase with no significant downstream bend migration, forming a ribbon geometry (Peakall *et al.*, 2000b).

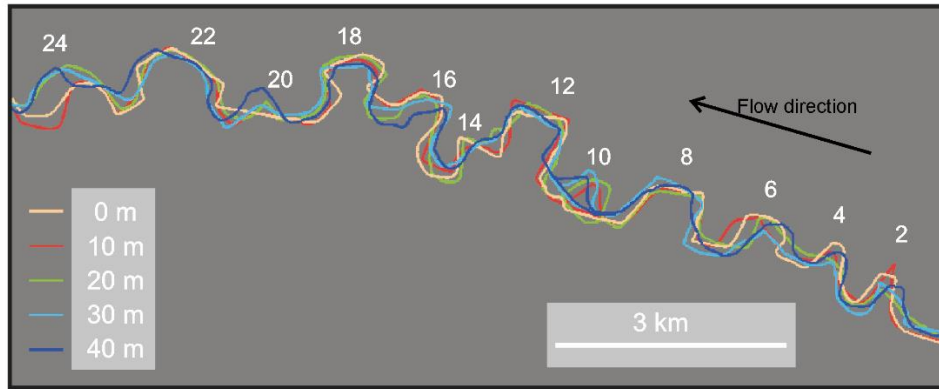


**Figure 2.10** Bend development in a subsurface example from the uppermost (~40 m) of a 120 m ( $\pm 20$  m) aggradational submarine channel stack that infills the upper fan valley on the west African margin. Successive position of the channel thalweg is shown; thalweg width is ~60 m, channel width is ~400 m. *Note:* Poor seismic resolution at bend 10. From Peakall *et al.* (2000a).

A 3-stage evolutionary (Figure 2.11) or “hockey-stick shape” model (Jobe *et al.*, 2016) for aggradational, moderate to high-sinuuous channels, based on observations, suggests that submarine channels are dominantly controlled by vertical aggradation rather than downstream migration (Peakall *et al.*, 2000a, b; Jobe *et al.*, 2016). Stage 1 exhibits lateral bend expansion, swing, and no to little downstream bend translation, sweep. Stage 2 is an equilibrium phase dominated by sediment bypass and vertical aggradation, followed by stage 3, where the channel gets abandoned and undergoes channel filling. These stages are idealised.

The model suggests that downstream migration occurs less for aggradational submarine channels on passive margins as has been recognised by the low number of bend cut-offs in such systems (Peakall *et al.*, 2000a, b). If downstream migration is observed for aggradational submarine channels (Posamentier, 2003; Posamentier and Kolla, 2003) it is typically on the order of 2-3 times channel widths (Wynn *et al.*, 2007). Exceptions from the rule with a greater downstream bend migration have been observed for non-aggradational controlled submarine channels (Abreu *et al.*, 2003), during the initially development stage (Kolla *et al.*, 2012), for confined-slope channels. (Deptuck *et al.*, 2003, 2007; Posamentier, 2003; Kolla *et al.*, 2012), in salt-

tectonic controlled settings (Covault *et al.*, 2020) and for the Bengal Channel (Schwenk *et al.*, 2003, 2005).

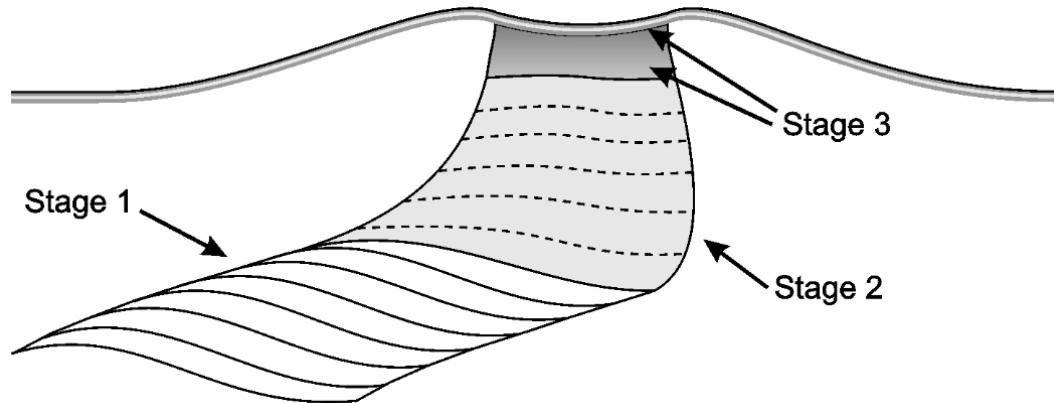


**Figure 2.11** Submarine channel evolution is controlled by a lateral bend expansion (Stage 1), followed by a zone of bypass and vertical aggradation (Stage 2) and ends with sediment filling of the channels, where the channel gets abandoned (Stage 3). From Peakall *et al.* (2000b).

Downstream bend migration increases for confined canyon-slope channels (Abreu *et al.*, 2003; Deptuck *et al.*, 2003, 2007). For example, the erosional Green Channel complex, the upper portion of a confined channel system offshore Angola, had 20% more bend cut-offs compared to the Einstein Channel, an aggradational slope channel. One suggestion is that lateral migration is initiated to fill up the accommodation space within the erosional master channel as the width of the channel complex increases over time (Abreu *et al.*, 2003; Deptuck *et al.*, 2007).

Lateral migration and hence cut-offs may increase during the early evolutionary stage (Sylvester *et al.*, 2011; Sylvester and Covault, 2016). When cut-offs occur, knickpoints increase followed by channel incision and hence terrace formation increases, similar to bedrock rivers (Finnegan and Dietrich, 2011). Overall, cut-offs create a broader and flat base (Sylvester and Covault, 2016). Once the deepest point is reached the erosional master surface (Sylvester *et al.*, 2011) is filled up by vertical aggradation. However, the causes of cut-off may be different for the other types of submarine channels.

Downstream-migration also increases in structurally controlled settings, such as environments which are salt-tectonically controlled (Covault *et al.*, 2020) due to a disequilibrium of channel sinuosity caused by the underlying structure. However, Jobe *et al.* (2016) showed that aggradational channels in tectonic settings can also be dominantly controlled by vertical aggradation. Hence, a tectonic control does not always explain observations of downstream bend migration greater than 2-3 times channel widths in aggradational channels, such as the Bengal Channel (Schwenk *et al.*, 2003, 2005).

The active Bengal Channel on the mid-fan at a water depth between 2480 m and 2680 m, an aggradational submarine fan channel, identified more cut-offs than the ancient aggradational Bengal Channel with a similar width-depth and slope (Schwenk *et al.*, 2005). Downstream translation in rivers acts to reduce channel sinuosity (Hooke, 2007; Zinger *et al.*, 2011), but channel sinuosity stayed the same over time for the Bengal Channel where regular cut-offs occurred (Schwenk *et al.*, 2003) and sinuosity for the Amazon and Indus is similar compared to the Bengal Channel although they exhibit less cut-offs. Hence a highly sinuous bend does not automatically cause cut-off in submarine channels. The upper Bengal Fan has been described as a fan valley complex with a network of narrower channels filling the confined valley (Kolla *et al.*, 2012), which is the same principle for confined slope channels and hence explains an increase of downstream bend migration in the upper Bengal Fan. The Bengal Channel in the mid-fan also has much narrower channels within a much larger leveed master channel (Schwenk *et al.*, 2005).

Although there are a few exceptions for aggradational channels, such as where the channels are smaller than the erosional master surface (confined slope channels, or submarine-fan valleys) or tectonic settings, the “hockey-stick shape” (Jobe *et al.*, 2016) model works most of the time which reinforces existing models that suggest that aggradational channels have a reduced downstream bend migration after their initial development. However, a key problem is that the majority of laboratory experiments and numerical models had sediment depositions at the inner bend and erosion just downstream of

the bend apex at the outer bend, which would suggest that channels should be dominated by strong downstream translation. The predict downstream translation would not lead to the “hockey-stick shape” model as has been observed in submarine channels (Keevil *et al.*, 2007; Peakall *et al.*, 2007; Straub *et al.*, 2008, 2012; Amos *et al.*, 2010; Darby and Peakall, 2012; Cossu *et al.*, 2015). Furthermore, the experiments and numerical models with sediment produced a point bar that was formed at the inner bend just downstream of bend apex, suggesting that if these channels had erodible banks rather than fixed geometries then erosion would occur at the outer bend (Keevil *et al.*, 2006; Straub *et al.*, 2008; Darby and Peakall, 2012; Cossu *et al.*, 2015). These results suggest that a key component required to understand channel evolution is missing in laboratory experiments and numerical models, such as Darby and Peakall (2012), which would reduce downstream migration, and which would act to restrict downstream migration as observed in the “hockey stick” model.

### **2.3 Evolution of river bends**

Theories for the initiation and evolution of a river bend can be divided broadly into bend theory and bar theory (Ikeda *et al.*, 1981). Bend theory argues that a meandering planform occurs in response to natural variation within the flow through turbulence. By contrast, bar theory argues that a variation of altering deposition along the banks causes a flow variation which initiates a meandering planform. In summary, bend theory argues that the flow controls bend evolution and bar theory argues that sedimentation controls bend evolution. However, neither theory can explain a meandering planform. For example, a meandering planform can be created in an environment without sediment, for example on a glacier or in bedrock (Leopold and Wolman, 1960), which suggests that bend theory may be favoured in these environments as a meandering planform can be formed without external influence. By contrast, laboratory experiments with sediment with variable flows run over a long time

period show that a meandering planform is transformed into a braided pattern (Murray and Paola, 1994; Frederici and Seminara, 2003). Hence, rather than considering flow variations and bank development separately, bend evolution in rivers is considered as a dynamic system with an interaction of flow perturbation, sedimentation, and bank processes, which lead to the concept of bend instability (Ikeda *et al.*, 1981). Lateral bend migration of rivers is driven by an excess flow at the outer bank (concave bank) of the bend causing erosion and a deflect flow at the inner bank (convex bank of the bend causing deposition). The variation of flow velocity between the outer and inner banks is influenced by factors, such as the secondary flow circulation due to the curvature, bed topography and channel width. Here, the role of channel width on bend evolution in rivers is discussed.

#### *Methodology for width measurements around river bends*

Channel width is defined as the reference line of bankfull discharge in rivers. Bankfull discharge is defined as the measurement at the reference of maximum channel capacity of the channel prior to overbank flooding. Three reference levels exist in rivers which can be used to define the bankfull discharge (Williams, 1978; Johnson and Heil, 1996; Navratil *et al.*, 2006) with three main sections: in-channel bar, the active channel, and main channel width (Wahl, 1984). Most studies have used the active channel width and have measured this bankfull channel width perpendicular to the flow discharge from vegetation break to vegetation break for vegetated banks and for unvegetated banks from top bank to top bank (Lagasse *et al.*, 2004; Luchi *et al.*, 2010, 2011, 2012; Eke *et al.*, 2014a). A consistent methodology is needed to compare the width around bends for a large dataset of rivers. Width is measured at the bankline perpendicular to the flow at inflection points and at apex points (Lagasse *et al.*, 2004). Additionally, width can also be measured through an automatic approach, where more measurements can be taken between inflection points and bend apex (Luchi *et al.*, 2010; Eke *et al.*, 2014a).



*Observations of the width around bends in rivers*

An analysis of 1,495 bends from 137 alluvial reaches in the USA suggests that the majority of river bends (~60%, Classes B2, C, D, G2 of Brice, 1975 – see Figure 2.12) are wider at the bend apex, followed by a constant channel width between inflection points and the apex point (~30%, Classes A, B<sub>1</sub>, G<sub>1</sub>, F of Brice, 1975), and an irregular channel width (~10%, Class E of Brice, 1975) around bends with no clear maximum width at the bend apex Figure 2.12 (Brice, 1975, 1982, 1984; Lagasse *et al.*, 2004). Along an individual reach, the majority of bends reveal a maximum channel width between two inflection points, and a minimum channel width at the inflection points, suggesting a general tendency of two points of maximum width over one meander wavelength (Figure 2.13; Luchi *et al.*, 2011).

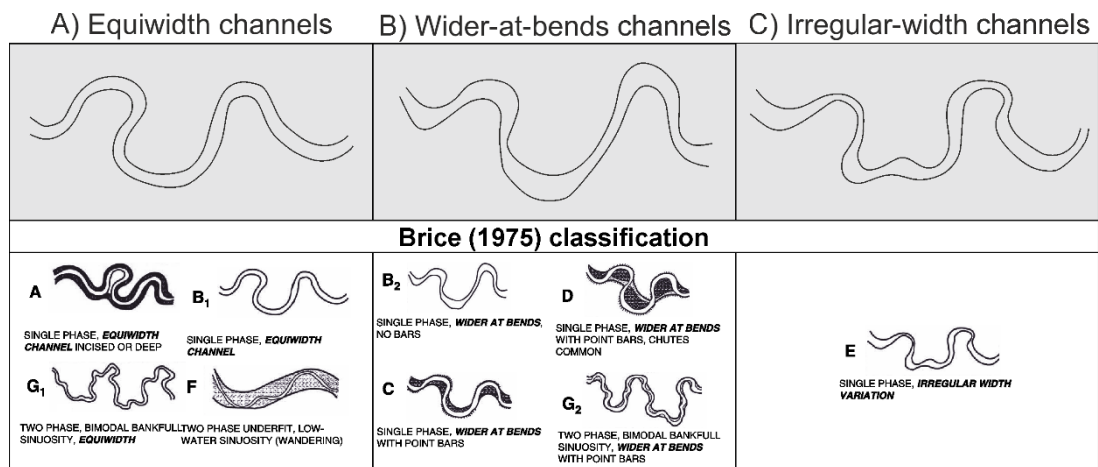


**Figure 2.12** Three types of channel width are identified from the Brice (1975) classification of single-thread alluvial rivers: A) Equiwidth channels with a constant width between inflections and apexes, B) Wider-at-bends channels are wider at bend apexes than at bend inflections and C) Irregular-width channels are wider at bend inflections and bend apexes. Classification is also divided on the dominant sedimentation style (modified from Zolezzi *et al.*, 2012).

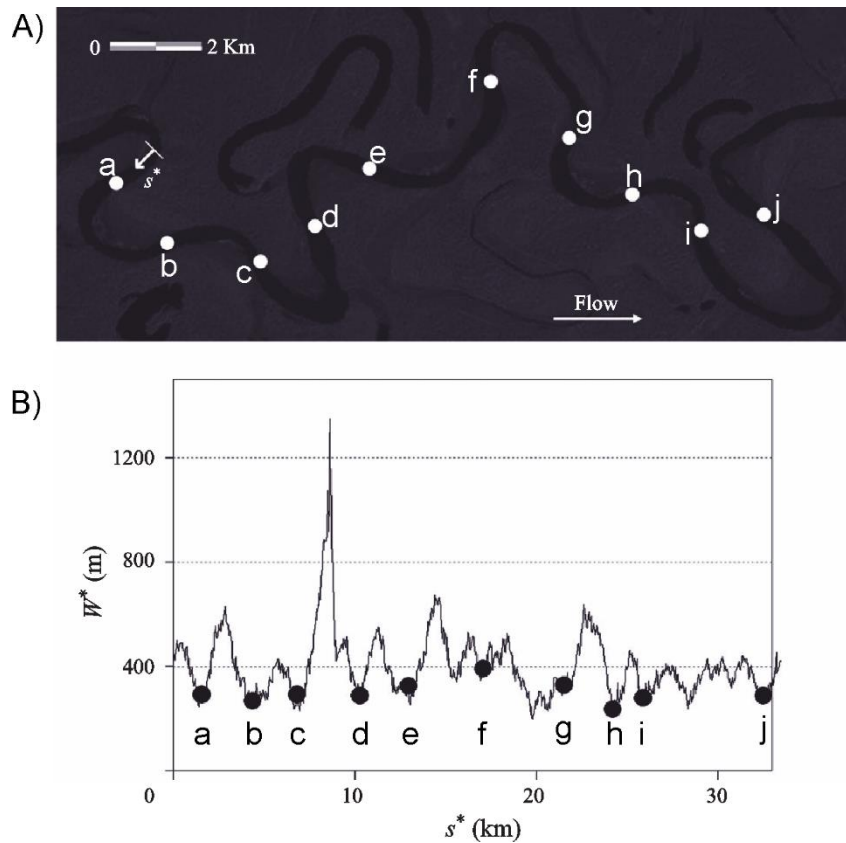


**Figure 2.13** A) Satellite images of a river reach with variable width of the Rio Beni (Bolivien Amazon). B) Variation of channel width along the reach. Small letters (a, b, c...) refer to inflection points,  $W^*$  to longitudinal channel width variation and  $s^*$  refer to a curvilinear arclength, channel centreline (modified Luchi *et al.*, 2011).

A riffle-pool sequence is composed of an alternating thalweg with riffle areas having a shallow water depth and pool areas having a deeper water depth. Average pool-to-pool spacing is between 5 to 7 times the average channel width and such sequences have been recognised for gravel-bed rivers (Leopold and Wolman, 1960; Keller and Melhorn, 1978; Hey and Thorne, 1986) and sand-bed rivers (Richards, 1976; Carling, 1991; Hudson, 2002; Gibson *et al.*, 2019). Riffle areas have been assigned to occur in areas with a wider width and pool areas have been assigned to occur in areas with a narrower width for straight gravel-bed rivers (Richards, 1976; Carling, 1991; Hudson, 2002; Nelson *et al.*, 2015). Observations suggest that riffle-pool-sequences occur in a pattern in terms of the bend planform, with riffle areas occurring at inflection regions, and pool areas occurring at apex regions (Keller and Melhorn, 1978). However, such rhythmic pool spacing, assigning

pools to apices and riffles to inflections is inconsistent (Carling, 1991; Gibson *et al.*, 2019) as pool-to-pool spacing is controlled by various factors. Autogenic controls, such as flow processes or morphological processes support a “rhythmic pool hypothesis” (Keller and Melhorn, 1978) and allogenic controls, such as obstacles, and geological controls support a “forced pool hypothesis”, whereby both pool mechanisms coincide (Montgomery, 1995; Gibson *et al.*, 2019). Hence a riffle-pool-sequence is not always coincident with bend morphology and therefore channel width.

A variable/irregular width or a wider-at-inflection width around bends often occurs in the presence of alternate bars (free bar; Zolezzi *et al.*, 2012; Duró *et al.*, 2016). Alternate bars, or free bars, are bars which develop spontaneously as a result of instability processes and may occur on either side of the bank or as mid-channel bars (Seminara and Tubino, 1989), which causes an increase of channel width at the position of the free bars (Zolezzi *et al.*, 2012; Duró *et al.*, 2016). Free bars have not been generated in laboratory experiments for submarine channels which may be due to a small aspect ratio in laboratory experiments as suggested by Peakall *et al.* (2007), as it is known from physical modelling of rivers that free bars start to form with aspect ratios  $>10$  and curvatures  $<10$  degrees (Whiting and Dietrich, 1993). However, alternate (free) bars may not be common in submarine channels as they are related to the formation of braided patterns in rivers (Richards, 1982). A braided river pattern is much less common in submarine channels (Wynn *et al.*, 2007; Foreman *et al.*, 2015) as a generally greater flow depth in submarine channels compared to rivers (Konsoer *et al.*, 2013; Shumaker *et al.*, 2018) prevents the formation of a braided pattern (Foreman *et al.*, 2015) and hence the formation of free bars. Although, free bar formation can lead to the development of a variable channel width, channel width is ultimately controlled by the relative rates of erosion at the outer bank (bank pull) and deposition at the inner bank (bar push; Nanson and Hickin, 1983; Braudrick *et al.*, 2009; Parker *et al.*, 2011; Eke *et al.*, 2014a, b; Matsubara and Howard, 2014; Van de Lageweg *et al.*, 2014; Wu *et al.*, 2016).

Bank pull is related to an initial channel widening, and bar push is related to initial channel narrowing (Eke *et al.*, 2014b). Independent results from laboratory experiments and models suggest that bend migration of rivers is dominantly controlled by bank pull, outer bank erosion, rather than bar push as deposition at the inner bend, point bar development occurred after the initial channel widening through outer bend erosion (Matsubara and Howard, 2014; Van de Lageweg *et al.*, 2014). However, evidence for bar push is that in some cases outer bank erosion requires excessive bed shear stress even during high flow stages, whereas inner bend deposition occurs during low flow stages (Matsubara and Howard, 2014; Wu *et al.*, 2016). Bends that are wider at bend-apexes experience the highest migration rates and have the most developed point bars and scroll bars (Figure 2.12; Brice, 1975, 1982, 1984; Lagasse *et al.*, 2004). Bends with a point bar (Class C) have on average a 14% wider width at the bend apex compared to the mean inflection width (Eke *et al.*, 2014a).

Bends with a constant width (equiwidth channels), which have been referred to as canaliform channels are related to restricted channel banks either through vegetation or silt/clay (Lagasse *et al.*, 2004; Luchi *et al.*, 2012; Matsubara and Howard, 2014); this acts to restrict the bank erosion rate (Luchi *et al.*, 2012), in turn limiting width variation. Luchi *et al.* (2010, 2012) argue that canaliform channels and wider-at-bend apex river bends are strongly related, but vary in terms of their “hydrodynamic” width, and their “morphologically active” width. The “hydrodynamic” width coincides with the free surface width, whereas the “morphologically active” width is the part of the cross-section where transport occurs during formative flow conditions. In wider-at-bend apex channels, the hydrodynamic width is not equal to the morphologically active width, whereas in canaliform rivers the hydrodynamic and active widths are the same as high bank resistance prevents the development of a distinct active channel width at high flow stage (Luchi *et al.*, 2010, 2012).

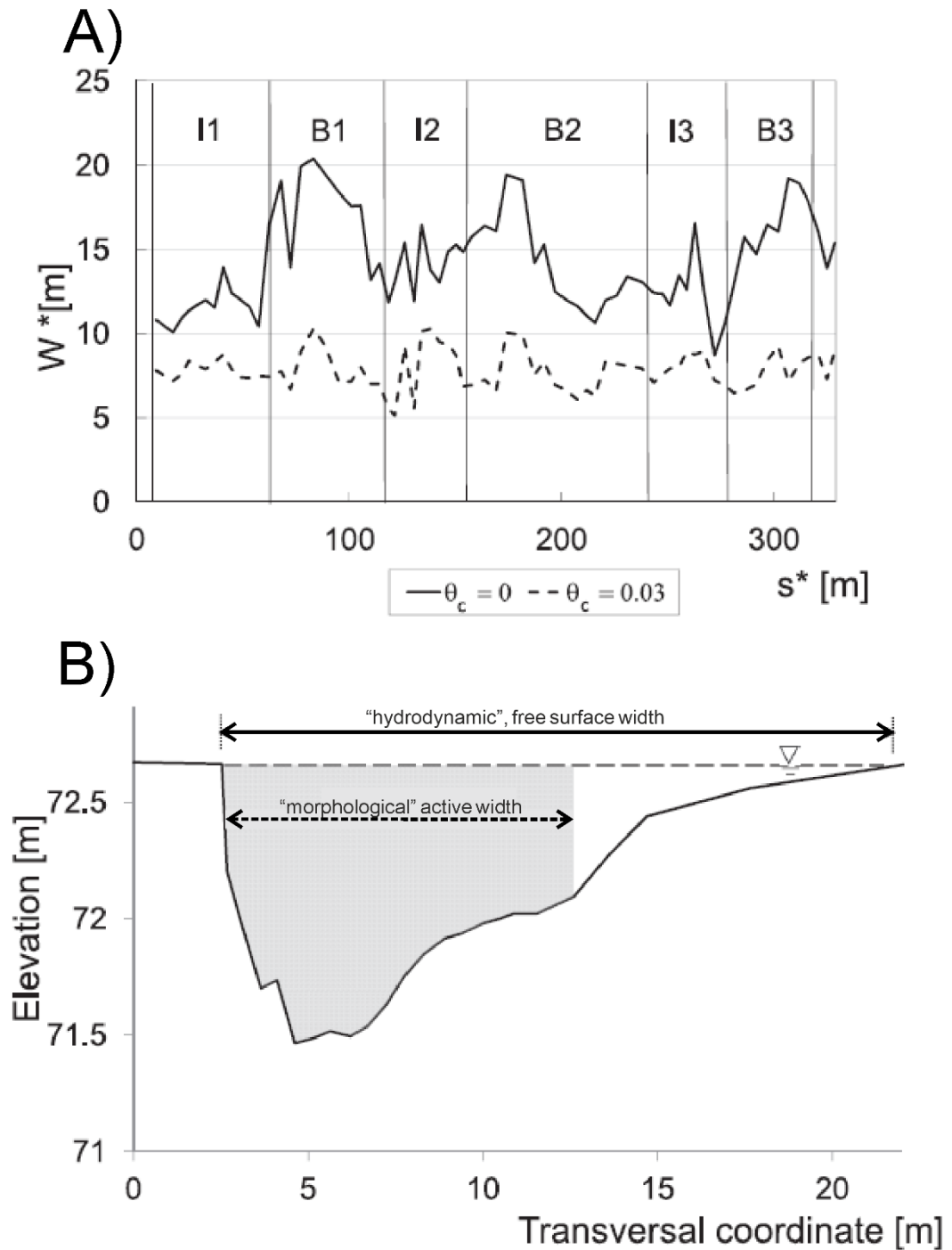


**Figure 2.14** A) Spatial distribution of the hydrodynamic (solid line) and morphologically active width (dashed line) along a meandering reach from the River Bollin. Letters I1, I2 and I3 refer to inflection regions and letters B1, B2, and B3 refer to apex region). B) Sketch of a cross-section at a point bar (Modified from Luchi *et al.*, 2012).

## 2.4 Morphometrics of submarine channels

### 2.4.1 Geometry of submarine channels

Cross-sectional dimensions (width-depth ratio) for submarine channels range over an order of magnitude between 10:1 and 100:1 (Figure 2.15). Channel depth ranges between 1 m and 1000 m and channel width ranges between 30 m and 10,000 m (Figure 2.15). For example, the Brunei channel has cross-sectional dimensions of a few hundred metres (width <600 m, depth <70 m; Straub *et al.*, 2011), whereas the North Atlantic Mid Ocean Channel (NAMOC; width <15 km, depth <200 m; Klaucke *et al.*, 1998a) has cross-sectional dimensions an order of magnitude greater than the Brunei channels.

The variety of submarine channels is reflected in the range of results obtained from different studies. The study from Konsoer *et al.* (2013) compiled a dataset from the modern seafloor, which included 177 cross-sections from 23 submarine channels, and identified a mean channel depth of 136 m and a mean width of 7820 m, which suggests that submarine channels exceed the largest rivers on Earth by an order of magnitude. In contrast, Jobe *et al.* (2016), compiled a dataset from seismic reflection and outcrop exposure for both rivers and submarine channels, and identified a mean channel depth of 40 m and a mean width of 600 m for submarine channels, compared to a mean depth of 10 m and a mean width of 300 m for rivers, suggesting that submarine channels have cross-sectional dimensions 2-4 times those of rivers. The Jobe *et al.* (2016) dataset has channel depths that are half that of Konsoer *et al.* (2013), and widths an order of magnitude narrower, which may reflect the choice of dataset as outcrops and subsurface examples are affected by compaction during burial and diagenesis (Wynn *et al.*, 2007). For example the Cullis *et al.* (2019) study that has a smaller channel width-to-depth ratio includes a wide range of systems from modern and outcrop studies and includes channels from a range of environmental setting, including canyons, and confined settings (Figure 2.15). However, even width-depth ratio from modern submarine channels show a wide variety: Clark and Pickering (1996a)

observed width-depth (aspect) ratio of 10:1, Konsoer *et al.* (2013) identified an aspect ratio of 50:1. The dataset used by Konsoer *et al.* (2013) as noted previously is composed of 177 cross-sections from 23 modern submarine channels. This includes 35 cross-sections from NAMOC, 23 cross-sections from Cascadia Channel, 11 cross-sections from Surveyor Channel, which suggests that at least 40% are from isolated deep-ocean channels, and only 24 cross-sections from submarine-fan channels (Amazon, Bengal and Magdalena Channel). By contrast, the Clark and Pickering (1996a) dataset consists of a wide of diversity of systems with 104 cross-sections from 14 modern systems including submarine-fan channels (Mississippi Channel, Indus Channel, Amazon Channel, Rhône Channel), and isolated deep-ocean channels (Cascadia Channel) with many channel from the East Coast USA (Monterey, Cascadia, Astoria, Arguello, Baltimore-Wilmington, Hudson, Atlantis). One suggestion may be that it depends on the regional setting with systems from the East Coast USA in general having a smaller width-depth ratio compared to other systems around the world and hence the differences between studies in terms of aspect ratio may relate to the chosen submarine channels. For example, the Congo Channel has a similar channel depth to the Tanzania Channel or NAMOC, whereas the Amazon Channel has a channel depth that is approximately half of the others (Figure 2.16). By contrast, channel width is on average twice as wide for the Tanzania Channel and NAMOC, isolated-deep ocean channels, compared to the Amazon Channel and Congo Channel, submarine-fan channels (Figure 2.16). Hence the difference may be related to the chosen submarine channels and the environmental setting of submarine channels, such as submarine-fan, isolated deep-ocean, slope, non-margin, and axial channels.

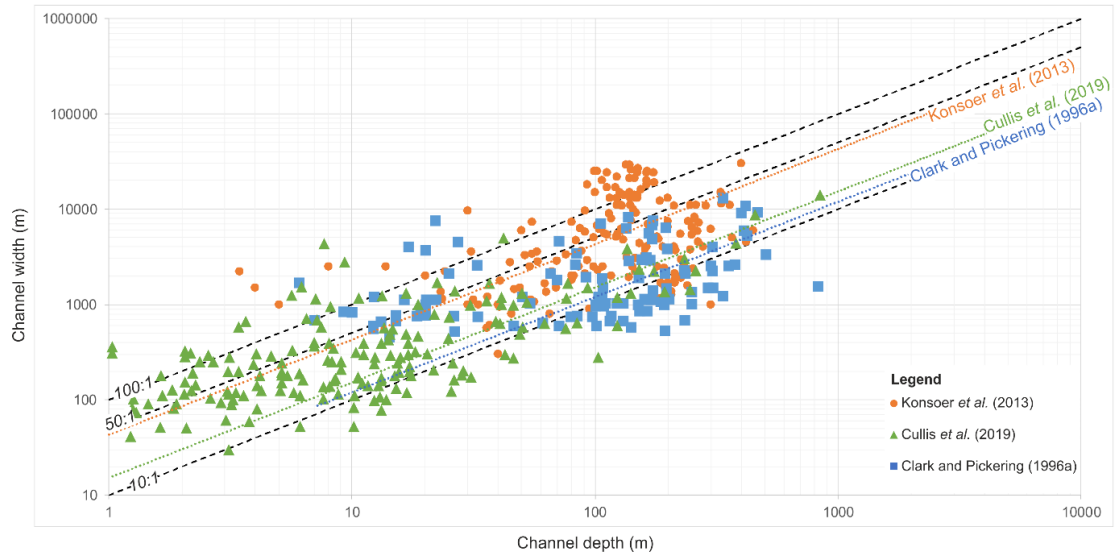


**Figure 2.15** Channel width vs. depth. Data from Clark and Pickering (1996a), Konsoer *et al.* (2013), and Cullis *et al.* (2019).

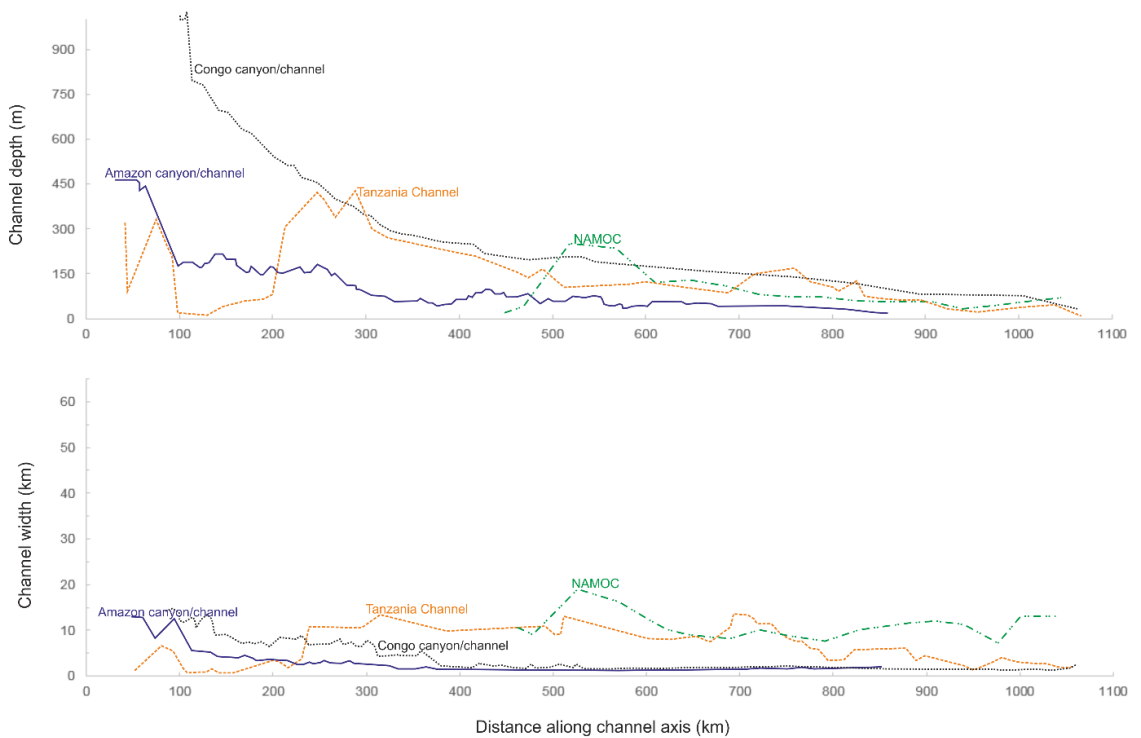


**Figure 2.16** Comparison of different submarine channels in the downstream direction. Curves are redrawn from Hesse *et al.* (1980), Babonneau *et al.* (2002), Pirmez and Imran (2003), Bourget *et al.* (2008) and Fournier (2016). A: Channel depth from channel bed to mean levee crest. B: Channel width between levee crest. Modified from Fierens *et al.* (2019).



## 2.4.2 Geometry around submarine channel bends

### *Terraces at inner bends*

A lower relief compared to the channel banks at the inner bend suggests width variation with height (Figure 2.17; Babonneau *et al.*, 2010). For example, at bend apexes, width is wider at channel banks and narrower near the channel bed (Figure 2.17).

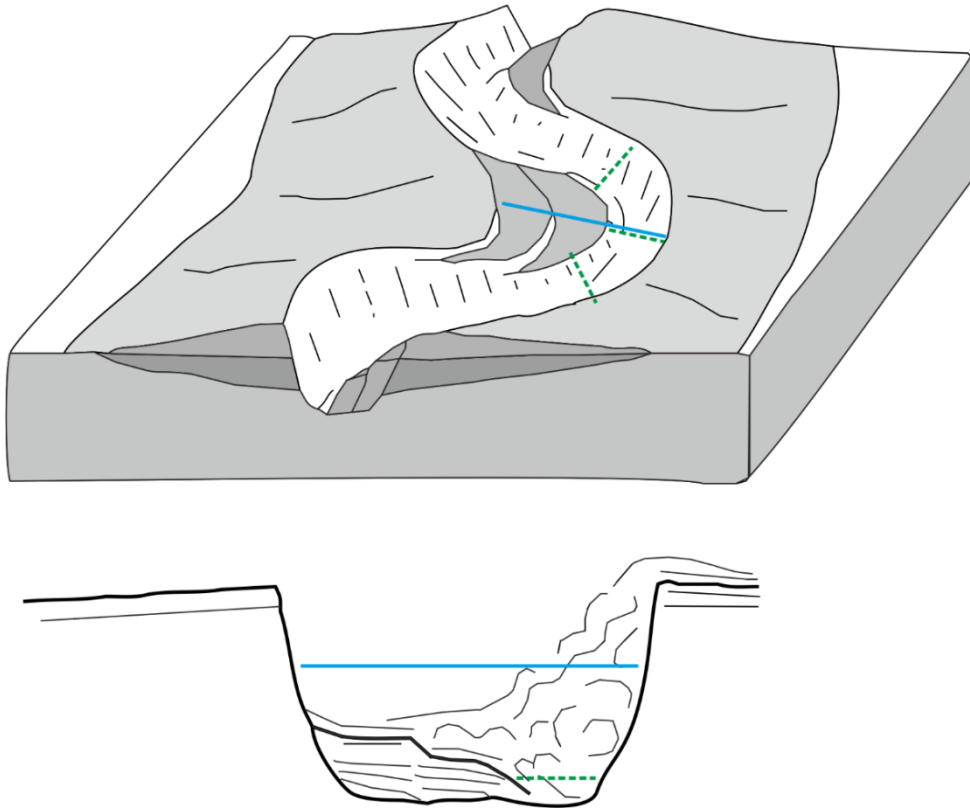


**Figure 2.17** A lower channel relief (green dashed line) compared to the channel banks (blue solid line) at the inner bend suggests width variation with height above the bend. Modified from Babonneau *et al.* (2010).

### *Erosion and deposition around bends*

Two surveys in 2008 and 2010 of the same channel in the Bute Inlet, a shallow marine channel, identified points of erosion and deposition around a bend

(Figure 2.18; Conway *et al.*, 2012). Erosion dominantly occurred at the outer bank and on the inner bend terraces and deposition dominantly occurred at the inner bank and at the channel bed, showing the interaction of erosion and deposition.

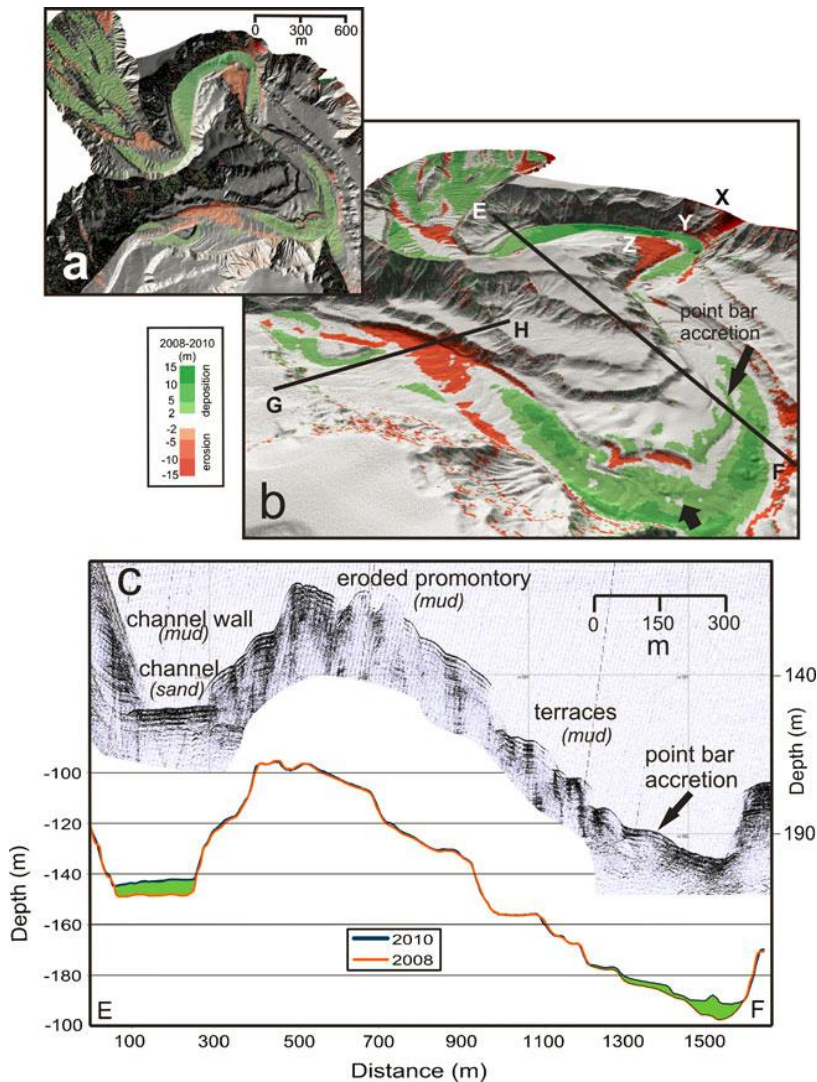


**Figure 2.18** Observations of a shallow marine channel showing the locations of erosion and deposition. From Conway *et al.* (2012).

### *Asymmetry varies with curvature*

Asymmetry is variable with curvature around bends in submarine channels (Reimchen *et al.*, 2016), similar to rivers (Knighton, 1982). Asymmetry refers

to the ratio between outer and inner bend cross-sectional shape. Cross-sections are more asymmetric with maximum curvature at bend apexes and in contrast cross-sections are more symmetrical with minimum curvature at bend inflections (Figure 2.19). A shift of asymmetry suggests that the position of the thalweg is near the centreline close to the inflection region and near the outer bank away from the centreline close to the bend apex region.

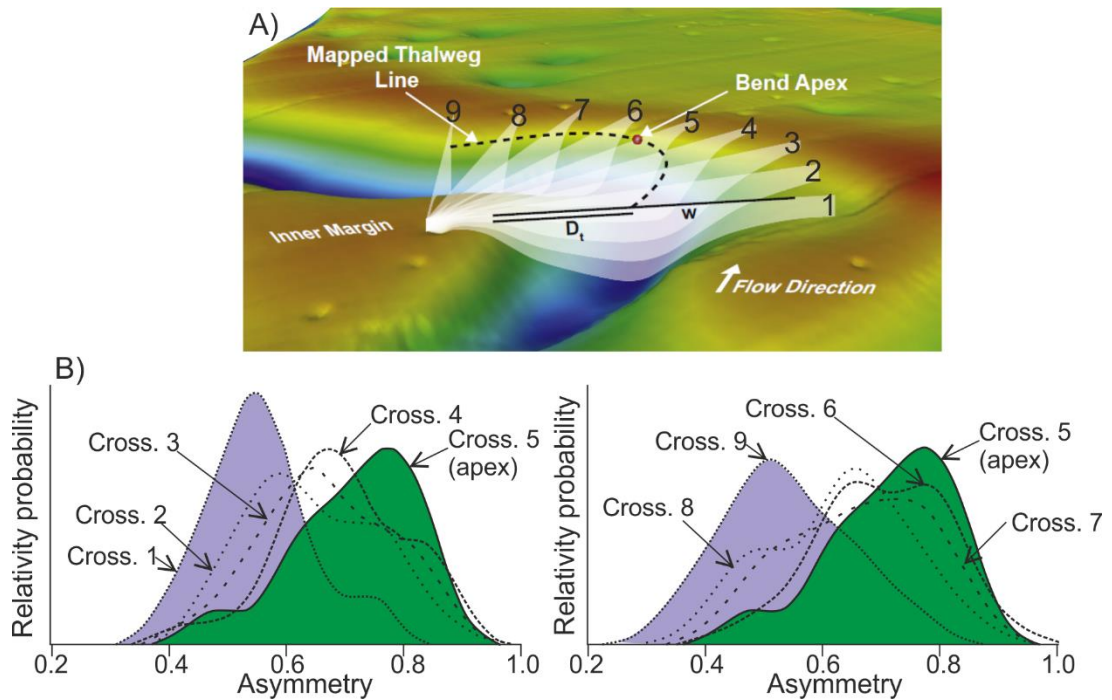


**Figure 2.19** A) Location of cross-sections. Cross-sections 1-4 are upstream of the bend apex and cross-sections 6-9 are downstream of the bend apex. Asymmetry is the ratio between the distance to the thalweg from the inner bend margin ( $D_i$ ) and the channel width ( $w$ ). B) Density probability plots of channel asymmetry upstream and downstream of the bend apex from the LUCIA Chica channel. Modified from Reimchen *et al.* (2016).

## 2.5 Flow processes from channel development to bend scale

### 2.5.1 Flows that generate a submarine channel

Submarine channels act as a conduit and transport pathway for submarine density flows. Hence, an understanding of the characteristics and dynamics of the flow is important for predicting bend evolution. A submarine density flow is a flow which is driven by a density difference caused by temperature, salt or sediment between the flow and the ambient sea water (Mulder and Alexander, 2001). Density flows driven by temperature and salinity help to understand flow characteristics around bends (Sumner *et al.*, 2014), but only density flows driven by sediment contribute to the formation of deposition around bends. Consequently, the interpretation of flows which form submarine channels are heavily based on studies of flow and deposition from laboratory experiments (Talling *et al.*, 2012; Peakall and Sumner, 2015). Submarine sediment density flows can be distinguished based on their mechanical behaviour (rheology), particle support mechanisms, concentration and the nature of flow deposition (Middleton and Hampton, 1973; Lowe, 1979; Mulder and Alexander, 2001). Broadly, flows can be distinguished based on the matrix strength support mechanism of the sediment within the flow into cohesive (viscous) and non-cohesive flows. Cohesive flows, such as debris flows are flows by which particles are supported by cohesion, and non-cohesive flows are characterised by low particle interaction and space between particles. Non-cohesive flows are composed of discrete particles with a high porosity between particles which is filled with seawater in the submarine environment or freshwater if formed from direct river input. Non-cohesive flows also include hyper-concentrated density flows, concentrated density flows, and, turbidity currents (Figure 2.20; Mulder and Alexander, 2001). Due to the continuous entrainment of water flows typically transform from hyper-concentrated density flows to turbidity currents (Figure 2.21; e.g. Felix and Peakall, 2006). Submarine channels are thought to be mainly formed by non-

cohesive flows that can be initiated by: hyperpycnal flows from rivers and glacier outwash, submarine landslides through flow transformation from a cohesive to non-cohesive flow, and suspended sediment from near the shelf edge through processes other than hyperpycnal flows (Piper and Normark, 2009).

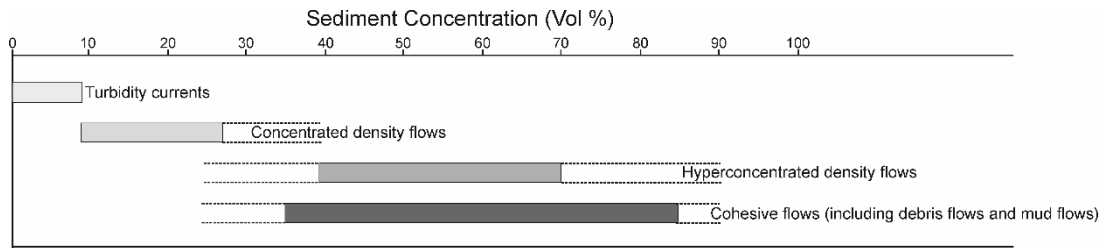


**Figure 2.20** Terminology of flow types for submarine sediment density flows as a function of sediment concentration based on percentage by volume (Modified from Mulder and Alexander, 2001).

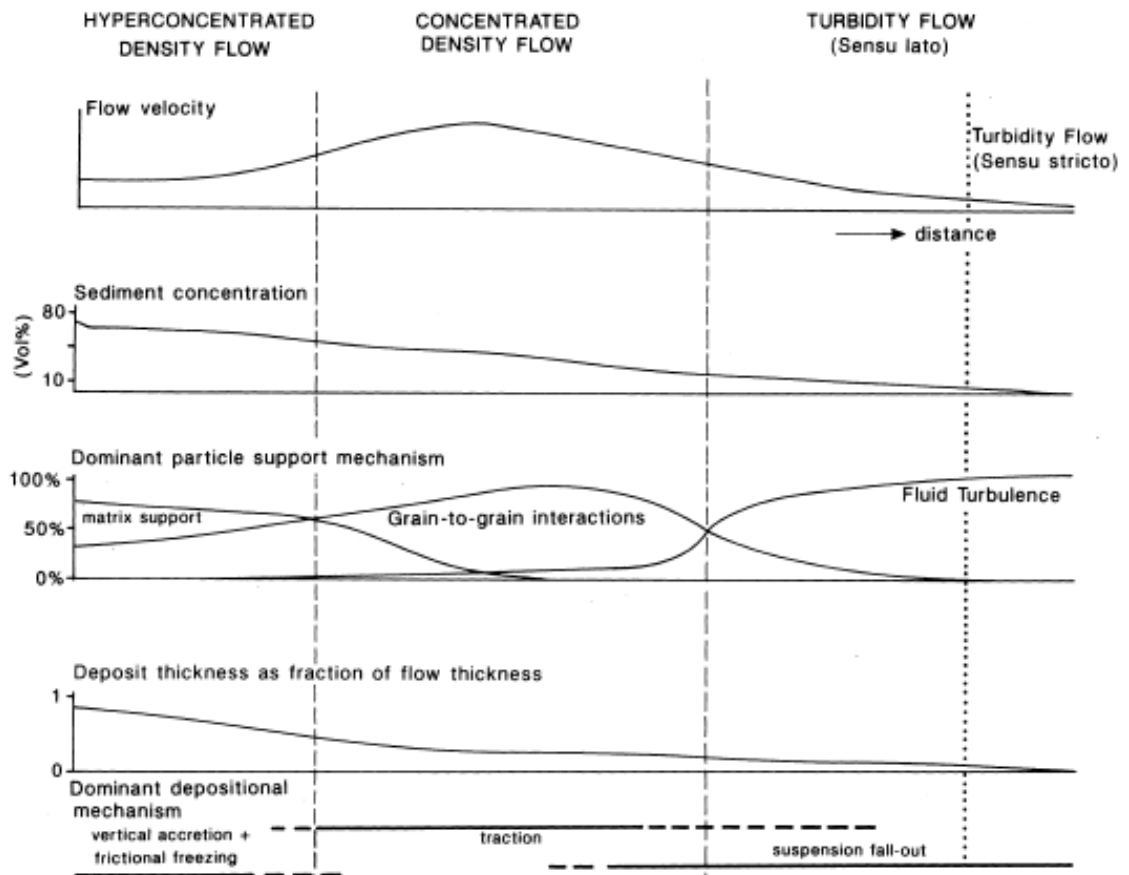


**Figure 2.21** Characteristics of flow transformation from hyper-concentrated density flow to turbidity flows. From Mulder and Alexander (2001).

### *Characteristics of flows within submarine channels*

Flows that form submarine channels are gravity-driven flows, and typically have the position of the maximum downstream velocity in the vertical profile near the bed rather than close to the top surface as in rivers (Hampton, 1972; Felix, 2002; Kneller and Buckee, 2000; Meiburg and Kneller, 2010). Furthermore, the density contrast near the top of the flow and their surrounding ambient fluid is far less than in rivers (Figure 2.22; Kneller and Buckee, 2000; Meiburg and Kneller, 2010). Sediment concentration of flows within submarine channels have not been measured directly due to sample difficulties (expensive and time consuming to access the flow: many inactive channels hence makes it hard to access an active channel, density stratification of the flow implies multiple measurements, flows can very destructive hence good equipment is needed) and can only be estimated. Sediment density flow concentrations have been estimated from numerical models (Pirmez and Imran, 2003; Konsoer *et al.*, 2013), derived from the backscatter obtained from Acoustic Doppler Current Profiling (ADCP) measurements (Azpiroz-Zabala *et al.*, 2017a) and interpreted from outcrops (Kuenen, 1966; Mulder and Alexander, 2001; Talling *et al.*, 2012).

Estimates from numerical models of submarine channels suggest a sediment concentration of 0.2% (Konsoer *et al.*, 2013), or between 0.6-2.5% (Pirmez and Imran, 2003). Sediment concentrations >0.02% and up to 0.17% by volume were calculated from backscatter observations from ADCP data, albeit there is no calibration for these estimations and the methodology assumes a single representative grain-size across all depths (Azpiroz-Zabala *et al.*, 2017a). By contrast, interpretation of outcrop studies suggests sediment concentrations ranging from ~7% up to 45% (Kuenen, 1966; Mulder and Alexander, 2001; Talling *et al.*, 2012). One suggestion may be that the observations record different kind of flows with low and high sediment concentrations, hence different flows transport different types of sediment through the channel. However, assuming, that the models are estimating the values correctly, Peakall and Sumner (2015) argue that sediment

concentration is stratified in the vertical, similar to velocity, and therefore the observations from outcrops represent concentrations near the bed interface. By contrast, estimates derived from ADCP data are unable to record measurement near the bed due to high sediment concentrations and due to sidelobe interference at the sediment interface, which may in part explain such low values compared to the other averaged values.

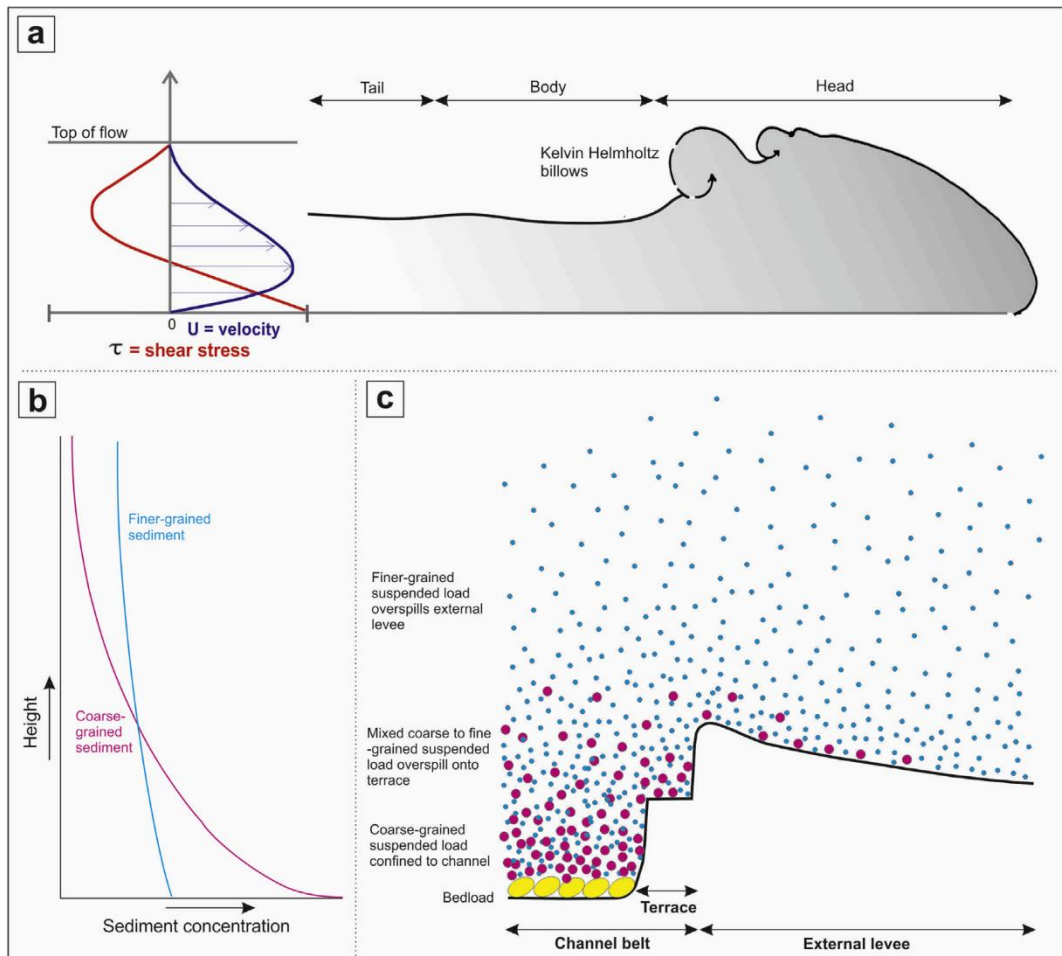


**Figure 2.22** Characteristics of flows within submarine channels (from Hansen *et al.*, 2015).

## 2.5.2 Flows around bends

### a) Rivers

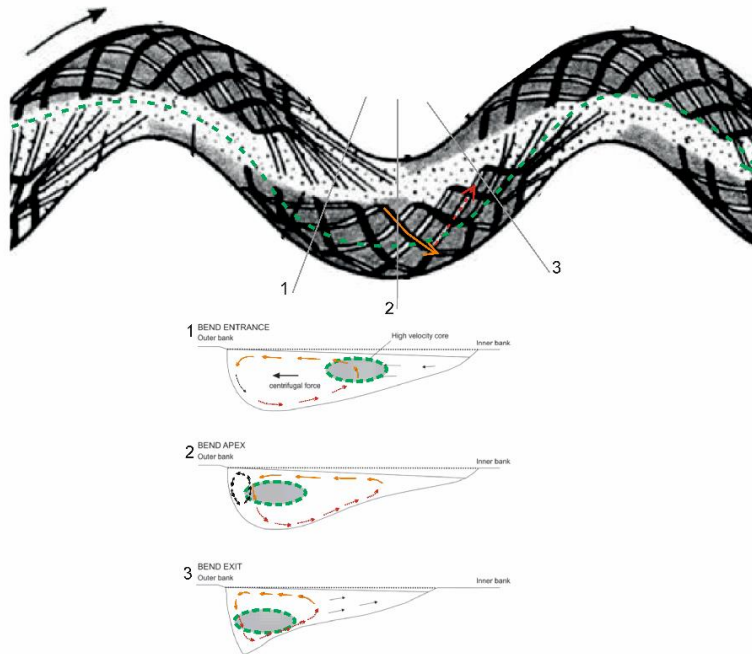
The 3-dimensional flow component around bends can be physically divided between a primary downstream and secondary lateral cross-sectional flow component due to the 3D flow helical flow structure initiated by the curvature (Figure 2.23A; Leopold and Wolman, 1960). The primary downstream component is the mean downstream directed flow. The maximum velocity of the primary downstream component, called the high velocity core, shifts due to the curvature from an inner bank position prior to the bend apex, towards an outer bank position at the bend apex due to the curvature in bends (Figure 2.23A; Leopold and Wolman, 1960; Dietrich and Smith, 1983; Dietrich, 1987). The secondary flow component is a “snap-shot” of the helical flow structure (laterally, across the channel) around the bend due to the centrifugal forces and pressure gradient forces. The centrifugal forces cause the flowing water around a bend to increase at the outer bend, causing a water surface elevation ( $z$ ). Due to the outward directed centrifugal force, an equal inward directed force that opposes the mean centrifugal force is created, the pressure-gradient force. The pressure gradient force acts as a balance to the centrifugal force (Rozovskii, 1957; Englund, 1974; Thorne *et al.*, 1985). The two forces are however generally unbalanced locally. The centrifugal force exceeds the pressure gradient force near the water surface and the pressure gradient force exceeds the centrifugal force near the channel bed, creating a helical or spiral motion around a curved bend. As you move towards bend inflections and away from a bend apex, the centrifugal force is reducing and hence the pressure gradient force as well. At straight sections (cross sections 1 and 4; Figure 2.23B) secondary flow is reduced, this then increases prior to the bend apex, is maximum at the bend apex, and decreases again after the bend apex (cross sections 2 and 3; Figure 2.23B).

Secondary flows are not just influenced by the induced curvature of the bend but also by the cross-sectional morphology of the bend, discharge and other



factors (e.g., Dietrich and Smith, 1983; Markham and Thorne, 1992). For example, outward shoaling of flow will occur above point bars (Figure 2.24); such variation between shoaling flows above point bars, the outer-flow component and a lateral flow component, has been directly observed in rivers (Figure 2.25; Markham and Thorne, 1992).

A) Schematic view of the primary and secondary flow component in a river



B) Schematic view of the generalised flow components in a river meander

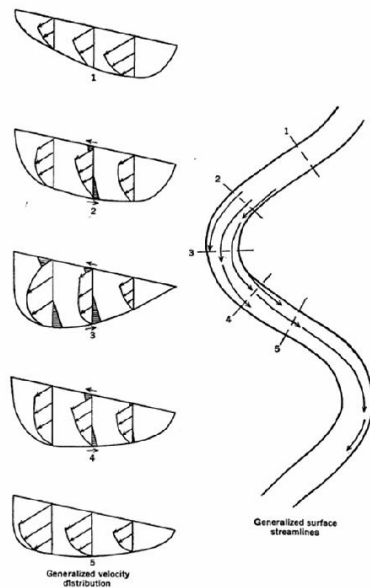


**Figure 2.23** A) Schematic view of flow components from the primary flow component (high velocity core, green) and secondary flow component (near-bed flow component, red and surface flow component, orange) Modified from Kasvi *et al.* (2015) and Lagasse *et al.*, 2004 based on Thompson (1986). B) Schematic view of the generalised flow components in a meander. Downstream primary flow (open parabolas with arrows) and lateral secondary flow (closely lined area) components of velocity as vectors and surface stream lines (From Leopold and Wolman, 1960).

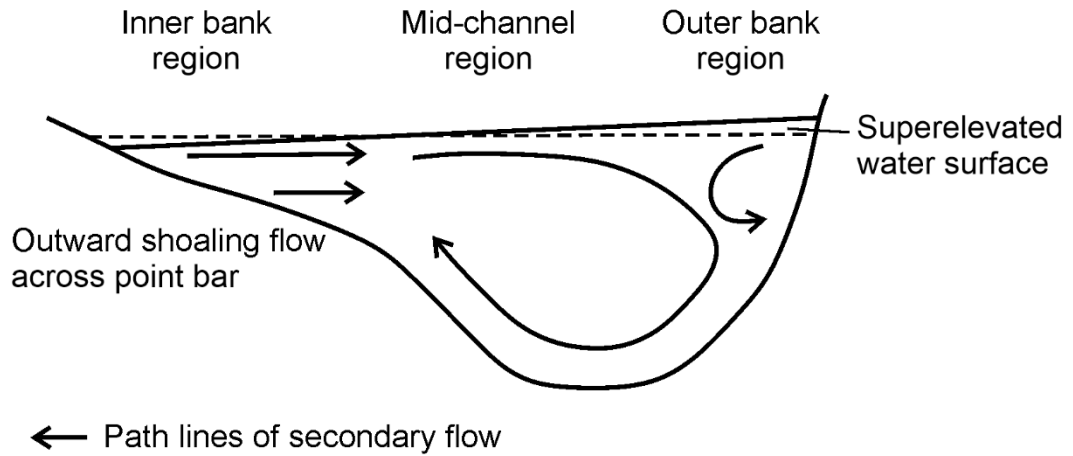


**Figure 2.24** Secondary flow at bend apex in rivers showing outward shoaling flow across point bar and outer bank cell (modified from Lagasse et al., 2004 based on Markham and Thorne, 1992).

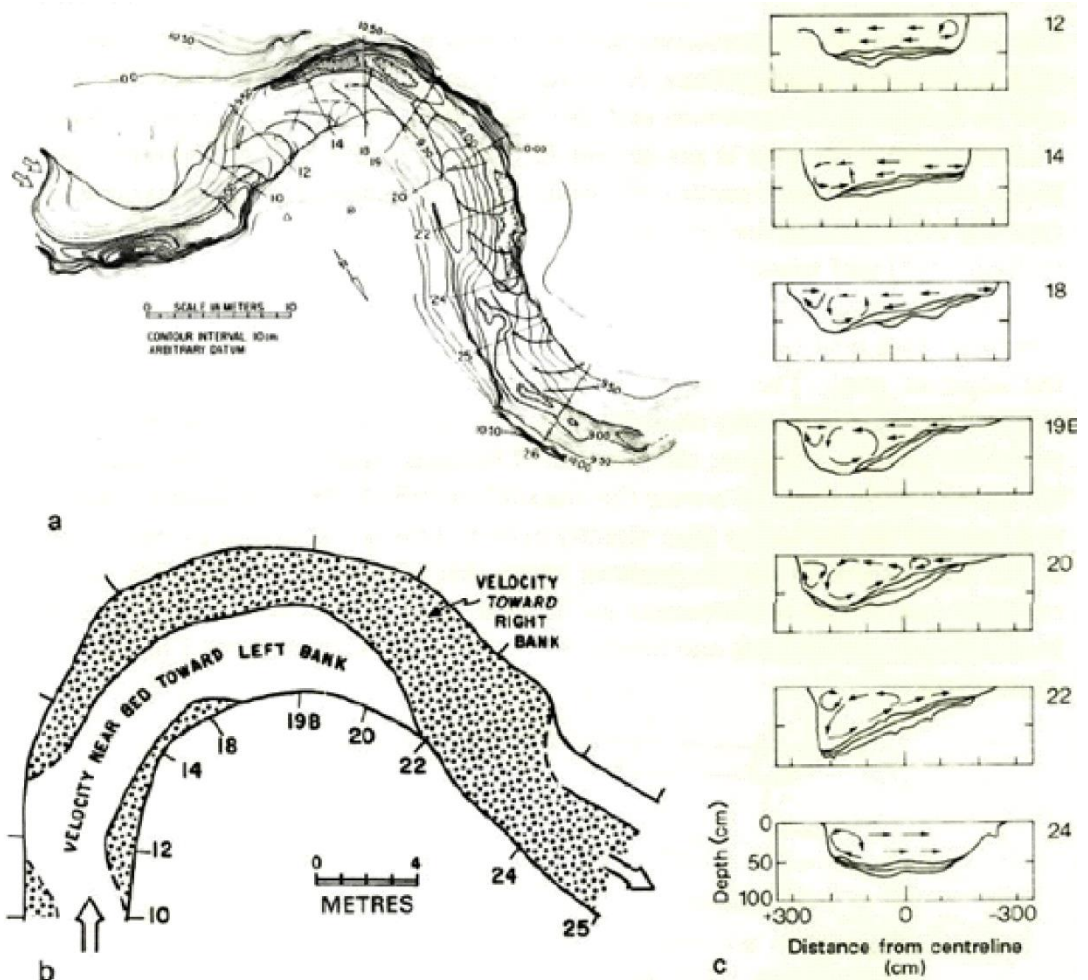
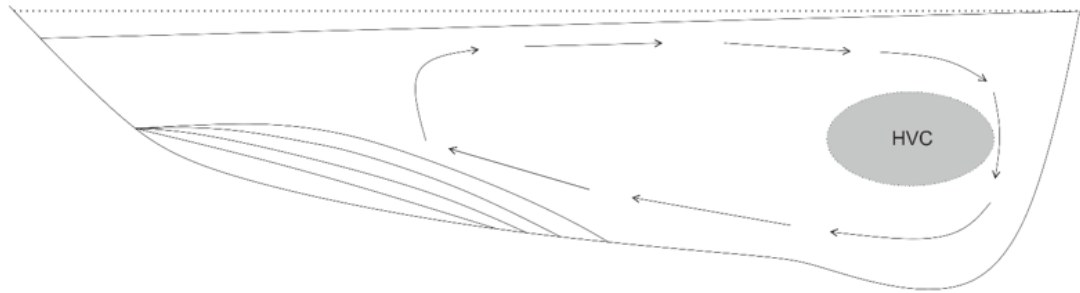


**Figure 2.25** Secondary flow component in a natural river bend. From: Dietrich and Smith (1983).

## **b) Submarine Channels**

Most observations of submarine channels in laboratory experiments and direct observations suggest that the secondary flow circulation in submarine channels does not exhibit a basal-inward directed flow at the bend apex, but rather has a basal-outward directed flow (Keevil *et al.*, 2006, 2007; Peakall *et al.*, 2007; Amos *et al.*, 2010; Sumner *et al.*, 2014). The change of secondary flow component direction is dependent on various factors, such as the maximum height of the flow velocity above the bed (Corney *et al.*, 2006), the material transported radially, which can vary depending on the flow super elevation and overspill (Dorrell *et al.*, 2013), Coriolis force, density stratification within the flow, and channel geometry (Peakall and Sumner, 2015). Additionally, the change of secondary flow component can have a direct effect on the primary flow component shifting the position of the high velocity core (Peakall and Sumner, 2015).

A) River with a clockwise flow structure



B) Submarine channels with an anti-clockwise flow structure

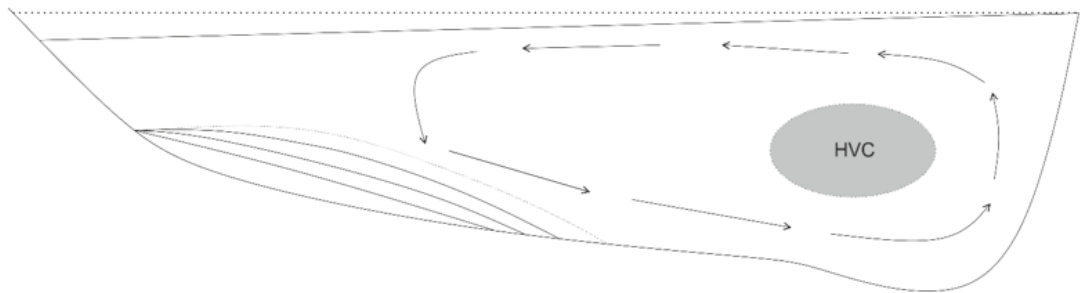


**Figure 2.26** Simplified flow structure model for A) clockwise or river-like in rivers and B) anticlockwise or river-reversed secondary flow for submarine channels at bend apexes. High velocity core (HVC) is situated close to the outer bend for rivers and HVC is similarly situated near the outer bend for an anti-clockwise (river reversed) flow structure or near the inner bend for a clockwise flow structure (river-normal) in submarine channels. Modified from Peakall and Sumner (2015) and Kasvi *et al.* (2015).

#### *Effect of channel geometry on the secondary flow component*

The channel geometry and the cross-section can have an influence on the secondary flow component (Amos *et al.*, 2010; Ezz and Imran, 2014). Ezz and Imran (2014) demonstrated through a 3D numerical model for saline flows from laboratory-scale channels that outward-directed bed flow at bend apexes increases for small bends with a small wavenumber in confined settings compared to large bends in unconfined settings (Ezz and Imran, 2014). Cross-sectional morphometrics have been analysed for different channel widths around bends (Ezz and Imran, 2014). Ezz and Imran (2014) demonstrated that the near-bed secondary flow component is outward-directed for a

rectangular channel with a narrow and wide channel width for confined flow settings, but significant density variations were observed for these two types (Figure 2.27). A rectangular wider channel width may favour a reduced outer-bed flow component with a high velocity core toward the outer bank (Imran *et al.*, 2007; Keevil *et al.*, 2007).

The influence of channel shape on secondary flow is important as channels in different environmental setting have been recognised to have different channel shapes. A “U”-shaped cross-section is more identified for isolated deep-ocean channels and a “V”-shaped cross-section is more identified for submarine-fan channels (Carter, 1988; Damuth *et al.*, 1988; Schwenk *et al.*, 2003), but it must be noted that the characteristics of “U” and “V”-shape classification in these studies is particularly subjective due to interpretation of cross-sections with a vertical exaggeration (Curry *et al.*, 2003). A trapezoidal channel shape with a narrow channel bed width favours outer-directed near-bed flows compared to a rectangular channel shape with a wider channel bed width (Ezz and Imran, 2014). Two stacked secondary flow cells can be observed for certain flow conditions in both rectangular and trapezoidal cross-sections with the bottom cell having either an outer-directed or inner-directed bed flow (Imran *et al.*, 2007; Islam *et al.*, 2008). Additionally, the cross-sections in these experiments were symmetrical, but observations show that cross-sections can be asymmetrical, similar to rivers (Reimchen *et al.*, 2016). It must be noted that Ezz and Imran (2014) identified variations of secondary flow in response to the cross-sectional shape for saline-density flows, but not for sediment-density flows which were not modelled.

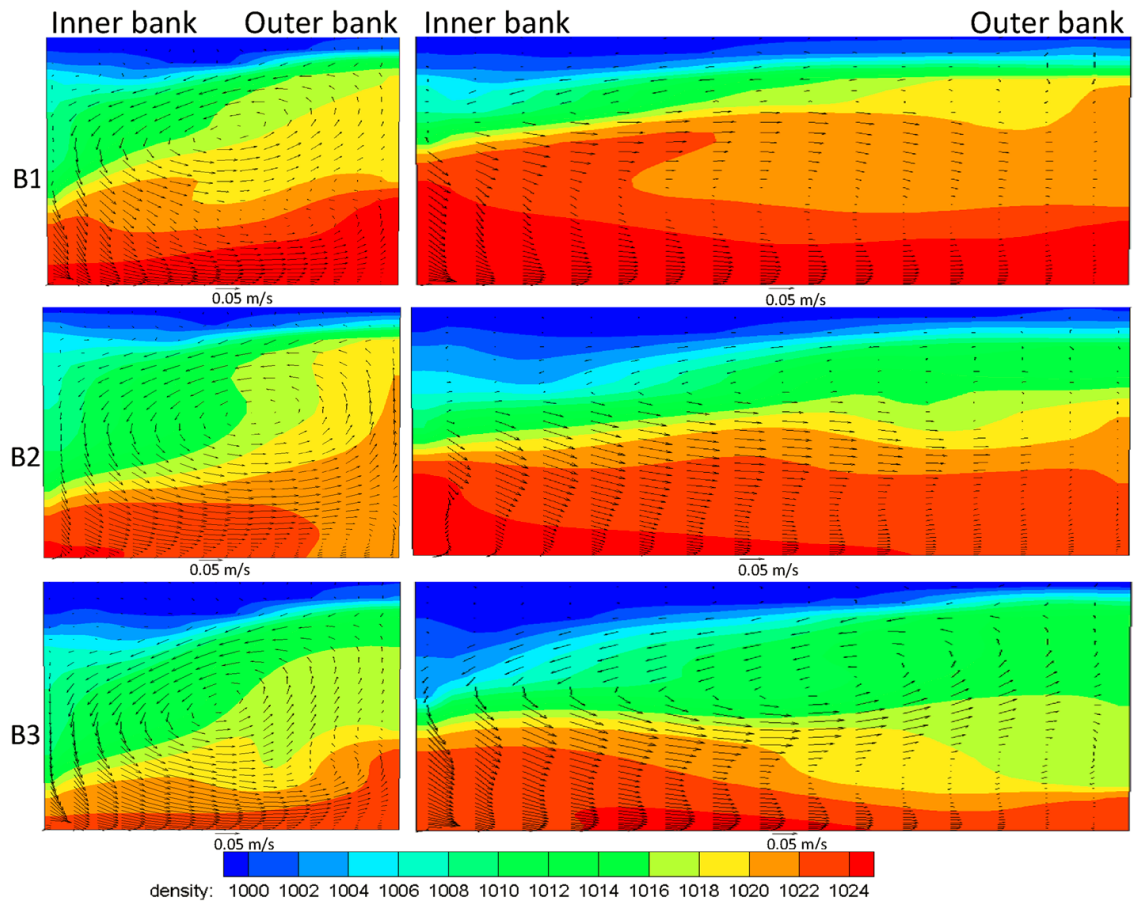


**Figure 2.27** Lateral velocity and density fields at three bend apices for confined flows with a 0.15-m-wide channel (left panel) and 0.30-m-wide channel (right panel). Curvature is constant. From Ezz and Imran (2014).

## 2.6 Sedimentation processes around bends in submarine channels

Multiple depositional areas can occur around submarine channels bends either on the outer and inner bank, which can be divided broadly into suspension-dominated or traction-dominated deposits. Suspension-dominated deposition is composed of sediment grains from suspension that underwent little traction during deposition, and traction-dominated deposition is associated with sediment bypass deposition (Figure 2.28; Peakall and Sumner, 2015). At bends, inner bend deposits consist of traction-dominated

point bars, and oblique accretion deposits, and outer bend deposits consist of outer-bank bars.

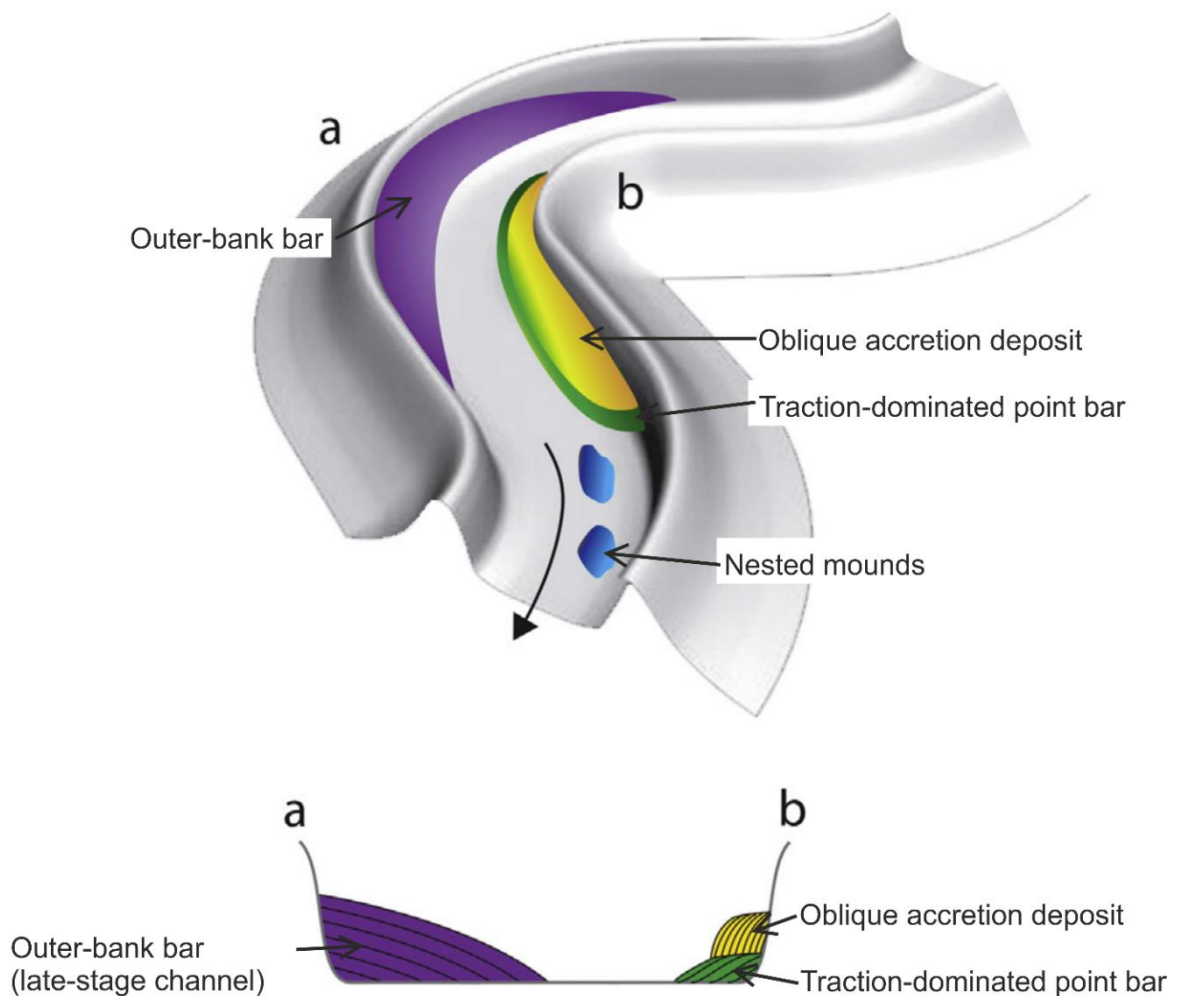


**Figure 2.28** Processes around submarine channel bends. Modified from Peakall and Sumner, 2015.

### *Traction-dominated point bars*

Traction-dominated point bars are deposits on the inner bend similar to point-bars in river. Traction-dominated point-bars are deposits from the lower part of the flow, where a higher sediment concentration occurs. However, since the lowest part of the flow is in general also the fastest, such flows may exhibit significant bypass, and only a relatively small component is deposited to form



traction-dominated point-bars. Hence, point-bars in submarine channels are different compared to point-bars in rivers since they are commonly thinner, if present, relative to channel depth (Nakajima *et al.*, 2009; Darby and Peakall, 2012; Peakall and Sumner, 2015). Inner bend deposition through suspension is developed above the point-bar or in the absence of point-bars; this has been termed oblique accretion deposition (Straub *et al.*, 2008; Peakall and Sumner, 2015).

#### *Oblique accretion deposits*

Suspension dominated oblique accretion deposition can form in the absence of point bars or above point bars and are composed of fine-grained clinofolds or low-angled dipping surfaces (Page *et al.*, 2003; Deptuck *et al.*, 2007; Babonneau *et al.*, 2010; Peakall and Sumner, 2015). In rivers, oblique accretion deposits are formed in low energy environments (Page *et al.*, 2003). Inner bend deposition of traction dominated point bars and oblique accretion deposition can occur on top of each other with the traction dominated point bars below the oblique accretion deposition (Fig. 2.29). Two mechanisms might explain the process, either through flow separation or through a low velocity zone transferring fine-grained sediment from the main flow to the inner bend region (Straub *et al.*, 2008; Peakall and Sumner, 2015). In rivers, where a traction dominated point bar is deposited below an oblique accretion deposition it occurs through the presence of bedload, hence the point bar and oblique accretion deposits are formed through converging sediment flux and a cross-stream velocity reduction in the combined downstream and secondary flow components towards the inner bend. The coarser material is deposited first at the inner bend, followed later by suspended sediment (Figure 2.29; Page *et al.*, 2003).

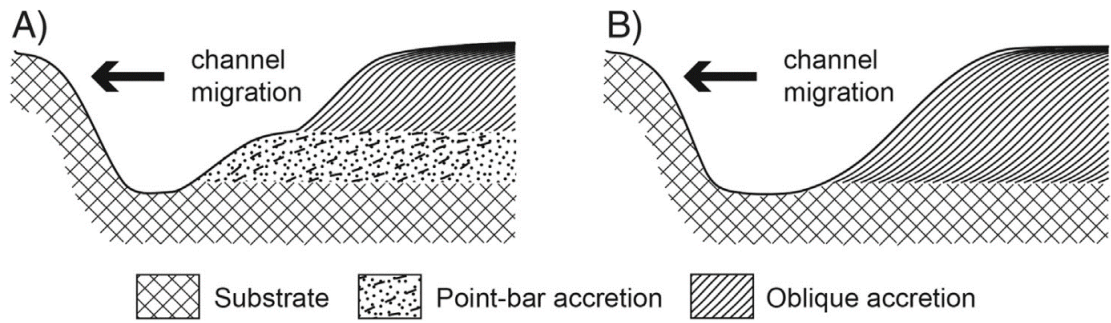


**Figure 2.29** Characteristics of oblique accretion deposits with A) point bar and B) without a point bar. Point bars develop from traction-dominated sedimentation and Oblique accretion deposition develop from suspension-dominated sedimentation. Modified from Page *et al.* (2003).

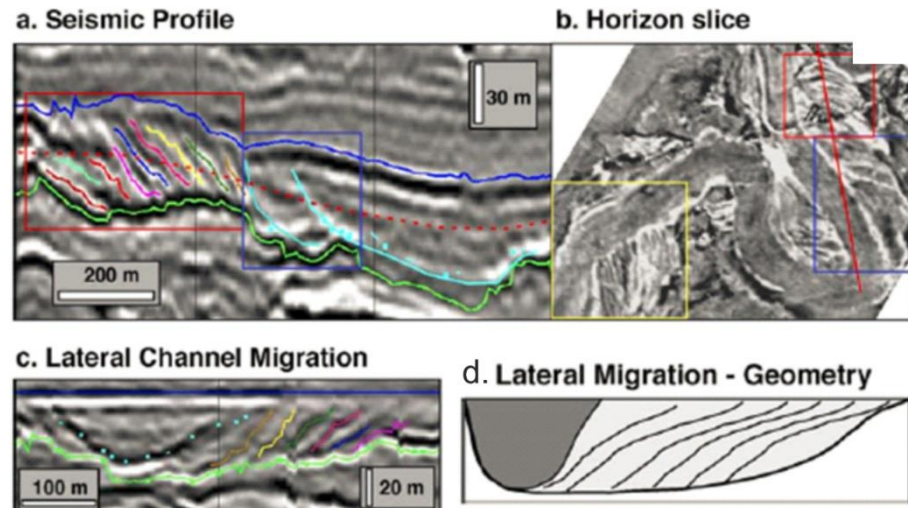
### *Scroll bars*

Scroll bars in rivers are a single topographic feature on a point bar (see Figure 2.6) which are composed of a ridge-and-swale topography on the inside of a bend to indicate the adjustment of past and present bend growth and hence can be used to extract information of bend migration and sedimentary architecture (Allen, 1965; Nanson, 1980).

Some studies have suggested that scroll bars exist for submarine channels (Clark and Pickering, 1996b; Abreu *et al.*, 2003; Kolla *et al.*, 2007), but a detailed study of these scrolls bars have not been conducted. Since a traction-dominated point bar is often reduced in submarine channels (Darby and Peakall, 2012; Peakall and Sumner, 2015), the formation of scroll bars through traction-dominated deposit, hence coarse-grained sediment, should be less common or nearly absent in submarine channels compared to rivers. Scroll-bars can also form through oblique accretion deposits in rivers, whereby the scroll bar formation is more complex compared to scroll bars from coarse grained point bars (Page *et al.*, 2003). Here, a comparison is made between observations in scroll-bars from submarine channels (Abreu *et al.*, 2003), assuming that scroll bar formation is through oblique-accretion deposits, and scroll-bars from rivers with oblique-accretion deposition (Page *et al.*, 2003; Figure 2.30). If the observed features are not similar to scroll bars in rivers,

the features may be inner channel terraces, which may have been created by channel incision, inner bend deposition, cut-off and margin failures (Hansen *et al.*, 2015).

## A) Submarine channels



## B) Rivers

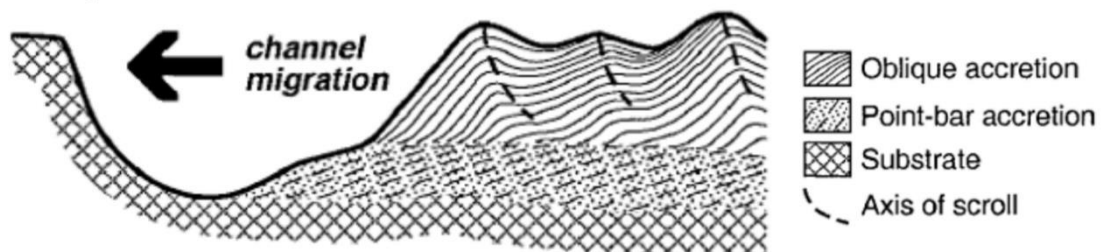


**Figure 2.30** Comparison of scroll bars in A) submarine channels (Abreu *et al.*, 2003) and B) rivers (Page *et al.*, 2003).

### Outer bank bars

Outer bank bars refer to relatively coarse-grained deposits at the outer bend, which have been suggested to occur during a late development stage for aggradational channels (Kane *et al.*, 2008; Straub *et al.*, 2008; Nakajima *et al.*, 2009). Interpretations of seismic data suggest that the dip angle of the outer bank bar is highest at the bend apex and decreases either side of the

bend apex. They can longitudinally occur simultaneous with a point-bar if it is present (Nakajima *et al.*, 2009). In the Amazon Channel, outer bank bars have only be identified in tight bends (radius of curvature < 2 km) and in narrow channels (width < 3 km, aspect ratio between 10 and 20; Nakajima *et al.*, 2009). Outer bank bars seem to be unique for submarine channels with no similar observation in rivers (Nakajima *et al.*, 2009), which may be due to capacity-induced deposition in turbidity currents (Hiscott, 1994) and the effect of superelevation of the flow towards the outer bank (Nakajima *et al.*, 2009; Straub *et al.*, 2011). Outer bank bars may play an important role in channel stability and channel evolution as outer bank bar deposition reduces bend sinuosity over time (Kane *et al.*, 2008; Nakajima *et al.*, 2009; Straub *et al.*, 2011).

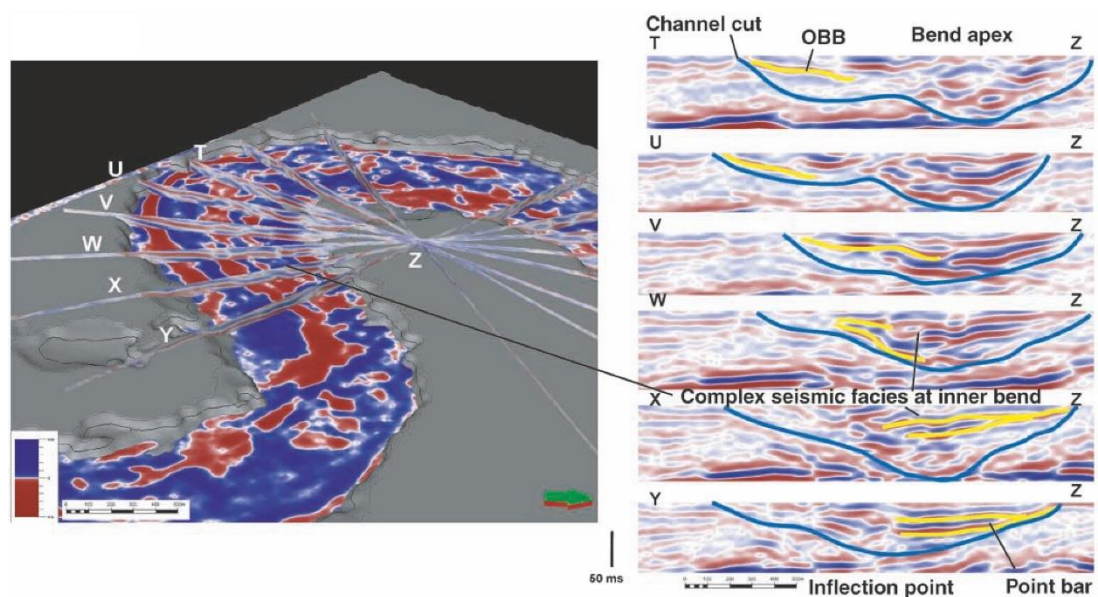


**Figure 2.31** Time slices from the Amazon Channel (Lower Channel Levee System) with reflection cross-sections around bends. Outer-bank bars (OBB) are observed at sections W-T. Green arrows indicate north. From Nakajima *et al.* (2009).

*Bend cut-off*

Bend cut-off in rivers and submarine channels is the process whereby the channel pathway is reduced by a neck cutoffs or chute cutoffs. In the case of neck cutoffs these increase with sinuosity in rivers (Hooke, 2007). Chute cut-off refers to the process whereby a new channel pathway is formed along a swale on the inner bend. In contrast, neck cutoff refers to the process whereby a new pathway occurs at the neck of the loop cutting off the old channel pathway around the bend (Allen, 1965). In alluvial rivers, cutoffs occur during periods of river floods in connection with increased meandering and lead to the formation of an oxbow lake. Most submarine channels have no to only a few cut-offs (e.g. Klauke *et al.*, 1998a; Peakall *et al.*, 2000a, b; Lewis and Pantin, 2002) and only a few channels exist which have regular cut-offs (Deptuck *et al.*, 2003; Schwenk *et al.*, 2003; Babonneau *et al.*, 2004). Submarine channels experience less cut-offs than rivers (Peakall *et al.*, 2000a; Kolla *et al.*, 2001), for example the Bengal Channel, an aggradational channel experienced 20 cut-offs along a 90 km channel length (Schwenk *et al.*, 2003) compared to for example 4 cut-offs within one season in a 600 m reach for a river (Hooke, 2004), which would be 600 cut-offs for a 90 km reach. Kane *et al.* (2008) argue that bend cut-offs occur less in submarine channels as they may regulate changes in channel sinuosity through the degree of bypassing flows through the channel. Strong bypassing and more confined flows deposit at the inner bend whereas weakly bypassing and less confined flows deposit at the outer bend. Inner bend deposits would create an increase in channel sinuosity over time (Nakajima *et al.*, 2009), whereas outer bend deposits act to decrease sinuosity with time, thus they may reach an equilibrium over time. By contrast, Kneller (2003) argues that bend cutoff occurs less in submarine channels as the flows are in disequilibrium with the channel gradient. If changes in the flow lead to an equilibrium slope with a steeper gradient then aggradational channels occur with vertical aggradation and if the flow changes so that the slope has a reduced equilibrium profile then erosional incision occurs (Kneller, 2003). Bend cutoff due to incision has been reported from the Congo submarine fan channel with arcuate channel-

facing scarps and occasional topographic highs in the centre which were formed on the inner bend prior to bend cutoff (Babonneau *et al.*, 2004). The new channel pathway occurs due to channel incision and the abandoned channel pathway is filled by overspilling deposits over time (Figure 2.32).

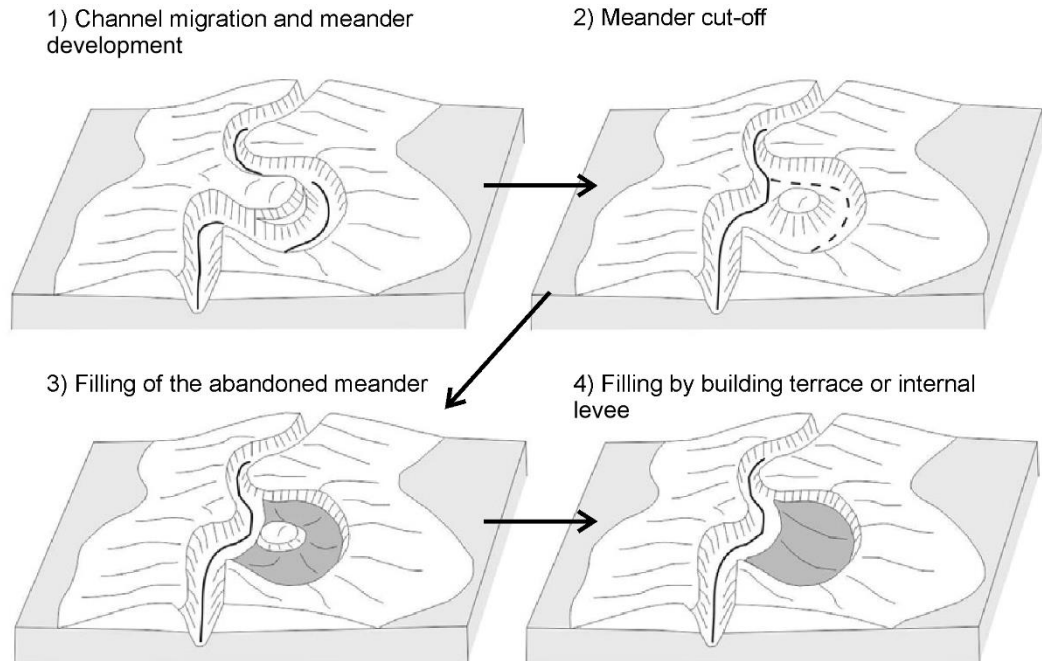


**Figure 2.32** Process of bend cut-off in submarine channels. Adapted from Babonneau *et al.* (2004).

## 2.7 Conclusions

Submarine channel dimensions range by an order of magnitude with different studies having contradictory results. Here it is postulated that this may be explained by considering different environmental settings and types of submarine channels (see Chapters 3, 5 and 6). Channel evolution in passive margin channels is shown from field examples to be dominantly controlled by a vertical aggradation component rather than down-stream bend migration, but laboratory experiments cannot reproduce the observed bend migration model, instead predicting a dominantly downstream migration. The effect cannot be obviously explained by flow or sedimentation processes alone,

hence it is hypothesised that these differences between field examples and experiments may in part be related to cross-sectional morphometrics, which have not been previously considered. The nature of width variations around submarine channel bends is considered in chapters 4, 5 and 6. The observations of width changes around bends in rivers may suggest the following for submarine channel evolution. Channel migration in submarine channels may be either explained by bar push, inner bend deposition, or bank pull, outer bank erosion. Again, these theories can be assessed by examining the nature of cross-sectional width variation around bends, and integrating this with the literature on sedimentation, see chapters 4, 5 and 6 for consideration of this.

# **Chapter 3 Morphometric variation as a function of submarine channel type: implications for hydraulic properties**

---

## **3.1 Chapter Summary**

Morphometric analysis is used to predict flow and sedimentation processes within submarine channels. Previous studies have aggregated data from multiple channels in order to examine average properties of submarine channels, and for comparison with fluvial channels. Results from these studies have been contradictory, with aspect ratios for submarine channels being suggested as either similar to, or much greater than, river channels. These previous studies are predicated on the assumption that submarine channels are all a single morphological type, and thus can be aggregated. However, submarine channels have been classified into a range of different types dependent on environmental setting (defined here following previous work as submarine-fan, isolated deep-ocean, axial, slope and non-margin ocean channels). Here it is examined whether these channel types exhibit different morphological properties, and thus should be considered separately in morphological analyses, and whether such distinctions might offer an answer to the present contradictory results when comparing submarine and river channels. More specifically, the present study examines the channel parameters of width, depth, aspect ratio and cross-sectional shape, utilising a new dataset based on cross-sections extracted from a number of multibeam echo sounding datasets and the top surface of multi-channel seismic (consisting of 2 submarine-fan, 3 isolated deep-ocean and 3 non-margin ocean channels). This dataset is then compared to a dataset of submarine channels compiled from the literature (based on 5 submarine-fan, 13 isolated deep-ocean, 2 axial and 3 slope channels). In turn, the submarine channel datasets are compared with single-thread alluvial rivers and bedrock rivers.



The results identify variations between cross-sections within individual submarine channels, between channels, and between channel types. Slope, submarine-fan, and non-margin channels are shown to have aspect ratios similar to rivers, whereas isolated deep-ocean and axial channels have aspect ratios (width: depth) much greater than rivers. Channel width varied by 2 orders of magnitude between channel types, and channel depth by an order of magnitude, in turn making slope channels the narrowest and shallowest channels and isolated deep-ocean channels the widest and deepest channels. Submarine-fan, slope and non-margin ocean channels exhibit a more “V”-shaped cross-section and axial and isolated deep-ocean channels a more “U”-shaped cross-section.

---

### 3.1 Introduction

Submarine channels are formed by gravity currents and act as conduits for sediment transport from the continental shelf edge (depths typically >100-200 m) across the continental slope, and on to the basin plain, in some cases extending to the abyssal plains at water depths of four to six kilometres (Menard, 1955; Lewis, 1994; Wynn *et al.*, 2007; Pickering and Hiscott, 2015). The widths and depths of submarine channels, that can be resolved on the modern seafloor, range from a few metres (e.g. LUCIA width <200 m, depth <25 m for some sections; Maier *et al.*, 2013) to hundreds of metres (e.g. North Atlantic Mid Ocean Channel (NAMOC) width <15 km, depth <200; Klaucke *et al.*, 1998a).

Morphometric analysis has been used in both rivers and submarine channels to predict hydraulic properties (Leopold and Maddock, 1953; Pirmez and Imran, 2003; Konsoer *et al.*, 2013; Shumaker *et al.*, 2018). These studies have shown that width, depth and velocity increase as power functions of discharge for rivers and submarine channels (Leopold and Maddock, 1953; Konsoer *et al.*, 2013). Additionally, analysis of channel parameters has been used to predict sedimentation processes and hence long-term evolutionary

process (Flood and Damuth, 1987; Clark *et al.*, 1992; Clark and Pickering, 1996a; Klaucke *et al.*, 1997; Babonneau *et al.*, 2002; Covault *et al.*, 2011; Jobe *et al.*, 2016; Reimchen *et al.*, 2016; Hansen *et al.*, 2017).

Flows that form submarine channels are gravity-driven, which in many cases have their position of the downstream maximum velocity in the vertical profile close to the bed rather than close to the top surface as in rivers (Peakall and Sumner, 2015). The density contrast near the top of the flow and their surrounding ambient fluid is also far less than in rivers (Hampton, 1972; Kneller and Buckee, 2000; Felix, 2002; Hansen *et al.*, 2015). Additionally, the Coriolis force can be a controlling factor for channel sinuosity unlike in rivers with larger channels having a higher sinuosity at low latitudes than at high latitudes (Cossu and Wells, 2010; Peakall *et al.*, 2012; Cossu *et al.*, 2015). In general, hydraulic properties reduce in magnitude downstream in contrast to rivers where hydraulic properties increase downstream (Kenyon *et al.*, 1995; Pirmez and Imran, 2003; Babonneau *et al.*, 2010).

A key issue when comparing a large dataset of hydraulic geometry of submarine channels and their comparison to rivers is that different studies have produced contrasting results. The average aspect ratios (width/depth) for submarine channels can be, depending on the study, smaller, similar or greater than rivers (Figure 3.1; Flood and Damuth, 1987; Clark *et al.*, 1992; Peakall *et al.*, 2000a; Konsoer *et al.*, 2013; Jobe *et al.*, 2016). Examining Figure 1 in more detail: three different submarine channel datasets (Pirmez and Imran, 2003; Konsoer *et al.*, 2013; Jobe *et al.*, 2016) are compared to three river datasets (Jerolmack and Mohrig, 2007; Wilkerson and Parker, 2011; Jobe *et al.*, 2016). Firstly, it is important to note that there are first order differences between the different submarine channel datasets (Figure 3.1), with Konsoer *et al.* (2013) predicting much greater aspect ratios than Jobe *et al.* (2016), with the Amazon dataset of Pirmez and Imran (2003), typically in between the two. Similarly, there are variations between the river datasets, although the Wilkerson and Parker (2011) and Jobe *et al.* (2016) datasets are similar, with Jerolmack and Mohrig (2007) very much an outlier. The river dataset of Jerolmack and Mohrig (2007) includes 23 branching or transitional channels with aspect ratios of 303, and only 4 single meandering channels

with aspect ratios of 159. Consequently, it makes a poor comparator for the single-thread submarine channels, and is not considered further. In contrast, the Wilkerson and Parker (2011) dataset is composed of single-thread alluvial channels. The Jobe *et al.* (2016) dataset is composed of measurements obtained from seismic reflection data and outcrops. Since the Jobe *et al.* (2016) dataset is similar to the Wilkerson and Parker (2011) dataset, it is assumed that it is composed of sing-thread alluvial channels. Comparing submarine channels to these two fluvial datasets reveals that the Jobe *et al.* (2016) dataset has lower aspect ratio, the Konsoer *et al.* (2013) has higher aspect ratio, and the Amazon dataset of Pirmez and Imran (2003) is the closest to the river datasets.

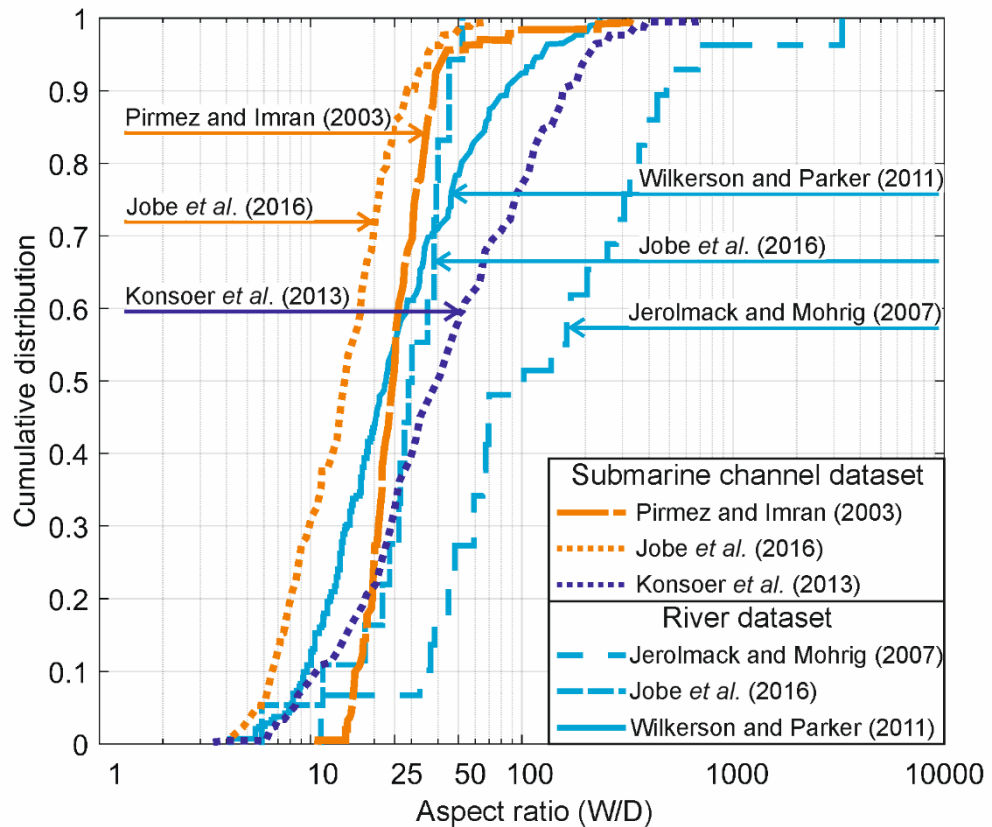


**Figure 3.1** Cumulative distribution of channel aspect ratio (W/D). Three submarine channel datasets (Pirmez and Imran, 2003; Konsoer *et al.*, 2013; Jobe *et al.*, 2016) are compared to three river datasets (Jerolmack and Mohrig, 2007; Wilkerson and Parker, 2011; Jobe *et al.*, 2016). Modified from Jobe *et al.* (2016).

The differences in the submarine channel datasets might be the product of the methodology used to measure channel parameters, or the choice of channels measured. Methodological differences may include, the equipment type used to collect data, data resolution, the orientation of cross-sections relative to channel banks, definition of parameters such as width and depth, and considerations of how to address complex topography. The equipment used to collect the data can influence the measurements. For instance, GLORIA side-scan sonar measures the channel bed, width which is 2-3 times smaller than the channel width at the channel banks (Pirmez and Imran, 2003). Previous studies that used GLORIA to measure the channel width concluded that the channel width is similar compared to rivers (Flood and Damuth, 1987; Clark *et al.*, 1992). The equipment used to collect the data also affects how the cross-sections were taken in relation to the channel path. If multibeam sonar is available then cross-sections can be taken perpendicular to the channel pathway (Reimchen *et al.*, 2016; Hansen *et al.*, 2017; Shumaker *et al.*, 2018). However, if cross-sections are taken from single-beam measurements then it depends how the ship-track line crosses the channel path (Carter and Carter, 1996; Pirmez and Imran, 2003; Schwenk *et al.*, 2003); in many cases there is no way of identifying how oblique the channel cross-section might be. Data obtained from outcrops (e.g. Jobe *et al.*, 2016) are also highly unlikely to be perpendicular to the channel path. Methodology also changes between studies. For instance, Shumaker *et al.* (2018) removed large width measurements arising from bend geometries by removing cross-sections whose width was more than 150% or 170% greater than the minimum width of the three previous measured cross-sections; this threshold varied for each channel. Additionally, a bias might exist towards larger channels due to limitations of data resolution. Although, these methodological aspects are undoubtedly important, they are unlikely to account for the differences between submarine channel datasets given that aspect ratios can vary by an order of magnitude at the upper end of the distributions (Figure 3.1). Variations in channel parameters also exist between channels when comparing them in the down-stream direction with a consistent methodology. For instance, channel width ranged from 550 m (Niger) to 4341 m (Surveyor) and aspect

ratios ranged from 12 (Niger) to 78 (Surveyor) in the dataset of Shumaker *et al.* (2018). The aim of the present study is to assess whether these variations between channels are a function of the type of channel, and whether these can account for the contradictions inherent in the literature with respect to aspect ratios in submarine channels.

### **3.2 Definition and classification of submarine channels**

Submarine channels are defined herein as seafloor channels dominated by turbidity currents and other sediment gravity flows (Peakall and Sumner, 2015), and that head dominantly downslope. These are in contrast to contourite channels that are dominantly along slope and driven by density differences caused by temperature and salinity (Peters *et al.*, 2005; Hernández-Molina *et al.*, 2006; Stow *et al.*, 2013; Rebesco *et al.*, 2014).

Submarine channels occur from shallow marine environments on the continental shelf to deep-marine environments on the continental slope all the way to the abyssal plain. Here, a distinction between shallow-marine to deep-marine channels is defined by the shelf break or shelf edge. Shallow-marine channels are channels on the continental shelf such as on river delta fronts (Kostaschuk *et al.*, 1992) or within fjords (Conway *et al.*, 2012; Dowdeswell and Vásquez, 2013; Gales *et al.*, 2018). Only deep-marine channels are included in the study and hence are considered in the present definition of submarine channels. Submarine channels beyond the shelf-break can occur in a range of environmental settings as network of channels on submarine-fans (e.g. Amazon, Bengal, Zaire and Indus Fan) or as deep-ocean channels (e.g. NAMOC), and these environmental settings have been used to classify submarine channels (Schweller and Kulm, 1977; Carter, 1988; Peakall and Sumner, 2015). However, only a few studies exist that recognise the variations between different channel types (Carter, 1988; Klauke *et al.*, 1998a). Here, the classification of Peakall and Sumner (2015) is adapted with the following channel types: submarine-fan channels, isolated deep-ocean channels, axial

channels, slope channels, and non-margin ocean channels (Figure 3.2). The term “deep sea channel”, which was previously exclusively used for isolated deep-ocean channels (Carter, 1988) has recently become a synonym for all “submarine channels” (Maier *et al.*, 2013; Reimchen *et al.*, 2016) hence the term “isolated deep-ocean channel” is used instead of the term “deep sea channel”. The characteristics of each channel type are:

- a) Submarine-fan channels build a complex network of channels on deep-sea fans, which are located at the distal part of continental margins on both passive and active margins (Kolla, 2007; Ortiz-Karpf *et al.*, 2015). Submarine-fans can be divided based on their feeding system (Reading and Richards, 1994; Richards *et al.*, 1998) into a single point-source (e.g. Amazon, Damuth and Flood (1984); Magdalena, Kolla and Buffer (1984); Astoria, Nelson (1976); Navy Fan, Piper and Normark (1983); Gulf of Corinth, Piper *et al.* (1990)) or multiple sources (e.g. Ebro, (Alonso *et al.*, 1995) and based on the characteristic of the submarine fan into mud, sand or gravel-dominated fan. Submarine fans can be generated from a variety of processes: sediment from longshore drift or rivers accumulating in canyon heads, delta failures or slumps from distal river sediments, or hyperpycnal flows from ice margins or rivers (Piper and Normark, 2001; Covault and Graham, 2010). Here, this study concentrates on mud-rich submarine-fan channels.
- b) Isolated deep-ocean channels are basement-controlled and develop in the early stage of ocean basin formation. They form a sediment pathway between submarine canyons/fans and abyssal plains. As the ocean basin developed, channels may get locked within the oldest and deepest oceanic crust, or may migrate from the older crust through a spreading ridge via a fracture zone. Isolated deep-ocean channels can stay active as long as the subsidence of the ocean basin at the channel terminus exceeds sediment deposition (Carter, 1988). Isolated deep-ocean channels can develop in areas of failed rift-valleys,

or aulacogens (Bounty Channel; Carter and Carter, 1996), interrupted oceanic basins ((North Pole Submarine Channel, NPSC; Kristoffersen *et al.*, 2004), Zambezi Channel (Droz and Mougnot, 1987)) and in areas parallel to a mid-ocean ridge (Upper Cascadia, Lower NAMOC). Older isolated deep-ocean may survive as relicts (Lower Cascadia, (Griggs and Kulm, 1973); Surveyor Channel, (Reece *et al.*, 2011)), with the continuous development of ocean basins and continental margins (Carter, 1988).

- c) Axial channels occur along axial trenches parallel to continental margins between two convergent plates (Schweller and Kulm, 1977; Thornburg and Kulm, 1987; Shimamura, 1989; Pickering *et al.*, 2013).
- d) Slope channels are restricted to continental slopes. Slope channels are not related to canyons nor gullies. Canyons are erosional features cut into bedrock or sediment at the shelf to slope and compared to submarine channels occur in general at a steeper slope gradient, increase in cross-section dimensions downstream and have poor to no leveed morphology (Shepard, 1973; Shepard and Emery, 1973; Pirmez and Imran, 2003; Lastras *et al.*, 2009). Gullies are parallel features occurring in clusters parallel to each other (Field *et al.*, 1999; Micallef and Mountjoy, 2011; Gales *et al.*, 2013). Slope channels can be orientated perpendicular to the shelf edge (e.g. Fuji Channel and Einstein Channel (Sylvester *et al.*, 2012); and Brunei (Straub *et al.*, 2012), or occur across the continental shelf flowing into a canyon ( e.g. LUCIA; Maier *et al.*, 2013)
- e) Non-margin ocean channels occur on volcanic arc-ridges or the down-dipping side of seamounts far from any continental margin and have no direct sediment source from terrestrial environments (Von Huene and Arthur, 1982; Gardner, 2010; Stern, 2010). The channels often occur perpendicular to the ridge.

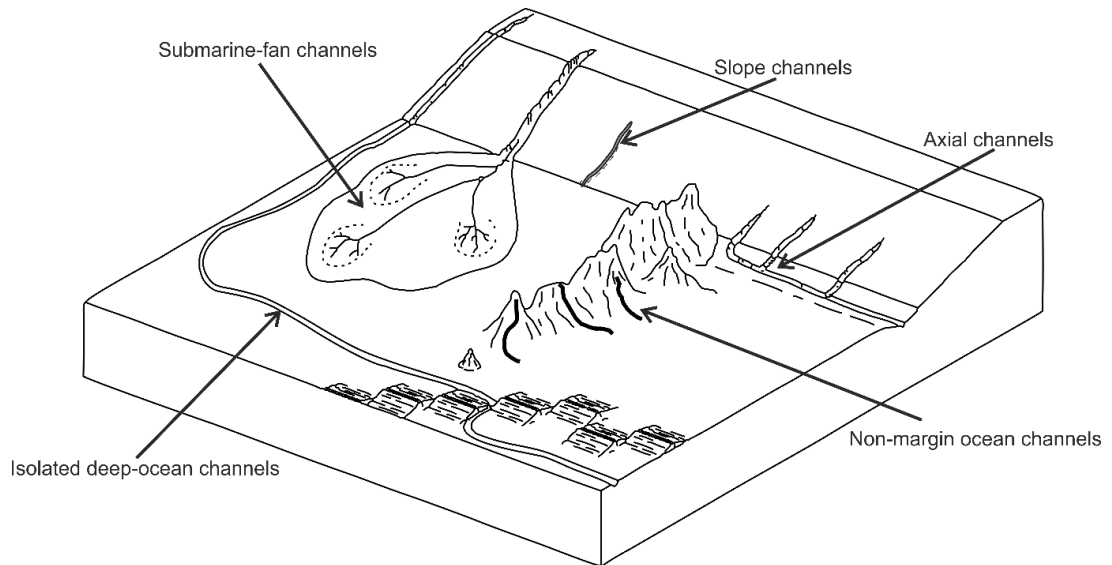


**Figure 3.2** Classification of submarine channels. Channel types are submarine-fan, slope, axial, non-margin ocean and isolated deep-ocean channels. Modified from Peakall and Sumner (2015).

### 3.3 Dataset and Methodology

The analysed sections were from the: Magdalena Channel, Bryant Channel, Horizon Channel, Baranof Channel and Surveyor Channel, Mariana Channels (Table 3.1). The Magdalena channel is situated in the Caribbean Sea and the Bryant Channel in the Gulf of Mexico. The Horizon Channel, Baranof Channel and Surveyor Channel are located in the Gulf of Alaska and the Mariana Channels are near the Mariana Trench. The bathymetry data from the Gulf of Alaska and Gulf of Mexico were obtained from the Law of the Sea U.S. UNCLOS Bathymetry Project, which were collected in 2005 (Gulf of Alaska), 2006 (Mariana Trench) and 2007 (Gulf of Mexico) and had a horizontal resolution of 100 m and a vertical resolution of 10% of the water depth (<40 m). The dataset for the Magdalena Channel in the Caribbean Sea was a seafloor horizon from a 3-D seismic survey from 2012 with a horizontal resolution of 12 m and a vertical resolution of 10 m. The Gulf of Alaska, Gulf of Mexico and West Mariana Ridge were projected into WGS 1984 world Mercator coordinates and the Caribbean Sea dataset was projected into



MAGNA Bogota coordinates. All datasets were processed in ESRI ArcMap 10.3.1 and measured in ImageJ.

**Table 3.1** Summary of analysed channel sections.

	Magdalena Channel	Bryant Channel	Horizon Channel Baranof Channel Surveyor Channel	Mariana Channel A, Mariana Channel B, Mariana Channel C
<b>Type</b>	Submarine-fan	Submarine-fan	Isolated deep-ocean	Non-margin ocean
<b>Study area</b>	Caribbean Sea	Gulf of Mexico	Gulf of Alaska	West Mariana Ridge
<b>Section Length (km)</b>	55.75	33.29	281.4; 267.4 244.2	13.04  8.87  8.25
<b>Water depth (m)</b>	1566 to 2320	3101 to 3204	2780 to 3030 2816 to 3105 3576 to 3815	4100 to 4188 3912 to 3997 3470 to 3608
<b>Slope (°)</b>	0.75	0.01	0.05 0.06 0.06	0.38 0.49 0.90
<b>Type of data</b>	3D seismic data	Bathymetry data	Bathymetry data	Bathymetry data
<b>Horizontal resolution</b>	12 m	100 m	100 m	100 m
<b>Vertical resolution</b>	< 10 m	30 m	< 40 m	30 - 40 m
<b>Coordinate System</b>	Magna Colombia Bogota	World Mercator	World Mercator	World Mercator

### *Magdalena Channel*

The Magdalena Channel section with a length of 56 km, at a water depth between 1566 m to 2320 m and a slope of 13.2 m/km is situated South-West on the Magdalena fan (area: ~237,000 km<sup>2</sup>; Idárraga-García *et al.*, 2019), offshore Colombia in the Caribbean Sea (Figure 3.3). The Magdalena Fan started to form during the late Miocene and its formation is linked to the

Magdalena River and is affected by tectonics since the Pliocene (Romero-Otero *et al.*, 2015; Idárraga-García *et al.*, 2019). Tectonically, the fan is situated on its southern side on a convergent margin and is divided between the Southern (SSBF) and Northern Sinu Folt Belt (NSBF). The analysed channel section is close to the SSBF. Major delta shifts created a fan which becomes younger toward the southwest. The studied channel section is part of the upper and middle part of the CLC-IIc4 Channel (Romero-Otero *et al.*, 2015). The upper part of the channel and the majority from the studied channel section is erosionally controlled with steep walls and a U-shaped profile. The middle to lower channel part (from 2000 m water depth) is controlled by aggradation, and external levees are present (Romero-Otero *et al.*, 2015). The change from erosional to aggradation dominated channel section is at around 54 km downstream, and a change of slope, interpreted as a knickpoints, is present between 10 and 20 km downstream of the channel section (Romero-Otero *et al.*, 2015). The Magdalena Channel is classified as a submarine-fan channel.

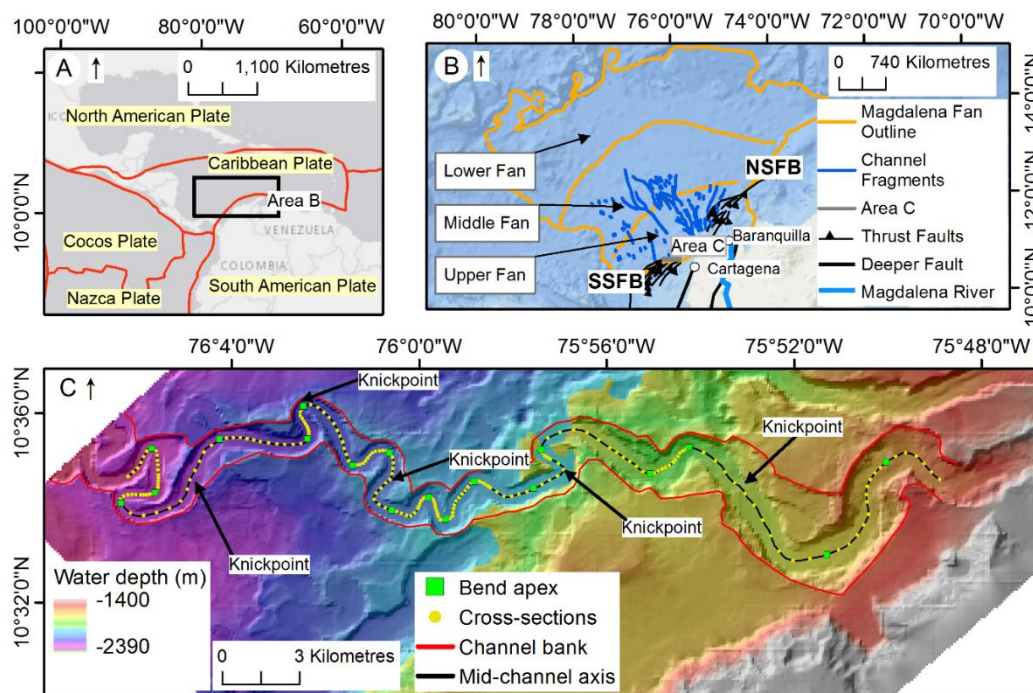


**Figure 3.3** Location and tectonic setting of the Magdalena Channel. A) The channel is located in the Caribbean Sea, offshore Colombia, where the Caribbean Plate converges with the South American Plate (Map data: Esri). B) The Magdalena Fan (Fan extent: Idárraga-García *et al.*, 2019) is between the Southern (SSBF) and Northern Sinu Folt Belt (NSBF).

The channel is part of a complex channel system (channel fragments from Kolla and Buffler (1984) and Ercilla *et al.* (2002)) and situated at the upper fan on the Southern Sinu Folt Belt (SSBF). C) Top surface of a 3D seismic survey with a horizontal resolution of approximately 15 m. In total, the channel section consists of 17 bends and a total of 217 cross-sections. DTM produced from seafloor horizon from a 3-D seismic survey – © Equión Energía Limited, Ecopetrol S.A. and Petrobras.

---

### *Bryant Channel*

The Bryant Channel (Figure 3.4) is situated on the continental rise after the Sigsbee Escarpment, off the Bryant Canyon at a water depth between 3100 and 3200 m in the Gulf of Mexico. The north-western continental slope off Texas and Louisiana in the Gulf of Mexico is controlled by salt tectonics with intraslope basins (Bryant *et al.*, 1990). Multiple canyons (e.g., Alaminos, Keathley, Bryant and Northern Canyon; Lee *et al.*, 1996) incise the salt-controlled continental slope. Bryant Canyon started to form 135 ka (Marine Isotope Stage 6; Tripsanas *et al.*, 2007) during a glaciated period when an ancient shelf-margin Mississippi River delta started to form (Tripsanas *et al.*, 2007). Turbidity currents were initiated by delta failures, storms and especially river discharge, which lead to the formation of a fan on the continental rise after the Sigsbee Escarpment. The Bryant fan, which is fed by the Bryant Canyon, is smaller than the Mississippi Fan and occurs at a water depth between 2600 m to 3200 m. The channel is highly erosional (Lee *et al.*, 1996; Twichell *et al.*, 2000). An analysis of mapped global canyons around the world, based on Google-Earth (data sources: SIO, NOAA, US Navy, NGA, GEBCO), classified the studied section as part of the Bryant canyon (de Leo *et al.*, 2010), but because of its location on the fan and its interpretation in previous studies the section analysed herein is classified as a submarine-fan channel.

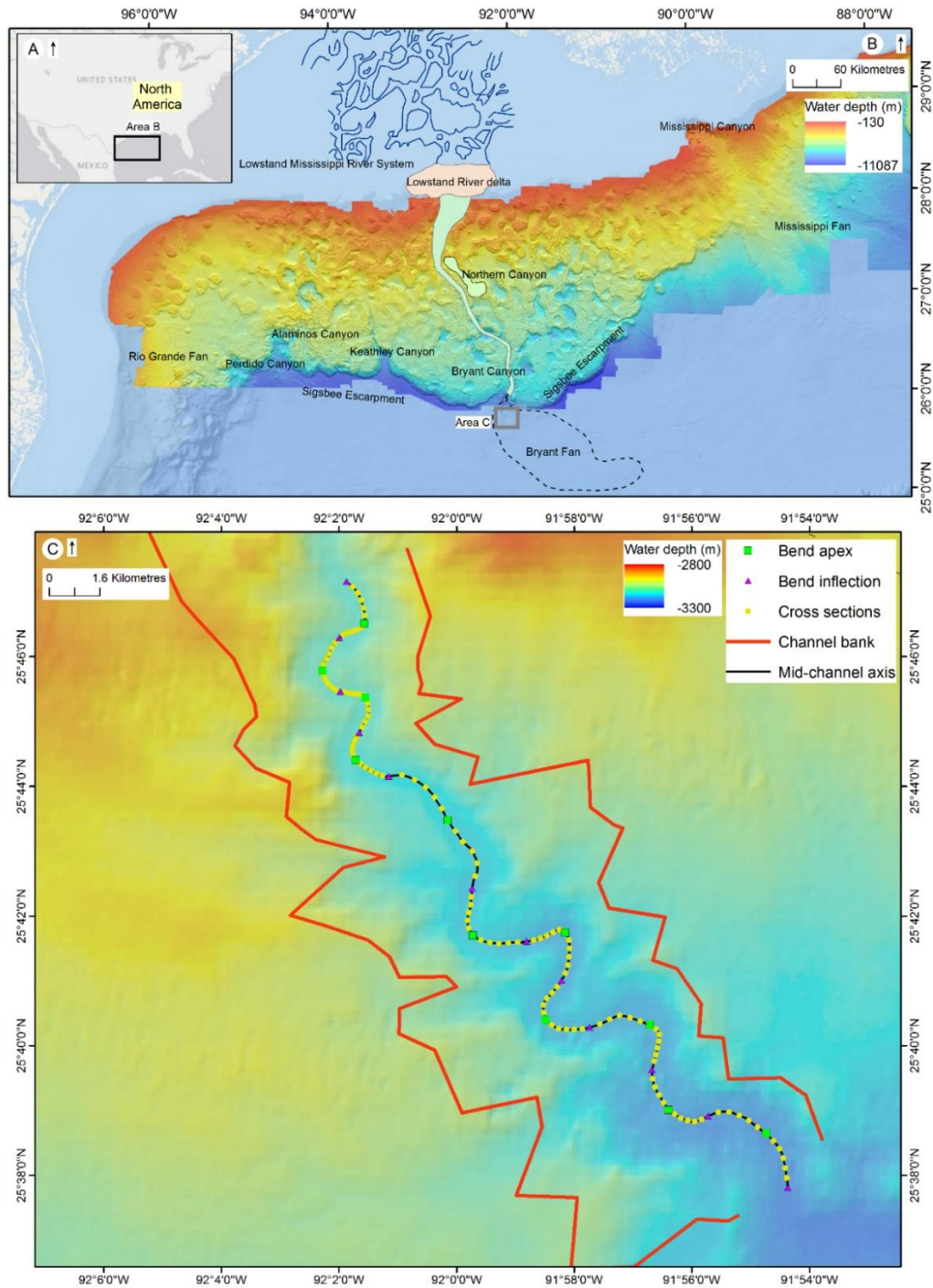


**Figure 3.4** Location of the Bryant Channel. A) The channel is located in the Gulf of Mexico (Map data: Esri, Basemap from BOEM). B) Bathymetric map of the north-western Gulf of Mexico showing the location of the Bryant canyon and fan with the position of the low stand Mississippi River and delta position (Suter and Berryhill, 1985). Fan outline and canyon location from Lee *et al.* (1996) and Twichell *et al.* (2000). C) Location of Bryant Channel section with 133 cross-sections. DTM data from Law of the Sea U.S. UNCLOS Bathymetry Project.

*Surveyor, Horizon and Baranof*

Three channel sections, the Surveyor, Horizon and Baranof Channels, are situated in the Gulf of Alaska (Figure 3.5). The channels are situated on two submarine-fans, which are the Surveyor (fan area:  $342 \times 10^3 \text{ m}^2$ , fan volume:  $680 \times 10^3 \text{ m}^3$ ; Reece *et al.*, 2011) and Baranof Fan (fan area:  $323 \times 10^3 \text{ m}^2$ , fan volume:  $301 \times 10^3 \text{ m}^3$ ; Walton *et al.*, 2014). The fans are controlled by tectonics and glaciated erosion (Ness and Kulm, 1973; Walton *et al.*, 2014; Zhang and Gulick, 2019), and have no direct river input but are fed from glacial erosion from the Chugach–St. Elias mountain range and additionally controlled by earthquakes (Walton *et al.*, 2014; Zhang and Gulick, 2019).

The Surveyor Fan is aligned to the north-west with the Aleutian Trench and to the north-east with the Baranof Fan. The Baranof Fan is aligned to the north-west to the Surveyor Fan and is controlled by a transform fault, the Fairweather Fault, to the north-east (Reece *et al.*, 2011; Zhang and Gulick, 2019). The north-eastern margin of the Gulf of Alaska is controlled by transition faults (Queen Charlotte and Fairweather Fault) with a north-south direction, shifting the oceanic plate towards the north. The north-western margin of the Gulf of Alaska is controlled by a subduction zone, forming the Aleutian Trench (Gulick *et al.*, 2007; Reece *et al.*, 2013). The major channel systems are away from the Aleutian Trench the Surveyor and Chirikof Channels on the Surveyor Fan and on the Baranof Fan the Baranof, Horizon and Mukluk Channels. The studied channel sections are part of the Surveyor and Horizon channel systems.

The Surveyor Channel originates from four tributaries called: Icy West Leg, Icy East Leg, Yakutat Leg and Alsek Leg (Reece *et al.*, 2011) and terminates in the Aleutian Trench south of Kodiak Island, Gulf of Alaska (Ness and Kulm, 1973; Reece *et al.*, 2011; Zhang and Gulick, 2019). The present channel section with a length of 244 km is part of the Alsek Leg tributary at a water depth between 3576 m and 3815 m, but for simplicity is here called Surveyor Channel. Given the direct connection between the Surveyor

Channel and the Aleutian Trench, it is classified here as an isolated deep-ocean channel.

The Horizon Channel is highly sinuous; whereas the Baranof Channel is located immediately to the east and is straight (Gardner and Mayer, 2005). The Horizon and Baranof channels are more difficult to classify; as has been previously noted that channels in the Gulf of Alaska are exceptionally large compared with many submarine channels (Shumaker *et al.*, 2018), and they are strongly erosional in their upper reaches. The straight channel section of the Baranof Channel has also been classified as a canyon based on automated ArcMap analysis (Harris and Whiteway, 2011). The Baranof Fan that they feed is amongst the largest deep-sea fans on Earth, equivalent in size to the Amazon Fan (Reece *et al.*, 2011; Walton *et al.*, 2014; Zhang and Gulick, 2019). However, the feeder channels are much larger than those on river-fed fans such as the Amazon and Bengal Fan (Shumaker *et al.*, 2018) presumably reflecting their sediment source from glacial output from the Cordilleran Ice Stream (Zhang and Gulick, 2019). In the present analysis, the Horizon and Baranof Channels are included with the isolated deep-ocean channels as they have closer characteristics to these than with river-fed submarine fan channels. Globally, there is an absence of similar sized glacially-driven deep-sea fans that have multibeam coverage, but it may be the case that such channels may require a separate classification of their own. Certainly, including them with river-fed submarine-fan channels will greatly skew the combined data.

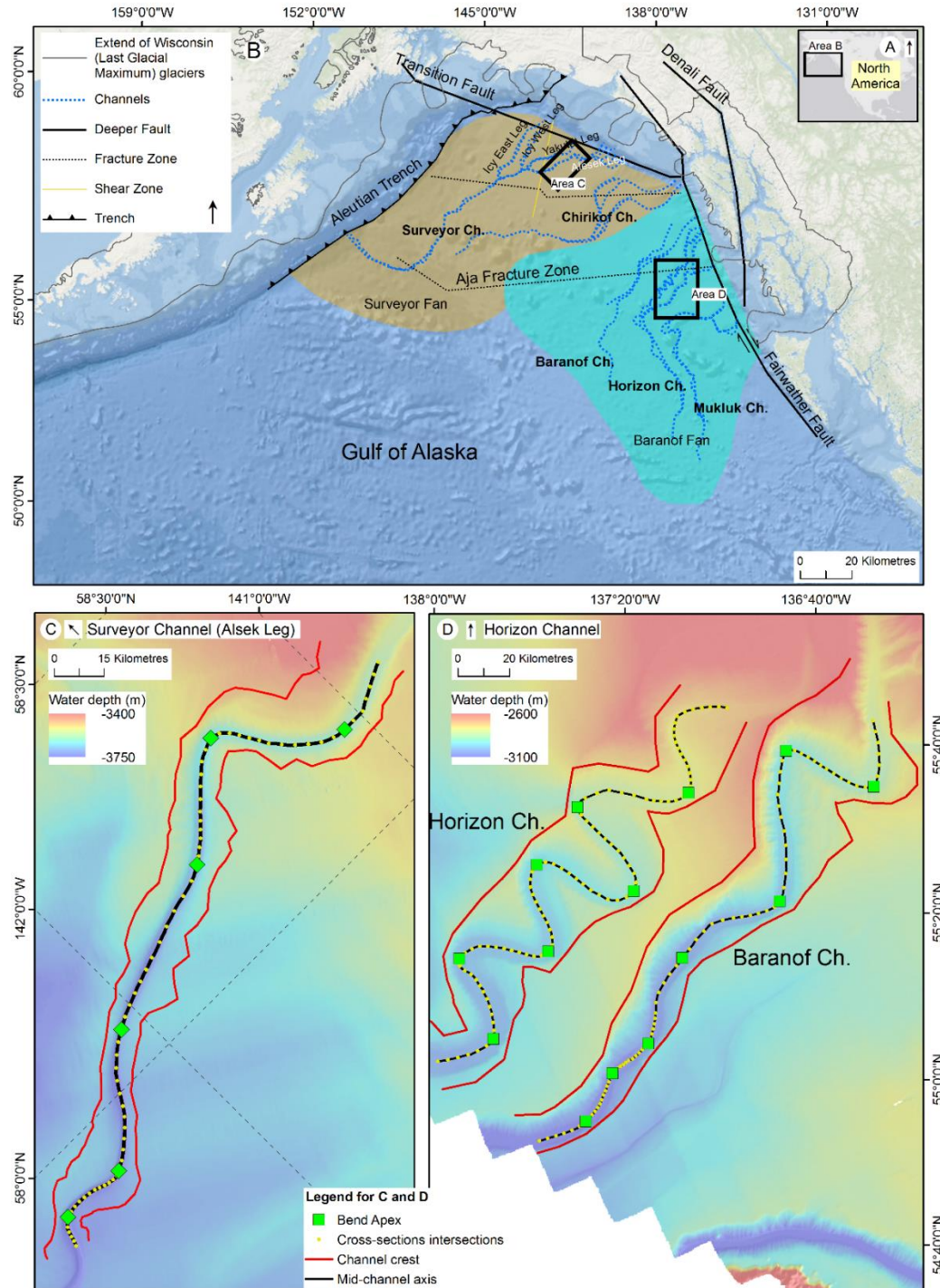


**Figure 3.5** Tectonic setting and channel locations from Surveyor, Baranof and Horizon Channel. A) The channels are situated in the Gulf of Alaska. B) Tectonic and channel extent derived from: Reece *et al.* (2011, 2013); Walton *et al.* (2014); and Zhang and Gulick (2019). Fan extensions from Walton *et al.* (2014). C) Location of Surveyor Channel with 73 cross-sections and D) Location of Baranof with 85 cross-sections and Horizon Channel with 97 cross-sections. Map data: Esri, Basemap. DTM data from Law of the Sea U.S. UNCLOS Bathymetry Project.

### *Mariana Channel*

Multiple channels are incising seamounts on the western flanks of the West Mariana Ridge west of the Mariana Trough in the Parece Vela Basin (Figure 3.6; Gardner, 2010). The Mariana Ridge separated two basins: the actively spreading back-arc Mariana Trough basin to the east, and the Parece Vela Basin to the west (Okino *et al.*, 1998). The west-facing flank has gentle slopes ( $3^{\circ}$ - $4^{\circ}$ ) in comparison to the east-facing flank of the Mariana Ridge, and is covered by volcanic apron sedimentation. Channels are possibly created by sediment erosion from volcano flanks (Gardner, 2010). Three channel sections were analysed: Mariana Channels A, B, and C, and are classified as non-margin ocean channels, giving its location on the West Mariana Ridge far away from any terrestrial sediment input.



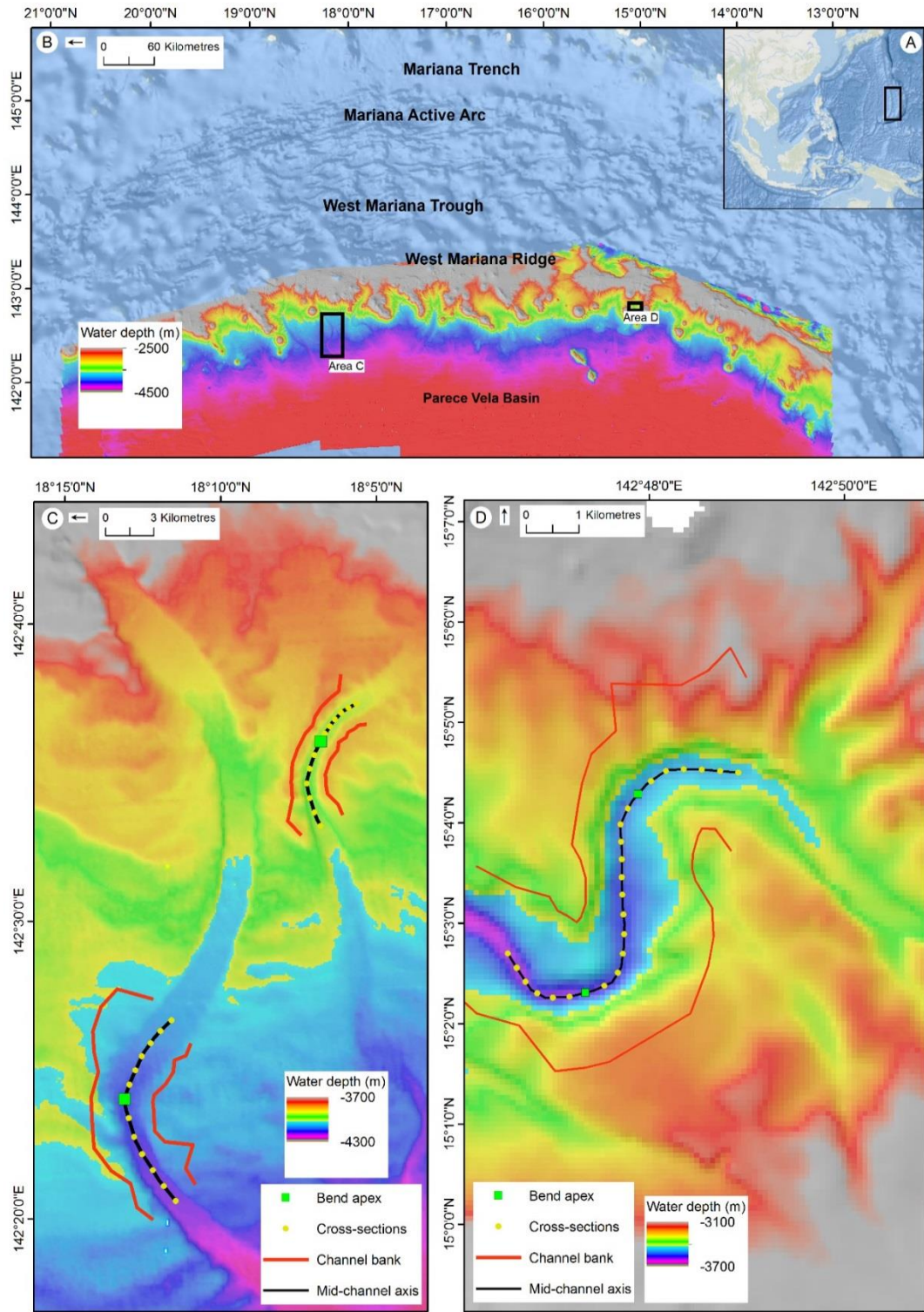


**Figure 3.6** Location of the studied Mariana Channels on the West Mariana Ridge. Map data: Esri, Basemap. DTM data from Law of the Sea U.S. UNCLOS Bathymetry Project.

### 3.3.1 Analysis of channel parameters

Channel parameters of mean width, mean height, bed width, area, aspect ratio and cross-sectional shape were obtained for each cross-section perpendicular to the channel centreline. The channel centreline was mapped in ArcGIS from a digital elevation model and was defined as the middle line of the channel bed. Along the centreline, bend apices were defined as positions of maximum curvature. Between two bend apices, an inflection point was identified as a position of minimum curvature. Perpendicular cross-sections to the centreline were extracted at the bend apex, at the inflection point and at six equally spaced positions between the bend apex and the inflection point, therefore 13 cross-sections were extracted in total from bend apex to the next bend apex.

#### *Width and depth*

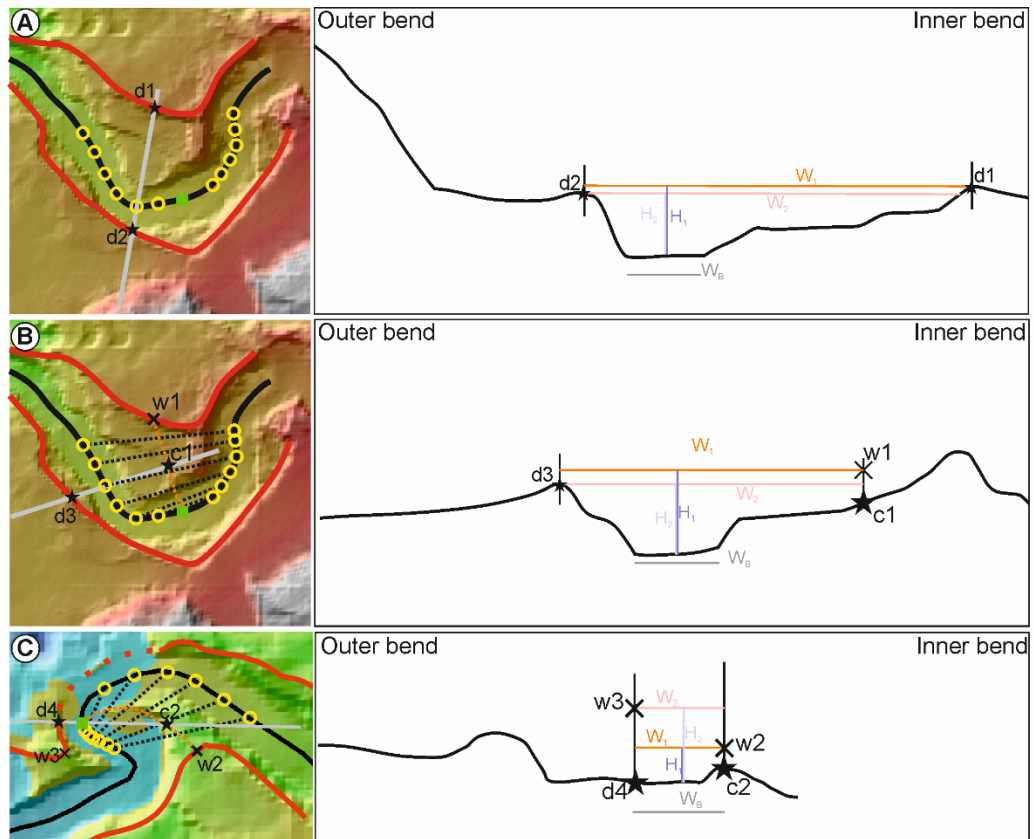
Previous studies defined channel parameters of width and height as “bankfull” width and height in analogy to cross-sectional measurements in rivers (Clark *et al.*, 1992; Pirmez and Imran, 2003; Konsoer *et al.*, 2013). Bankfull width and height in rivers are measured according to a reference, often bankfull level (Leopold and Maddock, 1953; Leopold and Wolman, 1960) defined as the level where maximum discharge occurs without flow overtopping the banks (Wahl, 1984; Copeland *et al.*, 2000). Consequently, bankfull level is commonly based on external parameters such as position of the active floodplain, change of vegetation and sedimentation, highest position of channel bars or position of active scours (Osterkamp and Hedman, 1977; Williams, 1978; Wahl, 1984; Johnson and Heil, 1996; Montgomery and Gran, 2001) and may represent the mean or maximum flow discharge of a river. Bankfull width is defined as the maximum distance of the bankfull level, and bankfull height is defined as the mean or maximum distance between the channel bed and bankfull level (Richards, 1982). However, the term “bankfull level” is misleading for submarine channels for two reasons. Firstly, channel banks in submarine channels often show a strong bank asymmetry with one channel

bank being taller than the other bank (e.g. Klaucke *et al.*, 1998a) hence the maximum discharge would always be at the lower bank as otherwise it would always overflow which would underestimate the flow discharge. Secondly and crucially turbidity currents become more dilute away from the channel bed and hence a defined boundary between the flow forming the channel and its ambient water may be weak (Hampton, 1972; Kneller and Buckee, 2000; Hansen *et al.*, 2015). Hence, the term “bankfull” width or height is not used here.

Channel width, for non-complex topography, was measured as the mean distance between channel banks (Figure 8A, mean of channel bank width ( $W_1$  and  $W_2$ )), rather than being measured as the maximum distance between channel banks (Babonneau *et al.*, 2002; Pirmez and Imran, 2003; Konsoer *et al.*, 2013; Shumaker *et al.*, 2018). Similarly, channel height (Figure 3.7A) was measured as the vertical distance between the channel bed and the mean elevation of the two channel banks (Figure 3.8A, mean of channel bank height ( $H_1$  and  $H_2$ ), see Appendix A, Section 4.5.2). For aggradational channels, channel banks are defined as the levee crests, which are the maximum point of aggradation and the highest point of the external levee (Kane and Hodgson, 2011; Hansen *et al.*, 2015). For channels with poorly developed or no levees the crest line was defined as the point where channel banks level-off relative to the surrounding seafloor, hence the rollover point between the cut bank and the surrounding seafloor (Shumaker *et al.*, 2018). Due to the nature of complex topography in submarine channels, particularly in the case of complex bend geometry or where bank failure occurred, the protocol for channel width and depth measurements needs to be adapted to avoid excluding any cross-sectional measurements (Figure 3.7B,C). Complex bend geometry occurred for tight bends with a low radius of curvature or where terraces were present at the inner bend (Figure 3.7B). In such cases, topography in the inner bend region was lower than the channel banks and therefore cross-sections at certain orientations will overestimate width. In extreme cases, this could lead to the channel being measured twice, on both sides of the meander neck (see orientation of section in Figure 3.7B). In the presence of terraces at the inner bend region, the channel width was the mean

of the outer bank crest to the trajectory line (Width between d3 and c1 in Figure 3.7B). The trajectory line was equivalent to the trajectory line used in the analysis of river meanders (Russell, 2017; Russell *et al.*, 2019; see Appendix A), but instead of following the migration of scroll bars, as no scroll bars were identified in these submarine channels, the trajectory line was a line at the inner bend, representing the mean distance between opposite cross-section points and the bend apex (orange dashed line in Figure 3.7B,C). The mean depth was the distance from the channel bed to the average elevation of the banks; these are defined as the outer channel bank (Figure 3.7B, Position d3) and the position where the trajectory line would intersect with the channel bank crest (Figure 3.7C, Position w1). Channel bed width ( $W_B$ ) was measured for each cross-section as the width of the flat surface between the positions where channel gradient starts to abruptly increase to create the channel walls.

Channel bank failure occurs for channels with or without levees, and this can cause the bank crest to have a lower topography than it would otherwise have had, thus leading to an underestimation of channel depth. In the example illustrated in Figure 3.7C, the bank failure occurred at the outer bend, and at the inner bend a terrace is present as in the previous example. Mean channel width was measured between the primary position of the channel bank prior to bank failure at the outer bend and the trajectory line at the inner bend (distance between position d4 and c2 in Figure 3.7C). Mean channel depth was measured between the channel bed and the position where the trajectory line intersects with the channel bank at the inner bend (w2) and the nearest position where the channel bank did not fail at the outer bank (w3). Any combination of the examples was possible and can be adapted according to the position and nature of the cross-section.



**Legend**

Central line		$W_b$	Channel bed width
Bend apex		$H_1, H_2$	Height of outer and inner bank
Cross-section		$W_1, W_2$	Width at outer and inner bank
Position of cross-sections		$c_1, c_2$	Position of cross-section at bend trajectory
Intact channel bank		$w_1, w_2, w_3$	Water depth at channel bank
Damaged channel bank		$d_1, d_2, d_3, d_4$	Position of cross-section at channel bank
Joined up-stream and down-stream cross-section position			
Bend trajectory			

**Figure 3.7** Three approaches for extracting channel width and height from a cross-section, a non-complex (Case A), and complex topography (Case B, C) in submarine channels. The approach adopted depends on the position of the cross-section in relation to the channel bank: A) Cross-section measured from channel bank to channel bank; B) Cross-section measured from channel bank to terrace; or, C) Cross-section measured from failed channel bank to terrace. Examples are shown from the Magdalena Channel.

### *Aspect ratio, channel bed width and cross-sectional area*

The aspect ratio for each cross-section was the ratio between mean width ( $\bar{W} = \frac{(W_1+W_2)}{2}$ ) and mean height ( $\bar{H} = \frac{(H_1+H_2)}{2}$ ), which was a point of equal interception of the two parameters for each cross-section.

Two approaches exist in the literature to calculate the cross-sectional area. Firstly, considering the cross-sectional shape to be rectangular in analogy to rivers with the approach:

$$Area_{Rectangular} = W_{max} \times \bar{H},$$

whereby  $W_{max}$  is the maximum channel width and  $\bar{H}$  is the mean height (e.g., Konsoer *et al.*, 2013; Shumaker *et al.*, 2018). Secondly, considering the cross-sectional shape to be trapezoidal with the formula:

$$Area_{Bed} = \frac{(W_B + \langle \bar{W} \rangle)}{2} \times \bar{H},$$

whereby  $W_{Bed}$  is the channel bed width,  $\bar{W}$  is the mean channel width and  $\bar{H}$  is the mean channel height (e.g., Hesse *et al.*, 1987; Fierens *et al.*, 2019). Since, submarine-channels have a dominantly trapezoidal shape, the second approach was used. Additionally, the first approach was adapted in order to compare datasets from the literature obtained assuming the rectangular case, to the second approach:

$$Area_{Simple} = \frac{(\bar{W} * \bar{H})}{2}.$$

### *Cross-sectional shape*

In addition, the shape of the cross-section was measured in order to quantitatively identify whether channels and channel types can be classified as either “U” or “V”-shaped cross-sections, or where on the continuum between the two they lie. Only cross-sections that reached from intact crest to intact crest were included in order to consider a precise cross-sectional shape interpretation. Here, the cross-sectional shape of submarine channels was calculated using a quantitative approach by using the General Power Law Program (<sup>G</sup>PL; Pattyn and Van Huele, 1998). The General Power Law

Program is based on the power law model, which was introduced to define the degree of glacification for glacial troughs (Svensson, 1959). Glacial troughs generally have a “U”-shaped cross-section, whereas troughs that underwent less glaciation tend to have a “V”-shaped cross-section (Harbor and Wheeler, 1992). The General Power Law Program has been extended beyond glacial troughs and has been widely used to examine the morphology of submarine gullies (Gales *et al.*, 2012, 2013; Swartz *et al.*, 2015). The General Power Law Program is based on the general power law equation:

$$y - y_0 = a|x - x_0|^b,$$

where “x” and “y” are the input arguments which correspond to the cross-sectional shape. “X”-values represent the length along the cross-section and “y”-values represent the depth of the cross-section in a submarine channel cross-section. The variables “x<sub>0</sub>” and “y<sub>0</sub>” correspond to the inflection point of the cross-section. The variables “a” and “b” are constant values, which are calculated by the program through the other parameters (y, x, x<sub>0</sub>, y<sub>0</sub>). The variable “b” represents the cross-sectional shape (Figure 3.8), whereby only positive values of the variable “b” are possible and is calculated by the minimum RMS misfit between the observed and calculated cross-section. A value of 0 ≤ b < 1 represents a convex-upward shaped cross-section (Figure 3.8a), a value of b = 1 represents a “V”-shaped cross-section (Figure 3.8b), a value of 1 < b ≤ 2 represents a “U” or parabolic-shaped cross-section (Figure 3.8c) and a value of b > 2 represents a box-shaped cross-section (Figure 3.8d), whereby a b-value closer to two represents a narrow box-shaped cross-section and a b-value further away from two represents a wider box-shaped cross-section.

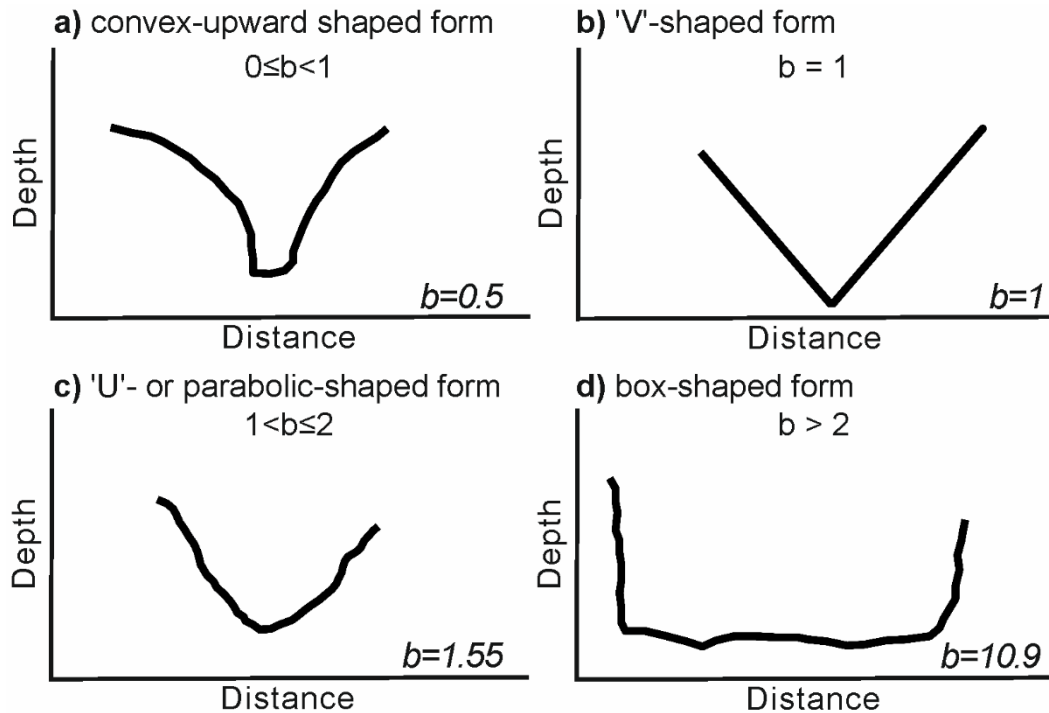


**Figure 3.8** Examples of cross-sectional shape (U/V index) and related b-values obtained through the General Power Law program: a) convex-upward shaped form,  $0 \leq b < 1$  (Example from Vidal Channel; Embley *et al.*, 1970); b) 'V'-shaped form,  $b = 1$ ; c) 'U'-shaped form,  $1 < b \leq 2$  (Example from Brunei Channel; Straub *et al.*, 2012); d) box-shaped form,  $b > 2$  (Example from Tanzania Channel; Bourget *et al.*, 2008).

### *Channel section length*

Submarine channel length is different between studied channel sections and hence the data are presented in two ways: a) with down-stream distance to compare channel parameters for a given channel section, and b) a normalised down-stream distance to compare different channel sections with each other. Three approaches exist to normalise the down-stream distance: firstly, on the basis of the channel/canyon length from canyon/channel head to the point of confinement, secondly from canyon/channel head to the point, where channel gradient reach gradients  $< 0.25^\circ$  and down-stream gradient is between  $-10^{-7}$  and  $10^7$  (Covault *et al.*, 2011), or thirdly by the maximum stream distance. For the first and second approach, the whole channel length needs to be known, but here only channel sections were studied hence the third approach was used:



$$\text{Normalised downstream distance} = \frac{\text{Stream distance}}{\text{Maximum downstream distance}},$$

whereby the start of the channel section represents 0, and the end of the channel section represents 1.

### 3.3.2 River dataset

Cross-sectional width and depth parameters from rivers were compiled from previous published literature (Table 3.2; Leeder, 1973; Van den Berg, 1995; Jerolmack and Mohrig, 2007; Whittaker, 2007; Wohl and David, 2008; Yanites *et al.*, 2010; Wilkerson and Parker, 2011): 358 measurements from alluvial and 293 measurements from bedrock rivers. The measurements are either from one cross-section or reach-averaged values from multiple cross-sections. Only single-thread rivers from meandering channels rather than straight channel sections were considered for the alluvial river dataset. The following references were used for the alluvial-river dataset: A1. Jerolmack and Mohrig (2007); A2. Leeder (1973); A3. Van den Berg (1995) and A4. Wilkerson and Parker (2011). Four data points were used from single meandering channels from Jerolmack and Mohrig (2007). All 57 data point from Leeder (1973) were used and were measured with a standardised methodology: one width and depth measurement at each bend. The width was measured between point bar top and the cut bank. The depth was measured perpendicular to the width into the channel thalweg. Only cross-sections from meandering rivers were taken from Van den Berg (1995). Alluvial river dataset from Wilkerson and Parker (2011) contained 219 data points from stable single-thread rivers and have been obtained from a wide range of literature. The dataset was previously used in a comparison of the morphometrics between rivers and submarine channels (Konsoer *et al.*, 2013). The bedrock-river data were obtained from mountain rivers from the following literature: B1. Wohl and David (2008); B2. Whittaker (2007); and B3. Yanites *et al.* (Yanites *et al.*, 2010). Reach-averaged width and depth measurements were obtained from Wohl and David (2008). The dataset included a wide range of bedrock rivers (step-pool, plane-bed or pool-riffle rivers; Wohl and Merritt, 2008). The

Whittaker (2007) data contained 158 data points from three tectonic-controlled rivers (Fosso Tascino, Rio Torto, Valleluce River) in the Italian Apennines. The width was measured with a hand-held laser range-finder and the depth is measured with a tape measure (width and depth precision: 1 cm) and were measured at least every 300 m downstream for each river. The measurements are equivalent to a high flow width which was recognised from the limits of active abrasion or vegetation, the highest level of bleaching on boulders and water-washed surfaces, and high stage flood debris Whittaker (2007). 89 data points from Yanites *et al.* (2010) were obtained from a stable tectonically controlled river in Taiwan.

**Table 3.2** Summary for the river dataset.

\* *Data source: A1. Jerolmack and Mohrig (2007); A2. Leeder (1973) Leeder (1973); A3. Van den Berg (1995); A4. Wilkerson and Parker (2011); B1. Wohl and David (2008); B2. Whittaker (2007); and B3. Yanites et al. (2010).*

Source*	No. of Cross-sections	No. of Rivers	How was the width obtained?	How was the depth obtained?
A1	4	4	Directly from literature	Directly from literature
A2	57	?	Between point bar top and the cut bank (bend apex, max. width around bend)	Between point bar top and the cut bank (bend apex, max. width around bend)
A3	78	78	Between point bar top and the cut bank (bend apex, max. width around bend)	Between point bar top and the cut bank (bend apex, max. width around bend)
A4	219	?	Directly from literature	Directly from literature
B1	46	37	- Average values of a river reach (reach is ten times the peak annual flow channel width with consistent gradient and geometry) - width for maximum flow through paeleo-stage indicators	Directly from literature
B2	158	3	Measured every 300 m downstream for each river at max flow stage using palaeostage indicators	- Average values of a river reach (reach is ten times the peak annual flow channel

			(vegetation, rock abrasion, discolouration of bedrock) with a hand-held laser range-finder	width with consistent gradient and geometry) - Height for maximum flow through palaeostage indicators
B3	89	1	Measured every 300 m downstream for each river at max flow stage using palaeostage indicators (limits of vegetation, rock abrasion, discolours of bedrock) with a hand-held laser range-finder	Measured every 300 m downstream for each river at maximum palaeostage indicators ( limits of vegetation, rock abrasion, discolours of bedrock) with a tape measure

### 3.3.3 Statistical analysis

Parameters of aspect ratio, cross-section shape and cross-sectional area between channel types are presented as box and whisker plots, cumulative distribution and kernel density estimation (Figure 3.9). Box and whisker plots (Figure 3.9a) identify a normal distribution with outliers (extreme values in regards to the average value within the dataset) in the dataset, whereby the lower and upper box borders represent the 25<sup>th</sup> (Q1) and 75<sup>th</sup> (Q3) percentiles, “+” identifies the median, “o” identifies the mean, whiskers indicates 99.3 % of the data in a normal distribution, and “x” indicates outliers. Outliers were identified as followed: a) if the outliers were larger than Q3 by more than  $Q3+(Q3-Q1)*1.5$  or b) if the outliers were smaller than Q1 by less than  $Q1-(Q3-Q1)*1.5$ .

The cumulative distribution, histogram and kernel density estimation is used to visualise the distribution of the data. The histogram (Figure 3.9b) and kernel density estimation (Figure 3.9d) are used to compare the cross-sectional shape and area between types. The histogram is the simplest form to represent the density estimation from an observed dataset. A more robust analysis to measure probability density function (pdf) is the kernel density

estimation. The kernel density estimator is defined for a data range  $(x_1, x_2, \dots, x_n)$  with a kernel,  $K$ , a window function, defined by:

$$\hat{f}(x) = \frac{1}{nh} \sum_{i=1}^n K\left(\frac{x-X_i}{h}\right),$$

where the parameter  $K$ , defines the interval range, and the parameter  $h$  is defined as the smoothing parameter or band width. Here, a kernel of a normal distribution and a bandwidth, which is assumed to be the optimal bandwidth for an underlying normal distribution of the dataset is chosen. The kernel density estimation can be imagined as multiple bars joined together, whereby the kernel function  $K$  represents the overall shape and the band width of the bars. If  $h$  increases too much, or is reduced too much, individual clusters of data will be not visible. Another problem is for a data distribution with a long-tailed distribution. Noise will appear at the end of tail, because of a fixed band width. For the above reasons, the histogram is used to identify any noise in the data of the kernel density estimation. Additionally, the kernel density estimation is used to identify the position, where the maximum distribution per channel type occurs for both channel shape and area and identify any differences between channel types. The cumulative distribution (Figure 3.9c) is useful to see how many data parameters are less or greater than a certain value, or between two values, and is used to compare the data distribution of width, depth and aspect ratio between channel types. The cumulative distribution function (cdf) estimates the probability that a value is less or equal to  $x$  and can be expressed as the integral of its probability density function:

$$F(x) = P(X \leq x) = \int_{-\infty}^{\infty} f(x)dt.$$

The cumulative distribution plot represents on the x-axis the probability with values between 0-1 and on the y-axis the range of the given probability function.

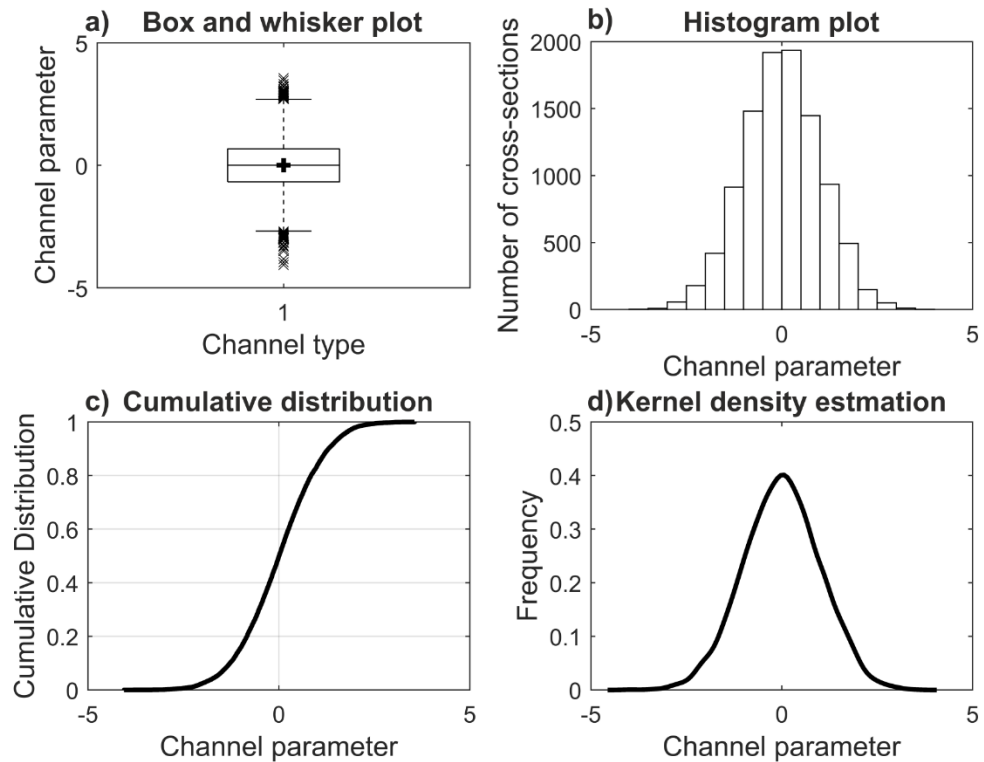


**Figure 3.9** Representation of a random dataset (range: -4.0 to 4.0) with a normal distribution. Mean and median are at 0. a) Box and whisker plot, b) Histogram plot with a histogram interval of 0.5, c) Cumulative distribution, and d) Kernel density estimation. For the box and whisker plot: the plot within each box indicates the median value, “+” indicates the mean, box ends are the 25<sup>th</sup> and 75<sup>th</sup> percentiles, whiskers represent 99.3 % in a normal distribution, and x indicates outliers. Data produced in MatLabR2016a.

### 3.4 Results

Channel parameters were examined for each channel, and then compared between channel types, prior to comparing these submarine channels with fluvial channels.

### 3.4.1 Comparison between channels within a channel type

#### *Submarine-fan channels (Magdalena Channel and Bryant Channel)*

Magdalena Channel and Bryant Channel are categorised as submarine-fan channels. Channel width (Figure 3.10B) decreased downstream for the Magdalena Channel from 2 km to 1 km. By contrast, the Bryant Channel had a variable channel width downstream ranging from 2 to 10 km with an average increase downstream. Channel height (Figure 3.10C) decreased downstream for the Magdalena Channels from 120 m to 90 m and for the Bryant channel from 150 to 100 m. Aspect ratio (Figure 3.10D) followed the trend of the channel width. Aspect ratio for the Magdalena Channel decreased downstream from 20 to 10, but aspect ratio for the Bryant Channel ranged from 5 to 125 with a mean increase from 25 to 60 over a length of 35 km. The cross-sectional shape was different between the two channels. The cross-sectional shape for the Magdalena Channel changed from a box-shaped to a “V”-shaped cross-section downstream, whereas the Bryant Channel was variable ranging from 0.3 (convex-upward shaped form) to 3.3 (box-shaped form) with one at 5.1 and a median of 1.3 (parabolic-shaped form) with no trend being identified downstream (Figure 3.10D). Cross-sectional shape for the Bryant Channel varied in general from a more box-shaped form to a parabolic-shaped form (“U”-shaped) downstream.

Internal variations of channel parameters for the Magdalena Channel are explained by the presence of knickpoints. Two large knickpoints were identified at 10 km and 20 km down-stream, and two small knickpoints were identified at 35, 40 and 52 km down-stream (Figure 3.10A). Channel parameters of width, height and aspect ratio increased (Figure 3.10B-D), and cross-section shape (Figure 3.10E) changed from a V-shaped to box-shaped cross-section at the first knickpoint and the three smaller knickpoint further downstream. After the knickpoint, channel parameters adjusted back to their values prior to the knickpoint. At the second knickpoint, channel width

decreased, channel height increased, aspect ratio decreased, and cross-sectional shape changed from a “V”-shaped to a box-shaped cross-section.

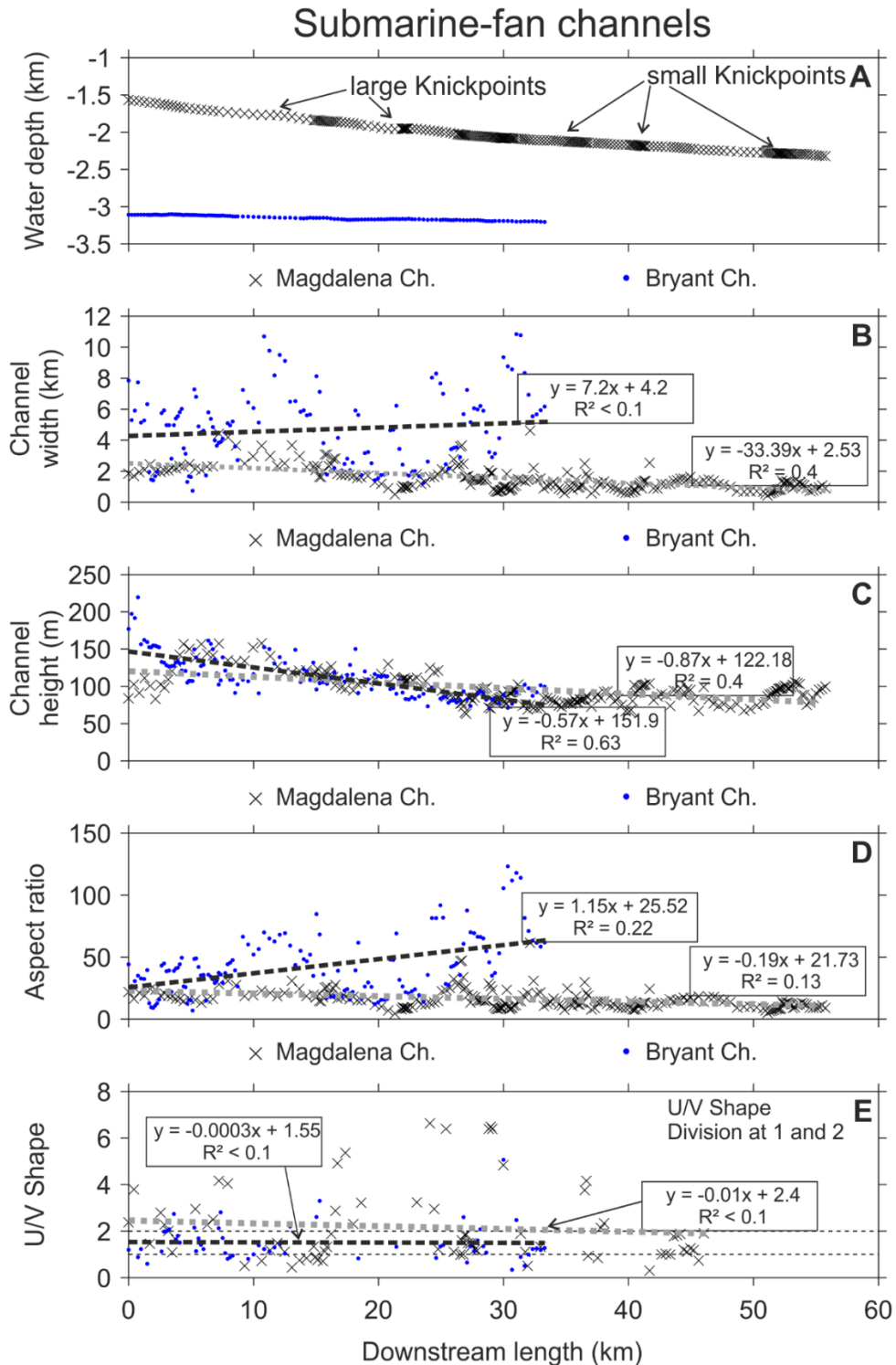


**Figure 3.10** Submarine-fan channel (Magdalena Channel: black cross, Bryant Channel: blue dot): (A) Longitudinal depth profile (Channel central line). (B) Channel width. (D) Channel height, (E) Cross-sectional shape with division at 1 and 2. Values of shape refer to: shape

< 1 convex-upward shaped form, shape = 1 "V"-shaped form, shape < 1 and shape  $\leq$  2 "U"- or parabolic-shaped form, shape > 2 box-shaped form.

---

*Isolated deep-ocean channels (Surveyor, Horizon, Baranof)*

Three isolated deep-ocean channels (Surveyor, Horizon and Baranof channels) occurred at a water depth between 2.8 km and 3.8 km (Figure 3.11a). Channel width for all three channels was between 10 and 46 km (Figure 3.11b). Channel width decreased downstream for the Baranof and Surveyor Channel and increased downstream for the Horizon Channel. The mean channel width was similar between the three channels with a mean channel width of 19.66 km for the Baranof Channel, 12.25 km for the Surveyor Channel, and 18.25 km for the Horizon Channel.

Channel height (Figure 3.11b) varied between 60 m and 230 m for all isolated deep-ocean channels. Channel height decreased downstream for Baranof Channel and Surveyor Channel and increased downstream for Horizon Channel. The maximum channel height was identified for the Baranof Channel with a mean channel height of 194.37 m. The Surveyor Channel has a mean channel height of 100.29 and the Horizon Channel has a mean channel height of 108.72 m. Aspect ratio (Figure 3.11d) for isolated deep-ocean channels ranges from 60 to 380 and decreases downstream for all three channels. Mean aspect ratio was for the Baranof Channel 100.78, for the Surveyor Channel 120.87 and for the Horizon Channel 174.27. The cross-sectional shape (Figure 3.11e) ranged from convex-upward (shape=0.6) to box-shaped (shape=2.2) with a mean of 1.1 (parabolic-shaped form) for all isolated deep-ocean channels. The Horizon Channel had a constant cross-sectional shape from 0.6 (convex-upward shaped form) to 1.8 (parabolic-shaped form) with a mean of 1.1 (parabolic-shaped form). The Baranof Channel cross-section shape ranged from 0.9 to 2.2 with one cross-sectional shape greater than 2.2 and a mean of 1.5 (parabolic-shaped form). The Surveyor Channels had a relative constant convex-upward shaped form



(shape < 1) with a mean of 0.64 with a few cross-sections toward a box-shaped form at the end of the channel section.

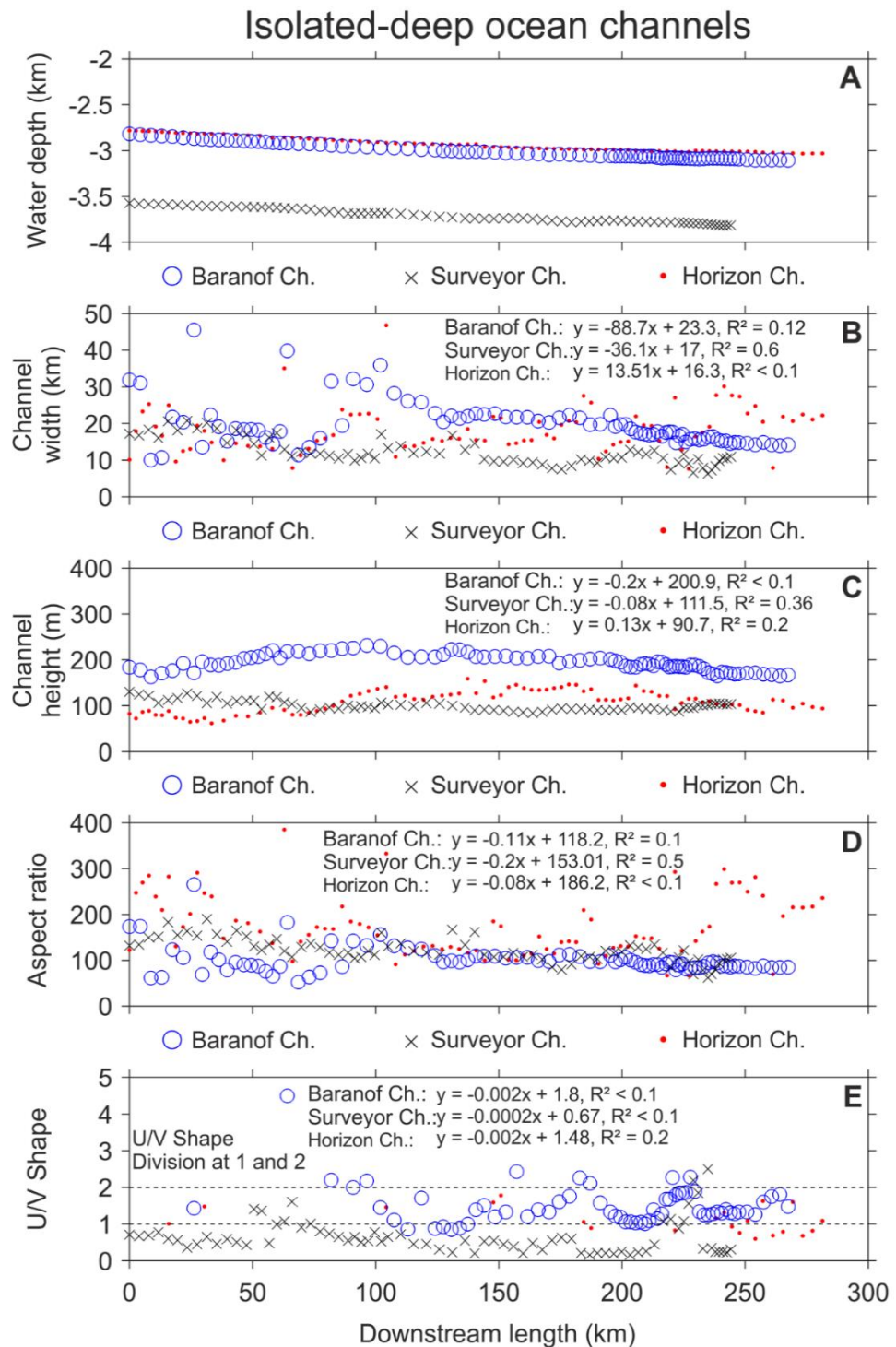


**Figure 3.11** Isolated deep-ocean channel (Baranof Channel: blue circle, Surveyor Channel: black cross, Horizon Channel: red point) measurements: (A) Longitudinal depth profile (Channel central line). (B) Channel width. (D) Channel height, (E) Cross-sectional shape with

division at 1 and 2. Values of shape refer to: shape  $< 1$  convex-upward shaped form, shape = 1 "V"-shaped form, shape  $< 1$  and shape  $\leq 2$  "U"- or parabolic-shaped form, shape  $> 2$  box-shaped form.

---

*Non-margin ocean channels (Marianna Channels A, B, C)*

Mariana Channels A, B and C ranged in channel width between 2 and 8 km (Figure 3.12b). Mariana Channel A width decreased in general downstream and ranged between 7 km and 3 km, whereas the channel width for Mariana Channels B and C was relatively constant, ranging between 2 km and 3 km. Mariana Channel C width increased to 4 km at 4 km downstream and to 5 km at 6 km downstream, but width decreased afterwards. Channel height (Figure 3.12c) was relatively constant with a channel height of around 100 m downstream for Mariana Channels A and B. The channel height for Mariana Channel C channel was more variable but decreased downstream from about 300 m to 200 m. The channel height for the Mariana Channel C channel is 2-times deeper compared to the channel height of the Mariana Channels A and B channel. The aspect ratio (Figure 3.12d) for Mariana Channel B (mean aspect ratio: 25) and Mariana Channel C (aspect ratio: 5-10) channel were relative constant along the course of the channel. By contrast, the aspect ratio for the Mariana Channel A (mean aspect ratio: 75) is 3-times greater than for the Mariana Channel B in the first half of its course, but decreased to 20 for the second half of its course. The cross-sectional shape (Figure 3.12d) for Mariana Channels A and B was mainly parabolic-shaped ("U"-shaped) along the channel length and only a few cross-sections were box-shaped for Mariana Channel A and convex-upward for Mariana Channel B. The cross-sectional shape for Mariana Channel C was mainly convex-upward.

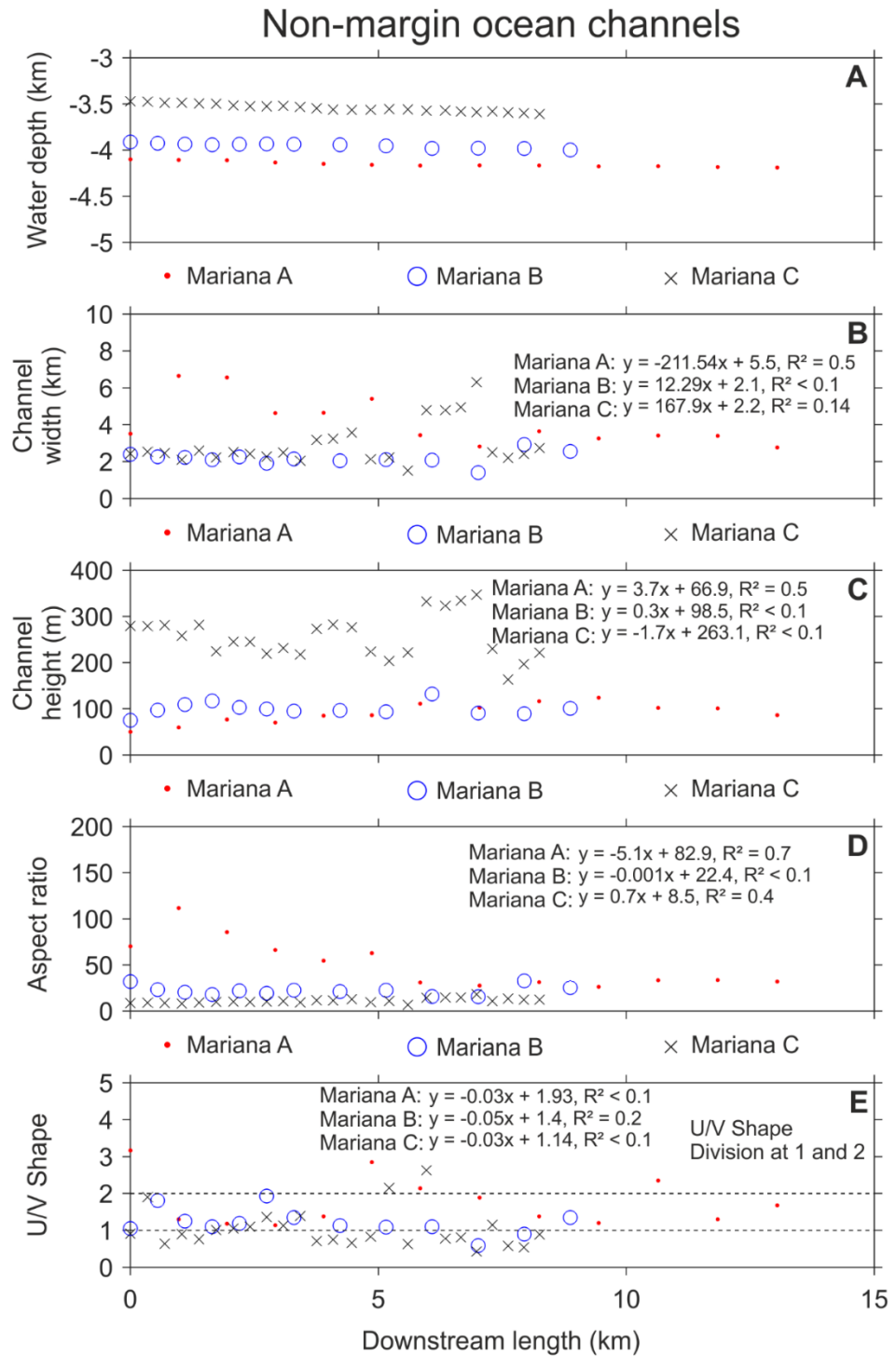


**Figure 3.12** Non-margin ocean channel (Mariana Channel A: red point, Mariana Channel B: blue circle, Mariana Channel C: black cross) measurements: (A) Longitudinal depth profile (Channel central line). (B) Channel width. (D) Channel height, (E) Cross-sectional shape with division at 1 and 2. Values of shape refer to: shape < 1 convex-upward shaped form, shape = 1 “V”-shaped form, shape < 1 and shape ≤ 2 “U”- or parabolic-shaped form, shape > 2 box-shaped form.

### 3.4.2 Comparison between channel types

Channel width (Figure 3.13a) was greatest for isolated deep-ocean channels, ranging between 10 and 40 km with a mean of 16.72 km, whereas the channel width for the Magdalena Channel (submarine-fan channel) was up 10-times narrower with a mean width of 1.5 km. Non-margin ocean channels (Mariana Channels) width was 2-times wider compared to the submarine-fan channel with a mean width of 3.05 km. The Bryant Channel (submarine-fan channel) with a mean width of 4.7 km had a width in general similar to the non-margin ocean channels (Mariana Channels). No channel types, except for the isolated deep-ocean channels were wider than 10 km.

Channel height (Figure 3.13b) was similar between channel types with a maximum channel height of 150 m (Figure 3.13b), except for the Baranof Channel (isolated deep-ocean channel) and Mariana Channel C (non-margin ocean channel).

Aspect ratios (Figure 3.13c) were variable between channel types. The aspect ratio for all isolated deep-ocean channels (Baranof Channel, Horizon Channel and Surveyor Channel) was greater than 100 with a maximum of 340 and a mean of 132. In contrast, submarine-fan channel had a mean aspect ratio range between 16 (Magdalena Channel) and 43 (Bryant channel), which is at least 2 times smaller than for isolated deep-ocean channels. Non-margin ocean channels had an aspect ratio similar to submarine-fan channels.

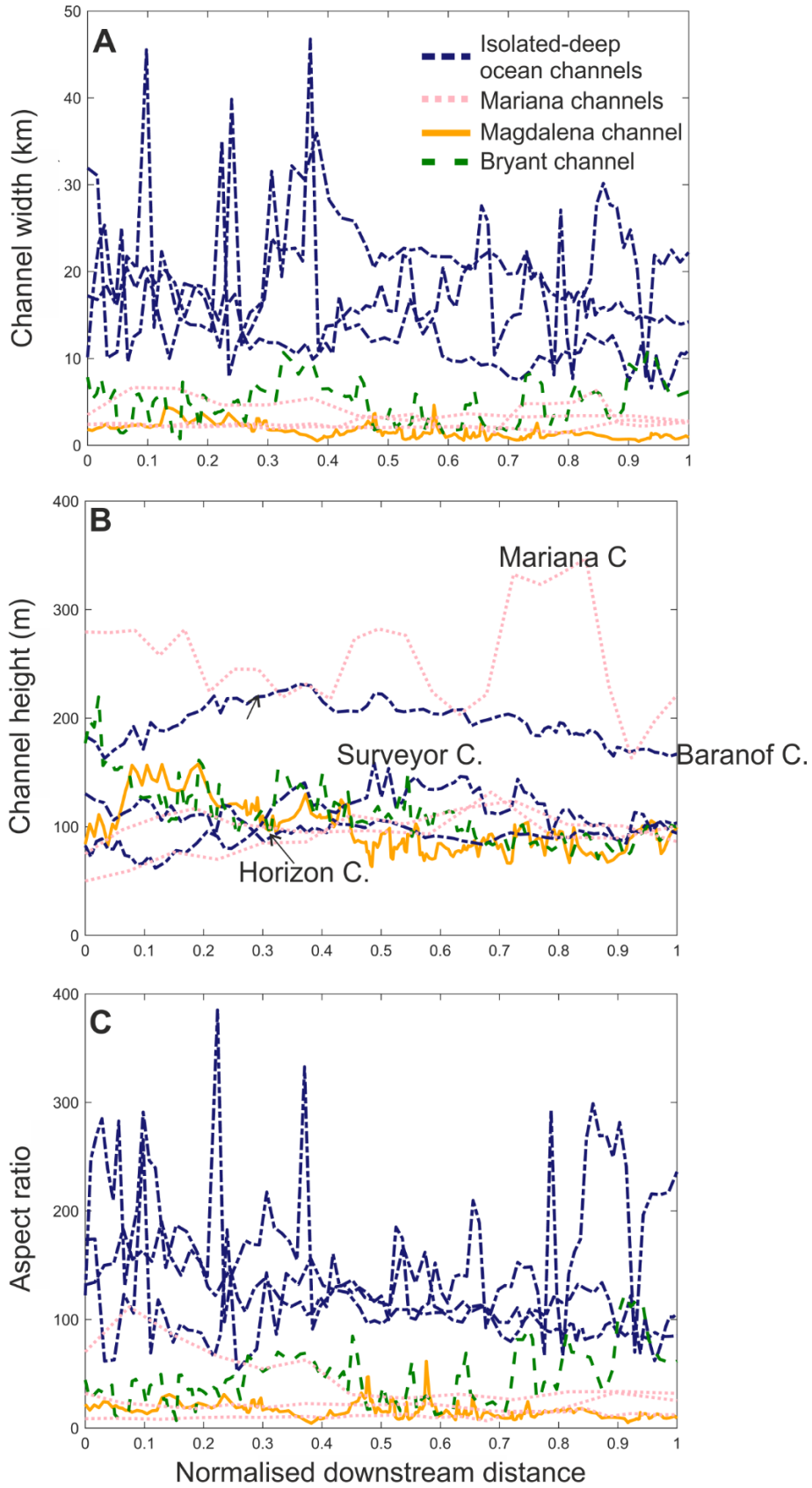


**Figure 3.13** Plots of normalised down-stream distance as a function of A) Width, B) Height and C) Aspect ratio and channel types.

### Channel-bed width

Channel-bed width varied between channel types (Figure 3.14). Channel-bed width was on average narrower than 1 km for submarine-fan channels (Magdalena Channel, Bryant channel) and non-margin ocean channels (Mariana Channels ). Channel bed was on average wider than 1 km for isolated deep-ocean channels (Horizon, Baranof and Surveyor Channel). The Horizon and Baranof had a mean channel bed width between 3 km and 3.55 km, whereas the channel bed width for the Surveyor Channels was half the channel bed width than for the Horizon and Baranof Channel. The greatest variability of the channel bed width was also identified from the three isolated deep-ocean channels.

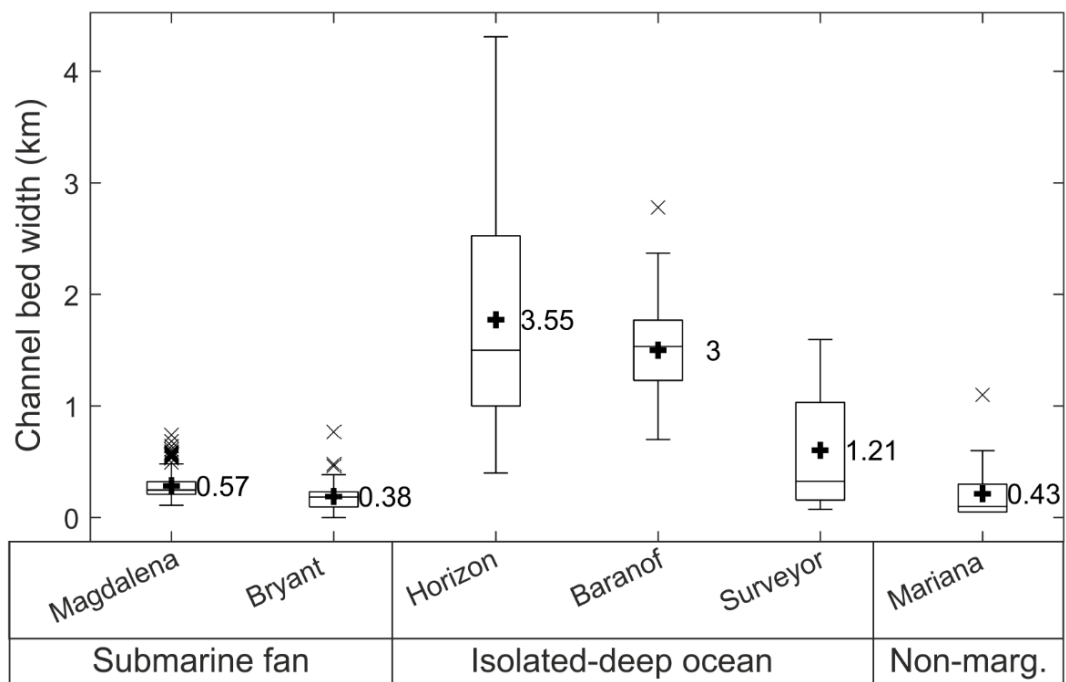


**Figure 3.14** Box and whisker plots of channel bed width (m) for studied channel sections (Magdalena, Bryant, Horizon, Baranof, Surveyor, and Mariana). Box indicates 25<sup>th</sup> and 75<sup>th</sup> percentiles, “+” indicates the mean, “-“ within the box indicates the median, whiskers indicate 99.3 % in a normal distribution and x indicate outliers. Mean for each category is shown.

*Cross-sectional area*

No differences existed between the two methodologies used to calculate the area for submarine channels (Figure 3.15a, b). The area was between 0.1 km<sup>2</sup> for submarine fan channels (Magdalena Channel) to 2.2 km<sup>2</sup> for the Baranof Channel (isolated deep-ocean channel). Non-margin ocean channels (Mariana Channels) and submarine fan channels (Magdalena Channel and Bryant Channel) had an area between 0.1 km<sup>2</sup> to 0.3 km<sup>2</sup> with the Magdalena Channel an area of 0.1 km<sup>2</sup> and Bryant and Mariana Channels an area of 0.3 km<sup>2</sup>. All isolated-deep ocean channels had a mean area between 0.7 km<sup>2</sup> and 2.2 km<sup>2</sup>, indicating that isolated deep-ocean channels had the greatest area of all submarine channel types. The most variable data was identified for the Horizon Channel and Baranof Channels.

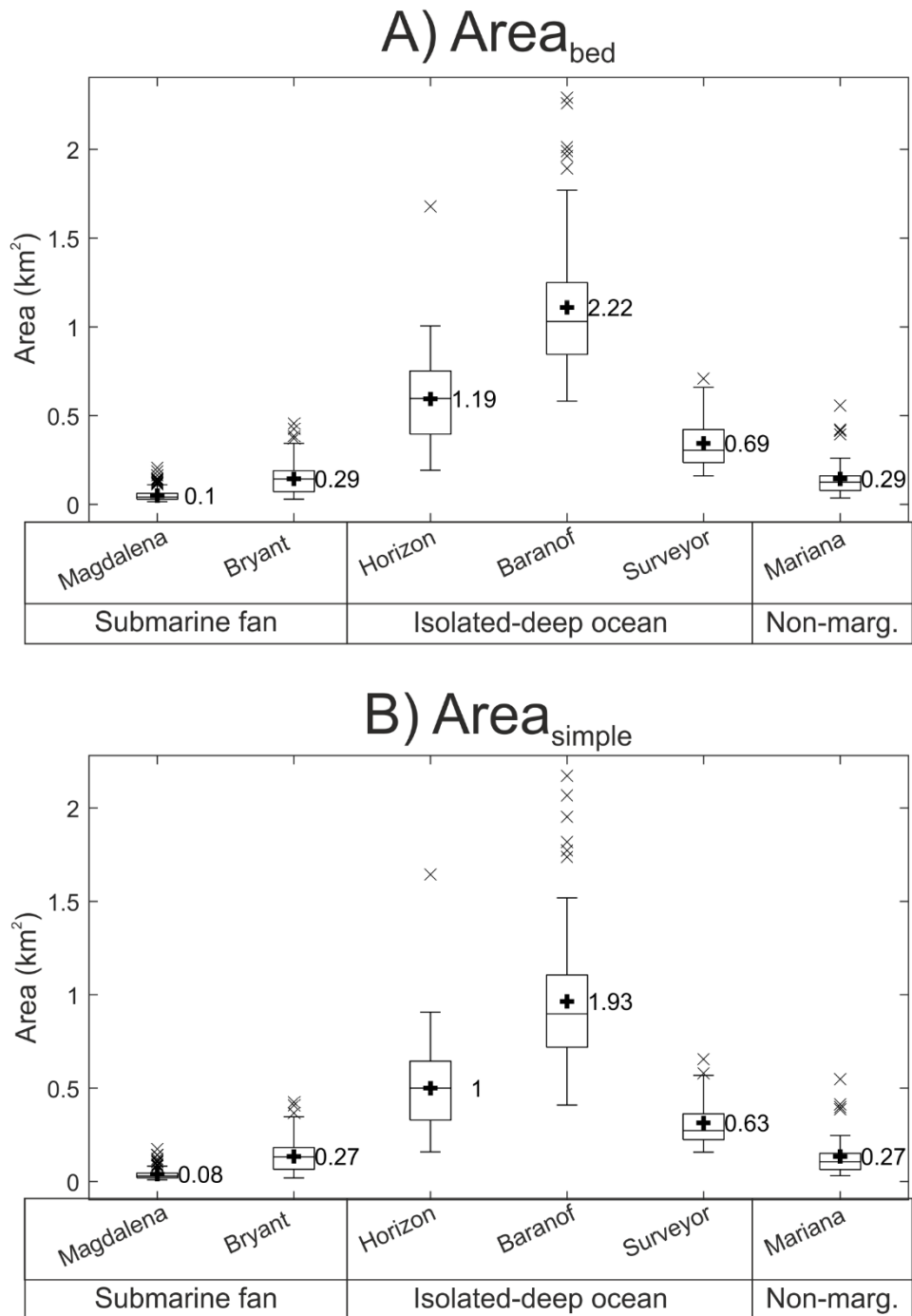


**Figure 3.15** Box and whisker plots of area ( $\text{km}^2$ ) for studied channel sections (Magdalena, Bryant, Horizon, Baranof, Surveyor, and Mariana). The area was either calculated as A)  $Area_{bed} = \frac{(W_B + \bar{W})}{2} \times \bar{H}$  or B)  $Area_{simple} = \frac{(\bar{W} * \bar{H})}{2}$ , where  $W_{Bed}$  is the channel bed width,  $\bar{W}$  is the mean channel width and  $\bar{H}$  is the mean channel height. Box indicates 25<sup>th</sup> and 75<sup>th</sup> percentiles, “+” indicates the mean, “-” within the box indicates the median, whiskers indicate 99.3 % in a normal distribution and x indicate outliers. Mean for each category is shown.



### **3.4.3 Comparison of morphometric parameters between submarine channel types and rivers**

Channel parameters of width, height and aspect ratio were compared between channel types and rivers (single alluvial and bedrock). Generally, submarine channels were wider compared to rivers (Figure 3.16a). Submarine-fan channels and non-margin ocean channels were at least 2- to 12-times wider compared to rivers. Isolated deep-ocean channels were significantly wider (at least 12-times) compared to rivers. Mean channel height (Figure 3.16b) for all submarine channel types (mean height varied between 96 m (submarine-fan channel) to 194 m (isolated deep-ocean channel) and was at 10-times greater than rivers (mean height was 5 m for alluvial and 2 m for bedrock rivers). Aspect ratios (Figure 3.16c) for submarine fan and non-margin ocean channels are within factor 2 of river channels, however, isolated deep-ocean channels exhibited 4 to 6 times higher aspect ratios compare to rivers.

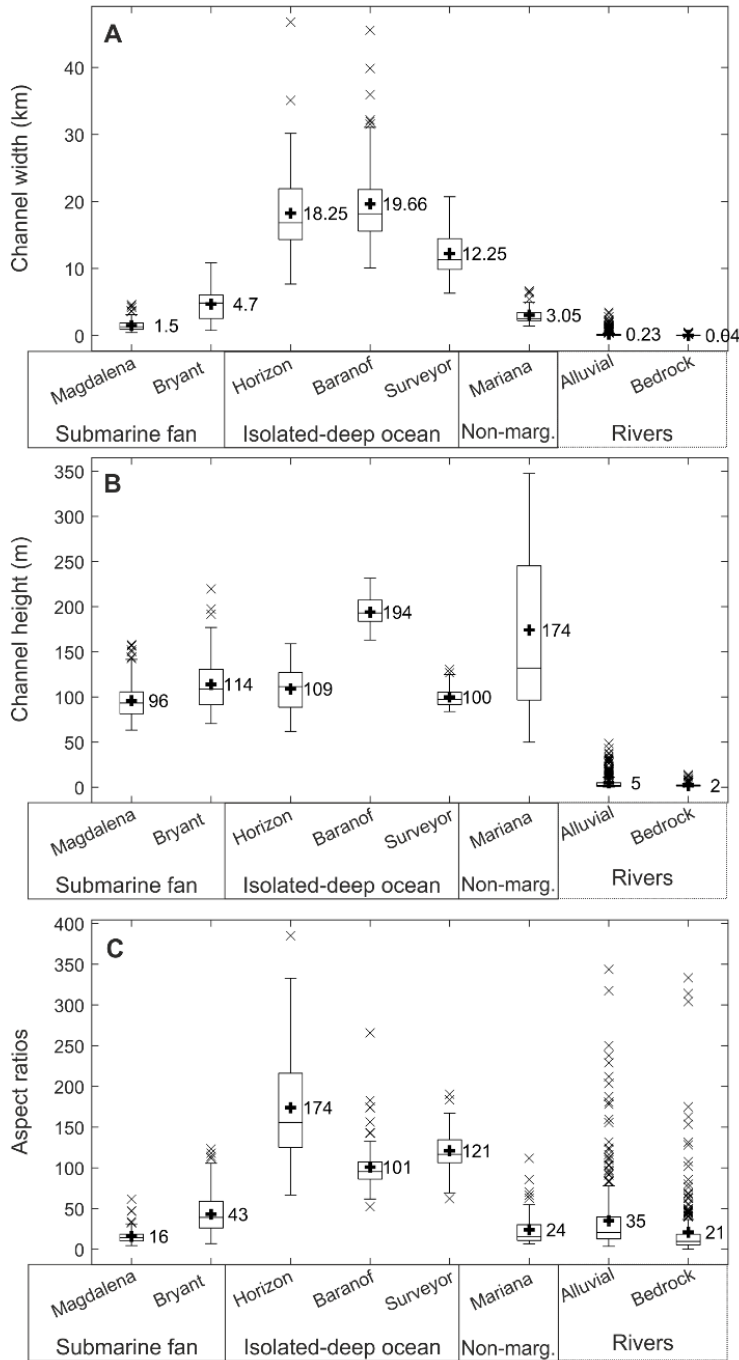


**Figure 3.16** Box and whisker plots of width, depth and width/depth ratio for 5 submarine channel sections and river data (Leeder, 1973; Van den Berg, 1995; Jerolmack and Mohrig, 2007; Whittaker, 2007; Wohl and David, 2008; Yanites *et al.*, 2010; Wilkerson and Parker, 2011). The line within each box indicates the median value, “+” indicate the mean, box ends are the 25<sup>th</sup> and 75<sup>th</sup> percentiles, whiskers represent 99.3 % in a normal distribution, and “x” indicated outliers. Mean for each category is written.

### 3.4.4 Application to a wider dataset

Analysis of the channels herein has identified variations between submarine channel types and rivers. In order to assess whether the observed variations between submarine channels and rivers are generic, a large dataset of submarine channels is compiled (Figure 3.17; Table 3.3; see Appendix C). Use of a literature-based dataset carries a number of limitations, common to previous studies utilising such as approach (Clark and Pickering, 1996a; Konsoer *et al.*, 2013; Shumaker *et al.*, 2018). The wider dataset contained only a limited number of cross-sections per channel. Cross-sections were either taken in relation to the ship-track line or perpendicular to the channel bed and data resolution was variable between studies. Parameter of width, depth, aspect ratio and cross-sectional shape were measured as previously, assuming that the cross-section represents a cross-section from intact to intact channel bank. Cross-sectional area was calculated as:

$$Area_{simple} = \frac{(\bar{W} * \bar{H})}{2}.$$

The dataset represented here was partly used by Konsoer *et al.* (2013). Twenty-three channels with 205 cross-sections belonging to four channel types (submarine-fan, slope, isolated deep-ocean and axial channels, Figure 3.17, Appendix 1) were used. The distribution of the channel types around the world were as followed: all submarine-fan channels occurred at low latitudes (30°N to 30°S), slope channels occurred between low to mid latitude (0° to 60°N), axial channels occurred at mid latitude (30-60°N and 30-60°S) and isolated-deep ocean channels were evenly distributed around the world (90°N to 60°S).

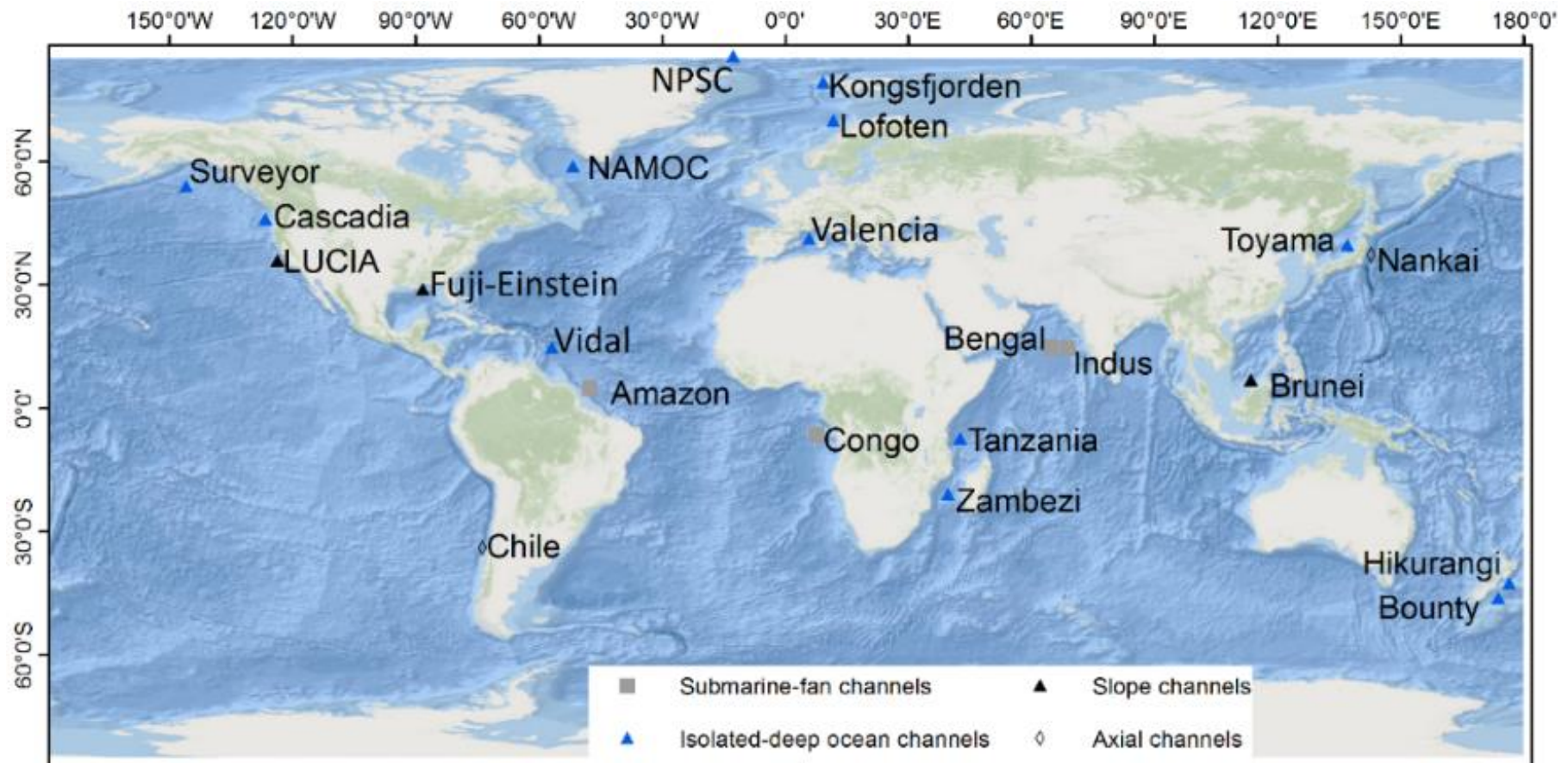


**Figure 3.17** World map showing the locations of 23 submarine channels used for the compiled dataset from four submarine channel types: Isolated deep-ocean (▲), Submarine-fan (■), Slope (▲), and Axial channels (◆).

**Table 3.3** Submarine channel dataset.

<i>Channel type</i>	<b>Submarine-fan</b>	<b>Isolated deep-ocean</b>	<b>Slope</b>	<b>Axial channel</b>
<i>No. of channels</i>	5	13	3	2
<i>No. of cross-sections</i>	37	109	40	19
<i>Name of channels</i>	Amazon, Bengal, Indus, Magdalena, Zaire	Bounty, Hikurangi, Cascadia, Kongsfjorden Channel System, Lofoten, NAMOC, North Pole Submarine Channel, Surveyor, Tanzania, Toyama, Valencia, Vidal, Zambezi	Brunei, Einstein, LUCIA	Chile, Nankai

*Width, depth and aspect ratio*

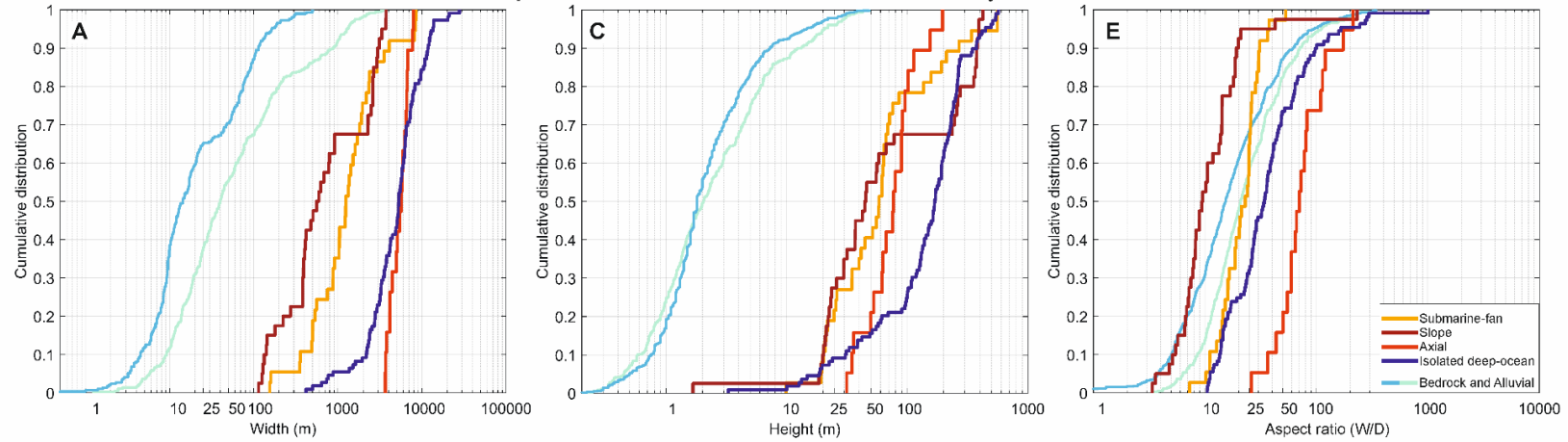
Variations of width, depth and aspect ratio between submarine-fan, slope, axial and isolated deep-ocean channels from the literature-based dataset were evident. Slope, submarine-fan, axial and isolated deep-ocean channels from the compiled dataset were at least 14-times wider (Figure 3.18A) and 22-times deeper (Figure 3.18C), but can have a similar aspect ratio (Figure 3.18D) than single meandering rivers. Slope channels (mean width: 595 m, mean depth: 45 m), had the narrowest width and the shallowest channel height of all submarine channels and hence an aspect ratio (mean: 9.4) similar to rivers (mean 15 and 20). The Magdalena Channel, a submarine-fan channel with a channel width of 1344 m, agreed with the channel width of the literature-based submarine-fan channel dataset (mean width: 1244 m), whereas the Bryant Channel (mean width: 5.2 km) had a mean channel width 5-times wider than the literature-based submarine-fan dataset (Figure 3.18B). The mean width of the Bryant Channel, a submarine-fan channel, was similar

to the literature-based axial channel (mean width: 5.7 km) and isolated deep-ocean channel (mean width: 5.3 km) dataset. The studied isolated deep-ocean channels (Baranof, Horizon and Surveyor) with a mean width of 16 km were 3-times wider compared to the literature-based isolated deep-ocean channel dataset.

Channel height was similar between datasets (Figure 3.18C). The channel height of the submarine-fan channel, Magdalena Channels (mean height: 94 m) and Bryant Channel (mean height: 109 m) was slightly greater than the literature-based submarine-fan channel dataset (mean height: 59 m). The studied isolated deep-ocean channels (Baranof, Horizon and Surveyor) had a channel height (mean height: 120 m), which was smaller than the literature-based isolated deep-ocean channel dataset with a mean height of 172 m.

Aspect ratio of the Magdalena Channels (mean aspect ratio: 14.46) was slightly smaller than the aspect ratio of the literature-based submarine-fan channel dataset with an aspect ratio of 22.99 (Figure 3.18F), which was similar to rivers, whereas the Bryant Channel, with a mean aspect ratio of 39, was nearly 2-times greater than the literature-based submarine-fan channel dataset and had an aspect ratio greater than rivers. Mean aspect ratio for isolated deep-ocean channels ranged from 35 for the literature-based dataset to 117 for the studied isolated deep-ocean channels (Baranof, Horizon and Surveyor).

Compiled dataset from the literature only and rivers



Compiled dataset from the literature, studied channels and rivers

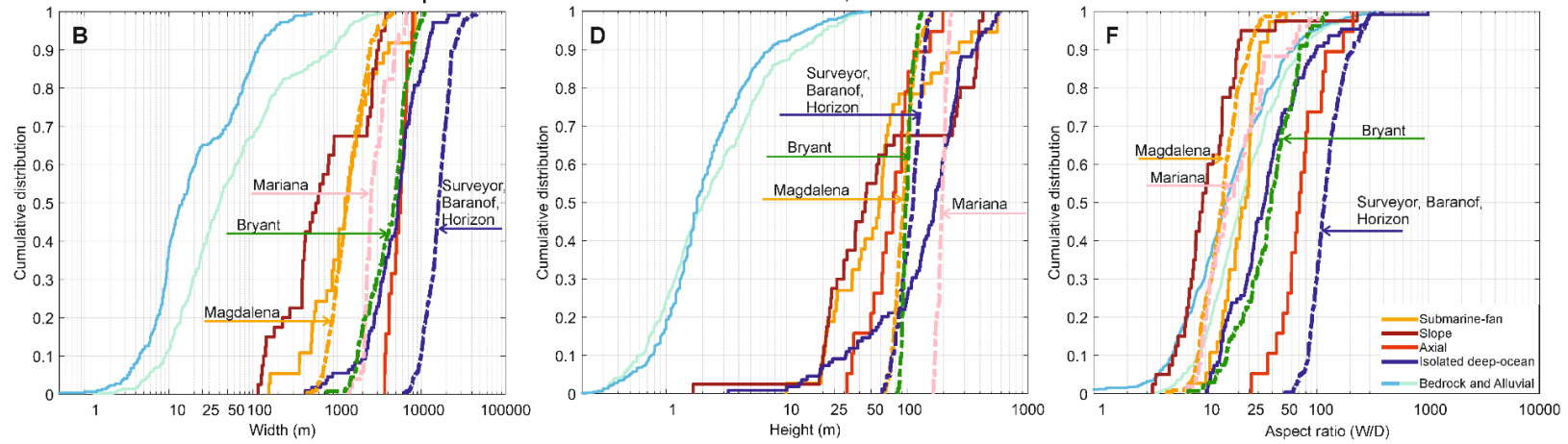


**Figure 3.18** Cumulative distribution of A and B) width (m), C and D) height (m), and E and F) aspect ratio. Figures A, C and E are composed of the compiled dataset from the literature only and rivers. Figures B, D and F are compiled dataset, rivers and studied channel types from the study herein. River datasets are from bedrock and alluvial rivers (Leeder, 1973; Van den Berg, 1995; Jerolmack and Mohrig, 2007; Whittaker, 2007; Wohl and David, 2008; Yanites *et al.*, 2010; Wilkerson and Parker, 2011); blue solid line), submarine channel types from compiled dataset are: submarine-fan (orange solid), slope (brown solid), axial (red solid) and isolated deep-ocean (dark blue solid). Studied channel types from the study herein are: submarine-fan (Magdalena, orange dashed; Bryant Channel, green dashed), non-margin (Mariana, pale pink dashed), and isolated deep-ocean (Surveyor, Baranof, Horizon; dark blue dashed).

---

### *Cross-sectional area*

The cross-sectional area of submarine channels varied between channel types from the literature-based dataset (Figure 3.19). Slope channels had the smallest area, with a mean of 0.005 km<sup>2</sup>, and isolated deep-ocean channels had the maximum area with a mean of 0.28 km<sup>2</sup>, which is 56-times a greater area compared to slope channels. Submarine-fan channels had an area of 0.02 km<sup>2</sup>, which is 14-times smaller than isolated deep-ocean channels and 4-times greater than slope channels. Axial channels with a mean of 0.14 km<sup>2</sup> had a cross-sectional area half of the size compared to isolated deep-ocean channels. A cross-sectional area greater than 2 km<sup>2</sup> was only identified for submarine-fan channels and isolated deep-ocean channels.

Cross-sectional area from the literature-based dataset was 2-times smaller than the studied channel sections (Figure 3.20). However, this is in close agreement, and in both cases isolated deep-ocean channels have at least a 5-times greater area compared to submarine-fan channels. The cross-sectional area for the Magdalena Channel, with a peak at 0.05 km<sup>2</sup>, is similar compared to the area of the literature-based submarine-fan channel dataset with a peak at 0.02 km<sup>2</sup>. The area for the Bryant Channel with a peak at 0.15 km<sup>2</sup> was 3-times greater compared to the literature-based submarine-fan channel dataset. The area for literature-based isolated deep-ocean channel



dataset with a peak at  $0.28 \text{ km}^2$  was half the area compared to the area of the studied isolated deep-ocean channels with a peak at  $0.65 \text{ km}^2$ .

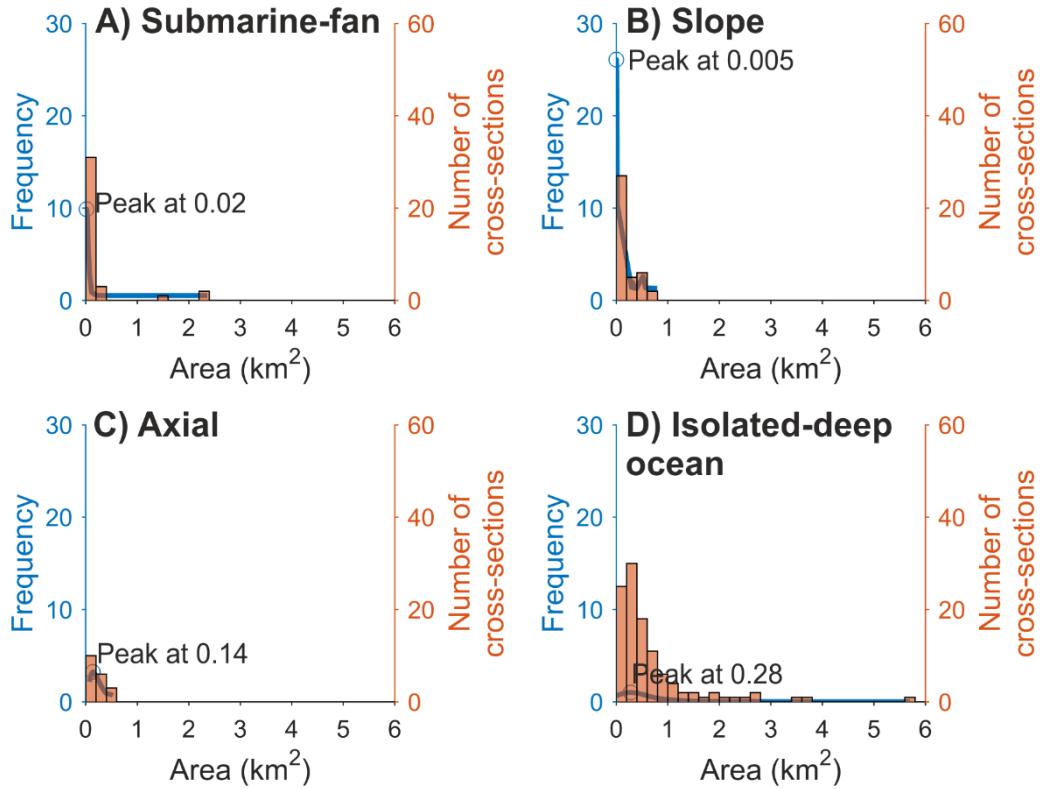


**Figure 3.19** Kernel density estimation (blue) and histogram with a bin interval of 0.2 (orange) of the cross-sectional area for A) submarine-fan, B) Slope, C) Axial and D) isolated deep-ocean channels. Data from the compiled dataset from the literature.

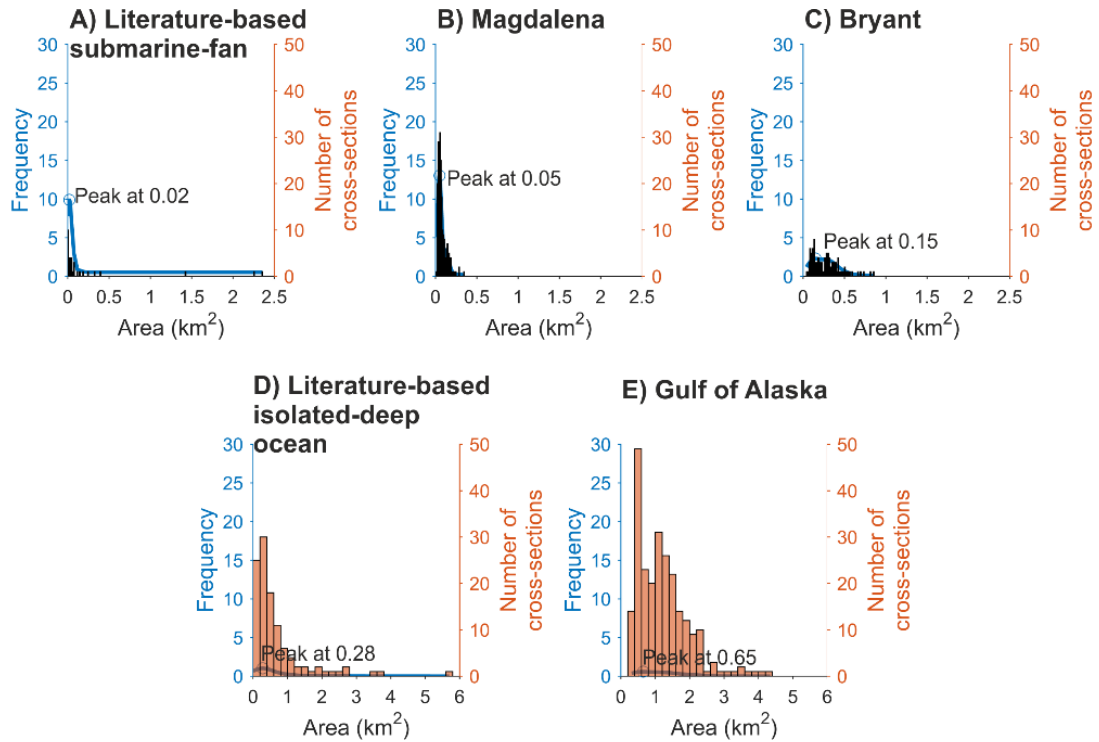


**Figure 3.20** Kernel density estimation (blue) and histogram with a bin interval of 0.01 (submarine-fan: A, B, C) and 0.2 (isolated deep-ocean: D, E) data (orange) of the cross-sectional area as a comparison between submarine-fan and isolated deep-ocean channel from the compiled dataset (A, D) and this study with Magdalena (B) and Bryant (C) and Surveyor, Horizon and Baranof compiled (D).

### *Cross-sectional shape*

Peak values of the cross-sectional shape were different between channel types (Figure 3.21). Submarine-fan channels had a peak value at 1 (“V”-shaped form), slope channel had a peak at 1.2, and axial channels a peak at 1.5, suggesting a parabolic-shaped form. However, more cross-sections with a “V”-shaped form were identified for slope channels and more cross-sections with a box-shaped form ( $shape > 2$ ) were identified for axial channels. Isolated deep ocean channels had a peak at 0.8 (convex-upward shaped form), but a few cross-section have a box-shaped form ( $shape > 2$ ). Most cross-sections with a box-shaped form were identified for axial and isolated deep-ocean channels.

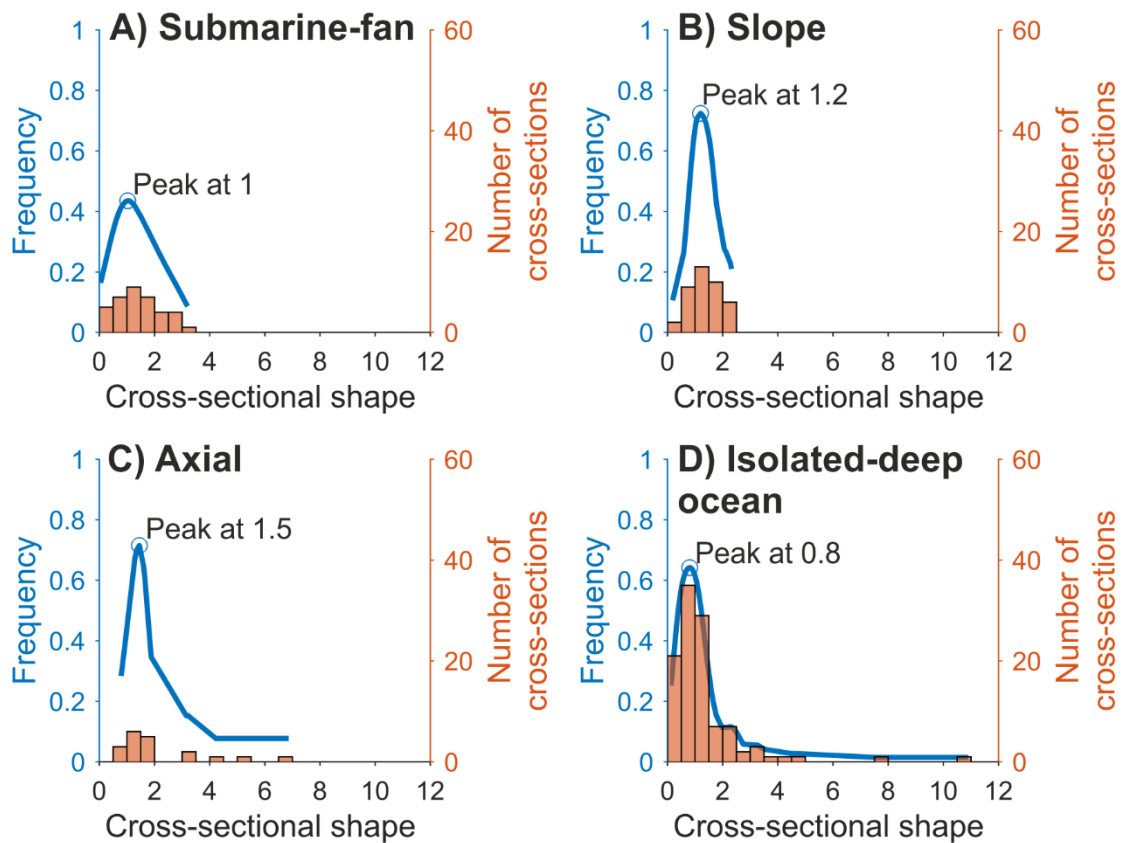


**Figure 3.21** Kernel density estimation (blue) and histogram with an interval of 0.5 (orange) of the cross-sectional shape for the compiled dataset.

Datasets of submarine-fan channels (Magdalena, Bryant) and Gulf of Alaska channels are in agreement with the literature-based dataset (Figure 3.22). Peak for Magdalena Channel, submarine-fan channel, was at 1.16 (parabolic-shaped cross-section) and Bryant Channel was at 1.23 (parabolic-shaped cross-section), which was similar compared to the literature-based submarine-fan channel dataset (peak at 1.03, V-shaped). More cross-sections with a box-shaped form existed for the Magdalena Channel compared to the literature-derived submarine-fan channel dataset. Channels in the Gulf of Alaska (Surveyor Channel, Baranof Channel and Horizon Channel) with a peak at 0.67 had a convex-upward shape cross-section, which agrees with the literature-based isolated deep-ocean channel dataset with a peak at 0.81.

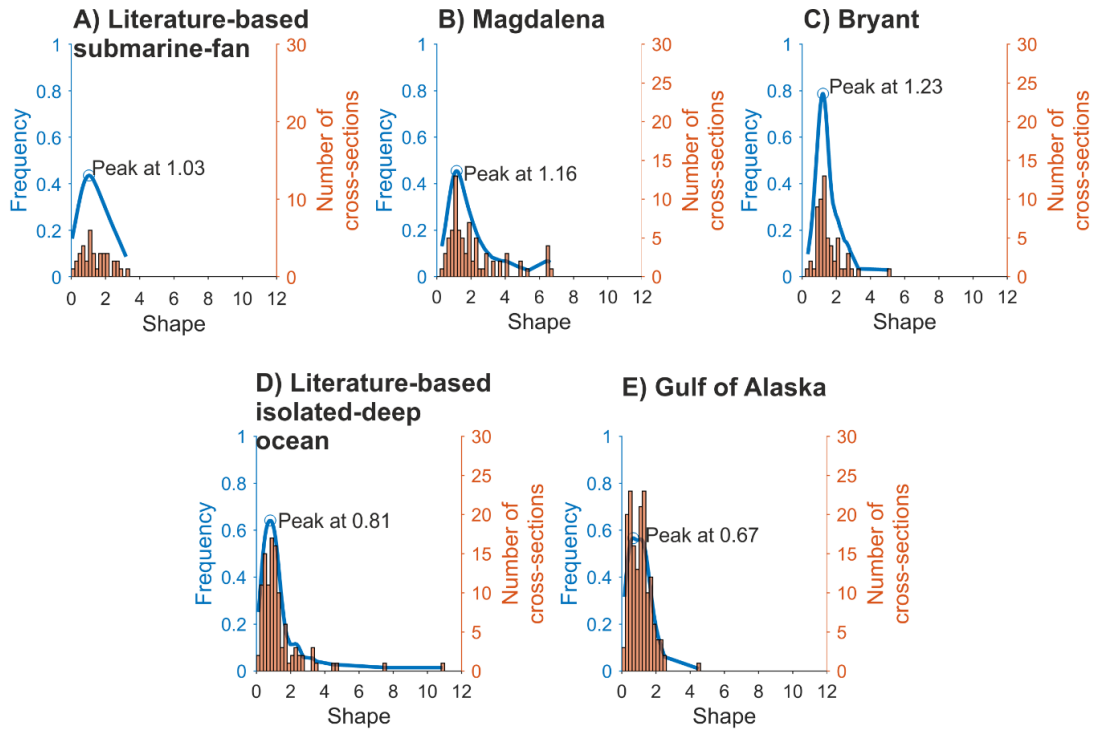


**Figure 3.22** Kernel density estimation (blue) and histogram with an interval of 0.2 (orange) of the cross-sectional shape as a comparison between Submarine-fan and isolated deep-ocean channel from the compiled dataset (A, C) and this study (B, D).

### 3.5 Discussion

The results indicate a variation of channel parameters on: (i) a small-scale (variation between cross-sections for a given channel), (ii) a medium-scale (variation between channels within a given channel type, e.g. Bryant Channel and Magdalena Channel) and (iii) a large-scale (variation between channel types).

A distinction based on morphometric parameters between submarine-fan, isolated deep-ocean, slope, axial and non-margin channels is identified, suggesting that the environmental setting of a submarine channel has a greater influence on the flow and sedimentation processes, and hence on the morphology of submarine channels, than previously thought. A comparison of aspect ratio between submarine channels and rivers identified two distinctive sub-groups. The first group is composed of submarine-fan, slope, and non-

margin ocean channels, and have a similar aspect ratio compared to rivers and the second group, which has a greater aspect ratio compared to rivers, is composed of axial and isolated deep-ocean channels. Nevertheless, submarine channels are wider and deeper than single meandering rivers.

Variation in cross-sectional shape for different submarine channel types was qualitatively identified: submarine-fan channels are general between “V”-shaped to “U”-shaped with a narrow channel width, isolated deep-ocean channels have in general a parabolic-shaped cross-section with a flat base, slope channels and non-margin channels are in general “V” to “U”-shaped and axial channels are in general “U” to box-shaped, suggesting a complex cross-sectional shape for all submarine channel types. Previous studies suggested that submarine-fan channels have a “V”-shaped and isolated deep-ocean channels have “U”-shaped cross-sections (e.g, Carter, 1988; Damuth *et al.*, 1988; Schwenk *et al.*, 2003; Fierens *et al.*, 2019), which agrees with this study in general that submarine-fan channels have a general narrow channel bed width and isolated-deep ocean channels have a wider channel bed width.

### **3.5.1 Aspect ratios of submarine channel types**

The contradiction between different studies in terms of aspect ratio is explained by the types of submarine channels analysed (Figure 3.23). The dataset of Jobe *et al.* (2016). gives aspect ratios similar to rivers and includes at least 204 from 276 cross-sections from modern submarine-fan channels (69 cross-sections from Bengal Channel, 91 cross-sections from Niger Channel, 11 cross-sections from Congo Channel, 24 cross-sections from Indus Channel, 9 cross-sections from Amazon Channel) and 8 cross-sections from the Einstein Channel, a slope channel, which have also similar aspect-ratio compared to rivers. Other studies which used submarine-fan channels (Amazon and Indus (Peakall *et al.*, 2000a); Amazon (Pirmez and Imran, 2003); and Indus (Kenyon *et al.*, 1995)) concluded that the width-depth ratio is similar compared to rivers. By contrast, a dataset with mainly isolated deep-

ocean channels (at least 93 from 177 cross-sections) concluded that submarine channels have a greater width-depth ratio compared to rivers (Konsoer *et al.*, 2013). Thus, it is clear that both conclusions that submarine-fan channels have similar aspect ratio compared to rivers and isolated deep-ocean channels have a greater aspect ratio compared to rivers agrees with the results obtained in the study herein. Despite having similar aspect ratios, submarine channels are in general wider and deeper than single alluvial and bedrock rivers.

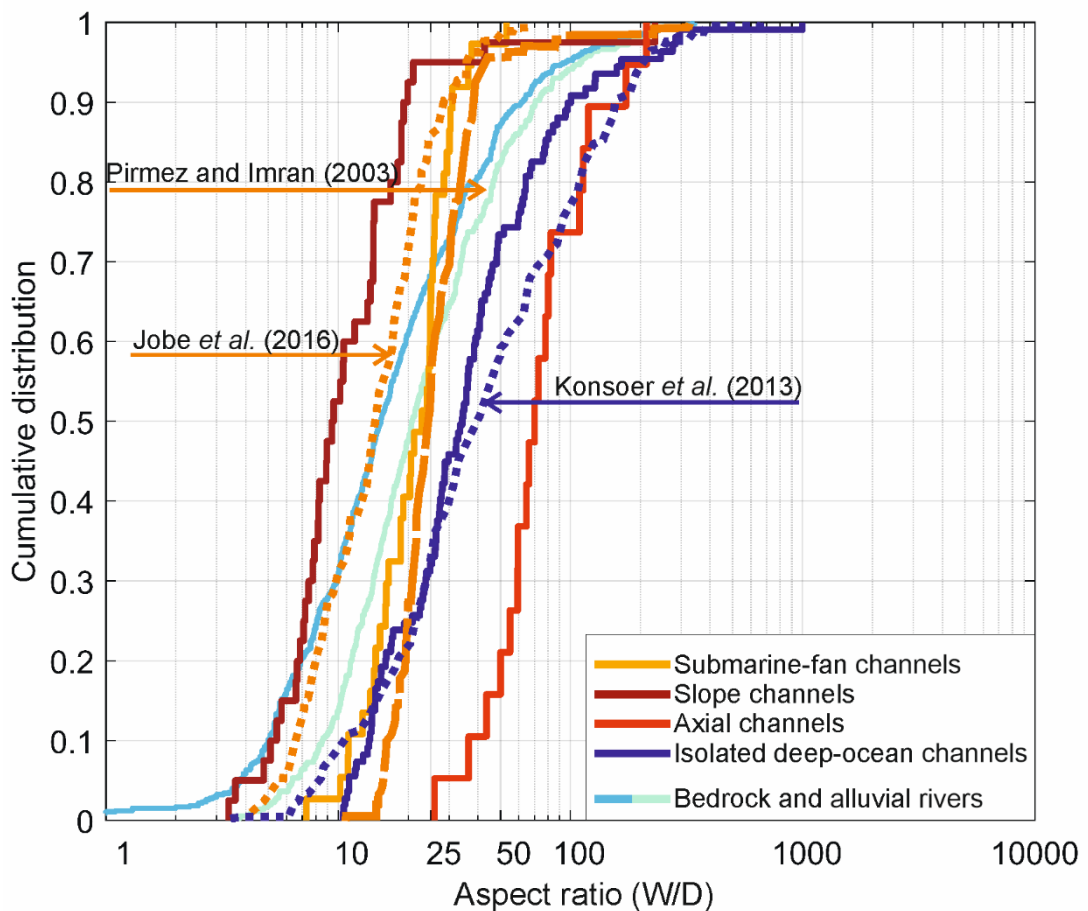


**Figure 3.23** Comparison of the literature-based dataset from this study to three submarine channel datasets (Pirmez and Imran, 2003; Konsoer *et al.*, 2013; Jobe *et al.*, 2016) and river datasets (bedrock and alluvial; Leeder, 1973; Van den Berg, 1995; Jerolmack and Mohrig, 2007; Whittaker, 2007; Wohl and David, 2008; Yanites *et al.*, 2010; Wilkerson and Parker, 2011).

### 3.5.2 “Bankfull condition” for submarine channels

Flow depth measurements within submarine channels are rare, therefore the height of the confinement (channel banks and levees), similar to alluvial rivers, is used as a reference for “bankfull condition”. However, not all turbidity currents are confined but overspill the bank and deposit sediment on the levees, and not all turbidity currents are powerful enough to reach channel banks and may die within the channel (Piper and Normark, 1983). Defining bankfull condition in rivers is also a debate (e.g., Leopold, 1994; Copeland *et al.*, 2000; Montgomery and Gran, 2001; Snyder *et al.*, 2003). In theory, bankfull level is defined as the level of maximum discharge without overflowing, which represents a mean flow depth with a reoccurrence interval between 1 and 2.5-years with many rivers reaching bankfull condition every 1.5 years (Leopold, 1994), but in other cases, reoccurrence interval of bankfull level can be 4 to 10-years (Pickup and Warner, 1976) or up to 32 years (Williams, 1978) and only one third of 36 studied rivers from the USA had recurrence intervals of near the 1.5-year interval. Nevertheless, the channel height is the best estimation for flow depth in both rivers and submarine channels at the moment.

Direct flow thickness measurements from the Congo Channels have been reported from at least 150 m up to 410 m (Khripounoff *et al.*, 2003; Vangriesheim *et al.*, 2009), but the recurrence interval of flows with this reported flow thickness is not known and hence such flows might be rare. Flow data from the Congo Canyon, which were measured over a four-month time period from Doppler current profilers (ADCPs), which were suspended between 66 and 85 m above the canyon bed, shows that flow thickness varied between 48 m and 77 m, which is at least 2-times less than the previous flow depth within the channel. Calculation of flow depth within the Amazon Channel, an submarine-fan channel, suggest that flow depth increases downstream and flow depth exceed channel depth at the upper fan section with flow depths of 280 m, which is 20 times greater than the channel depth (Pirmez and Imran, 2003). However, the flow thickness values do not consider flow concentration.

Flows in submarine channels and rivers are stratified differently in terms of their flow properties. For example, sediment concentration and velocity, which has an influence on the morphometrics (Peakall and Sumner, 2015). Near the channel bed, turbidity currents are in general coarser, more dilute and faster (Peakall *et al.*, 2000a; Azpiroz-Zabala *et al.*, 2017a), whereas the upper part of the turbidity current is slower and more dilute compared to the lower part. The upper flow may be not confined and is thicker than the channel banks in contrast to rivers, causing a deposition of sediment on the channel banks (Peakall *et al.*, 2000a; Mohrig and Buttles, 2007; Savoye *et al.*, 2009), which may explain a greater channel depth of submarine channels compared to rivers.

Channel height and hence flow depth is variable between submarine channel types. A dataset by Konsoer *et al.* (2013) included 177 submarine channel cross-sections with at least 93 cross-sections from isolated deep-ocean channels and only 22 cross-sections from submarine-fan channels reported a mean channel height value of 136 m. By contrast, a study with at least 21 submarine-fan channels from 4 systems (Niger, Bengal, Amazon, Western Gulf of Mexico) out of 37 channels from 6 systems identified a mean channel height of 37 m (Shumaker *et al.*, 2018), which is 3-times lower than the reported value by Konsoer *et al.* (2013). Submarine-fan channels from the present study had a channel height value of 58.6 m for the literature-based dataset, which is similar to the Shumaker *et al.* (2018) dataset. By contrast, extracted submarine-fan channels (Amazon, Bengal and Magdalena) from the Konsoer *et al.* (2013) dataset had a mean depth of 97 m, which is similar to the Magdalena and Bryant channel. Such differences between channel heights for submarine fan channel might reflect their evolutionary stage or flow properties through an interaction between levee development through suspended sediment (Savoye *et al.*, 2009), and channel bed aggradation, and hence reflect a general decrease of channel depth downstream (Flood and Damuth, 1987; Babonneau *et al.*, 2002; Pirmez and Imran, 2003) as turbidity current overspill and flow stripping is common and concentrated further downstream than upstream (Savoye *et al.*, 2009).



Channel depth for isolated deep-ocean channel ranges between 100 and 300 m (Carter, 1988), which agrees with the Konsoer *et al.* (2013) dataset with a mean channel depth of 153 m and this dataset. Additionally, as noted by Carter (1988) and this study, channel depth in general increases towards the distal end in contrast to submarine-fan channels. Isolated deep-ocean channels are controlled by subsidence of the channel terminus, hence flows within isolated-deep ocean channels height is controlled by channel incision due to the subsidence of the distal channel end (Carter, 1988), hence overflows within isolated-deep ocean channels may be dilute and uncommon.

Channel width is variable between submarine channels within a channel type. Possible explanations for differences between submarine channels within a channel type could be related to channel maturity and hence channel evolution, topographic variation such as presence of faults and knickpoints (Heiniö and Davies, 2007; Jolly *et al.*, 2017), amount of sediment transported to channels (Wetzel, 1993; Peakall *et al.*, 2000a; Kneller, 2003) or just the nature and magnitude of the input flow (Reading and Richards, 1994; Piper and Normark, 2001). Nevertheless, isolated-deep ocean channels are deeper and wider compared to submarine-fan channels.

### 3.6 Conclusions

This study analysed the hydraulic geometry of submarine channels, which suggest that based on the morphometric analysis deep-sea submarine channels can be distinguishing into submarine-fan, isolated-deep ocean, non-margin, slope and axial channels. Channel width varied by 2-orders of magnitude between channel types and channel depth by an order of magnitude, in turn making slope channels the narrowest and shallowest channels and isolated deep-ocean channels the widest and deepest.

Distinguishing channel-forms into different channel types can explain the contradiction when comparing a large dataset of hydraulic geometry and their comparison to rivers. Slope, submarine-fan, and non-margin channels

are shown to have aspect ratios similar to rivers, whereas isolated deep-ocean and axial channels have aspect ratios much greater than rivers. Differences between submarine channel types may reflect their variable formation setting, and hence their allogenic control. For example, submarine-fan channels are controlled by aggradational processes and isolated deep-ocean channels are controlled a subsidence of the channel terminus. Obtained morphometric parameters from different channel types can be incorporated into numerical models and laboratory experiments to constrain processes of sediment gravity flows, for example flow velocity, flow height and sediment concentration, within a conduit better.

# Chapter 4 Width variation around submarine channel bends: Implications for sedimentation and channel evolution

---

## 4.1 Chapter Summary

Submarine-fan channels can build the largest sediment accumulations on Earth, but our understanding of flow and sedimentation processes related to channel evolution remains limited. Results from physical and numerical modelling predict dominantly downstream channel bend migration. However, observations and evolutionary models for aggradational submarine channels on passive margins suggest that bends are dominated by lateral expansion. This paradox may be due to limitations induced by the use of constant width channels in process studies. Constant width has been used for two reasons: partly because this is the simplest possible case, but primarily because the width variation around submarine channel bends is unknown. Channel width variations are examined from an active channel reach with 49 bends and three inactive but unfilled channel reaches with a total of 35 bends from the Congo Fan. Each bend was divided into 13 cross-sections, and for each cross-section, channel width was measured for the channel base, and at 10 m vertical increments up to the height of the channel banks. The results indicate that channels are typically wider around bend apices than around inflections. This morphology suggests that channels are controlled by bank-pull (outer bank erosion), with later deposition at the inner bend, similar to many rivers. The implications of these spatial changes in channel width around bends for sedimentation and channel evolution are explored, and it suggests that such changes may account for the contradictions between physical and numerical modelling, and seafloor observations. Integration of these channel width data with the known climate history of the Congo Fan, further suggests that the magnitude of channel width variation at bend apices may be controlled by

allogenic forcing, with larger flows associated with greater width variations around bends.

---

## 4.2 Introduction

Many large submarine-fan channels derive their sediment source from large rivers (e.g. Amazon, Indus, Bengal, Congo and Magdalena). Over time, channels on submarine-fans develop a complex network, which build the largest sediment accumulations on the ocean floor (Flood and Damuth, 1987; Kolla and Coumes, 1987; Curray *et al.*, 2003). Generally, sediment gravity flows enter a network of distributary channels, via a single canyon, of which usually only one channel is active at a time. These flows can interact with the channel by eroding and depositing sediment, before finally depositing sediment as lobes at the end of the channel (Wynn *et al.*, 2007; Prélat *et al.*, 2010; Pickering and Hiscott, 2015). Additionally, the sediment-laden flows can be highly destructive for seabed infrastructure such as seafloor cables and pipelines (Heezen *et al.*, 1964; Carter *et al.*, 2009; Pope *et al.*, 2017). Furthermore, the deposits of submarine channel systems, particularly channel fills and lobes, can form significant hydrocarbon reservoirs (Clark and Pickering, 1996a; de Ruig, 2003; Mayall *et al.*, 2006). A better understanding of how channels migrate, and the depositional processes associated, can help improve geohazard assessment, and understanding of the internal architecture of such reservoirs.

During sea level highstand, many submarine-fan channels show reduced activity since most river load is trapped on the inner continental shelf and is not transported to the canyon head (Wetzel, 1993; Burgess and Hovius, 1998; Covault and Graham, 2010). However, a channel on a submarine fan may stay active during highstand (e.g. Burgess and Hovius, 1998; Covault and Graham, 2010), for instance if the canyon is directly connected to the river, as observed for the Congo River (Heezen *et al.*, 1964; Babonneau *et al.*, 2002; Savoye *et al.*, 2009) or through storm-induced flows transporting

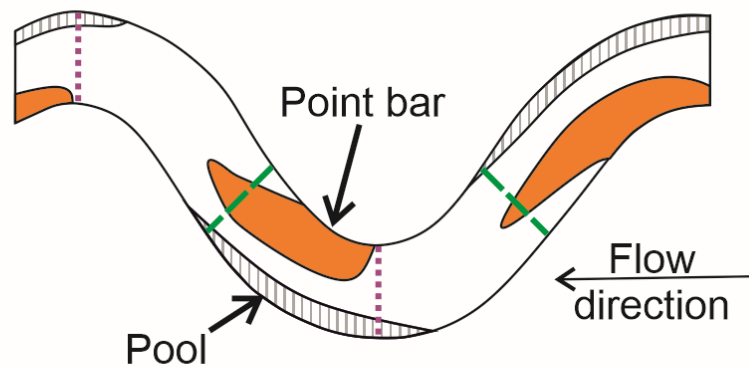
sediment across the shelf and into the channelised system (Kudrass *et al.*, 1998; Guiastrennec-Faugas *et al.*, 2020).

Laboratory experiments and numerical simulations have suggested that submarine channel bends have thinner point-bars relative to channel depth compared to rivers, and these are located further downstream of the bend apex than in fluvial systems (Figure 4.1A; Keevil *et al.*, 2007; Peakall *et al.*, 2007; Straub *et al.*, 2008; Amos *et al.*, 2010; Darby and Peakall, 2012; Cossu *et al.*, 2015). These experiments, and simulations, have all used fixed (non-erodible) channel banks. However, in channels with erodible banks the point-bar position would be associated with erosion occurring preferentially at the outer bank, at and beyond the bend apex (Fig. 1A). This imbalance of deposition further downstream of the bend apex and erosion at the outer bend beyond the bend apex would lead to downstream bend migration. However, observations and evolutionary models from aggradational channels on passive margins suggest that submarine channels are dominated by lateral bend expansion, and that significant downstream bend migration (more than 2-3 times the channel width) is typically restricted relative to rivers (Peakall *et al.*, 2000a; Deptuck *et al.*, 2007; Jobe *et al.*, 2016); consequently relatively few bend cut-offs form (Peakall *et al.*, 2000a, b). This contradiction between experimental and numerical models, and observations from modern submarine channels, suggests that a key component in the process of sediment deposition around bends is missing. One possible answer to this paradox is that submarine channel bends may exhibit a width variation around bends, similar to that observed in most rivers and incorporated in models (Figure 4.1B; Dietrich, 1987; Eke *et al.*, 2014a, b), rather than the constant channel width which has been used in laboratory experiments and numerical simulations of submarine channels (Imran *et al.*, 1999; Straub *et al.*, 2008; Amos *et al.*, 2010; Sylvester *et al.*, 2011; Ezz and Imran, 2014).

Quantitative analyses of the geometry of submarine channels have been undertaken (Clark *et al.*, 1992; Pirmez and Imran, 2003; Konsoer *et al.*, 2013; Shumaker *et al.*, 2018; Lemay *et al.*, 2020). However, detailed characteristics of cross-sectional morphologies with curvature are rare and

typically concentrate on intra-channel deposition and erosion (Babonneau *et al.*, 2004, 2010; Nakajima *et al.*, 2009) rather than on the morphology of the cross-section around bends. Cross-sectional asymmetry around submarine channels increases with curvature, with maximum cross-sectional asymmetry at bend apices (Reimchen *et al.*, 2016), similar to rivers (Knighton, 1982). Such variation of asymmetry around bends further suggests that there is an inter-relationship between flow and morphology. Nonetheless, Reimchen *et al.* (2016) is a single study from a channel system high on the slope, feeding into a canyon, and it focuses on channel asymmetry. It remains unknown whether there are variations in channel width around submarine channel bends, and if present what the nature of these variations are. Herein, this question is examined using data from the active and several inactive channels on the Congo Fan. In summary, the main aim is to examine the variation of channel width around bends within individual channels, and between channels, which will be addressed by meeting the following objectives: i) to identify appropriate methodologies for measuring channel width in complex submarine channel geometries; ii) to elucidate the variation of width around bends, and compare to results from alluvial rivers; iii) to examine the implications of these variations in channel width around bends in terms of sedimentation and channel evolution; iv) to assess whether submarine channel bends are dominated by bank-pull (outer bank erosion) or bar-push (inner-bend deposition); and, v) to examine the role of climate forcing in controlling variations in width around bends.

### A) Experimental submarine in-channel morphology



### B) River in-channel morphology

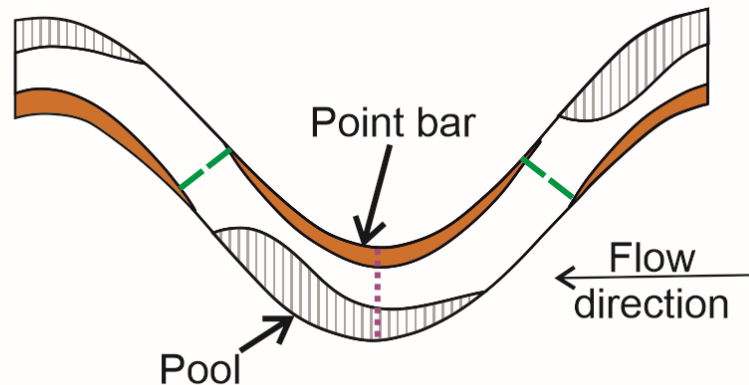


**Figure 4.1** Schematic diagram of in-channel morphology as a function of bend position and curvature for A) an experimental submarine channel with a constant width, adapted from Peakall et al. (2007) and Amos et al. (2010); and B) a river channel with greater width at the bend apex relative to the inflections, adapted from Trush et al. (2000) and Rossi (2012). Positions of maximum erosion (black stripes) and aggradation (orange area) are shown. Purple dotted lines represent apex cross-section and green dashed lines represent inflection cross-sections. Note that the areas of enhanced aggradation and erosion are located further downstream relative to the apex in the submarine channel than in the river case.

### 4.3 Width variations around river bends

Bends in rivers typically exhibit a maximum width at the bend apex, although there is a full range of morphology, including constant width, wider at bend inflection, and channels where bends exhibit no clear pattern (Brice, 1975, 1982; Lagasse *et al.*, 2004; Hooke, 2007). Bends in actively migrating meandering rivers, the 'sinuous point bar rivers' of Brice (1984) exhibit greater widths at bend apices, whereas 'sinuous canaliform rivers' show constant widths (Brice, 1982; Lagasse *et al.*, 2004). Canaliform rivers are marked by greater bank strength as a result of higher clay content or bank vegetation, and consequently they exhibit lower lateral migration rates at bend apices (Brice, 1984; Luchi *et al.*, 2012). Notably, an analysis of 1495 alluvial river bends, demonstrates that over 60% had their maximum width at the bend apex, with a point bar commonly present (Lagasse *et al.*, 2004). Wider-at-apex channels had a 14% wider width at the bankline from vegetation to vegetation line at the bend apex point compared to mean inflection points (Eke *et al.*, 2014a).

In contrast, a wider-at-inflection width is recognised for many sand-bed and gravel-bed rivers and has been incorporated into the concept of a riffle-pool sequence (Tinkler, 1970; Keller and Melhorn, 1978; Hudson, 2002). Riffle-pool-sequences may occur in a pattern in terms of bend planform with riffle areas occurring at inflection regions and pool areas occurring at apex regions (Tinkler, 1970; Keller and Melhorn, 1978; Hudson, 2002). A variable width or a wider-at-inflection width around bends is often controlled by alternate bar (free bar) formation (Zolezzi *et al.*, 2012; Duró *et al.*, 2016). Alternate bars, or free bars, are bars that develop spontaneously as a result of instability processes and may occur on either side of the bank or as mid-channel bars (Seminara and Tubino, 1989), which causes the channel width to increase at the position of free bars (Zolezzi *et al.*, 2012; Duró *et al.*, 2016).

Although the formation and movement of free bars can initiate width changes, ultimately width changes in rivers are controlled by the relative rates



of erosion at the outer bank and deposition at the inner bank (Eke *et al.*, 2014a, b). Where this variation is high, greater width variations occur (Eke *et al.*, 2014a, b). This process of width variation, and in turn bend migration, is therefore controlled by deposition at the inner bend (bar push) or erosion at the outer bank (bank pull), and their relative magnitudes (Nanson and Hickin, 1983; Braudrick *et al.*, 2009; Parker *et al.*, 2011; Eke *et al.*, 2014a, b; Matsubara and Howard, 2014; Van de Lageweg *et al.*, 2014; Wu *et al.*, 2016). Bank pull is related to initial channel widening, and bar push is related to initial channel narrowing (Eke *et al.*, 2014a). Independent results from laboratory experiments and numerical simulations suggest that bend migration of rivers is typically controlled at the bend apex by bank pull through outer bank erosion rather than bar push, for both bed-load and suspended-load deposition (Matsubara and Howard, 2014; Van de Lageweg *et al.*, 2014). However, the observed positive relationship between suspended sediment load and migration rate in certain systems may suggest that bar push dominates in these rivers (Constantine *et al.*, 2014; Donovan *et al.*, 2021).

Constant width, canaliform channels are related to restricted channel banks either through vegetation or silt/clay (Lagasse *et al.*, 2004; Luchi *et al.*, 2012; Matsubara and Howard, 2014); this acts to restrict the bank erosion rate (Luchi *et al.*, 2012), in turn limiting width variation. Some mixed-load and suspended-load alluvial rivers composed of fine sand to silt/clay also have a nearly constant channel width with steep banks (Page *et al.*, 2003; Matsubara and Howard, 2014). Inner bend deposition of these latter mixed-load, and associated suspended-load, rivers consists of oblique accretion deposits, which can form in the absence, or on top of, point bars. Oblique accretion deposits form in a low-energy environment from suspended load and consist of alternating thin sand and mud beds. These beds dip mostly towards the channel. Channel migration is low in these mixed-load and suspended-load rivers but scroll bars and bend cut-offs are formed (Page *et al.*, 2003; Matsubara and Howard, 2014). Hence a constant channel width might be related to a balance between low energy flows and sedimentation, whereby only enough erosion occurs at the outer bank to be balanced by deposition of

suspended sediment at the inner bend by secondary flow circulation (Nanson, 1980; Matsubara and Howard, 2014).

#### **4.4 Geological setting and study area**

The Congo Fan is a large active mud-rich submarine fan situated offshore Gabon, Congo and Angola, south of the Gulf of Guinea, on a mature passive margin, reaching a maximum water depth of around 5600 m (Figure 4.2; van Weering and van Iperen, 1984; Droz *et al.*, 1996). The fan is composed of at least 100 channel-levee systems from three sub-fans (from north to south: the Northern, Axial, and the Southern Fan) with the Axial Fan (210 ka-present) the youngest sub-fan. Within the sub-fan a single channel-levee system is active at any given time (Droz *et al.*, 2003; Marsset *et al.*, 2009). Abandonment of an active channel is initiated through avulsion (Droz *et al.*, 1996, 2003; Kolla, 2007; Marsset *et al.*, 2009).

The channels on the Axial Fan are chronologically recorded by the avulsion of the feeder channel (Marsset *et al.*, 2009; Picot *et al.*, 2016) and show a total of 52 almost complete channel-levee-lobe systems, called channel-lobes (Ax1-Ax52) by Picot *et al.* (2016). Four prograding-retrograding architectural cycles were observed from analysis of the channel length and avulsion length, whereby channel length and avulsion length reach a minimum at the end of each cycle: cycle A (Ax01-Ax13), cycle B (Ax14-Ax19), cycle C (Ax20-Ax44), cycle D (Ax45-Ax52), with the current active channel being Ax52 (Picot *et al.*, 2016). The age and timing of each architectural cycle is constrained by dating and/or proxies from cores (Picot *et al.*, 2019). Cycles A and B occurred between 210-70 ka with an average channel duration of 7.4 kyr; cycle C occurred between 70-11 ka with an average channel duration of 2.2 kyr; and cycle D occurred between 11-0 ka with an average 1.4 kyr channel duration (Picot *et al.*, 2019). The 52 channel-lobe systems belong to one of the Northern, Central or Southern Channels, which are independent

from the architectural cycles (Marsset *et al.*, 2009; Picot *et al.*, 2016). The Northern Channels with the current active Ax52 channel are the youngest channels on the Axial Fan and follow an E-W orientation. The Southern Channels, which are the oldest channels, follow a NE-SW direction (Picot *et al.*, 2016). The Northern and Southern Channels are separated by a topographic low, where the Central Channels occur. The Ax52 channel is known to be active from frequent cable breaks (Heezen *et al.*, 1964), direct flow measurement (Khripounoff *et al.*, 2003; Vangriesheim *et al.*, 2009; Azpiroz-Zabala *et al.*, 2017a) and recovery of Holocene fine-grained turbidites from cores (van Weering and van Iperen, 1984; Savoye *et al.*, 2009).

The activity of the Ax52 channel is explained by its connection to the canyon and is linked to periods of maximum river discharge (Heezen *et al.*, 1964; Picot *et al.*, 2019). The canyon extends 30 km from the shelf edge into the Congo River Estuary (Heezen *et al.*, 1964). The architecture and timing of avulsion of the channel-lobe systems on the Axial Fan have been connected to climatic factors controlled by the West African monsoon. During humid periods, river discharge increases and the fan progrades, whereas during arid periods the fan retrogrades (Picot *et al.*, 2019).

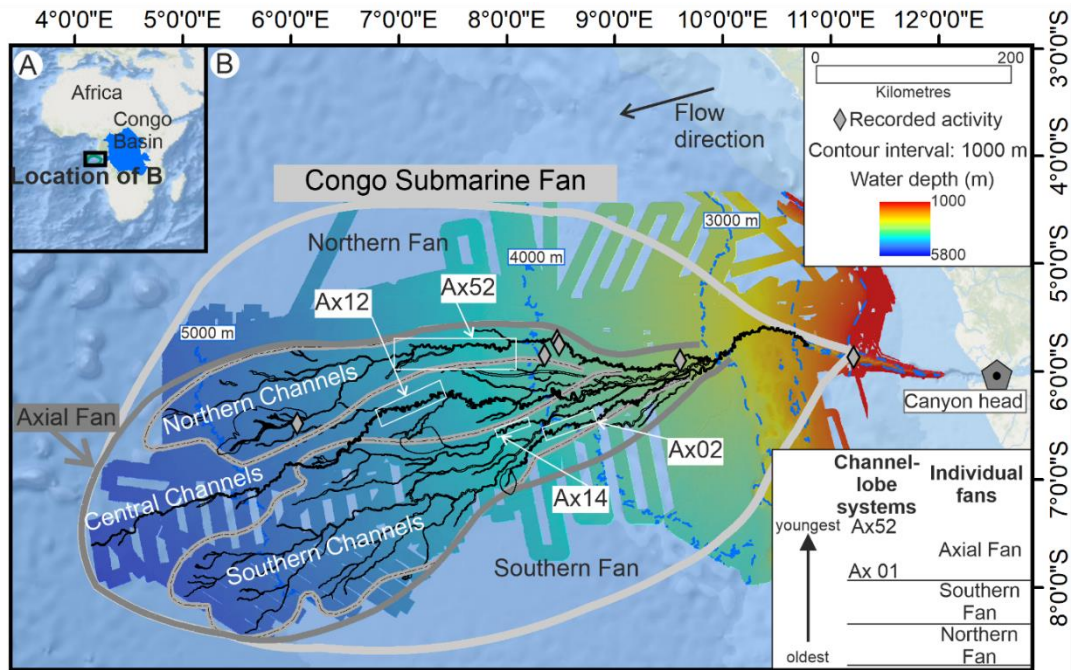


**Figure 4.2** A) Location of the Congo Submarine Fan and Congo basin. B) Bathymetry map of the Congo Submarine Fan with its individual fans (Northern, Southern and Axial Fan). The study area is situated on the Axial Fan, the youngest individual fan of the Congo Submarine Fan. The studied channel reaches are part of the Northern (Ax52), Central (Ax12) and Southern Channels (Ax02, Ax14). Channel Ax52 is currently active. The canyon head is the starting point for channel length measurements and is 77 km upstream, as measured by along channel distance, from the point of origin used by Babonneau *et al.* (2002). Grey diamonds represent positions of recorded activity; data obtained from Khripounoff *et al.* (2003), Vangriesheim *et al.* (2009) and Azpiroz-Zabala *et al.* (2017a). Studied channel reaches are shown as white boxes. Outline of fans, location of channels and relative age of channels are based on Picot *et al.* (2019).

## 4.5 Dataset and methodology

Bathymetric maps of the area were constructed during nine scientific cruises between 1992 and 2001 by IFREMER in partnership with TOTAL. Processed EM12 multibeam echo sounder (MBES) data provided a Digital Terrain Model (DTM) with a 100 m horizontal resolution and processed SeaBat7150 MBES data provided a DTM with a 50 m horizontal resolution. Absolute vertical accuracy of the water depth for both DTMs was 0.5% or lower, corresponding to between 10 m for 2000 m water depth and 25 m for 5000 m water depth.

ArcGIS 10.3.1 was used to analyse the channels, produce slope maps and to generate cross-sections perpendicular to the channel centreline. Matlab and ImageJ were used to interpret each extracted cross-section and to measure the channel width and height (see Section 4.5.1).

The channel base was identified as a reference level for each channel because channel bank crestlines can be irregular due to previous mass failure events (Kane and Hodgson, 2011), and crestline heights can vary substantially between inner and outer banks (Imran *et al.*, 1999), and spatially around bends, as a result of deposition from super-elevation (Imran *et al.*, 1999). It is noted that channel bases themselves can be spatially variable as a result of knickpoints of the order of 5-30 m in height (e.g. Vendettuoli *et al.*, 2019; Heijnen *et al.*, 2020; Guiastrennec-Faugas *et al.*, 2021). However, in the observed cross-sections, knickpoints were not observed; if present they are too small to be detected. The channel base is defined as those central parts where the slope approximates to zero, between the points where the lateral gradient abruptly increases. These gradient changes were identified manually using the bathymetry in combination with the slope map of the bathymetric data. The centreline of the channel was determined based on the midpoint of these channel base edges. Note that the centreline is preferred over the thalweg, the deepest part of the channel, as this is simpler to define geometrically and can be measured more accurately. Along the channel base centreline, bend apices were identified manually as points of maximum curvature and inflections as points of minimum curvature between two bend apices.

Sinuosity,  $P$ , defined as the ratio between the distance along the channel, and the straight distance between two points, was calculated for each channel reach and for each bend (Figure 4.3A). For bends, sinuosity is given by the channel centreline distance between the up-stream and down-stream inflection points, divided by the straight-line distance between these two points (Micheli and Larse, 2010). Classifications of straight, low and high sinuosity divisions are variable. The transition between straight and low sinuosity has been taken at: 1.05 (Reimchen *et al.*, 2016); 1.15 (Clark *et al.*,

1992); 1.25 (Babonneau *et al.*, 2010); or, 1.3 (Van den Berg, 1995). Here, the division between straight and low sinuosity was chosen as 1.2, which is an average of all the studies and the same value as Wynn *et al.* (2007). The transition between low and high sinuosity was defined as 1.5 (Leopold and Wolman, 1960; Clark *et al.*, 1992). Consequently, the following divisions were used: straight ( $1 \leq P \leq 1.2$ ), low sinuosity ( $1.2 < P < 1.5$ ), high sinuosity ( $P \geq 1.5$ ).

#### **4.5.1 Methodology for cross-section measurement around bends**

Cross-sections perpendicular to the channel base centreline (Figure 4.3B, see Appendix A) were taken using the right angle and split tool in the editor of ArcMap, for each bend at a series of positions. For each bend measurements were taken at the apex (7a), inflection points (1ui, 13di), and respectively five equally spaced cross-sections between the upstream inflection point and bend apex (2u-6u), and between the bend apex and downstream inflection point (8d-12d); giving 13 cross-sections for each channel bend. The cross-sections were divided into an inflection region (1ui-3u, 11d-13di; 6 cross-sections) and an apex region (4u-10d; 7 cross-sections, see Figure 4.3B).

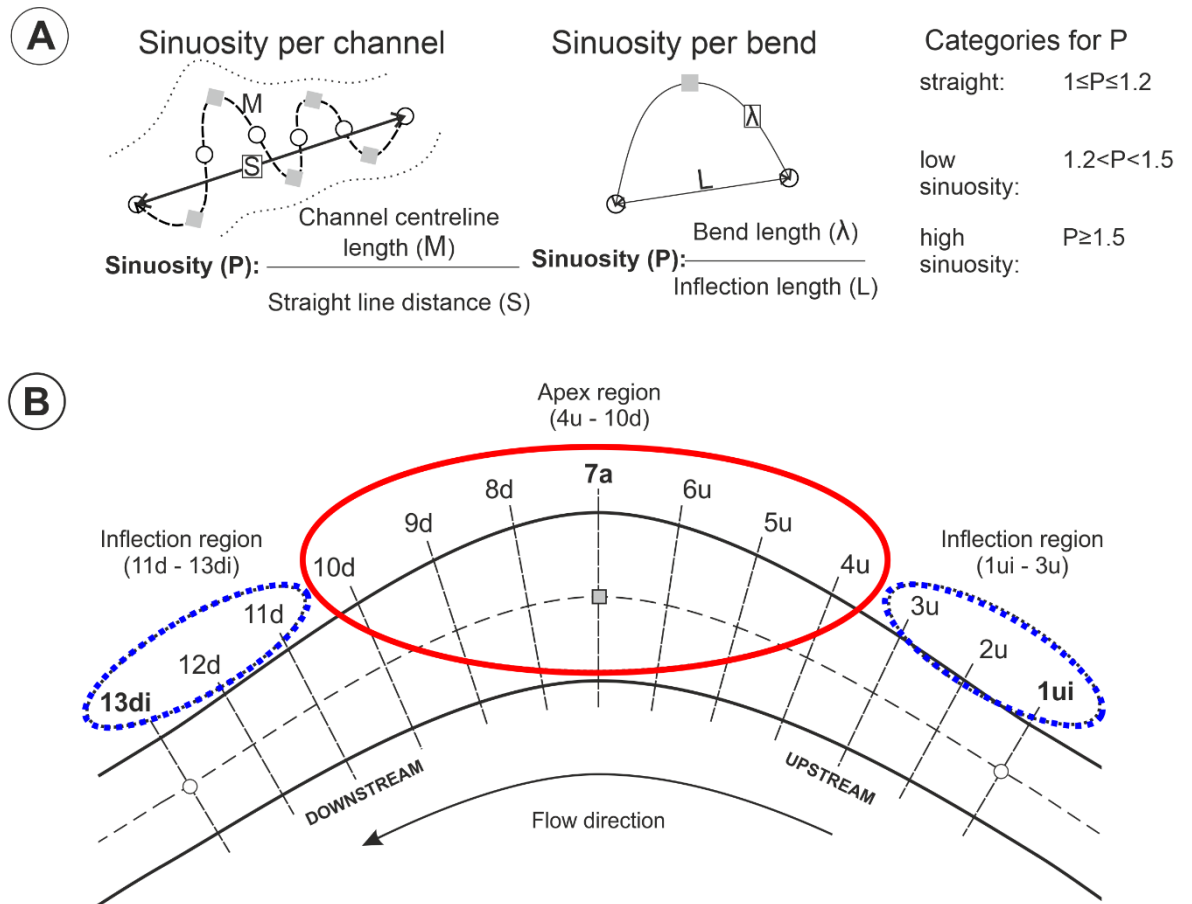


**Figure 4.3** Methodology for measuring: A) sinuosity, and B) width variation around bends. A) Sinuosity was measured per channel and per bend. B) Methodology for measuring cross-sections around a bend. Flow is from right to left. Thirteen cross-sections per bend were measured perpendicular to the channel base centreline (dashed line): at the up-stream inflection (1ui, white circle), at the down-stream inflection (13di, white circle), at bend apex (7a, grey square) and 5 cross-sections between the bend apex and up-stream (2u, 3u, 4u, 5u, 6u), and 5 between the bend apex and the down-stream inflection point (8d, 9d, 10d, 11d, 12d). Cross-sections were divided into an inflection region (blue dashed ellipses) and an apex region (red solid ellipse).

For each cross-section of a bend, channel height ( $H$ ) was measured from the channel base ( $H_0$ ) centreline up to the outer and inner channel bank crests ( $H_{Outer}$  and  $H_{Inner}$ , Figure 4.4B, C). Similarly, channel width was measured at the channel base ( $W_0$ ), and at vertical increments (on the channel centreline) of 10 m, up to the outer and inner channel bank crests ( $W_{Outer}$  and  $W_{Inner}$ , Figure 4.4B, C). The channel base width was defined as the distance between the points where lateral gradient abruptly increases. These points were

identified using the bathymetry in combination with the slope map. It should be noted that this definition of the channel base, may in the case of the inactive channels, incorporate latter stage infill and post-abandonment draping of the channel both of which would act to increase the width relative to that of the original active channel. In a few V-shaped cross-sections that lack a flat floor the channel base width was equivalent to a single point within the resolution of the DTM. In these cases the channel base width was taken as the width of the two adjacent measurement points on the channel cross-section.

For aggradational channels, channel banks are defined between the external levee crests (Kane and Hodgson, 2011; Hansen *et al.*, 2015). The positions of the two channel bank crests on the planform map (Figure 4.4A) were identified using a combination of bathymetric and slope maps. For individual cross-sections the bank crests are typically easily identified. In some cases where the crestline position is poorly defined, for instance due to a gentle rise of the banks (e.g., Figure 4.4B, inner bend and Figure 4.4C, inner bend), planform mapping of crestlines (Figure 4.4A) is used to identify the correct position.

Due to the nature of complex topography present within many submarine channels, a cross-section from bank to bank may lead to “erroneous measurements” (Shumaker *et al.*, 2018). Such “erroneous measurements” occur in the Congo channels because of the presence of terraces, which cause the inner bend topography to be lower than the topography at the channel bank crests. These changes to inner bend topography could lead to an overestimation of the channel width due to measuring the channel cross-section twice, either side of the meander neck, and incorrect estimates of maximum channel height (see for example cross-sections D-D’ and E-E’ in Figure 4.4D, E). Previous workers have resolved this issue by excluding such erroneous cross-sections (Shumaker *et al.*, 2018). However, a new methodology is introduced that can be used to collect cross-section data from all cross-sections in complex topography. An imaginary bank line is introduced that compensates for the missing topography at inner bend areas with lower elevations; it is here called a



trajectory line as it is equivalent to the trajectory line for the migration of scroll bars in rivers (Russell, 2017; Russell *et al.*, 2019). The trajectory line (red dashed lines in Figure 4.4) is obtained by connecting the midpoints of opposite cross-sections (1ui and 13di, 2u and 12d, 3u and 11d, 4u and 10d, 5u and 9d, 6u and 8d; see Figure 4.3) to the bend apex (7a), and linking this line to the intersection with the inner channel bank crestline. By way of an example, if a terrace was present at the inner bend which would lead to an “unrealistic measurement” (Figure 4.4D, E), channel height and width were measured normally up to the channel crest at the outer bend (e.g. Figure 4.4D, E; position D' of line D-D', or position E of line E-E'). However, at the inner-bend, bank-top channel width was measured up to the intersection with the trajectory line (e.g., Figure 4.4E, position c1 for line E-E'). In rare cases an exception occurred if the cross-section did not intersect with the trajectory line. In these cases, channel width was measured up the position of the maximum elevation of the inner bend along the cross-section (e.g., Figure 4.4D, position b1 for line D-D'). In all cases the corresponding channel height is given as the point where the trajectory line intersects with the channel bank crest at the inner bend (Figure 4.4D, E, position w1 for line D-D', and position w2 for line E-E').

In terms of workflow, the cross-sections were extracted from ArcMap using the 3D analyst tool and inserted into Matlab where channel base, bank crests, channel base centreline, and the vertical 10 m increments above the channel base centreline were annotated for each cross-section. Afterwards cross-sections were extracted as an image and loaded into ImageJ where channel height, and channel widths at different height increments were measured.

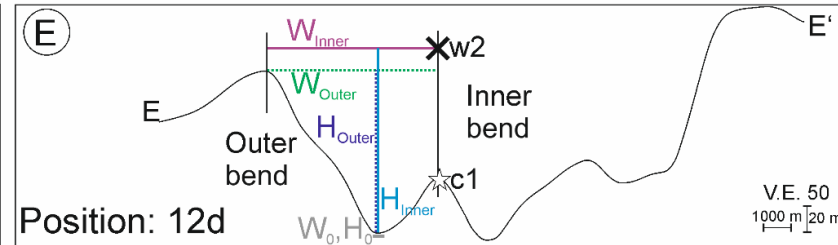
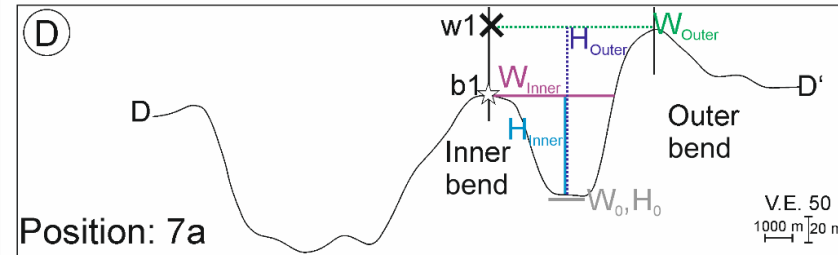
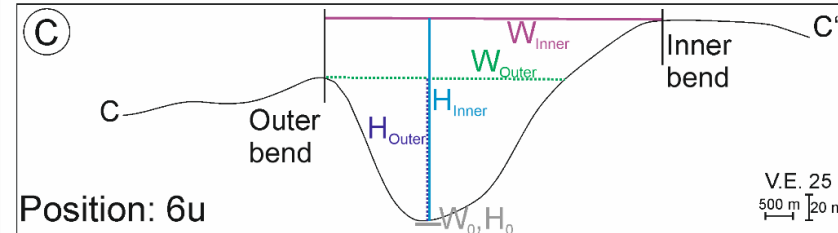
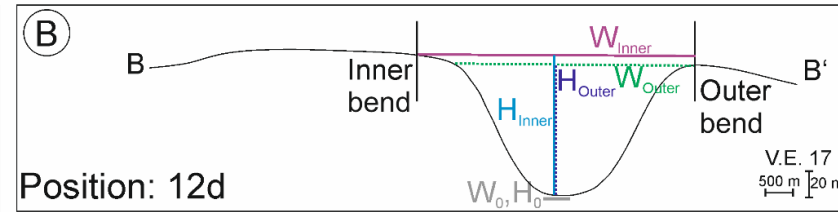
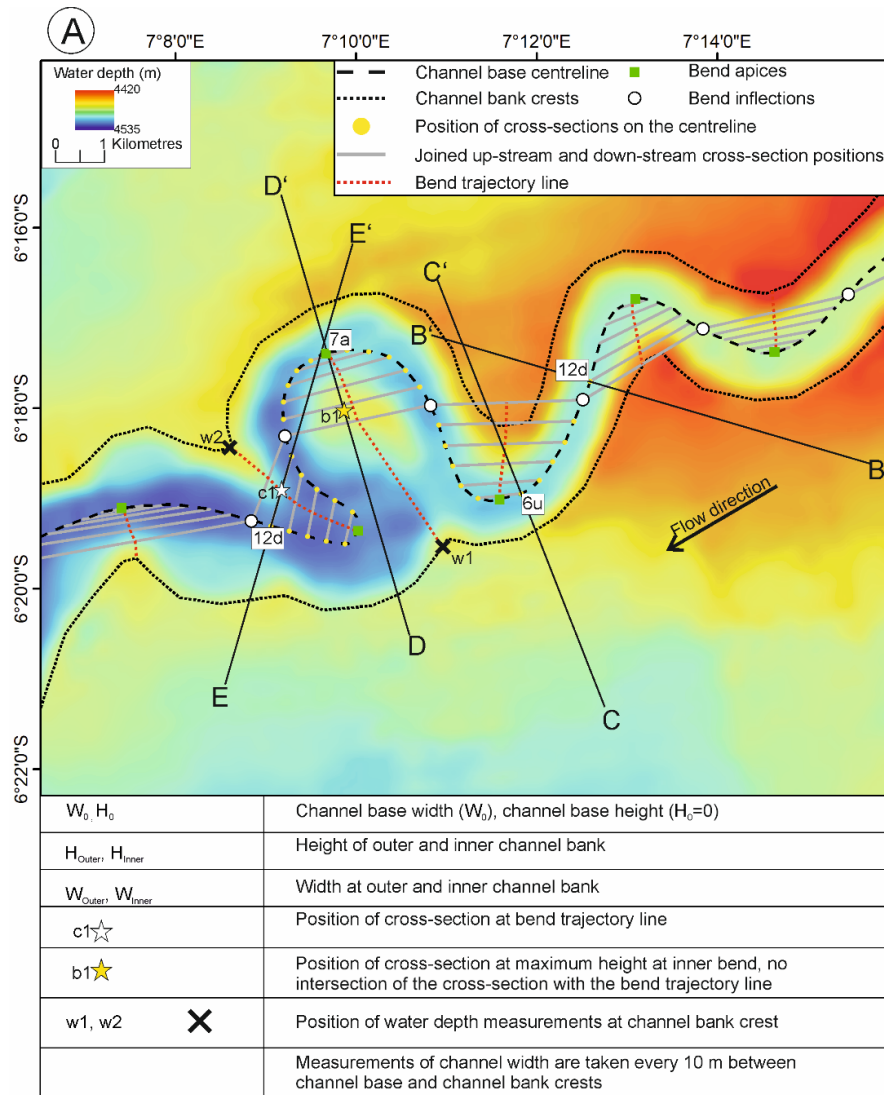


**Figure 4.4** Methodology for cross-section measurements in submarine channel bends. A) Bathymetric map showing an example of a channel reach with the channel base centreline, channel bank crestlines, bend trajectory lines, and the points on the centreline (yellow dots) where cross-sections would be taken from (see Figure 4.3 for details of the cross-sections themselves). For simplicity only 4 channel cross-sections are shown; lines B-B' to E-E'. The grey lines join the centreline points (yellow dots) at equivalent downstream and upstream positions around the bend (e.g., points 6u and 8d, see Figure 4.3). Trajectory lines are connected along the mid-points of these grey lines. B-E) Examples of width and height measurements from channel cross-sections. At each perpendicular cross-section width and height were measured as followed: channel width was measured at the channel base ( $W_0$ ), at the channel banks ( $W_{Outer}$ ,  $W_{Inner}$ ), and at height intervals of 10 m between the channel base and channel banks; channel heights were measured between the channel base ( $H_0=0$  m) and channel banks ( $H_{Outer}$ ,  $H_{Inner}$ ). B) Simple cross-section close to bend inflection, showing an inner bend without a clear crestal position; crestal position and height are estimated from the planform map of the crestline on part A. C) Simple cross-section close to the bend apex. D) Complex cross-section at the bend apex, where the bank to bank section at the height of the crestline, crosses the channel twice as a result of a lower elevation of the inner bend. Here, atypically, there is no intersection of the cross-section with the trajectory line (red dotted line). In this case the measured inner bend position is the position of the maximum elevation of the inner bank along the cross-section (position b1). The estimated channel height at the inner bend is measured up to the intersection of the trajectory line (red dotted line) with the bank crest (w1). E) Complex cross-section close to the bend inflection, showing multiple crossings of the channel. The intersection of the cross-section with the trajectory line (c1) is used to identify the inner bend position, and therefore identify the true width (see text for details). The estimated channel height at the inner bend (w2) is calculated as in D. DTM produced by IFREMER Géosciences Marines – ©IFREMER.

---

## 4.5.2 Channel width measurements: definitions and methodology

There are a number of approaches to measuring channel width variation around bends. At the simplest level, and analogous to many measurements in rivers, bank-top channel width can be measured at the bend apex, and compared to the average of the two inflection points (7a, and 1ui, 13di, respectively; see Figure 4.3). For each of these 3 cross-section positions, the following parameters are measured:

$$\text{Bank-top channel width: } \overline{W}_{Bank} = \frac{(W_{Outer} + W_{Inner})}{2},$$

where  $W_{Inner}$  and  $W_{Outer}$  are the widths as measured at the height of the inner and outer banks respectively (see Figure 4.4 for details).

A second approach is to measure the *depth-averaged channel width* by averaging the width measurements at different heights within the channel, for the bend apex section, and for the two inflection points:

$$\overline{x}_{7a} = \frac{1}{n} \sum_{i=0}^{Banks} x_i = \frac{x_0 + x_{10} + x_{20} + \dots + x_{Inner-1} \text{ OR } x_{Outer-1} + x_{Banks}}{n}$$

and

$$\overline{x}_{1ui,13di} = \frac{1}{n} \sum_{i=0}^{Banks} x_i = \frac{x_0 + x_{10} + x_{20} + \dots + x_{Inner-1} \text{ OR } x_{Outer-1} + x_{Banks}}{n},$$

where  $x_0$  is the position at a height of 0 m, equivalent to the channel base,  $x_{10}$  is 10 m above the channel base centreline,  $x_{Inner-1}$  or  $x_{Outer-1}$  refers to the last position with a 10 m increment from the channel centreline before the positions of the lowermost of the inner channel and outer channel banks,  $x_{Banks}$  is the mean position of the two channel banks ( $x_{Outer}$ ,  $x_{Inner}$ ) and  $n$  is the total number of measurements at all vertical positions for each cross-section.

One additional factor potentially needs to be taken into account when comparing depth-averaged channel width measurements around submarine channel bends is that channel bank height likely varies spatially around bends. Although super-elevation of flow in rivers is very small (Leopold, 1982), it can be two orders of magnitude higher in submarine channels (Dorrell *et al.*, 2013), and therefore bank

crestlines vary spatially around bends (Imran *et al.*, 1999). This spatial variation in bank heights in submarine channels may lead to a variation in the number of points in the vertical between different cross-sections, potentially influencing comparisons between sections by making those with more points in the vertical look wider than they are. To account for any bias induced by this variation of points a *comparative depth-averaged channel width* is introduced, where the number of points in all cross-sections at 10 m vertical increments from the channel base (thus excluding channel bank positions), is equal to the cross-section with the least vertical increments within a bend, and is calculated:

$$\overline{x_{7a}} = \frac{1}{n} \sum_{i=0}^{x_{max}} x_i = \frac{x_0 + x_{10} + x_{20} + \dots + x_{max}}{n} \text{ and } \overline{x_{1ui,13di}} = \frac{1}{n} \sum_{i=0}^{x_{max}} x_i = \frac{x_0 + x_{10} + x_{20} + \dots + x_{max}}{n}$$

where  $x_{max}$  is the height exhibited by the highest 10 m increment in the cross-section with the least number of points in the vertical.

An alternative to only focusing on the bend apex and inflection cross-sections, is to examine width changes around a given bend by using cross-sections from around a bend, and sub-dividing these into the apex region (4u, 5u, 6u, 7a, 8d, 9d, 10d, see Fig. 3 for cross-section nomenclature) and the inflection region (1ui, 2u, 3u, 11d, 12d, 13di). Such an approach has the advantage of synthesising data from the whole bend, and is not reliant on a single cross-section (the apex) or pair (inflections) of cross-sections which may not be fully representative of the broader bend. In particular, studies in rivers have demonstrated that maximum width is often at some point upstream or downstream of the bend apex (Eke *et al.*, 2014a). These aspects, in combination with the greater channel depths and the associated topographic complexity of the Congo channels, relative to rivers, suggest that this approach has potential for providing a broader comparison of bend regions. This approach enables the smoothing of any outliers at apices and inflections, and the capture of maximum width if it is not located at the bend apex. Afterwards, it is examined how these region-based measures compare to those derived from focusing on the individual apex section relative to the two inflection cross-sections. As with the apex and inflection cross-section, the *depth-averaged channel width* for these apex and inflection regions, contain all measurements per cross-section from the channel base to the channel banks:

$$\overline{x_{4u-10d}} = \frac{1}{n} \sum_{i=0}^{Banks} x_i = \frac{x_0 + x_{10} + x_{20} + \dots + x_{Inner-1} \text{ Or } x_{Outer-1} + x_{Banks}}{n}$$

and

$$\overline{x_{1ul-3u,11d-13d}} = \frac{1}{n} \sum_{i=0}^{Banks} x_i = \frac{x_0 + x_{10} + x_{20} + \dots + x_{Inner-1} \text{ Or } x_{Outer-1} + x_{Banks}}{n}.$$

A comparative depth-averaged channel width for these apex and inflection regions is also calculated in the same way as for the individual bend apex and inflection cross-sections:

$$\overline{x_{4u-10d}} = \frac{1}{n} \sum_{i=0}^{x_{max}} x_i = \frac{x_0 + x_{10} + x_{20} + \dots + x_{max}}{n}$$

and

$$\overline{x_{1ul-3u,11d-13d}} = \frac{1}{n} \sum_{i=0}^{x_{max}} x_i = \frac{x_0 + x_{10} + x_{20} + \dots + x_{max}}{n}.$$

For each of these definitions of channel width, a comparison is made of the relative increase at the apex (or apex region), relative to the inflections (or inflection region):

$$\% \text{ width increase at apex (or apex region)} = \frac{\overline{W}_A}{(\overline{W}_I/100)} - 100.,$$

where  $\overline{W}_A$  is the apex (or apex region) width, and  $\overline{W}_I$  is the inflection (or inflection region) width.

In order to compare variations in channel width in the vertical between different channel bends, the depth-averaged channel width is utilised. The channel height was normalised since channel height of submarine channels can vary: i) in the downstream direction by a few tens of metres (Klaucke *et al.*, 1997), ii) between different channel systems (Shumaker *et al.*, 2018; Jobe *et al.*, 2020) and iii) between channels from the same system (Straub *et al.*, 2012; Maier *et al.*, 2013). Each cross-section measurement was normalised by the maximum channel bank height for that cross-section. Thus a normalised height of 0 represents the channel base, and 1 is equivalent to the maximum channel bank height of a cross-section. In order to enable aggregation of different cross-sections across multiple bends, width measurements

were taken for each cross-section at each intercept of an increments of 0.1 of the normalised height. Subsequently, the mean width was calculated per normalised channel height increment for the apex and inflection, for both points (apex cross-section vs the two inflection cross-sections) and regions, for all channel reaches.

### 4.5.3 Error analysis

In this analysis, a differentiation is made for horizontal errors between the error arising from the DTM resolution, and the standard error of the mean associated with the sampled distributions. The different studied channel reaches have DTMs with either a horizontal resolution of 50 m or 100 m (cell size). The maximum absolute horizontal error for each point,  $P_i$  (Figure 5.5A), associated with gridding at a given resolution is given by:

$$|\delta_{max}P_i| = \sqrt{(25)^2 + (25)^2} = 35.4 \text{ m for the 50 m resolution dataset,}$$

and

$$|\delta_{max}P_i| = \sqrt{(50)^2 + (50)^2} = 70.7 \text{ m for the 100 m resolution dataset.}$$

Therefore each width, measured between two points, has a maximum absolute horizontal error of 70.7 m for the 50 m resolution DTM or 141.4 m for the 100 m resolution DTM. The absolute error distribution around a grid point,  $P_i$ , on the DTM is shown in Figure 5.5B, and the absolute mean is 0.54 of the maximum value, thus 19.1 m or 38.2 m for the 50 m and 100 m DTMs respectively; giving mean absolute width errors of 38.2 m or 76.4 m.

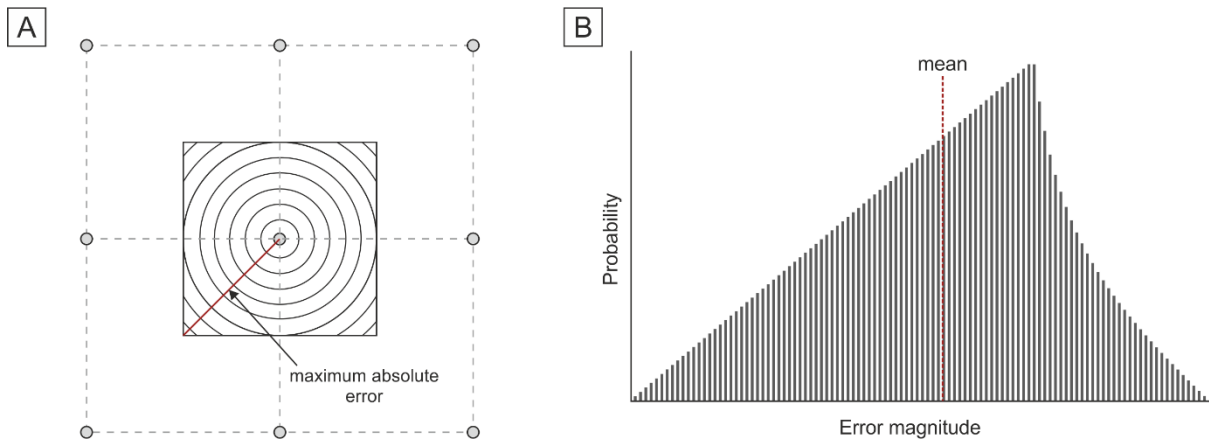


**Figure 4.5** Absolute error distribution around a point on a DTM grid. A) Planform view of a DTM grid, showing the distribution of distances (errors) around a point; the length of the maximum absolute error is shown with a red line. B) The probability density function of absolute errors around a DTM point; generated from choosing randomly selected points in the unit square and calculating the distance to the centre. The mean absolute value is 0.38 of the cell size (Weisstein, 2021), thus 0.54 of the maximum absolute error.

When taking width measurements from a DTM grid, however, the errors of interest are not absolute values, as there will be both positive and negative errors. With increasing numbers of measurement points the mean error would tend towards zero. Although the absolute error distribution for a point,  $P_i$ , (Figure 5.5B) is not a Gaussian distribution, an approximation of the effect of the number of measurement points can be given by considering the standard error of the mean,  $\sigma_{\bar{x}}$ :

$$\sigma_{\bar{x}} = \frac{\sigma}{\sqrt{n}}$$

Where  $\sigma$  is the standard deviation, and  $n$  is the number of measurement points. The best fit Gaussian to the distribution has a standard deviation of 0.20 of the maximum absolute error (0.14 of the cell size), giving values of 7.1 m and 14.2 m for the 50 m and 100 m DTMs respectively. However, as the true distribution is non-Gaussian, as a precaution the standard deviation is used twice:

$$\sigma_{\bar{x}} = \frac{2\sigma}{\sqrt{n}}$$

$n$  values for mean channel width estimates in this study range from 26 to 780 for the 50 m resolution, and from 54 to 4879 for the 100 m resolution datasets. Considering each end of the width measurement separately, this conservatively gives the standard



error of the mean for the location error due to each grid point,  $P_i$ , as 0.5-2.8 m, and 0.4-3.9 m for the 50 m and 100 m DTM datasets respectively. Thus taking the standard error of the mean for the points at either end of a width measurement, gives combined width errors of 1-5.6 m and 0.8-7.8 m for the 50 m and 100 m DTM datasets respectively. It is noted, that as 2 standard deviations from the mean is used, actual errors will be considerably lower than those estimated here. Lastly, it is noted that consideration of a planar surface is the conservative case, and that incorporation of a slope as present in reality, will further reduce the width errors; the error progressively diminishing with increasing slopes.

Although it is helpful to understand the magnitude of DTM grid related errors in the horizontal as discussed above, it is noted that the estimates of mean channel width in the present study, include systematic effects from variations in the width measurements themselves reflecting true changes in channel morphology, as well as the associated DTM grid errors as discussed above. Given the comparatively small values of the mean grid errors, it is not specifically considered them further. Instead, the standard error of the mean of the width distributions, of which the grid error is a component of the observed variation is used.

The error ( $\delta H$ ) for a single measurement point arising from the vertical resolution can be calculated using the instrumental error of 0.5% of the water depth,  $d$ , (Picot *et al.*, 2016):

$$\delta H = d * 0.005$$

Thus the absolute maximum vertical error,  $|\delta H_{\max}|$ , arising from one height measurement (two measurement points) is 1% of water depth and varies between channels from 40-45 m for the water depths in our study (**Error! Reference source not found.**). Non-maximum vertical errors can be estimated through error propagation:

$$\delta H_{Banks} = \sqrt{(\delta H_{Base})^2 + (\delta H_{Mean Bank})^2}$$

giving an error of 0.7% of water depth (Table 4.1). However, such an approach to estimating vertical errors is highly misleading since for this study there is no interest in the true depth value for a given point, which has these associated errors, but rather in relative errors between two points in the vertical, which have a high degree of spatial correlation (Calder, 2006, 2007; Czuba *et al.*, 2011). The spatially smooth nature of

the extracted cross-sections (e.g., Fig. 4) also demonstrates that relative errors across the DTM are far smaller than those calculated assuming errors from true depths. Thus it is demonstrated via the cross-sections that it is possible to take width measurements at regular 10 m height increments that reflect the broad morphology of the channel form.

**Table 4.1** Summary of the vertical error for height, for each channel system

<i>Channel name</i>	<b>Ax02</b>	<b>Ax12</b>	<b>Ax14</b>	<b>Ax52</b>
<i>Water depth (m)</i>	3909 to 4062	4409 to 4633	4105 to 4252	4170 to 4499
<i>Average water depth (m)</i>	4005	4535	4180	4340
Error ( $\delta H$ ) for height measurements (m)	28	33	30	31
Absolute maximum error ( $ \delta H_{\max} $ ) for height measurements (m)	40	45	42	43

Statistical analysis was conducted using the two-sample Student's t-test to test if a significant difference exists between bend apex and bend inflection widths, for a range of different width measurements for each channel. The two-sample Student's t-test is used for two samples with different sizes, that are not paired, and which exhibit an underlying normal distribution. The test analyses whether the two means are significantly different, or they are random. The hypothesis is the same for each tested channel. The null hypothesis is that the apex width is not larger than the inflection width. The alternative hypothesis is that apex width is larger than the inflection width. The null hypothesis is rejected if the p-value is less than 0.05, representing a confidence limit of 95%. As discussed later, p-values of  $<0.05$  for the overwhelming majority of our width measurements were calculated, suggesting that despite the

epistemic (systematic variations in channel width spatially) and aleatoric (random grid error) uncertainties discussed above, channel widths are larger at bend apices than at bend inflections.

## 4.6 Characteristics of studied channel reaches

The four studied channel reaches are situated on the Axial Fan of the Congo Submarine Fan and are part of the following channels which are from oldest to youngest: Ax02, Ax12, Ax14 and Ax52 (Picot *et al.*, 2016, 2019; Figure 4.6). Ax52 is the active channel and the others are classified as inactive channel reaches. The characteristics of each analysed channel reach can be seen in Table 4.2. The chosen channel reach for Ax52 is part of the lower channel-levee complex (Babonneau *et al.*, 2002) and was chosen as the degree of overspill starts to increase rapidly in this morphological region (Savoye *et al.*, 2009). Additionally, channel slope is relatively low and channel width is relatively constant (Babonneau *et al.*, 2002). The inactive channels (Fig. Figure 4.6A-C) were chosen as they have similarities in planform to the active channel (Figure 4.6D), but have different locations on the Axial Fan, and were active at different points of prograding/retrograding cycles (termed architectural cycles; Picot *et al.*, 2016). Additionally, Ax02 and Ax14, are covered by higher resolution bathymetric data (50 m resolution compared to 100 m for Ax52 and Ax12). The Ax02 and Ax12 channels were formed during the first architectural cycle, cycle A, of the Axial fan, whereby Ax02 occurred at the beginning of a prograding period and Ax12 occurred during the peak prograding period of cycle A (Picot *et al.*, 2016). Ax14 occurred during architectural cycle B during a peak retrograding phase.

**Table 4.2** Characteristics of each studied channel reach.

<i>Name of Channel</i>	<b>Ax02</b>		<b>Ax12</b>		<b>Ax14</b>		<b>Ax52</b>	
<i>Channel activity</i>	Inactive		Inactive		Inactive		Active	
<i>Horizontal resolution</i>	50 m		100 m		50 m		100 m	
<i>Water depth (m)</i>	3909 to 4062		4409 to 4633		4105 to 4252		4170 to 4499	
<i>Along channel distance from canyon head (km)</i>	653		853		694		796	
<i>Straight distance of reach (km)</i>	52		73		34		124	
<i>Distance along channel centreline (km)</i>	70		117		47		179	
<i>Sinuosity</i>	low (1.36)		high (1.6)		low (1.42)		low (1.44)	
<i>Channel-reach slope (m/m)</i>	0.002		0.002		0.003		0.002	
<i>Number of bends with terraces (Total bends)</i>	7 (19)		16 (27)		12 (13)		17 (49)	
<i>Number of apex (A) and inflection (I) region cross-sections</i>	133 A	114 I	189 A	162 I	91 A	78 I	343 A	294 I
<i>Fan development</i>	Beginning of prograding period		Peak of prograding period		Peak of a retrograding period		Prograding period	

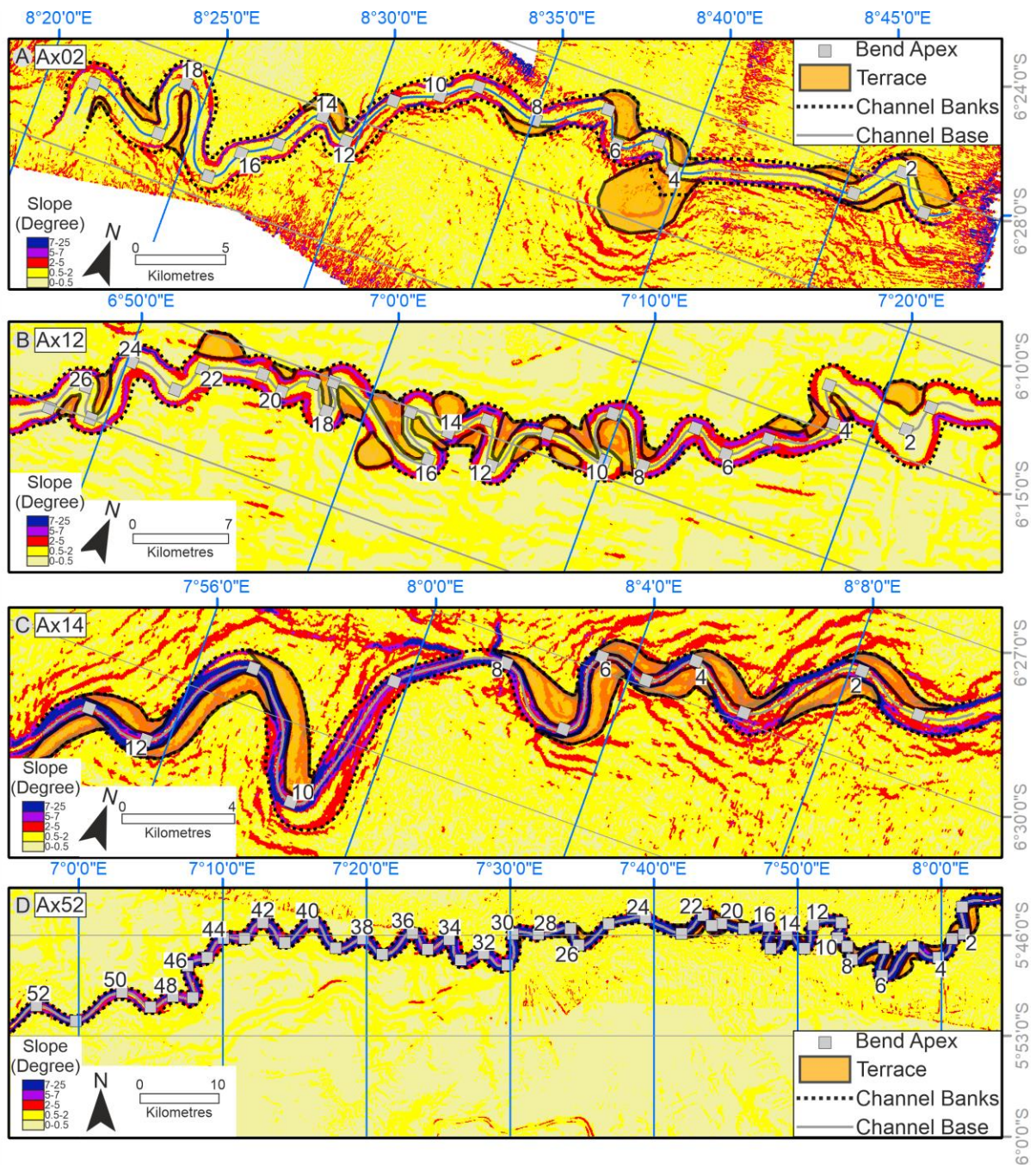


**Figure 4.6** Slope map with identified terraces and bend apices shown for each studied channel reach. (A) Ax02-channel. (B) Ax12-channel. (C) Ax14-channel. (D) Ax52-channel. Flow direction is from right to left.

## 4.7 Results

Here, firstly width variation around bends in individual channel reaches is examined, prior to examining the vertical distribution of channel width, and the relationship between width variations and sinuosity. Subsequently, an analysis of width variations is made for the compound dataset across all four of the channels reaches.

### 4.7.1 Variation of channel width around bends in individual channel reaches

#### *Overview*

Bank-top channel widths along each channel reach are plotted in Figure 4.7, and show that the channels vary between ~1 and ~5 km in width, with Ax14 the narrowest channel at ~1-2 km wide, and Ax12 the widest at ~1-4.5 km. The mean bank-top channel width is greater at the apex point compared to the inflection points for the majority of bends in all channel reaches, with 18 of 19 bends (95%) for Ax02 (Figure 4.7A), 20 of 27 (74%) for Ax12 (Figure 4.7B), 10 of 13 (77%) bends for Ax14 (Figure 4.7C), and 31 of 49 (63%) bends for Ax52 (Figure 4.7D) wider at the apex point. Most bends (15 of 19 bends) for Ax02 were at least 5% wider at the apex point compared to the inflection points with 6 bends (Figure 4.7A) more than 25% wider, and 2 bends greater than 50% wider. Similarly, most bends (19 of 27 bends) for Ax12 were at least 10% wider at the apex point compared to the inflection points, with 8 bends (Figure 4.7B) more than 50% wider. In contrast, 6 of 13 bends in Ax14 were more than 10% wider at the bend apex point, with 2 bends >40% wider (Figure 4.7C). For Ax52 there were 18 bends more than 10% wider, and 7 bends more than 40% wider. Almost identical results are observed when examining the data in terms of apex regions versus inflection regions (see Appendix C).

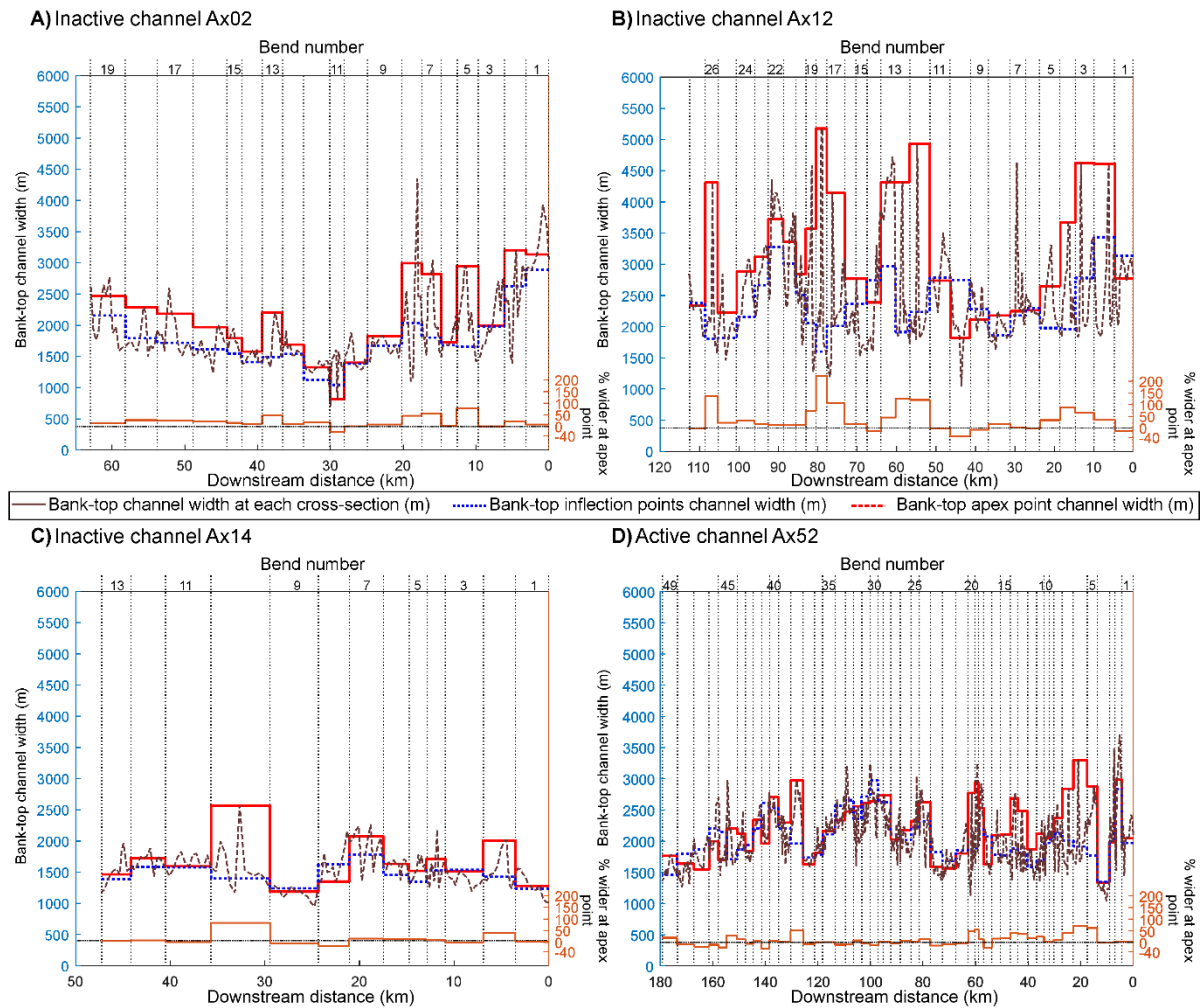


**Figure 4.7** Bank-top channel width at individual cross-sections (brown dashed-pointed line), at mean bank inflection points (blue dotted line), at bank apex point per bend (red solid line), and % wider at apex point, against downstream distance (km) and bend number for individual channel reaches A) Ax02, B) Ax12, C) Ax14 and D) Ax52. Flow direction is from right to left.

*Variation of channel width around bends: bend apex relative to bend inflection points*

The simplest measure of width variation around bends, is to compare the bend apex cross-section to the two bend inflection cross-sections. Examining the variation in terms of the bank-top channel width it is observed that the width is wider at the apex point than at the inflection points for all submarine channels (Ax02, 22% or 379 m wider; Ax12, 36% or 856 m wider; Ax14, 13% or 193 m wider; Ax52, 9% or 177 m wider; Figure 4.8). These differences between

bank-top channel widths around bends are all statistically significant ( $p < 0.05$ ; Table 4.3).

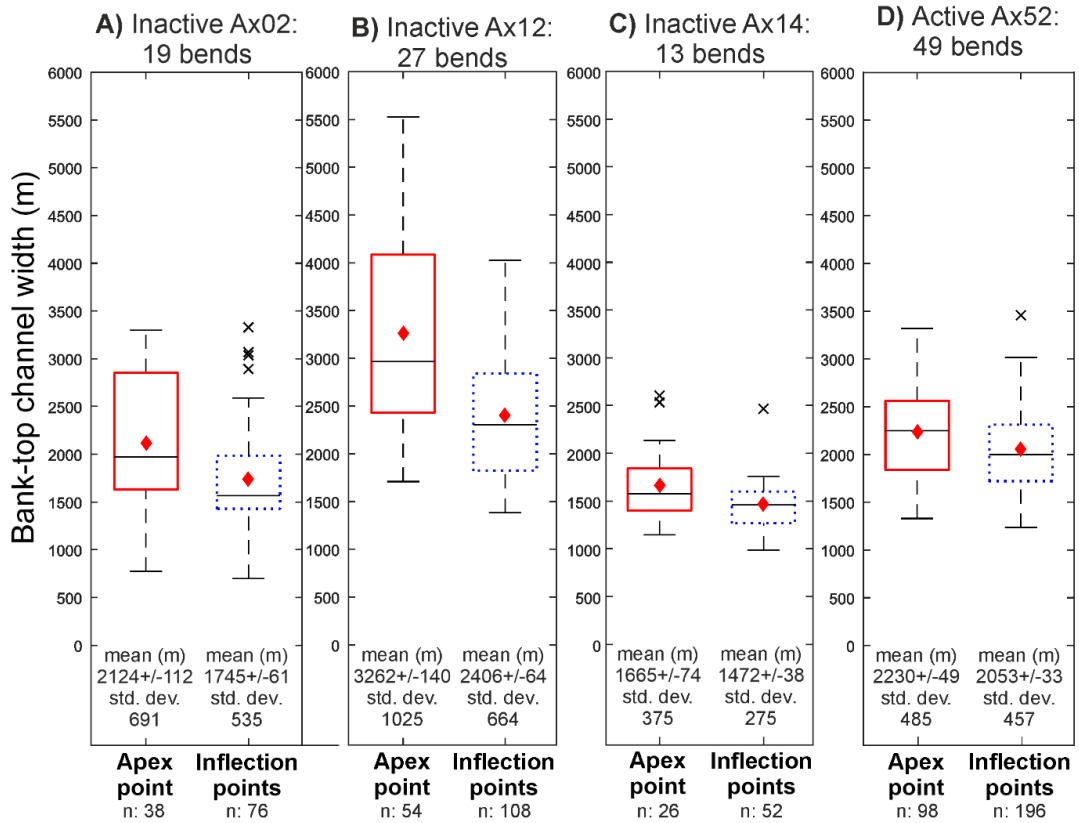


**Figure 4.8** Box and whisker plots of the bank-top channel width between apex point (7a, red solid line) and inflection points (1ui, 13di, blue dotted line) for A) Ax02, B) Ax12, C) Ax14 and D) Ax52. Data include the widths as measured at the height of the inner and outer banks. Box indicates 25th and 75th percentiles, “red diamond” indicates the mean, “-” within the box indicates the median, whiskers indicate 99.3% in a normal distribution and “x” indicate outliers. Mean  $\pm$  standard error of the mean, standard deviation (std. dev.) and the number of measurements (n) are shown for each position.

Looking at depth-averaged measures of the variation between bend axis width and bend inflection width, the mean comparative depth-average channel width (equal points in the vertical), and the depth-averaged channel width (all points in the vertical) is assessed; see Section 4.5.2. The mean comparative depth-average channel width is also wider at the apex point than at the inflection points for all submarine channels (Ax02, 22% or 234 m wider; Ax12, 38% or



548 m wider; Ax14, 6% or 35 m wider; Ax52, 8% or 69 m wider; Figure 4.9). All of these variations in channel width are statistically significant ( $p < 0.05$ ) except for the narrowest channel Ax14 (Table 4.3).

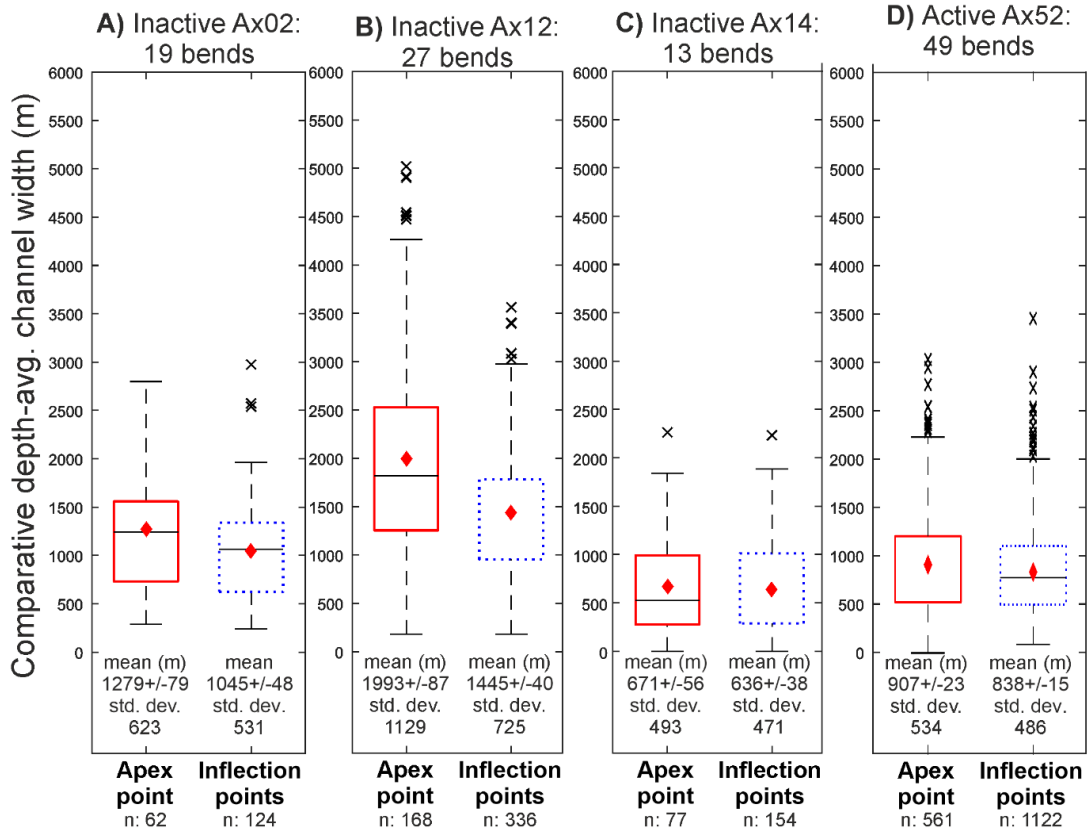


**Figure 4.9** Box and whisker plots of the comparative depth-avg. channel width between apex point (7a, red solid line) and inflection points (1ui, 13di, blue dotted line) for A) Ax02, B) Ax12, C) Ax14 and D) Ax52. Data include an equal number of measurements per cross-section for each bend and exclude the bank-top channel width. Box indicates 25th and 75th percentiles, “red diamond” indicates the mean, “-” within the box indicates the median, whiskers indicate 99.3% in a normal distribution, and “x” indicate outliers. Mean  $\pm$  percentage error of the mean, standard deviation (std. dev.) and the number of measurements (n) are shown for each position.

The data on depth-average channel width that incorporates all the points in the vertical are shown in Figure 4.10. Bend apices are again shown to be consistently wider than bend inflection positions. Although the channel width variations are different in absolute terms to those from the comparative

depth-averaged width analysis, the percentage differences are markedly consistent between the two (Ax02, 23% or 315 m wider; Ax12, 38% or 648 m wider; Ax14, 7% or 64 m wider; Ax52, 8% or 90 m; Figure 4.10). As with the comparative depth-averaged width data, all of these variations in channel width are statistically significant ( $p < 0.05$ ) except for the narrowest channel Ax14 (Table 4.3).

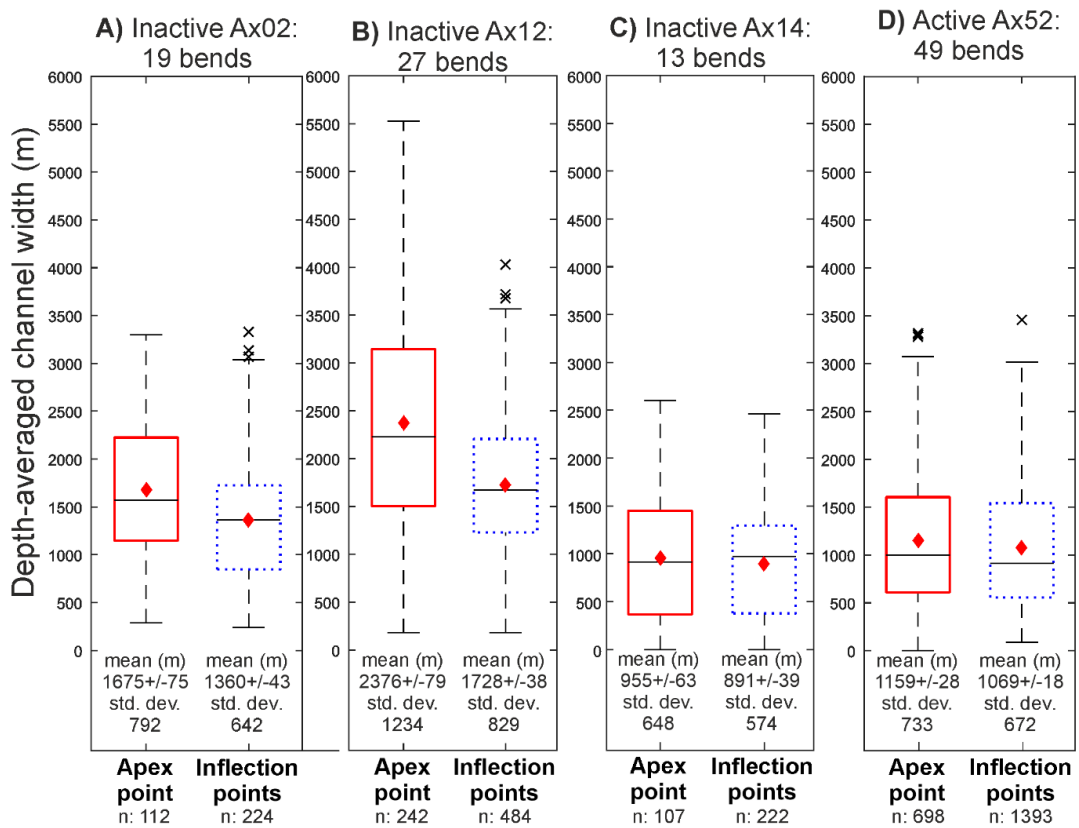


**Figure 4.10** Box and whisker plots of the depth-averaged channel width between apex point (7a, red solid line) and inflection points (1ui, 13di, blue dotted line) for A) Ax02, B) Ax12, C) Ax14 and D) Ax52. Data include the widths as measured at the height of the inner and outer banks. Box indicates 25th and 75th percentiles, “red diamond” indicates the mean, “-” within the box indicates the median, whiskers indicate 99.3% in a normal distribution and “x” indicate outliers. Mean  $\pm$  standard error of the mean, standard deviation (std. dev.) and the number of measurements (n) are shown for each position.

*Variation of channel width around bends: bend apex region relative to bend inflection region*

Although, assessing variation in channel width between bend apex and bend inflection points has the advantage of being most comparable to typical river methodologies, this approach may not capture the maximum width, nor provide an assessment of variations around the whole bend. Therefore, variations between bend apex and bend inflection regions is examined. The bank-top channel width is wider at the apex region than at the inflection region for all submarine channels (Ax02, 9% or 167 m wider; Ax12, 11% or 248 m wider; Ax14, 4% or 64 m wider; Ax52, 1% or 21 m wider; Figure 4.11). These variations in channel width between regions are statistically significant ( $p < 0.05$ ) except for the active channel Ax52 (Table 4.3). This contrasts with bank-top channel width data from the comparison of the apex and inflection points where the bend apex was significantly wider than the bend inflections in the active channel, Ax52.

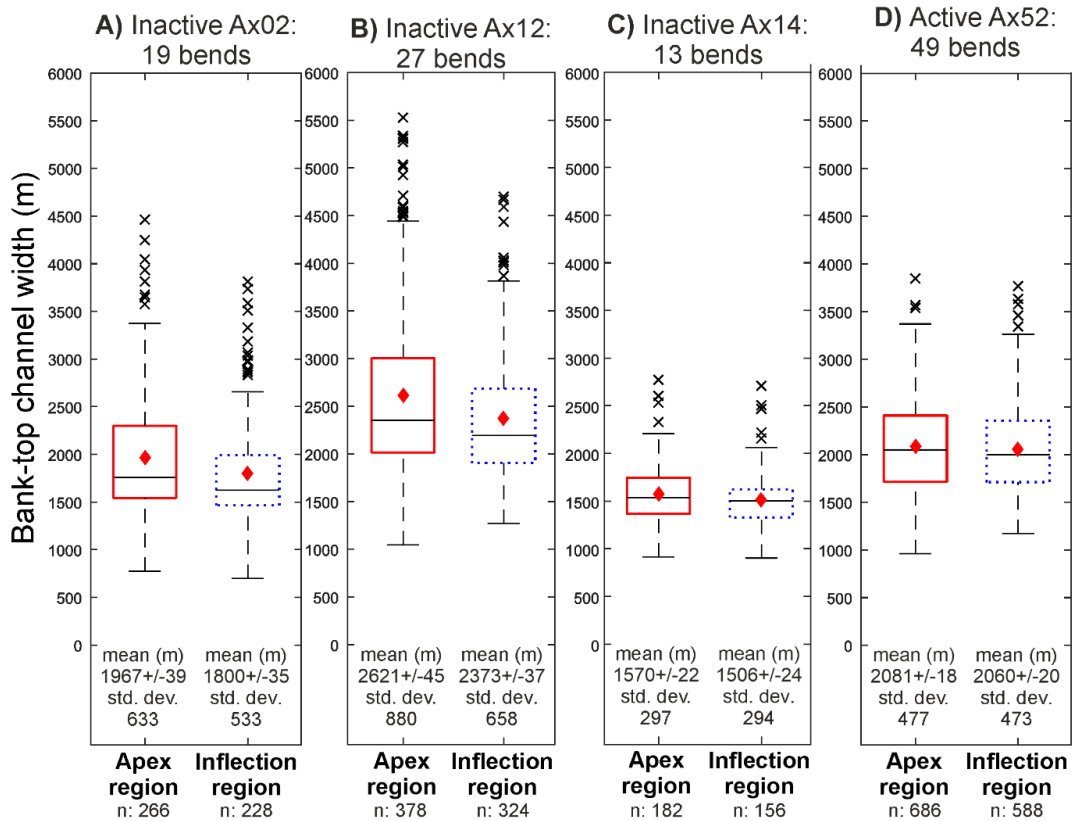


**Figure 4.11** Box and whisker plots of the bank-top channel width between apex (4u-10d, red solid line) and inflection (1ui-3u, 11d-13di, blue dotted line) regions for A) Ax02, B) Ax12, C) Ax14 and D) Ax52. Data include the widths as measured at the height of the inner and outer banks. Box indicates 25th and 75th percentiles, “red diamond” indicates the mean, “-” within the box indicates the median, whiskers indicate 99.3% in a normal distribution and “x” indicate outliers. Mean  $\pm$  standard error of the mean, standard deviation (std. dev.) and the number of measurements (n) for each region are shown.

The mean comparative depth-average channel width is also wider at the apex region than at the inflection region for all submarine channels (Ax02, 13% or 139 m wider; Ax12, 11% or 162 m wider; Ax14, 3% or 18 m wider; Ax52, 4% or 32 m wider; Figure 4.12). With the exception of the narrowest channel, Ax14, all of these variations in channel width between regions are statistically significant ( $p < 0.05$ ; Table 4.3).

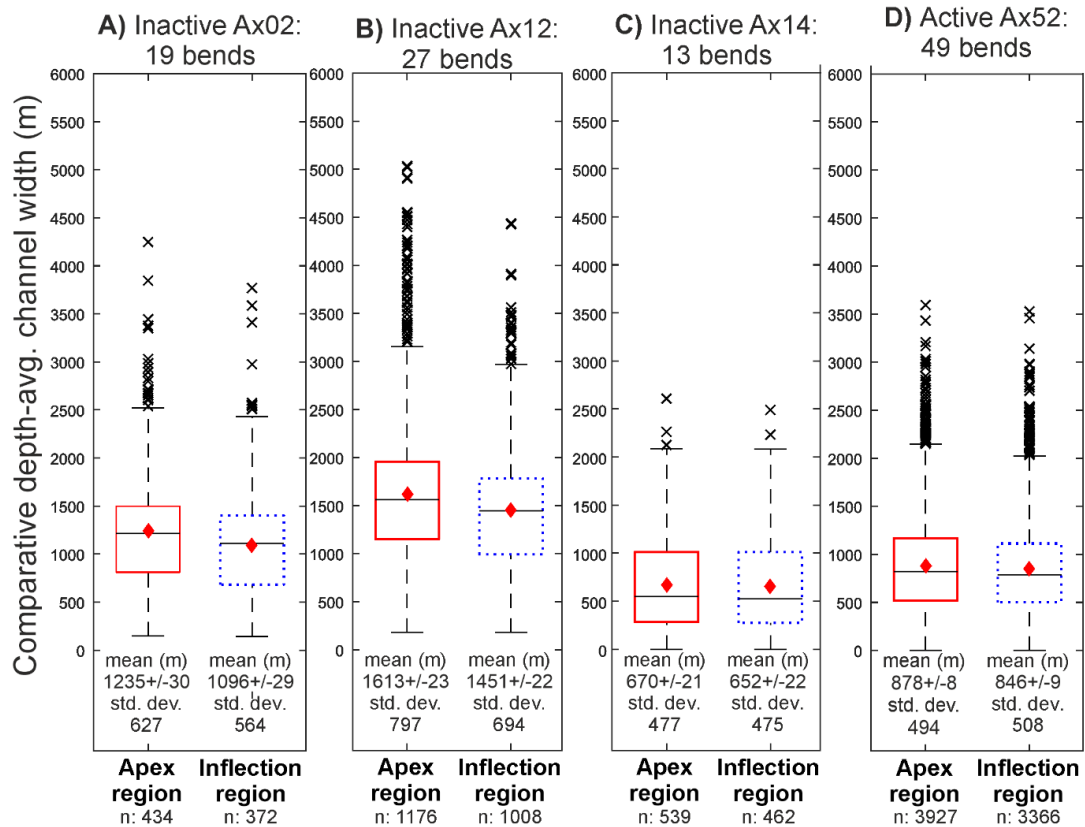


**Figure 4.12** Box and whisker plots of the comparative depth-avg. channel width between apex (4u-10d, red solid line) and inflection (1ui-3u, 11d-13di, blue dotted line) regions for A) Ax02, B) Ax12, C) Ax14 and D) Ax52. Data include an equal number of measurements per cross-section for each bend and exclude the bank-top channel width. Box indicates 25th and 75th percentiles, “red diamond” indicates the mean, “-” within the box indicates the median, whiskers indicate 99.3% in a normal distribution and “x” indicate outliers. Mean  $\pm$  percentage error of the mean, standard deviation (std. dev.) and the number of measurements (n) for each region are shown.

Lastly, the mean depth-average channel width is assessed. On this measure, the channel is also wider at the apex region than at the inflection region for all submarine channel reaches (Ax02, 11% or 151 m wider; Ax12, 11% or 189 m wider; Ax14, 1% or 12 m wider; Ax52, 3% or 32 m wider; Figure 4.13). With the exception of the narrowest channel, Ax14, all of these variations in channel width between regions are statistically significant ( $p < 0.05$ ; Table 4.2). As observed with the points data, the two measures of depth-averaged width produce strikingly similar results. In the case of the regions data, not only are

the percentage differences similar, but even the absolute magnitude of the variations are very close to one another.

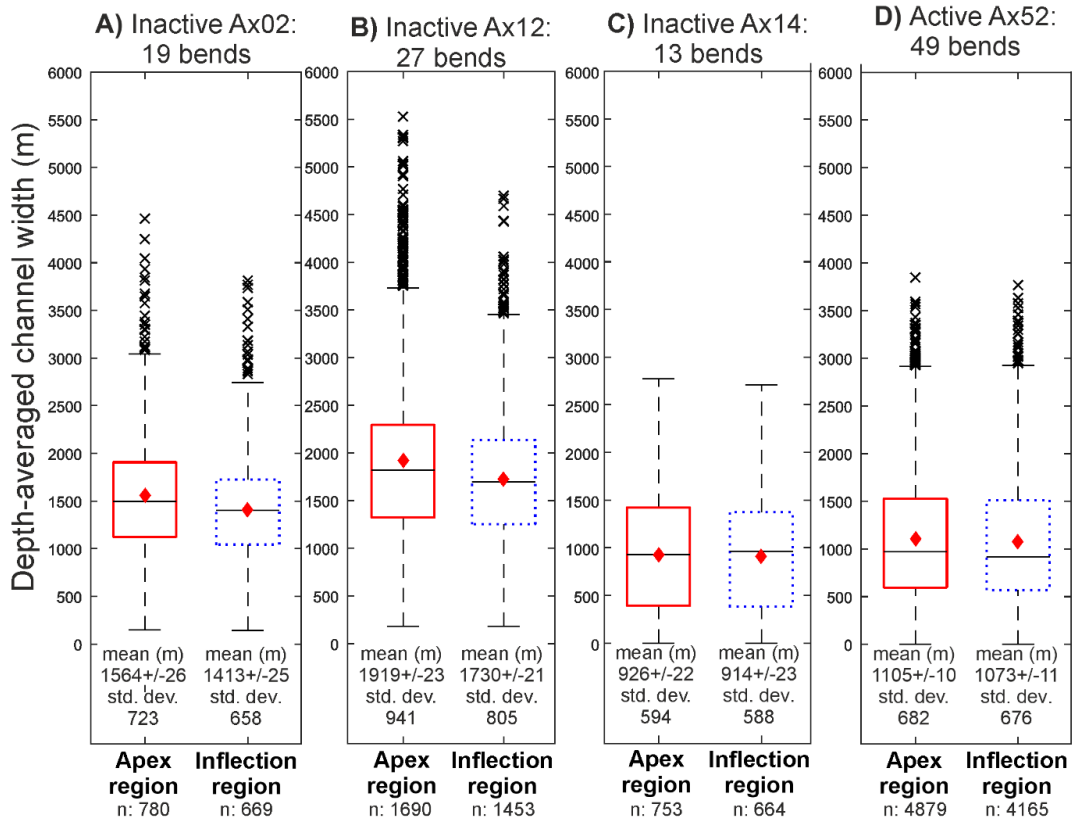


**Figure 4.13** Box and whisker plots of the depth-averaged channel width between the apex (4u-10d, red solid line) and inflection (1ui-3u, 11d-13di, blue dotted line) regions for A) Ax02, B) Ax12, C) Ax14 and D) Ax52. Data include the widths as measured at the height of the inner and outer banks. Box indicates 25th and 75th percentiles, “red diamond” indicates the mean, “-” within the box indicates the median, whiskers indicate 99.3% in a normal distribution and “x” indicate outliers. Mean  $\pm$  standard error of the mean, standard deviation (std. dev.) and the number of measurements (n) for each region are shown.

#### 4.7.2 Summary of width variations around bends in individual channels

All three measures of channel width, at both points (bend apex, and bend inflection cross-sections), and regions, produced a consistent result that in all cases the bend apex was wider than the bend inflection (Figure 4.14). The

magnitude of these variations varied from 1% to 38% depending on the width measure and the channel reach (Figure 4.14). For three of the channel reaches, Ax02, Ax12 and the active Ax52, all measures were statistically significant ( $p < 0.05$ ), with the one exception of the bank-top channel width for regions, where Ax52 was not significant (Table 4.3). In contrast, the narrowest channel, Ax14, only showed a significant ( $p < 0.05$ ) variation between bend apex and bend inflection width for the two measures of bank-top channel width (points, and regions); the depth-averaged measures were not significant (Table 4.3). The two-sample t-test therefore rejected the null hypothesis that the apex-width was not larger than the inflection region width, for Ax02, Ax12, Ax52 bar one measure, and for the bank-top channel width measures for Ax14 (Table 4.3). The alternative hypothesis that the apex width is wider than the inflection width was therefore accepted for almost all cases (Table 4.3). Measured variations in channel width between bend apices and bend inflections are two to three times greater when measuring width at bend apex and bend inflections points (6-38% greater at bend apices), than they are for bend regions (1-13%, Figure 4.14). This indicates that maximum channel width is somewhere close to the bend apex in these systems, and therefore measuring width changes by region has the effect of smoothing out these variations. Nonetheless, even when measured across these regions there remains, in most cases, a statistically significant enhancement in bend apex widths.

The different channel reaches range in the degree to which bends are wider at apices relative to inflections (Figure 4.14). The widest channel Ax12 shows the greatest difference between bend apices and bend inflections, with a difference of 36-38% on the apex to inflection points measures, and 11% for regions. Ax02 is the second widest channel on the depth-averaged measures, and also shows a substantial variation between bend apex and inflection, of 22-23% on points measures, and 9-13% for regions. Ax52 is the third widest on depth-averaged measures, although it is wider than Ax02 on bank-top channel width measures. Bend apices are 8-9% wider than inflections for the points data, but only 1-4% wider at regions, of which the 1% difference for bank-top channel width at regions is not statistically significant ( $p < 0.05$ ). Finally, Ax14 is the narrowest of the channels, and here only the bank-top channel width variations of 13% (points) and 4% (regions) are statistically significant.

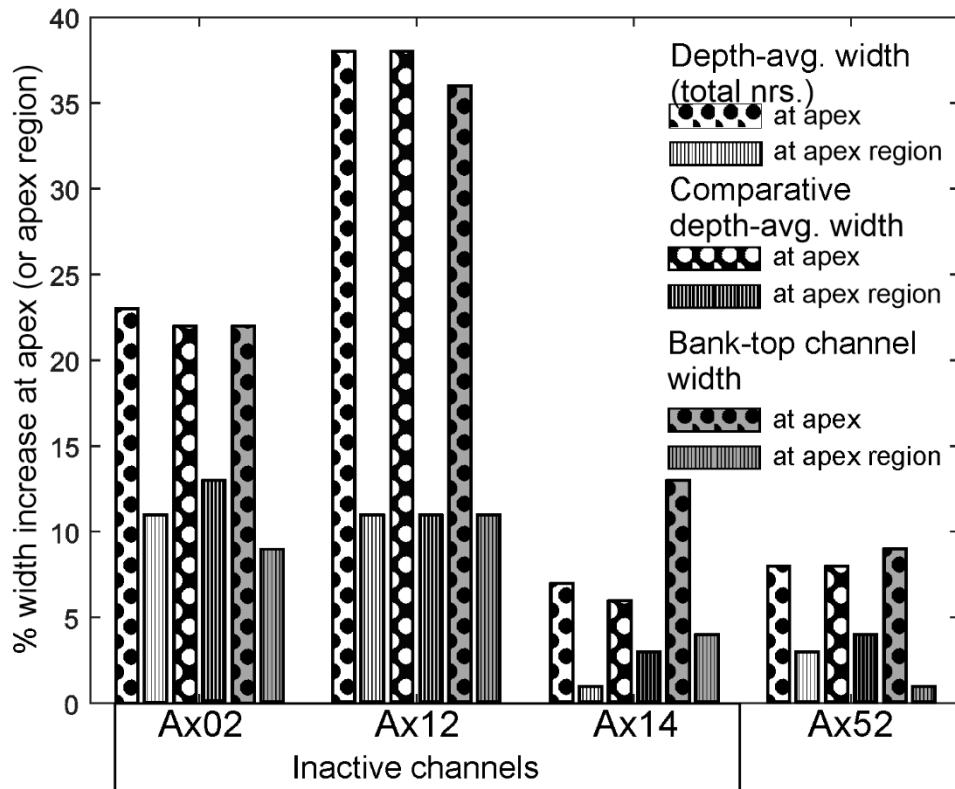


**Figure 4.14** Bar charts showing the percentage width increase at bend apices compared to the inflection points (symbol: dots), or between apex and inflection regions (symbol: vertical lines), for different measures of channel width. The different width measures are depth-avg. width (symbol: white box), comparative depth-avg. width (symbol: black box) or the bank-top channel width (symbol: grey box). The inactive channels are Ax02, Ax12 and Ax14 and the active channel is Ax52. All results are statistically significant ( $p < 0.05$ ) other than both depth-averaged measures for Ax14, and the depth-averaged region data for Ax52 (see Table 4.3).



**Table 4.3** Results of two-sample Student's t-test between bend apex and bend inflection widths, for a range of different width measurements, for the four channel reaches. The null hypothesis was that the apex-width was not larger than the inflection region width. The table reports p-values, or probability values, that identify whether a statistically significant relationship exist between two sample groups. A p-value of <0.05 identifies a statistical significance between two sample groups with a 95% confidence interval, and rejects the null hypothesis and thus confirms the alternative hypothesis. The alternative hypothesis is that bend apex width is greater than bend inflection width. 'None' represents no significant relationship.

<b>Width measure</b>	<b>Ax02</b>	<b>Ax12</b>	<b>Ax14</b>	<b>Ax52</b>
Bank-top channel (points)	<0.005	<0.0005	<0.025	<0.0025
Comp. depth-average (points)	<0.01	<0.0005	None	<0.01
Depth-average (points)	<0.0005	<0.0005	None	<0.005
Bank-top channel (regions)	<0.001	<0.0005	<0.025	None
Comp. depth-average (regions)	<0.001	<0.0005	None	<0.005
Depth-average (regions)	<0.0005	<0.0005	None	<0.025

Lastly, it is noted that the two measures of depth-averaged width, one with an equal number of points for every cross-section (comparative depth-averaged width), and one including all data (depth-averaged channel width) are shown to give very similar results. This indicates that any height variations around channel bends as a result of the enhanced super-elevation in submarine channels, are not unduly biasing the measurement of width variations around bends. Given this result, all subsequent data analysis uses the depth-averaged width data, therefore retaining all of the measured data points. The inclusion of channel banks in the depth-averaged width measurement also enables a reference point for normalisation and comparison of width data from the four channel reaches (see Section 4.5.2).

### 4.7.3 Width variation between channel base and channel banks

The depth-averaged width at both apex and inflection points, and at apex and inflection regions, increases with height above the bed for all submarine channels, but for Ax02 and Ax12 the magnitude of this difference between the width at the apex and at inflections is greater (Figure 4.15 and 4.16). The percentage depth-averaged width variation between the apex and inflections is relatively constant with height for most of the channels, however more variability is shown for Ax14 (Figure 4.16).

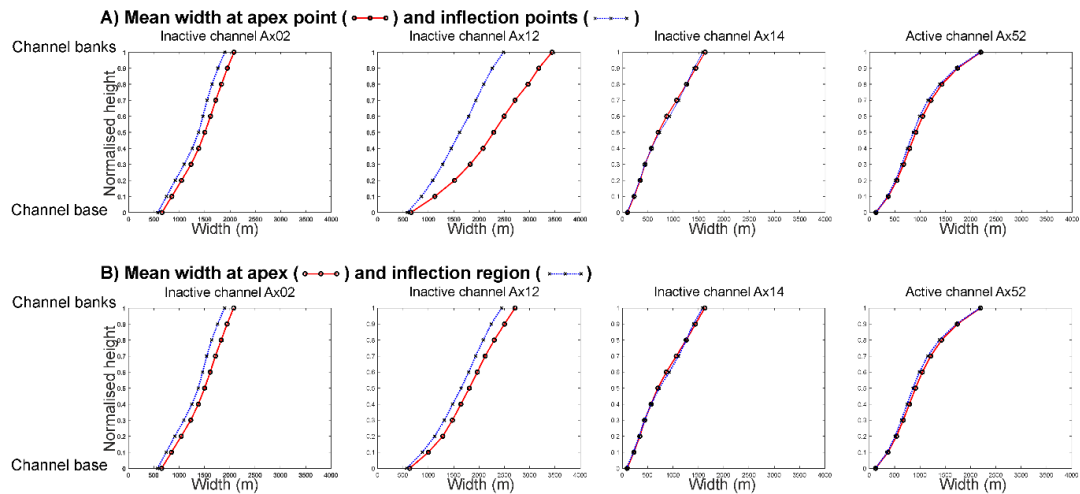


**Figure 4.15** Depth-averaged width with normalised height at A) apex point (red dashed line) and inflection points (blue dotted line), and B) apex (red dashed line) and inflection region (blue dotted line) for all channel reaches (Ax02, Ax12, Ax14, and Ax52). The normalised height was calculated using the maximum height of each cross-section. Width measurements were calculated by taking the intersection of the normalised height at 0.1 increments with the extracted cross-section profile. Afterwards the data were averaged. Each data-point corresponds to the average of all bends of a reach.

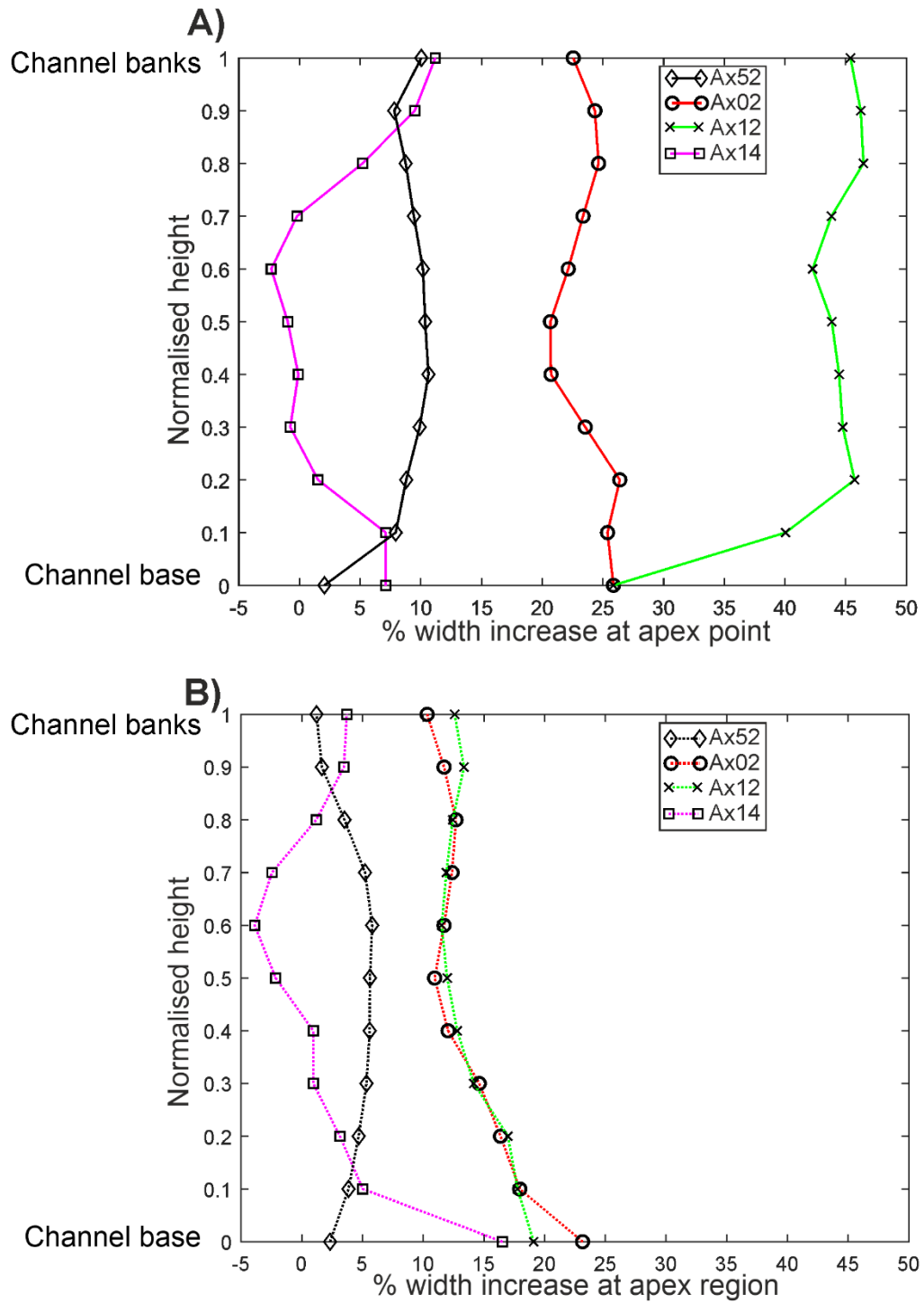


**Figure 4.16** Percentage width increase at the apex with normalised height, at A) apex point, and B) apex region, for all channel reaches (Ax02, Ax12, Ax14, and Ax52). The normalised height was calculated using the maximum height of each cross-section.

#### 4.7.4 Channel width variation as a function of sinuosity

Here, the relationship between sinuosity and variations in channel width around bends are examined. In Figure 4.17 the apex-inflection ratio is plotted against sinuosity, with the ratio representing the depth-averaged width at the bend apex region, divided by the depth-averaged width at the bend inflection region, for a given bend. The apex region width was wider than the inflection region width in the majority of cases for bends across all sinuosity classes; straight ( $P \leq 1.2$ ), low sinuosity, and high sinuosity (Figure 4.16 and 4.17). The majority of bends were classified as straight ( $n=53$ ), with a more equal distribution between low sinuosity bends ( $n=24$ ) and high sinuosity bends ( $n=31$ ).

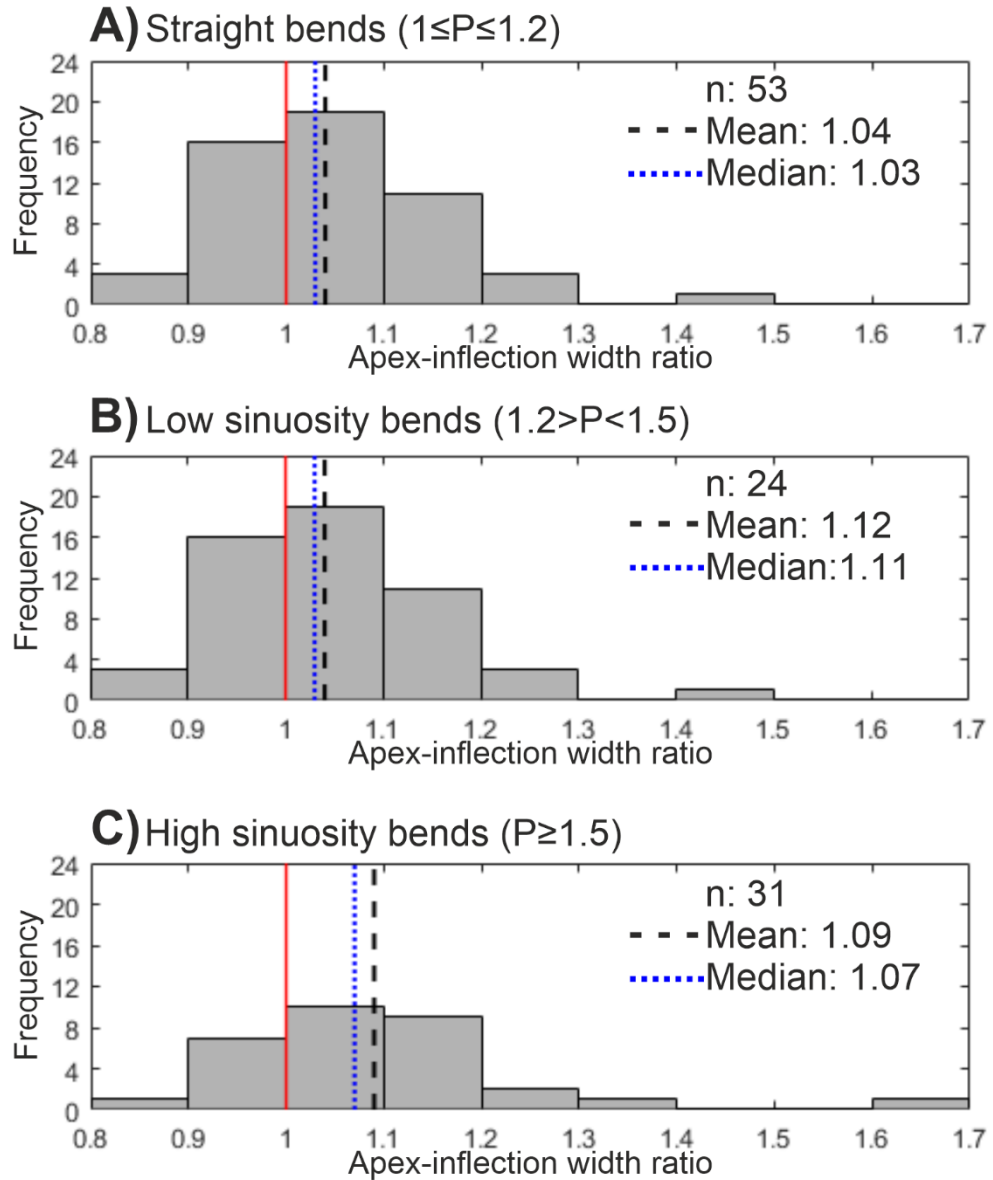


**Figure 4.17** Bar charts showing the apex-inflexion width ratio for A) bends classified as straight ( $1 \leq P \leq 1.2$ ), B) low sinuosity bends ( $1.2 < P < 1.5$ ), and C) high sinuosity bends ( $P \geq 1.5$ ). Sinuosity was obtained for each bend and corresponds to the ratio between bend length and inflection length (see Figure 4.3A). A second way to assess the relationship between sinuosity and variations in width around channel bends, is to plot mean apex width at regions, against mean inflection width at regions, as a function of sinuosity classes (Figure 4.18). The linear regression varied little between bends classified as straight, low sinuosity, and high sinuosity, suggesting that there is little if any relationship between sinuosity and a wider apex region width (Figure 4.18). No difference is seen between different channel reaches.

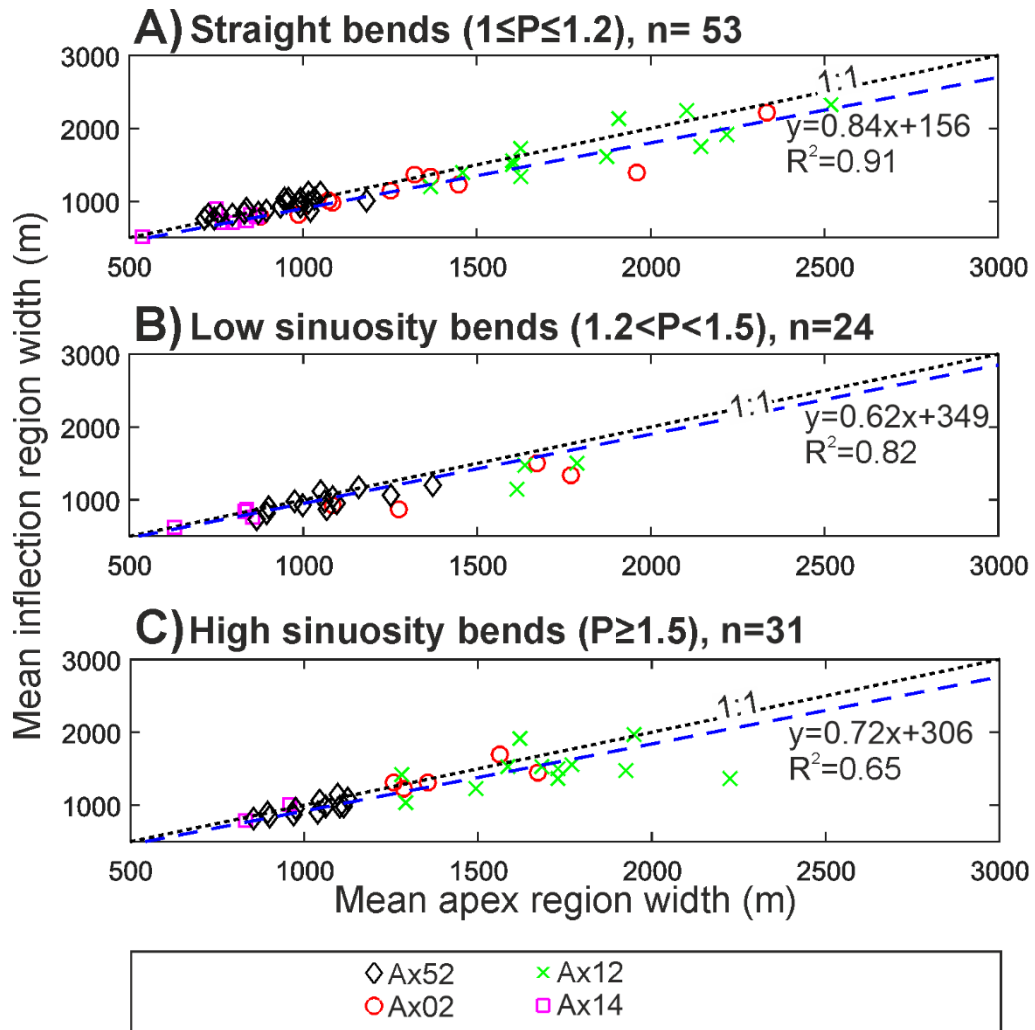


**Figure 4.18** Mean apex region width versus mean inflection region width for A) bends classified as straight ( $1 \leq P \leq 1.2$ ), B) low sinuosity bends ( $1.2 < P < 1.5$ ), and C) high sinuosity bends ( $P \geq 1.5$ ). The following channels were used: Ax02 (19 bends, circle), Ax12 (27 bends, cross), Ax14 (13 bends, square) and Ax52 (49 bends, diamond). Each point represents one bend and contains measurements from the depth-averaged channel width. Sinuosity was obtained for each bend and corresponds to the ratio between bend length and inflection length (see Figure 4.3A).

### 4.7.5 Channel width variation as a function of radius of curvature

The relationship between the percentage bank-top channel width increase at the bend apex point relative to inflection points is plotted as a function of radius of curvature normalised by the bank-top channel width (Figure 4.19). These data can be fitted by an envelope that describes the maximum width increase at bend apices relative to inflections for a given normalised radius of curvature. This envelope shows that channel apices are at their widest relative to inflections for tight bends, peaking at a radius of curvature-channel width ratio between 0.3 and 0.4 for Ax02, Ax12 and Ax52 and slightly above 0.4 for Ax14.

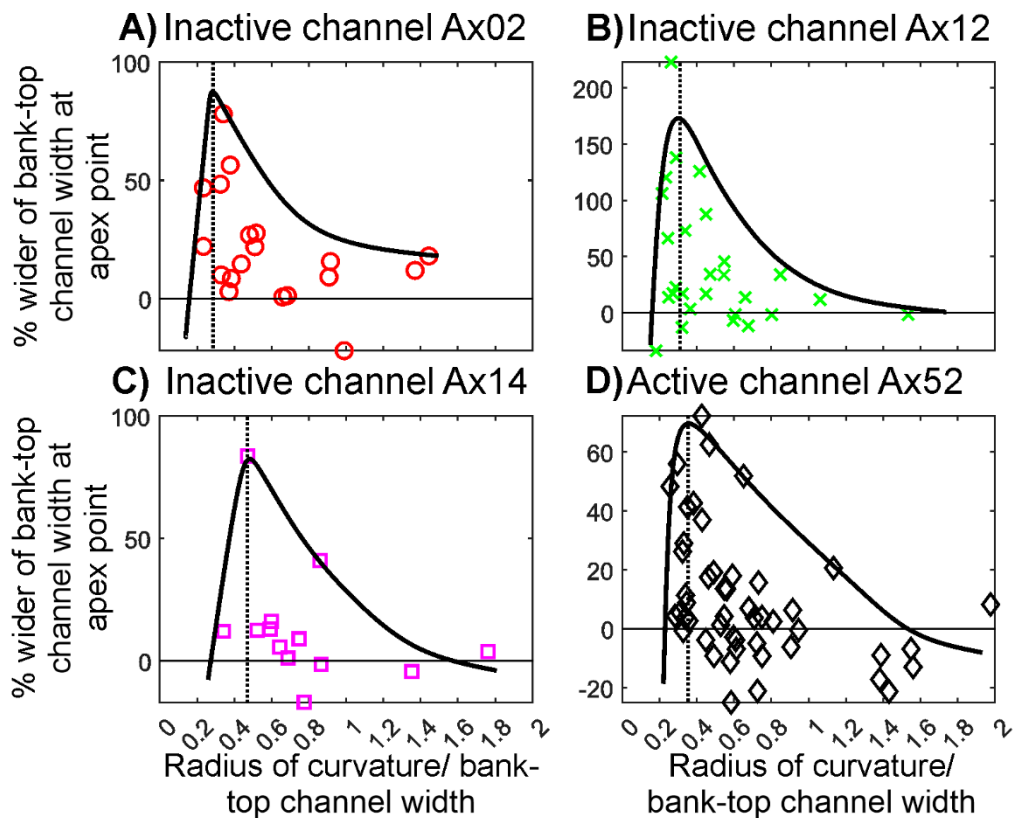


**Figure 4.19** Relationship between the percentage bank-top channel width increase at the bend apex point relative to inflection points, and the ratio of radius of curvature to bank-top channel width, is shown for A) Ax02 (19 bends), B) Inactive channel reach Ax12 (27 bends), C) Inactive channel reach Ax14 (13 bends) and D) Active channel reach Ax52 (49 bends). Each point represents one bend. The radius of

curvature was measured for each bend using the curve-fitting method (Brice, 1973, 1974) along the channel base centreline. The channel width is the bank-top channel width of the 13 cross-sections along the bend.

---

#### **4.7.6 Overall trend of channel width variation around bends**

A strong correlation is observed between the mean depth-averaged apex region width and the mean depth-averaged inflection region width (Fig. 20A) with an  $R^2$  value of 0.85 (linear) for all 108 bends from the four channel reaches. The majority (70%) of bends (76 from 108 bends) were on average 161 m or 10% wider at the apex region compared to the inflection region. For the remaining 32 bends, the inflection region was on average 92 m or 7% wider compared to the apex region. Bends with terraces or no terrace present at the inner bend had a similar trend (Figure 4.20B) with an  $R^2$  of 0.83 (terrace) and 0.81 (no terrace). Bends without terraces exhibited slightly wider bends at apex regions relative to bend inflection regions, compared with those bends with terraces, for bends greater than 1000 m wide.

80% of bends from the inactive channel reaches are wider at the apex region (Figure 4.21; 17 out of 19 bends for Ax02, 21 out of 27 bends for Ax12 and 9 out of 13 bends for Ax14) with  $R^2$  values between 0.50 and 0.78, whereas the active channel reach has 59% of bends wider at the apex region (Figure 4.21; 29 out of 49 bends for Ax52), with an  $R^2$  value of 0.7.



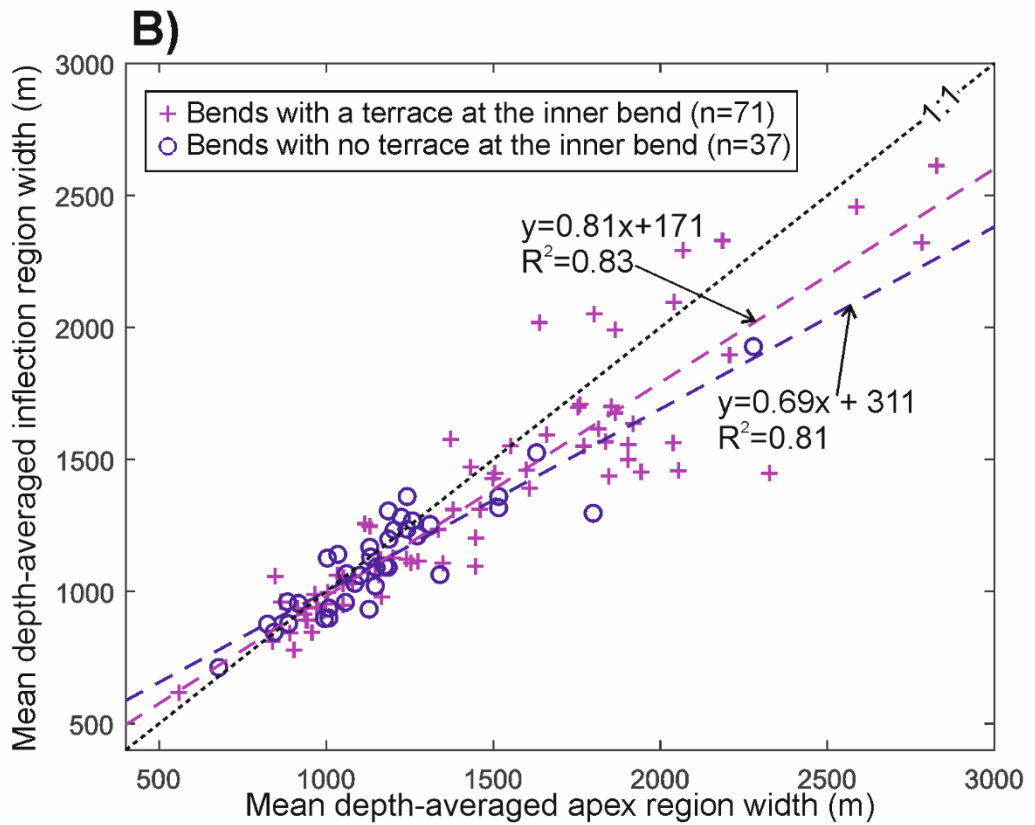
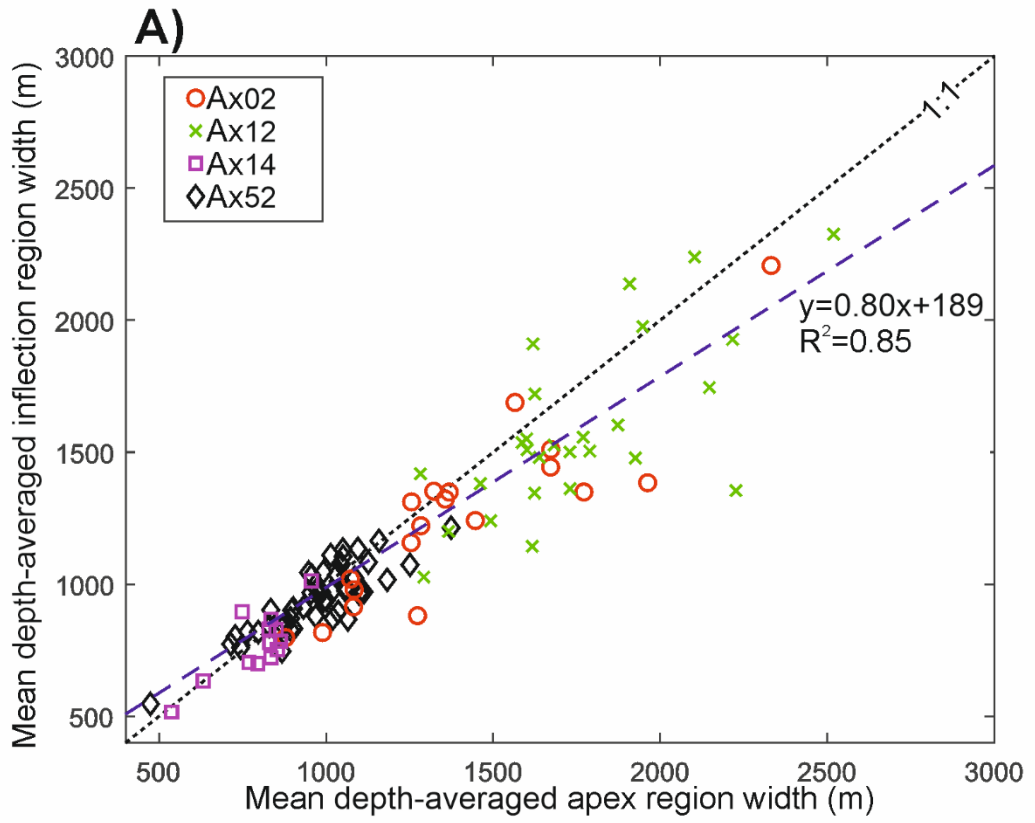


**Figure 4.20** A) Mean apex-region width versus mean inflection region width. Each point represents one bend and contains measurements of the depth-averaged channel width. The mean width for a bend was obtained from six cross sections for mean inflection-region and seven cross-sections for mean apex region width. A high correlation (blue dashed line,  $R^2=0.85$ ) is shown. The active channel reach is Ax52 (49 bends, diamond). Inactive channel reaches are Ax02 (19 bends, circle), Ax12 (27 bends, cross) and Ax14 (50 m resolution, 13 bends, square). B) Mean apex region width versus mean inflection region width for bends with terraces present or not. Bends with a terrace (cross) had an  $R^2$  of 0.83 and bends with no terrace (circle) had an  $R^2$  of 0.81. Black dotted line represents an equal mean inflection region and apex region width.

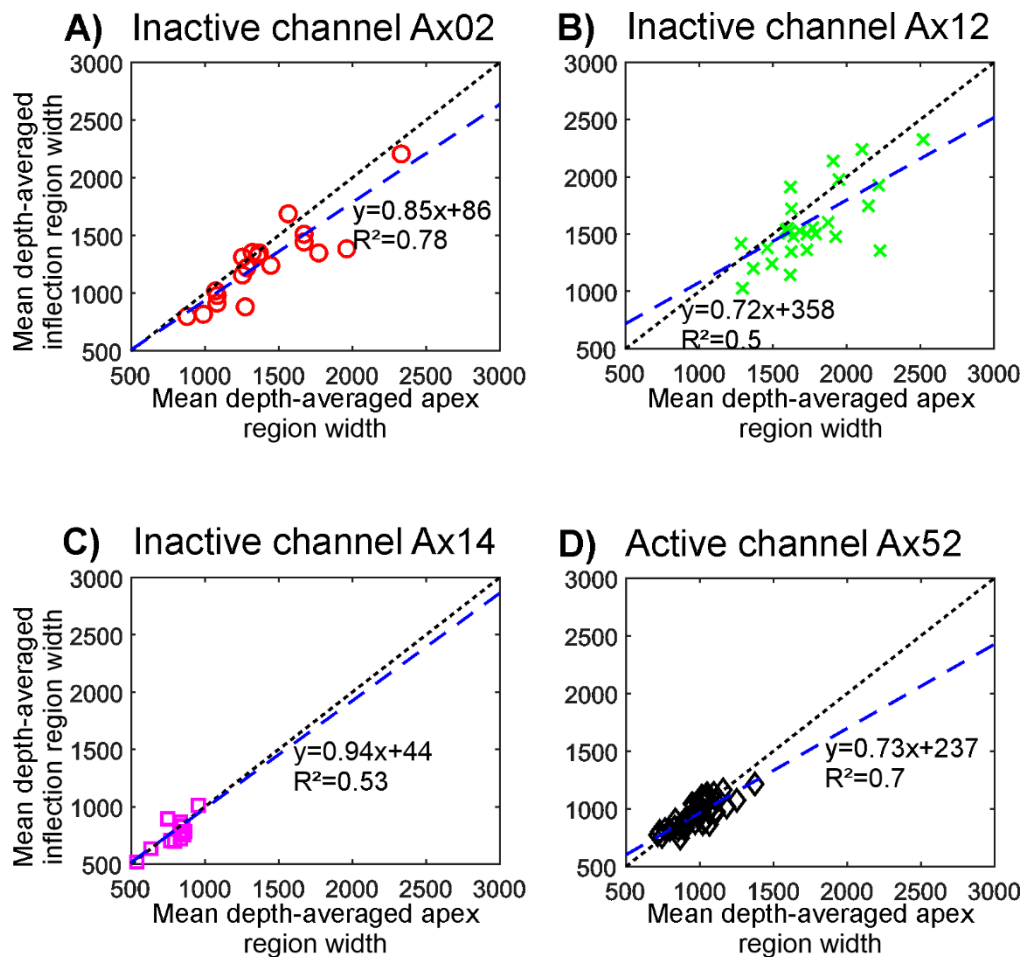


**Figure 4.21** Mean apex region width versus mean inflection region width. Each point represents one bend and is based on depth-averaged measurements. Blue dashed line represents the linear regression and black dotted line represents equal mean apex and inflection region width. A) Active channel reach Ax52 (49 bends), B) Inactive channel

reach Ax02 (19 bends), C) Inactive channel reach Ax12 (27 bends), and D) Inactive channel reach Ax14 (13 bends).

---

## 4.8 Discussion

Clear evidence in inactive and active reaches of the Congo channel have been presented, which show that submarine channel bends are significantly wider at bend apices than they are at bend inflections, for both points and regions. Here, it is explored how these results compare to alluvial river channels, and examine the implications for sedimentation at channel bends, and bend evolution. The question of whether these channels are dominated by bank pull or bar push processes is then examined. Lastly, the potential role of climate forcing in controlling variations in width around bends was assessed.

### 4.8.1 Comparison of submarine channel bends to river bends

In order to directly compare these submarine channels to the results obtained from sinuous point-bar rivers (type C of Brice (1975) classification; Lagasse *et al.*, 2004; Eke *et al.*, 2014a), the mean width at the channel banks, which is equivalent to bankfull level in rivers (Clark *et al.*, 1992; Pirmez and Imran, 2003; Konsoer *et al.*, 2013), from the inflection points and apex point is taken. The results show that bend apices for the Congo channel reaches had bank-top channel widths that were between 9 and 36% greater than bend inflections. This compares to a 14% increase in width at the apex point for rivers as observed by Eke *et al.* (2014a). However, this width difference may be an overestimation for submarine channels as they exhibit lower gradient banks than rivers (rather V-shaped cross-sections; Islam *et al.*, 2008). If it is assumed that rivers essentially have vertical banks, then a more appropriate comparison for submarine channels may be the depth-averaged widths at the bend apex and inflection points. However, the Congo channels exhibit a very

similar variation as for the bank-top channel widths, with bend apices 7-38% wider than bend inflections.

There may be ambiguity by looking solely at the apex and the two inflection points for both rivers and submarine channels as comparison between regions might be a better guide to the width variations around bends as this approach acts to smooth out outliers at the apices and inflections. However, it is not possible to directly compare such figures to the data from rivers. A simpler measure is to compare the number of bends that are wider at the apex region, and in this respect the observed submarine channels from Axial Congo Fan are similar to rivers (60%; Eke *et al.*, 2014a), with active channel reaches very similar (59%) and inactive channel reaches a little higher (70%-89%) based on depth-averaged widths.

The results from the apex and inflection points suggest that there is an increased variation in width changes around bends for Ax02 and Ax12 (23% and 38% greater at bend apices in terms of depth-averaged width; 22-36% for bank-top channel width), whereas Ax14 and Ax52 exhibit a smaller variation (7-8%, and 9-13% on the same measures) respectively, compared to sinuous point-bar rivers (Eke *et al.*, 2014a, b). The reason(s) for a difference in width variation between rivers and Ax02 and Ax12 and also within/between submarine channels is unclear. Possible explanations include super-elevation which is around two orders of magnitude greater compared to rivers (Dorrell *et al.*, 2013), and may vary between submarine channels and within submarine channels. Strong overspill related to super-elevation can lead to sandier deposits at the outer bank, forming spillover lobes and sediment waves (Nakajima *et al.*, 1998; Wynn and Stow, 2002; Posamentier, 2003; Morris *et al.*, 2014a). Sediment waves resulting from this overspill have been observed in the Congo system (Migeon *et al.*, 2004). Potentially these less cohesive sandier deposits may be more erodible than equivalent outer bank deposits in rivers. Asymmetry in exhumed levees has been reported (Kane and Hodgson, 2011), with outer bank external levees being thicker and having a higher sand content. Furthermore, erodibility of submarine levees would be enhanced in systems prone to avulsion and progradation, such as the Congo,

where the base of the levee is commonly a sand-prone frontal lobe (e.g. Morris *et al.*, 2014b; Picot *et al.*, 2016). Alternatively, such variation between bank erodibility might be related to strongly variable flow structures and induced shear stresses. The 3D-helical flow structure in submarine channels is composed of a downstream primary flow component, and a cross-stream secondary flow component, as in rivers (e.g., Peakall and Sumner, 2015; Davarpanah Jazi *et al.*, 2020; Wells and Dorrell, 2021). However, the orientation of the helix is frequently reversed relative to rivers, with basal flow at bend apices going from the inner to outer bank (e.g., Peakall and Sumner, 2015; Dorrell *et al.*, 2018; Wells and Dorrell, 2021).

Experiments and simulations have shown that this reversal in secondary flow causes the downstream flow velocity core (the area with the highest downstream velocities) to increase in magnitude and be moved towards the outer bank (Keevil *et al.*, 2006; Giorgio Serchi *et al.*, 2011). This movement of the downstream flow core may intensify outer bank erosion. However, it remains unclear how the position and strength of the downstream velocity core varies between rivers and submarine channels, and between submarine channels. Reversal of the secondary flow field does lead to flow impinging (impacting at an oblique angle) on the outer bank further around the bend than in rivers, at least for constant width channels (e.g. Keevil *et al.*, 2006), and again this may cause enhanced erosion at the outer bank due to deflection of the flow towards the outer bank.

One might expect these factors to apply to all of the submarine channels, yet there is a lot of variation between the channel reaches. Later, the variation between channel reaches is discussed further at the end of the discussion where possible differences in external forcing between channels are discussed.

#### 4.8.2 Sedimentation at channel bends

The evidence for wider bend apices has profound implications for sedimentation within submarine channels. Point-bars are often not observed in submarine channels, likely because such tractional forms only form when migration is rapid relative to aggradation (Sylvester *et al.*, 2011). However, where present, observations from fixed width channel experiments (Peakall *et al.*, 2007; Amos *et al.*, 2010; Cossu and Wells, 2010; Wells and Cossu, 2013) and simulations (Darby and Peakall, 2012), suggest that point-bars are preferentially formed downstream of bend apices. This position beyond the bend apex is because, as noted earlier, secondary circulation is frequently reversed in turbidity currents relative to river channel flows (Corney *et al.*, 2006, 2008; Dorrell *et al.*, 2013; Peakall and Sumner, 2015), and this leads to flow being outwardly directed for further around the bend than in rivers. These experiments and simulations also exhibit tight bends where there may be an enhanced phase lag between curvature and secondary flow strength (Zhou *et al.*, 1993; Ezz and Imran, 2014). As a consequence, the point at which flow and sediment flux converge, in turn driving sedimentation and point-bar development (Nelson and Smith, 1989), is beyond the bend apex, rather than dominantly at the bend apex as in rivers (Peakall *et al.*, 2007; Amos *et al.*, 2010; Peakall and Sumner, 2015).

This delay in the convergence of flux at the inner bend as a result of reversed secondary circulation will still occur in natural submarine channels but the increased width at the bend apex will affect the flow dynamics. The increased width at bend apices will lead to a reduction of the outwardly directed centrifugal force in the upstream part of the bend where channel width is increasing, leading to reduced flow super-elevation relative to constant width channels, and a corresponding decrease in the pressure gradient force at the base of the flow. Past the bend apex as the channel narrows, super-elevation and the pressure gradient force will be maintained for longer than in a constant width channel, and the flow towards the inner bank will be enhanced; in turn these aspects will lead to flow convergence and traction-

dominated sedimentation further upstream than in fixed width channels (cf. Nelson and Smith, 1989). Interestingly, channel width at bend apices relative to inflections increases to a maximum for bends where radius of curvature is relatively small (Figure 4.19), suggesting that as bends tighten the channel undergoes adjustment therefore reducing the associated increase in centrifugal forces, and enhancing the flow patterns described above. For suspension-driven deposition, increasing width at bend apices, particularly at tight bends where apices are relatively widest, is likely to further enhance flow separation at the inner bank relative to that observed in fixed width channels (Straub *et al.*, 2008, 2011; Janocko *et al.*, 2013; Basani *et al.*, 2014), thus driving sedimentation and formation of oblique accretion deposits at the inner bend (Straub *et al.*, 2011; Peakall and Sumner, 2015). Such suspension-dominated sedimentation is in keeping with observations of modern and ancient submarine channel-fills where low-angle, inclined, low-amplitude (fine-grained in ancient examples), sediments are observed at inner bends, often above thinner point-bar deposits (Schwenk *et al.*, 2005; Deptuck *et al.*, 2007; Babonneau *et al.*, 2010; Hodgson *et al.*, 2011; Peakall and Sumner, 2015).

Taken together, the effects of wider channel apices on tractional- and suspension-driven sedimentation will result in point-bar development much closer to the bend-apex (Figure 4.22). This result suggests resolution of a contradiction at the heart of our understanding of submarine channel bend development. Theoretical, experimental and numerical work have all indicated that point-bar development is further downstream in submarine channels than in rivers, which would be expected to be associated with bank erosion beyond the bend apex and enhanced downstream migration (sweep; Peakall and Sumner, 2015). However, planform studies of aggradational channels on passive margins have paradoxically long indicated that bend development is instead dominated by bend amplitude growth (swing; Peakall *et al.*, 2000a, b; Jobe *et al.*, 2016). Our understanding has been based on an absence of knowledge of width variation in submarine channels, and thus has assumed the simplest possible case, that of fixed width channels (i.e. canaliform). As shown here for the Congo submarine channels, a width variation does occur,

with bend apices typically wider than inflections, and this clearly has important ramifications, leading to deposition closer to bend apices (Figure 4.22). Consideration of width variation changes around submarine bends and their likely influence on sedimentation appears to be the 'missing link' for a holistic understanding of bend dynamics in submarine channels.

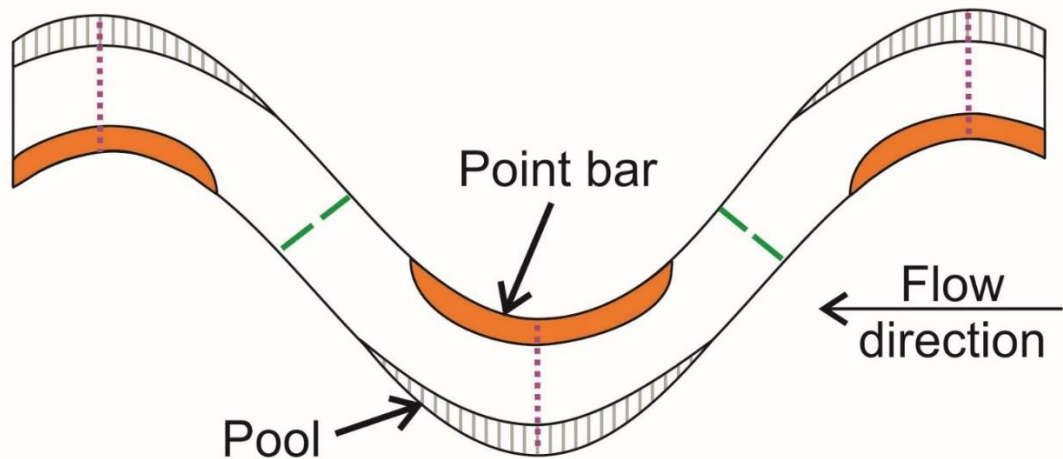


**Figure 4.22** Summary diagram of submarine channels illustrating that they are wider at bend apices compared to inflections. Purple dotted line represents apex cross-section and green dashed lines represent inflection cross-sections. Postulated positions of maximum erosion (white area) and aggradation (black area) are shown. This schematic diagram also suggests that point bars and zones of outer bank erosion are located more symmetrically around the bend apex, rather than prominently downstream of the bend apex; for channels without significant external tectonic or topographic influence.

### 4.8.3 Bank pull or bar push?

The clear and consistently wider bend apices relative to inflections, observed in these Congo channels, are consistent with actively migrating channels, as observed in rivers. However, there is a question as to what is driving this migration. Is this a result on inner bend deposition (bar push) or outer bank erosion (bank pull)? Point-bar deposits composed of high amplitude deposits are relatively thin in the Congo channels, in the small number of examples



where data allows them to be recognised (Babonneau *et al.*, 2010). This is in keeping with other submarine channels, where point-bars, if present, typically do not scale with flow depth as they do in alluvial rivers (Nakajima *et al.*, 2009; Darby and Peakall, 2012). Overlying these high amplitude deposits are vertically accreting, low-angle inclined finer-grained units that have similar seismic response to the external levee deposits (Babonneau *et al.*, 2010). The geometry of these finer-grained deposits suggests that they were deposited after the initial formation of the point-bar (Babonneau *et al.*, 2010). Consequently, only deposition of the thin point-bar deposit could act as bar push, and it is not clear if this would be sufficient to control channel migration. The overlying finer-grained material is filling in space at the inner bank, and thus is responding to bank pull at that level. The presence of very wide bend apices relative to inflections as observed in Ax02 and Ax12 casts further doubts on the applicability of bar push in this system. Instead such width variation, suggests that bank pull may be the dominant process here, leading to the creation of space at the inner bend. Given the thin point-bars, this may also be the case for Ax14 and Ax52 with their smaller relative increases in width at bend apices compared to inflections. These observations, notably the marked increases in channel width at bend apices, support the conceptual ideas of Peakall and Sumner (2015) who previously suggested that submarine channels may be controlled by bank pull as submarine channels frequently do not have point bars and in many cases the inner bend deposits are instead composed of finer-grained deposits analogous to oblique accretion deposits in mixed load rivers. It is therefore suggested that submarine channels may be dominated by bank pull, in contrast to rivers where there is evidence for both bar push and bank pull depending on the system exist (e.g., Constantine *et al.*, 2014; Eke *et al.*, 2014a, b; Van de Lageweg *et al.*, 2014; Donovan *et al.*, 2021).

#### 4.8.4 Control on width of submarine channel bends

The results of this study, in combination with the theoretical arguments of Peakall and Sumner (2015), suggest that bank pull, and channels that have wider bend apices, are likely typical for submarine-fan channels. One key question is whether the variation in channel width, caused by the ratio of the relative rates of erosion at the outer bank, and deposition at the inner bank (Eke *et al.*, 2014a, b), is a function of flow properties such as sediment yield and composition, and volume, and by extension the type of turbiditic flows. If such flow properties are a key driver, then changes in channel width would be expected geographically, and for a given system then changes over time are predicted if affected by allogenic forcing. The present dataset allows this question to be examined. Monsoonal cycles have been linked to the architectural cycle of the Congo Fan for the last 40 kyr (Picot *et al.*, 2019). Picot *et al.* (2019) suggest based on pollen assemblages (proxy for vegetation cover), kaolinite/smectite (K/S) ratio (proxy for freshwater plume intensity and thus discharge of the Congo River), and monsoon index, that prograding periods are related to an increase in monsoonal intensity and therefore humidity and freshwater input. Furthermore, retrograding periods are related to a low monsoonal intensity and hence decrease in humidity and freshwater input. Picot *et al.* (2019) identified three types of monsoonal periods in the last 40 kyr: arid, humid, and transition monsoonal period from humid to arid. During arid monsoonal periods there is low discharge, increased sediment yield (Jansen *et al.*, 1984), and more coarse sediment relative to mud, which leads to a low transport capacity of turbidity currents and channel infill. In contrast, humid periods correspond to higher discharge, and reduced sediment yield (Jansen *et al.*, 1984) producing clays and a higher mud/sand ratio, which leads to high capacity turbidity currents and probably increased confinement by channel erosion and levee construction (Picot *et al.*, 2019). A transitional monsoonal period from arid to humid causes the retrogradation due to an increase in precipitation and river runoff, prior to re-establishment of vegetation, which increases erosion and coarse sediment production, and hence channel infill.

Here, the degree to which the apex is wider than the inflections based on depth-averaged width measurements was utilised for each channel. A relative age constraint for each channel (Picot *et al.*, 2019) is then utilised and compared to a monsoonal cycle extending over the past 200 kyr, as predicted by numerical models (Caley *et al.*, 2011), which gives an environmental setting during channel formation (Figure 4.23). The assumption is made that the relationship between monsoon period and progradation/retrogradation identified by Picot *et al.* (2019) for the past 40 kyr, holds over this 200 kyr period and that the width measurements are interrelated to the monsoonal cycle. It must be noted that this comparison has a number of assumptions including a small sample size. However, it might explain width variations between different submarine channels. Ax14 was formed during a retrograding period at the beginning of cycle B during a peak dry monsoonal period (Picot *et al.*, 2019). An arid climate may have led to flow sizes and capacity being small, and therefore less sediment being eroded at outer banks, which would have led to a narrow apex (7% wider depth-averaged width at the apex point relative to the inflection points). Ax12 may have occurred during an arid to humid period with a peak prograding phase at the end of cycle A (Picot *et al.*, 2019), and so flow sizes and capacity would have increased, and more sediment was likely subsequently eroded at outer banks. Hence, the apex was comparatively wide (38% wider depth-averaged width at the apex point relative to the inflection points). Ax02 also has a high apex width (23% wider on the same measure) as it occurred at the beginning of the prograding period of cycle A which follows a retrograding peak. An increase in river freshwater input and a decrease in solid discharge at the beginning of the progradation that follows the retrogradation maximum may explain the increase in capacity of turbidity currents and a high apex-region width for Ax02. Lastly, the active channel Ax52 occurred during the maximum progradation of cycle D, which correlated with a transition towards a more arid west African monsoonal system (Figure 4.23; Caley *et al.*, 2011), where vegetation cover and river liquid and solid discharge decrease and hence sediment capacity reduced, which would fit with the apex-region width being comparatively low (8% wider on the same measure). All of these comparisons

assume that there is no significant change in submarine channel cross-sectional morphology during the process of avulsion and shutdown. For instance, smaller flows may be expected to run up and deposit their sediment on outer banks, potentially forming outer bank bars (Nakajima *et al.*, 2009). That said, the variations between different climatic conditions is probably greater than channels being currently active or not, and hence the data may suggest that there is a relationship between channel bend variation and turbiditic flow characteristics driven by climatic conditions. In summary, turbidity currents with enhanced transport capacity appear to be associated with channels with an enhanced width variation, with wider bend apices relative to inflections.

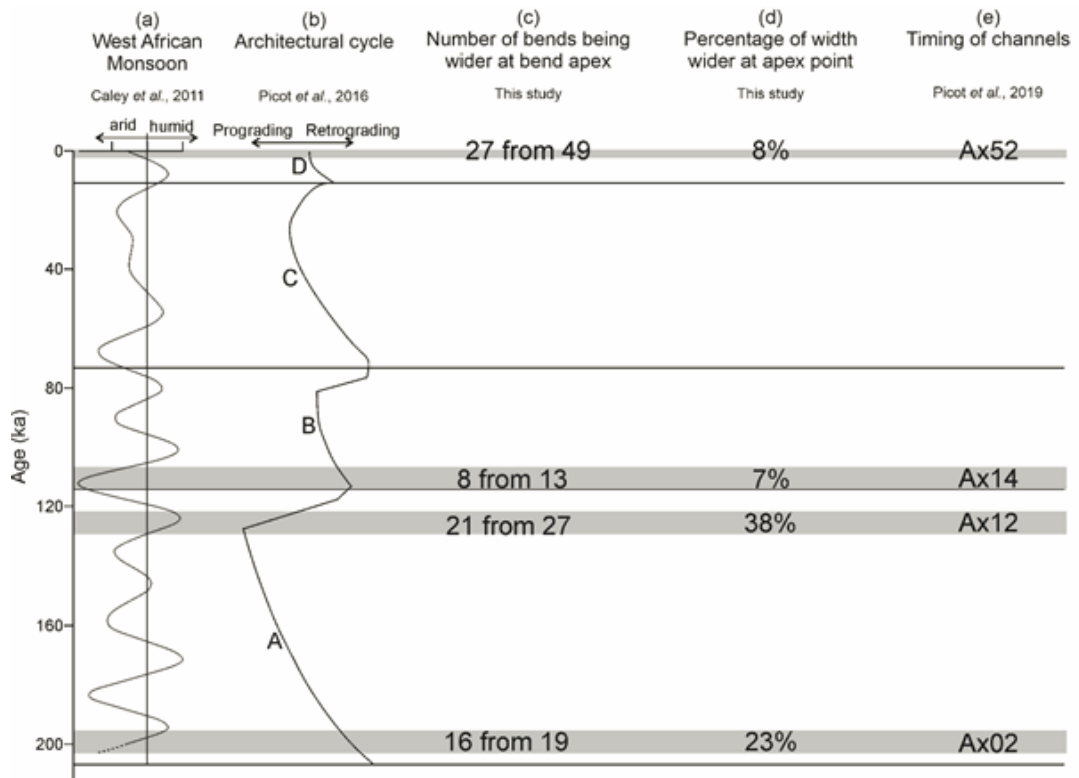


**Figure 4.23** Relationship between climate, progradation/retrogradation, and channel bend width variations. Aspects modified from Caley *et al.* (2011) and Picot *et al.* (2016, 2019). Channel bend width variations are based on depth-averaged width measurements from the apex point and inflection points.

## 4.9 Conclusions

This study has analysed the nature of cross-sectional width variation around submarine channel bends, from both active and inactive channels on the Congo Fan. All the studied submarine-fan channels were dominated by bends where the apex is wider than the inflections, which is similar to actively migrating meandering rivers. The result that bends are in general wider at bend apices, combined with consideration of depositional processes, suggests that bend migration in submarine channels is controlled by outer-bank erosion (bank pull) rather than by inner-bend deposition (bar push). A key paradox in our understanding of the dynamics of aggradational submarine channels has been that field observations typically indicate dominantly lateral bend expansion, whereas laboratory and numerical models predict downstream translation of bends. In the absence of any data, and for simplicity, all numerical and experimental work has assumed constant width channels. Herein it is shown that this assumption is incorrect, and increased channel width at bend apices provides an answer to this paradox. The three-dimensional flow dynamics in bends with wider bend apices are predicted to lead to the locus of tractional sedimentation, in the form of point-bars, moving towards the bend apex, compared to that modelled in previous process studies. Enhanced flow separation in bends also likely leads to suspension-driven sedimentation in the additional space at the inner bend. Asymmetry in the erodibility of the outer and inner banks due to super-elevation and overspill of sandier parts of flows will further enhance bank pull dynamics. Comparison of the morphological changes between channels and the climate conditions at the time of their formation, suggests that there may be a relationship between channel bend variation and climatic-driven variation in sediment source composition and turbiditic flow characteristics. Flows with a higher transport capacity appear to be associated with channels with an enhanced width variation, with wider bend apices relative to inflections.

# Chapter 5 Width variation around submarine channel bends for different channel types: implications for bend migration

---

## 5.1 Chapter summary

Width analysis around bends is used to predict flow and sedimentation processes around bends. Width is regulated by processes of deposition at the inner bend and erosion at the outer bend. Here, width around bends of three different channel types are analysed (submarine-fan, isolated deep-ocean, and non-margin ocean channels). Width was analysed at 13 cross-sections (6 cross-sections for the inflection region and 7 cross-sections for the apex region) from bend inflection to bend inflection. For each cross-section width was measured at the level of the channel bed and then at 10 m increments up to the height of the channel banks. Width was analysed at each channel height on either side away from the centreline, here called the outer and inner bank width, according to their location towards the inner and outer bend. Channel width was widest at bend apexes for all channel types. Outer bank width is wider than inner bank width for all channel types. Interpretation of width around bends suggests that submarine channels are controlled by bank pull, outer bank erosion rather than bar pull, similar to rivers. Variations between channel types exists in terms of channel width around bends. Submarine-fan channels are wider at the apex-region, whereas isolated deep-ocean channels have a constant width around bends. Such variations between channel types may be related to bank resistance for isolated deep-ocean channels.

## 5.2 Introduction

Submarine channels form a transport pathway for sediment-gravity flows from the continental shelf edge to the basin plain, in some cases extending all the way to the abyssal plains at water depths of four to six kilometres (Menard, 1955; Lewis, 1994; Wynn *et al.*, 2007; Pickering and Hiscott, 2015). Channel lengths can range from only a few km (e.g. Kongsfjorden Channel System, ~1-20 m; Forwick *et al.*, 2015) to hundreds of kms (e.g. Valencia, ~200 km, O'Connell *et al.*, 1985; Amazon, ~800 km, (Pirmez and Imran, 2003) to some that are >1000 km (~1500 km, Indus, (Kolla and Coumes, 1987); ~3800 km, Northwest Atlantic Mid-Ocean (NAMOC), (Johnson *et al.*, 1971)). Through the process of sediment transport, submarine channels can build over time, the largest sediment accumulations on Earth (Curry *et al.*, 2003). Furthermore deposition of lobes and submarine-fan channels may hold potential hydrocarbon reservoirs (Clark and Pickering, 1996b; Mayall *et al.*, 2006).

Width variation around bends is controlled by erosion and deposition of the inner and outer banks (Nanson and Hickin, 1983; Parker *et al.*, 2011; Eke *et al.*, 2014a, b). Erosion and deposition of these banks ultimately controls bend migration. In rivers, it is known that bend migration is either controlled by a faster eroding outer bank (bank pull), which leads to a wider channel width or a faster depositing inner bank (bar push), which leads to a more constant channel width around bends (Eke *et al.*, 2014a, b; Van de Lageweg *et al.*, 2014), hence a channel with a constant width relates to a relative balanced erosion and deposition. However, channel narrowing and widening can occur at any time at any position around the bend (Eke *et al.*, 2014a). This said, most rivers are likely controlled by bank pull rather than bar push (Eke *et al.*, 2014a; Matsubara and Howard, 2014; Van de Lageweg *et al.*, 2014).

Channel migration of aggradational submarine channels are thought to be rather constant with limited downstream bend translation 2-3 times channel width (sweep) and a dominance of lateral bend translation (swing), followed by a phase of equilibrium with relatively constant bend sinuosity and finally an abandonment phase (Peakall *et al.*, 2000a, b; Deptuck *et al.*, 2007; Sylvester *et al.*, 2011; Jobe *et al.*, 2016). However, laboratory experiments and numerical models are unable to reproduce the above migration model for submarine channels. In these models and simulations a

less developed point-bar is deposited further downstream of the bend apex compared to rivers suggesting that erosion would occur at the outer bank beyond the bend apex if these had erodible banks (Keevil *et al.*, 2007; Peakall *et al.*, 2007; Straub *et al.*, 2008, 2012; Amos *et al.*, 2010; Darby and Peakall, 2012; Janocko *et al.*, 2013; Cossu *et al.*, 2015). The modelled imbalance of deposition further downstream of the bend apex and erosion beyond the bend apex would therefore lead to downstream bend migration, similar to rivers. Additionally more expansive, downstream bend migration has been observed in a number of other setting, particularly in non-aggrading or channel phases (Posamentier, 2003; Posamentier and Kolla, 2003; Kolla *et al.*, 2012). Downstream, bend-migration may be favoured in rapid deforming locations, such, as salt basins (Covault *et al.*, 2020), but local down-stream bend migration in terms of bend cut-off have also been observed for the Amazon, Congo and Indus Channels (Damuth *et al.*, 1988; Schwenk *et al.*, 2003; Babonneau *et al.*, 2010). Some of these contradictions between natural channels and experimental/numerical approaches might be explained by variations between aggradational and erosional channels (Abreu *et al.*, 2003), or through variation of flows around bends (Dorrell *et al.*, 2018). However, the results of laboratory experiment and numerical models and their inability to produce deposits that are compatible with reduced downstream bend migration, suggests that a key component in our understanding of bend migration is missing.

Width around bends has been kept constant in laboratory experiments and numerical models (Kassem and Imran, 2004; Imran *et al.*, 2007; Peakall *et al.*, 2007; Amos *et al.*, 2010; Straub *et al.*, 2012; Janocko *et al.*, 2013), and it is unknown whether width around bends in submarine channels may vary. However, some laboratory experiments and observations suggest that deposition may vary around bends, increased outer bank deposition at bend apexes may occur during abandonment (Kane *et al.*, 2008; Straub *et al.*, 2008; Nakajima *et al.*, 2009), which would for example reduce the width at the apex region compared to the inflection region. Additionally, evidence for a wider-at-apex region compared to the inflection region has been observed in the previous chapter for channels on the Congo Fan. In the Congo, a wider-at-apex-region was observed, which created space at the apex region for sediment to deposit at the inner bend and would therefore reduce downstream bend migration in submarine channels. However, the analysis was limited to one channel type, submarine-fan channels, and also a single system within that channel type. A



key question is whether different channel types may experience variable width around bends and if so what the nature of this width variation around bends would be. The aim of the present study is to assess width variations around bends between different channel types. Additionally, the width around bend is compared from an upstream and a downstream channel reach to assess whether there are longitudinal variations in width variation around bends.

## 5.3 Methodology

### *Dataset*

This study analyses reaches from the Amazon, Magdalena, Bryant, Horizon, Baranof, Surveyor and Mariana Channels. Horizontal data resolution from Digital elevation models (DEM) ranged from 12.5 m to 100 m and a depth accuracy of 1% of the water depth (maximum 40 m at 4000 m water depth). Datasets were processed in ESRI ArcMap 10.3.1 and cross-sections were measured in ImageJ. The Amazon, Magdalena and Bryant Channel are considered as submarine-fan channels. The Surveyor, Horizon and Baranof Channel are considered as isolated deep-ocean channels, and the Mariana Channels are considered as non-margin ocean channels.

Submarine-fan channels build a complex network of channels on deep-sea fans, which are located at the distal part of continental margins on both passive and active margins (Kolla, 2007; Ortiz-Karpf *et al.*, 2015). Two Amazon Channel reaches were analysed, one from the middle fan and one from the lower fan section. The Amazon Fan system is situated off northeast Brazil in the equatorial Atlantic and has an area of 3,330,000 km<sup>2</sup> and reaches 4800 m water depth (Flood and Damuth, 1987). The Amazon Fan is fed by the Amazon River, which has an annual sediment discharge of just under one gigaton per year (Milliman and Meade, 1983). The Quaternary fan is composed of eight channel-levee systems with the Amazon Channel being the youngest channel and Brown channel being the oldest (Jegou *et al.*, 2008). The

Amazon Channel has been inactive since around 10 ka BP (Showers and Bevis, 1988; Piper and Deptuck, 1997).

The Magdalena Channel reach is situated at a water depth between 1566 m and 2320 m in the South-West of the Magdalena fan, offshore Colombia in the Caribbean Sea. The Magdalena Fan started to form during the late Miocene and its formation is linked to the Magdalena River and has been affected by tectonics since the Pliocene (Romero-Otero *et al.*, 2015; Idárraga-García *et al.*, 2019). Tectonically, the fan is divided between the Southern (SSBF) and Northern Sinu Fold Belt (NSBF). The analysed channel reach is close to the SSBF. Major delta shifts created a fan which becomes younger toward the southwest. The studied channel reach is part of the upper and middle part of the CLC-IIc4 channel (Romero-Otero *et al.*, 2015). The upper part of the channel and the majority from the studied channel reach is erosionally controlled.

The Bryant Channel reach is situated on top of the Bryant Fan on the continental rise after the Sigsbee Escarpment at a water depth between 3100 and 3200 m in the Gulf of Mexico. The Bryant Fan is fed through the Bryant Canyon, which started to form 135 ka (Tripsanas *et al.*, 2007) during a glaciated period when an ancient shelf-margin Mississippi River delta started to form (Tripsanas *et al.*, 2007), hence turbidity currents were triggered by delta failures, storms and especially river discharge (Bryant *et al.*, 1990; Lee *et al.*, 1996; Twichell *et al.*, 2000). The Bryant Fan occurs at a water depth between 2600m and 3200m. Since the Bryant Channel reach is situated on a submarine-fan and previous studies classified it as a channel (Lee *et al.*, 1996; Twichell *et al.*, 2000), it could be classified as a submarine-fan channel. An analysis of mapped global canyons around the world, based on Google-Earth (data sources: SIO, NOAA, US Navy, NGA, GEBCO), classified the studied section as part of the Bryant Canyon (de Leo *et al.*, 2010), but because of its location on the fan and its interpretation in previous studies the section analysed herein is classified as a submarine-fan channel. However, due to a greater channel width and an increase in channel width downstream compared to the Magdalena Fan the Bryant Channel is considered separately in this study (Chapter 3).

Isolated-deep ocean channels are basement controlled and develop in the early stages of ocean basins formation. Here, the Horizon, Baranof and Surveyor Channels

are considered to be all in this group. The analysed reach of the Surveyor Channel is part of the four tributaries feeding the Surveyor Channel. The analysed reaches of the tributaries has similar widths and heights compared to channel sections further downstream (Ness and Kulm, 1973), suggesting that the analysed reach is representative for the Surveyor Channel. Given the termination of the Surveyor Channel into the Aleutian Trench, it is classified as an isolated-deep ocean channel. The Horizon and Baranof Channel have no direct connection with the Aleutian Trench. The Baranof Fan that they feed is equivalent in size to the Amazon Fan (Reece *et al.*, 2011; Walton *et al.*, 2014; Zhang and Gulick, 2019), which would classify them as submarine-fan channels. However, the Horizon and Baranof Channel are exceptionally large in comparison with many submarine channels, see Chapter 3. Additionally, due to their similar size to the Surveyor Channel and convex-upward cross-sectional shape with a flat bases (“U”-shape) rather than “V”-shaped cross-sections with narrow bases, and their location next to the Surveyor Channel, the Horizon and Baranof Channels are classified as isolated deep-ocean channels. Hence three channels from the Gulf of Alaska, Surveyor, Horizon and Baranof Channels are considered as isolated deep-ocean channels.

All bends from the isolated deep-ocean channels are obtained from channels from one area, the Gulf of Alaska. Hence, the data obtained for bends from isolated deep-ocean channels may not be applicable for other isolated deep-ocean channels, such as Cascadia (Griggs and Kulm, 1973), NAMOC (Klaucke *et al.*, 1998a, b), Vidal (Embley *et al.*, 1970), Valencia (O’Connell *et al.*, 1985), Toyama (Nakajima and Satoh, 2001), Hikurangi (Lewis and Pantin, 2002) or the Kongfjorden (Forwick *et al.*, 2015). In Chapter 1, a comparison of morphometric parameters was compiled between the studied submarine channels from the Gulf of Alaska and other isolated deep-ocean channels, which suggests that the three submarine channels from the Gulf of Alaska are on average 3-times wider than other isolated-deep ocean but in general they have a similar cross-sectional shape (convex-upward shaped form), which suggests similar flow and sedimentation processes to create the cross-sectional shape.

The Mariana Channel reaches are classified as non-margin ocean channels given their location far from any terrestrial sediment source as they are situated off seamounts on the western flanks of the West Mariana Ridge west of the Mariana

Trough in the Parece Vela Basin (Figure 5.3; Gardner, 2010). The Mariana Ridge separated two basins: the actively spreading backarc Mariana Trough basin to the east and the Parece Vela Basin to the west (Okino *et al.*, 1998) The western-facing flank has gentle slopes ( $3^{\circ}$ - $4^{\circ}$ ) in comparison to the eastern-facing flank of the Mariana Ridge and is covered by volcanic apron sedimentation. Channels are possibly created by sediment erosion from volcano flanks (Gardner, 2010).

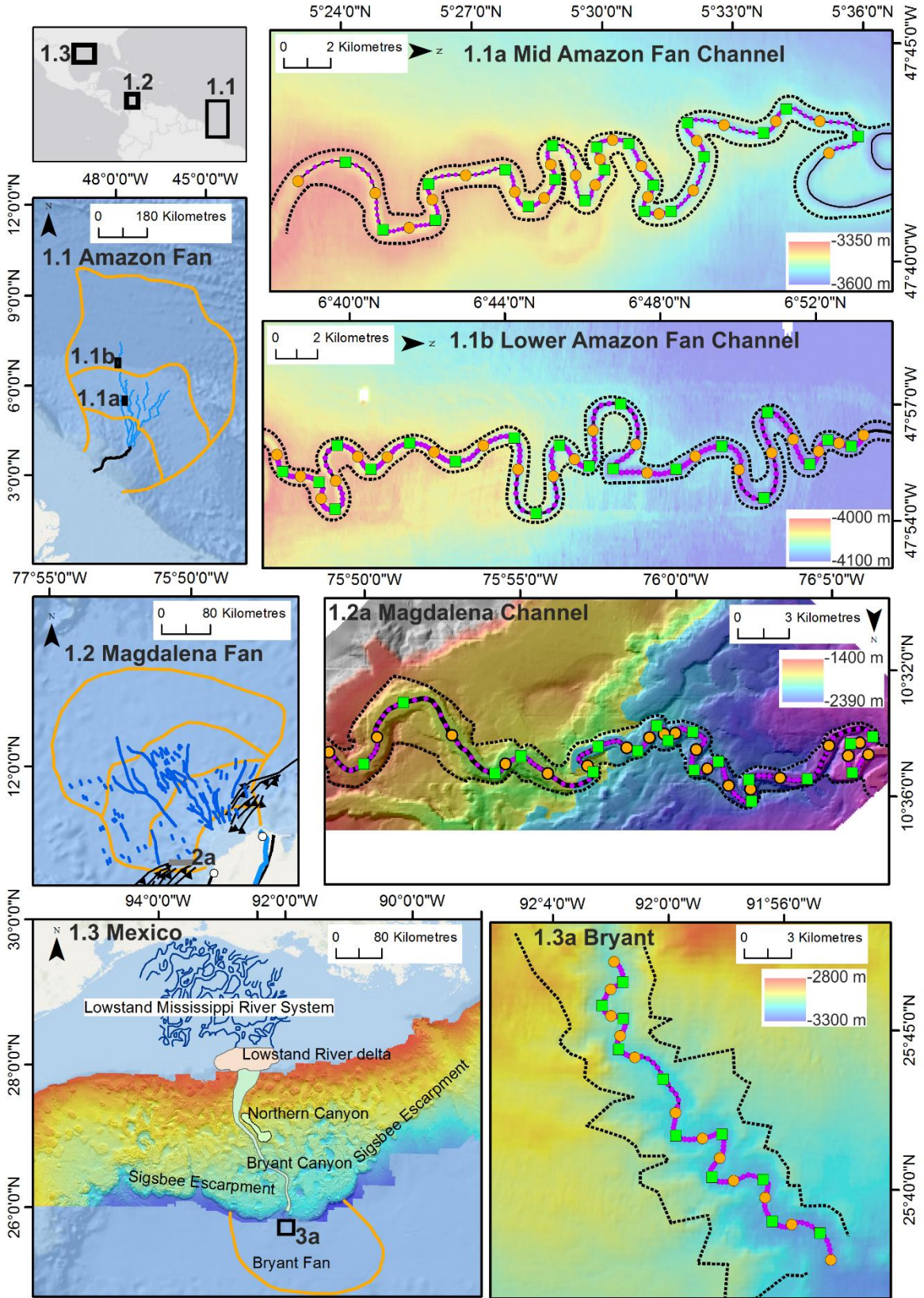


**Figure 5.1** Location of submarine-fan channels: 1.1) Amazon, 1.2) Magdalena, and 1.3) Bryant Channel. 1.1) Fan extension for A) Amazon Fan (extension from Damuth and Flood, 1984) with channel segments (blue) and black (canyon). 1.1a) Middle fan channel section with 20 bends analysed and 1.1b) Lower fan section with 20 bends analysed. DTM produced by IFREMER Géosciences Marines – ©IFREMER. 1.2) The Magdalena Fan (Fan extension: Idárraga-García *et al.*, 2019) is between the Southern (SSBF) and Northern Sinu Fold Belt (NSBF). The channel is part of a complex channel system (channel fragments from Kolla and Buffler, 1984; Ercilla *et al.*, 2002) and situated at the Upper Fan on the Southern Sinu Fold Belt (SSBF). 1.2a) Top surface of a 3D seismic survey with a horizontal resolution of approximately 15 m. 18 bends were analysed from the channel. DTM produced from seafloor horizon from a 3-D seismic survey – © Equión Energía Limited, Ecopetrol S.A. and Petrobras. 1.3) Bathymetry map of the north-western Gulf of Mexico (Basemap from Esri and BOEM) showing the location of the Bryant canyon and fan with the position of the low-stand Mississippi River and delta position (Suter and Berryhill, 1985). Fan outline and canyon location from Lee *et al.* (1996) and Twitchell *et al.* (2000). 1.3a) Bryant Channel location with 11 bends. DTM data from Law of the Sea U.S. UNCLOS Bathymetry Project.

---

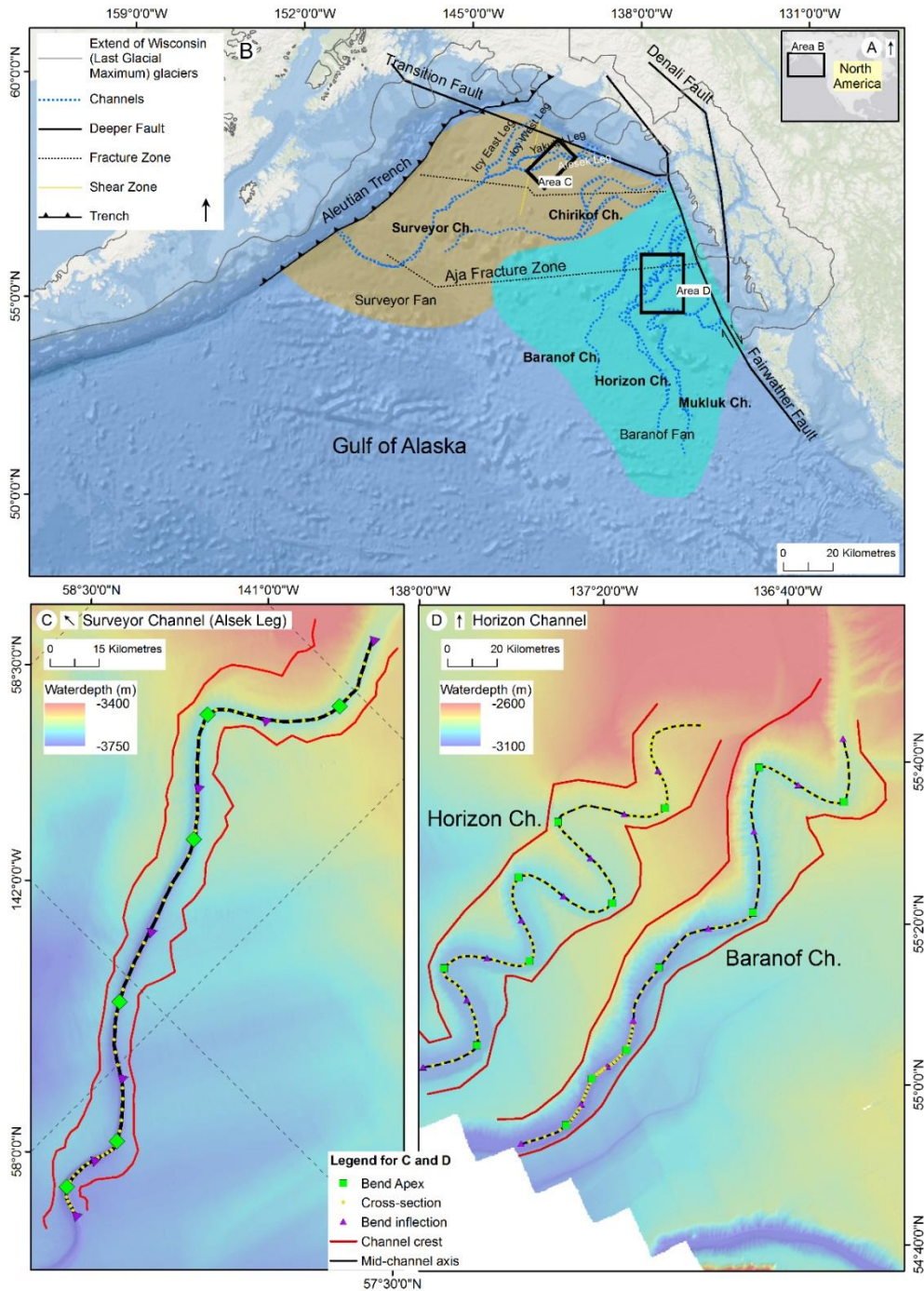


**Figure 5.2** Tectonic setting and channel locations from Surveyor, Baranof and Horizon Channel. A) The channels are situated in the Gulf of Alaska. B) Tectonic and channel extension derived from: Reece *et al.* (2011, 2013); Walton *et al.* (Walton *et al.*, 2014); Zhang and Gulick (2019). Fan extensions from Walton *et al.* (2014). C) Location of Surveyor Channel with 6 bends. D) Location of Horizon and Baranof Channel with 7 bends each. DTM data from Law of the Sea U.S. UNCLOS Bathymetry Project.

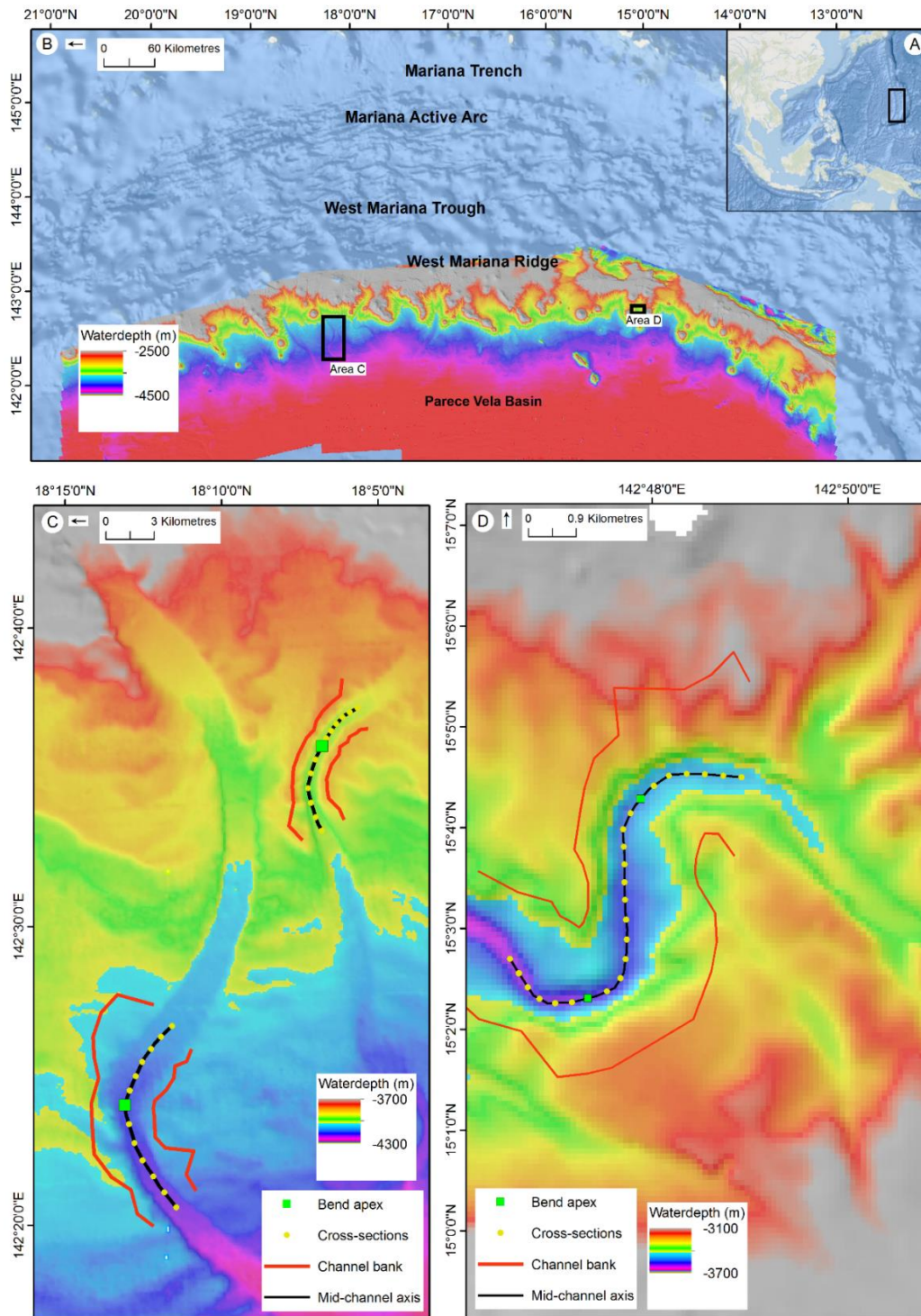


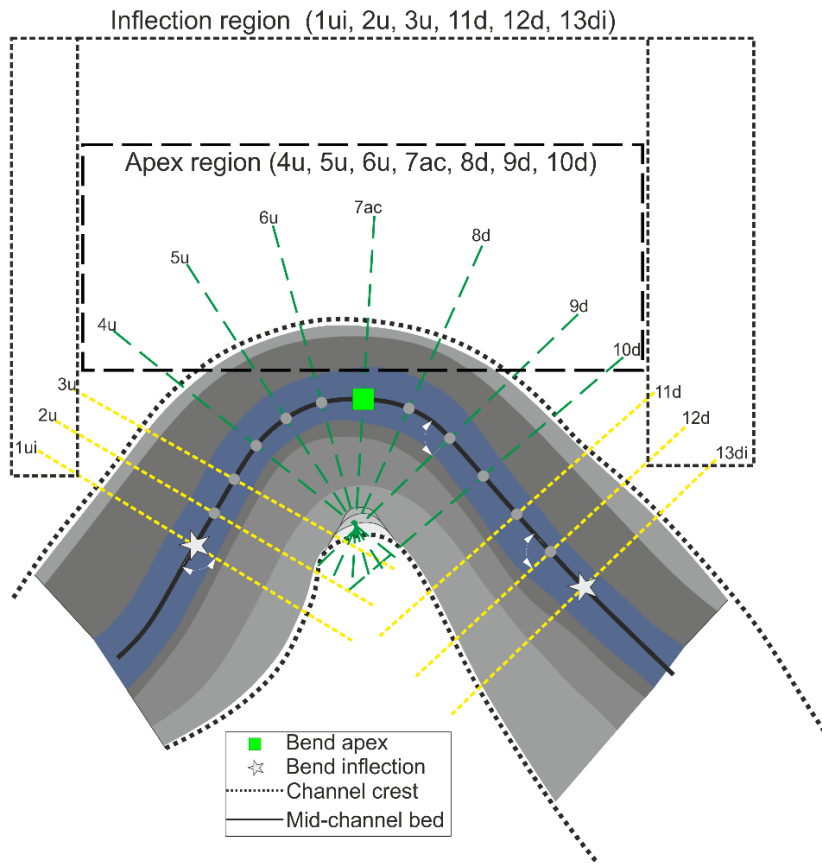
**Figure 5.3** A, B) Channels locating along the West Mariana Ridge. C, D) Location of the studied Mariana Channels on the West Mariana Ridge with 4 bends. DTM data from Law of the Sea U.S. UNCLOS Bathymetry Project.



*Bend analysis*

For each channel, the channel bed centreline was used as a reference for each analysis. The channel bed centreline was identified as the mid channel-bed line. The channel-bed was identified as the flat surface between the points where the slope of the channel banks rapidly increases. Along the centreline, bend apices represent points of maximum curvature and bend inflections represent points of minimum curvature. A bend is composed of an upstream and downstream inflection point with one bend apex in between (Figure 5.4A; see Appendix A, Section 4.5.2). 13 Cross-section were taken perpendicular to the centreline for each bend: one cross-section each at upstream inflection (1ui), bend apex (7ac), downstream inflection (13di), 6 equally-spaced cross-sections from upstream inflection to bend apex (2u, 3u, 4u, 5u, 6u) and an additionally 6 equally-spaced cross-sections from bend apex to downstream inflection (8d, 9d, 10d, 11d, 12d). Cross-sections were also grouped into an inflection region (1ui, 2u, 3u, 11d, 12d, 13di) and an apex region (4u, 5u, 6u, 7a, 8d, 9d, 10d). Additionally, half-width was measured equally away from the centreline at the inner and outer bend for each channel height, the sum represented the total width at each height position away from the channel bed (Figure 5.4B).

**A**



**B**

Cross-section: 7ac

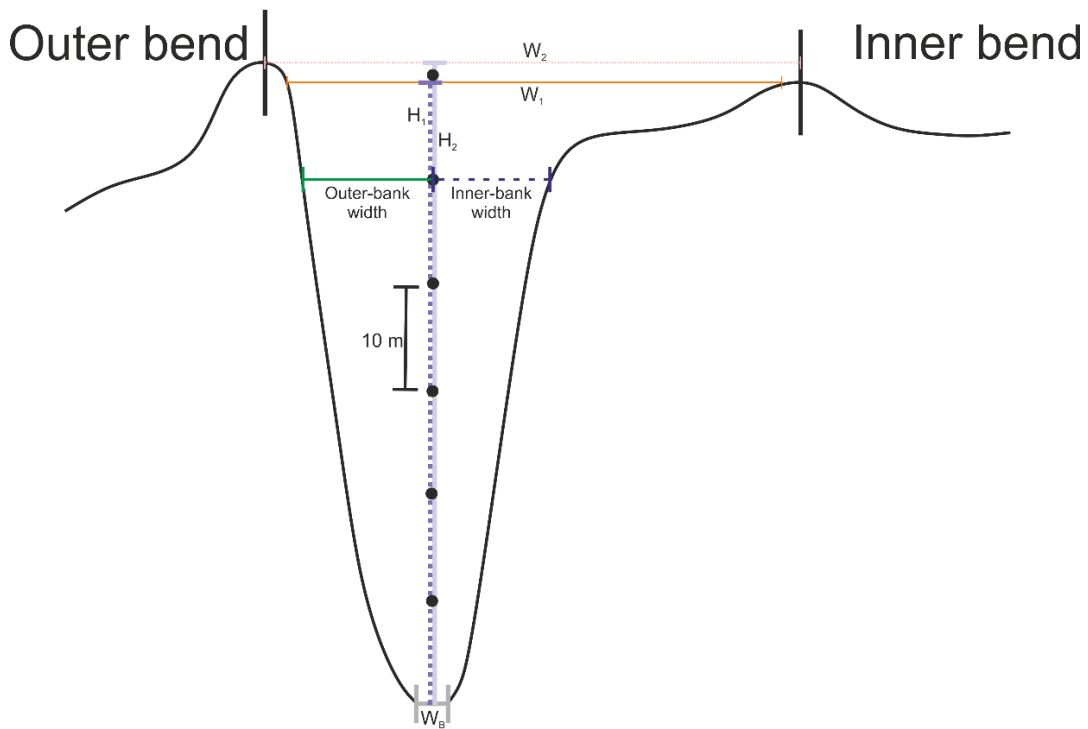


**Figure 5.4** Methodology of (A) bend analysis and (B) cross-section analysis. A) Methodology for cross-section measurements around a bend. Flow is from left to right. 13 cross-sections per bend were measured perpendicular to the channel bed centreline: at the up-stream inflection (1ui), at the down-stream inflection (13di), at the bend apex (7a) and 5 cross-sections between the bend apex and up-stream (2u, 3u, 4u, 5u, 6u) and equally down-stream inflection points (8d, 9d, 10d, 11d, 12d). Cross-sections were divided into an inflection region (orange ellipse: 1ui, 2u, 3u, 11d, 12d, 13di) and an apex region (yellow ellipse: 4u, 5u, 6u, 7a, 8d, 9d, 10d). B) At each cross-section channel width and height were measured at the channel bed and at vertical intervals of 10 m away from the channel bed up to the top of the channel banks. Additionally, width was measured at each position, and separately the outer and inner bank widths were measured to either side of the bed centreline position.

---

### *Cross-sectional analysis*

As noted earlier a cross-section was defined from channel bank to channel bank perpendicular to the channel-bed centreline (Figure 5.5A; see Appendix A, Section 4.5.2). Channel banks or crest lines are defined for aggradational channels with well-developed levees as the highest point of the external levee, which represents the point of maximum aggradation (Kane and Hodgson, 2011; Hansen *et al.*, 2015) and for channels with poorly developed or no levees, as the point at which the gradient of the inner channel bank levels off to the surrounding sea floor, hence this is the roll-over point between the bank and the surrounding sea floor (Shumaker *et al.*, 2018). Cross-sectional measurements in submarine-channel needed to be adjusted in order to not exclude any measurements. This adjustment is needed where cross-sections did not reach from channel bank to channel bank due the often complex topography of submarine channels (Figure 5.5B,C; see Appendix A, Section 4.5.2). A complex topography in submarine channels may arise for example from bend geometry due to the presence of terraces at inner bends, especially for bends with a low radius of curvature, or due to terrace formation resulting from bend cut-off, or an absence of a channel bank section due to channel bank failure. In such cases, topography is lower at regions where terraces are present and also where the bank failure occurred than at the channel banks, hence channel width will be overestimated, and height will be underestimated. In extreme cases channel width will be measured twice if a cross-section extends across the inner-bend region or channel height will be close to 0 m if

measured at a point at the inner-bend region. One possible approach to adjusting cross-sections with complex topography is to exclude any cross-section in which channel width exceeds 150% or 170% of the minimum width of the three previous upstream cross-sections (Shumaker *et al.*, 2018) which can vary for each channel (Shumaker *et al.*, 2018). Furthermore, the three upstream cross-sections could still incorporate complex morphology that would still lead to erroneous measurements. Such an approach may also be a subjective adjustment leading to cross-sections being excluded or in other cases retained.

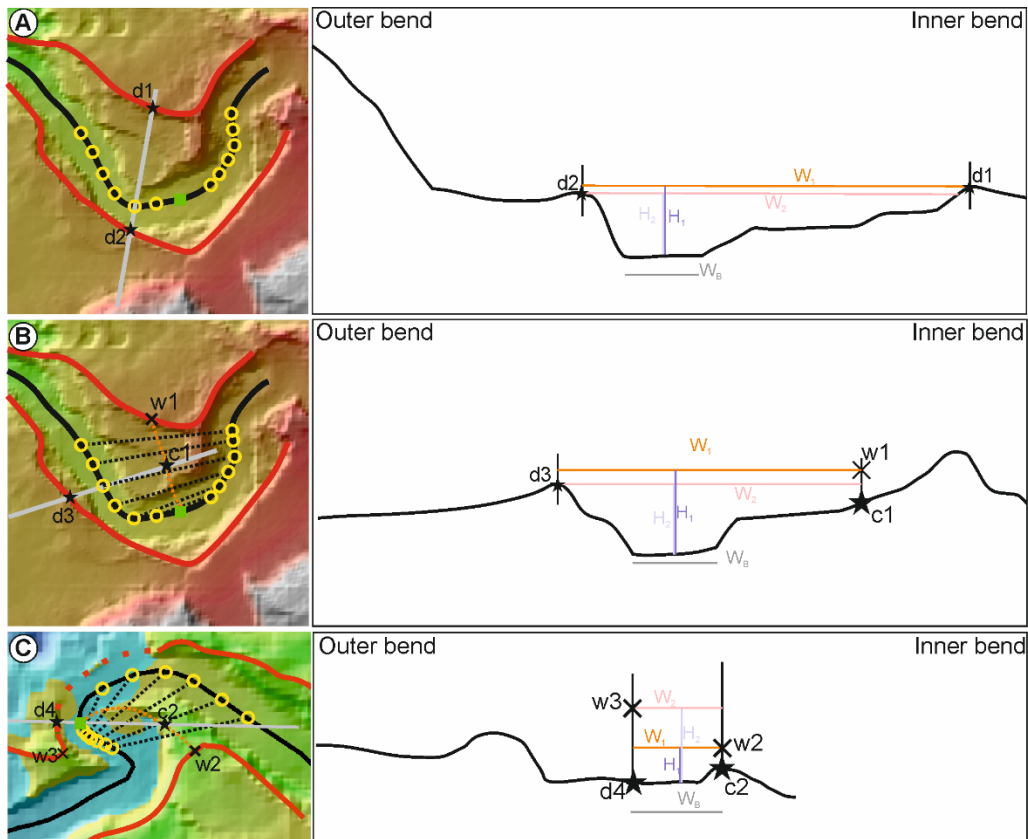
For cross-sections crossing tight bends with a low radius of curvature or terraces at the inner bend (Figure 5.5B), the position of the channel bank at the inner bend was equivalent to the trajectory line. The trajectory line was equivalent to the trajectory line used in the analysis of river meanders (Russell, 2017; Russell *et al.*, 2019), but instead of following the migration of scroll bars, as no scroll bars were identified, in these submarine channels, the trajectory line was a line at the inner bend, representing the mean distance between opposite cross-section points and the bend apex (orange dashed line in Figure 5.5 B,C). Mean channel width was the mean of the two outer bank crest to trajectory line measurements (Width between d3 and c1 in Figure 5.5B). Mean channel height was the distance from the channel bed to the average elevation of the banks; these are defined as the outer channel bank (Figure 8b, Position d3) and the position where the trajectory line would intersect with the channel bank crest (Figure 5.5C, Position w1). Channel bed width ( $W_B$ ) was measured for each cross-section as the width of the flat surface between the positions where channel gradient starts to rapidly increase to create the channel walls.

Channel bank failure occurs for channels with or without levees and this can cause the bank crest to have a lower topography than it would otherwise have had, thus leading to an underestimation of channel depth. In the example illustrated in Figure 5.5C the bank failure occurred at the outer bend, and at the inner bend a terrace is present as in the previous example. Mean channel width was measured between the primary position of the channel bank prior to bank failure at the outer bend and the trajectory line at the inner bend (distance between position d4 and c2 in Figure 5.5C). Mean channel depth was measured between the channel bed and the position where the trajectory line intersects with the channel bank at the inner bend (w2) and the nearest position where the channel bank did not fail at the outer bank (w3). Any

combination of the examples was possible and can be adapted according to the position and nature of the cross-section.

**Table 5.1** Total number of cross-sections measurements, and subdivided by non-complex, and complex topography.

	<b>Magdalena</b>	<b>Amazon</b>	<b>Bryant</b>	<b>Surveyor</b>	<b>Horizon</b>	<b>Baranof</b>	<b>Mariana</b>
Total number -of cross-sections	217	484	133	73	85	85	52
Non-complex topography	76	382	60	73	64	64	
Complex topography	141	102	73	0	21	21	



**Legend**

Central line		$W_B$	Channel bed width
Bend apex		$H_1, H_2$	Height of outer and inner bank
Cross-section		$W_1, W_2$	Width at outer and inner bank
Position of cross-sections		$c1, c2$	Position of cross-section at bend trajectory
Intact channel bank		$w1, w2, w3$	Water depth at channel bank
Damaged channel bank		$d1, d2, d3, d4$	Position of cross-section at channel bank
Joined up-stream and down-stream cross-section position			
Bend trajectory			

**Figure 5.5** Three approaches for extracting channel width and height from a cross-section for the case of a non-complex (Case A) and complex topography (Case C) in submarine channels. The approach adopted depends on the position of the cross-section in relation to the channel bank: A) Cross-section measured from channel bank to channel bank; B) Cross-section measured from channel bank to terrace; or, C) Cross-section measured from failed channel bank to terrace. Examples are shown from the Magdalena channel.

### *Analysis of channel parameters*

The apex (4u, 5u, 6u, 7ac, 8d, 9d, 10d, see Figure 4 for cross-section nomenclature) and inflection region width (1ui, 2u, 3u, 11d, 12d, 13di) contain all data from the channel bed to the channel banks:

$$\overline{W_{1ui}Total} = \{W_0, W_{10}, W_{20}, \dots, W_{Banks}\} \dots \dots \dots$$

$$\overline{W_{13di}Total} = \{W_0, W_{10}, W_{20}, \dots, W_{Banks}\}$$

, where for  $W_0$  is the width at 0 m,  $W_{10}$  at 10 m, ....., and  $W_{Banks}$  at left and right bank.

The outer-inner bank width ratio was calculated for each cross-section away from the centreline at the inner and outer bank width for each channel height per cross-section:

$$\overline{W_{1ui}outer} / \overline{W_{1ui}inner} \dots \dots \overline{W_{13di}outer} / \overline{W_{13di}inner},$$

whereby an outer-inner bend width ratio of  $1 \pm 0.005$  represented no difference between inner and outer bend width, an outer-inner bend width ratio  $< 0.995$  represented a wider inner bend width and outer-inner bend width ratio  $> 1.005$  represented a wider outer bend width.

The mean apex and inflection region width was obtained for each bend by calculating the mean width for each cross-section from channel bed to channel banks first:

$$\overline{W_{1ui}Total} = \{W_0, W_{10}, W_{20}, \dots, W_{Banks}\} / n \dots \dots \dots$$

$$\overline{W_{13di}Total} = \{W_0, W_{10}, W_{20}, \dots, W_{Banks}\} / n$$

and then calculating the mean apex region width (4u, 5u, 6u, 7ac, 8d, 9d, 10d) and mean inflection-region width (1ui, 2u, 3u, 11d, 12d, 13di):

$$\overline{W_A}Total = \{\overline{W_{4u}}, \overline{W_{5u}}, \overline{W_{6u}}, \overline{W_{7ac}}, \overline{W_{8d}}, \overline{W_{9d}}, \overline{W_{10d}}\} / 7 \text{ and}$$

$$\overline{W_I}Total = \{\overline{W_{1ui}}, \overline{W_{2u}}, \overline{W_{3u}}, \overline{W_{11d}}, \overline{W_{12d}}, \overline{W_{13di}}\} / 6.$$

The apex-inflection width ratio is the ratio of the mean apex region width (4u-10d) and the mean inflection region width (1ui-3u, 11d-13di) per bend:

$$\text{Apex - inflection width ratio} = \overline{W_A}Total / \overline{W_I}Total,$$

whereby an A-I width ratio of  $1 \pm 0.005$  represented no difference between apex and inflection width, an A-I width ratio  $< 0.995$  represented a wider width at inflection region and an A-I width ratio  $> 1.005$  represented a wider width at apex region.

The apex-inflection width ratio was also calculated with height per bend. The width per height was calculated between the channel bed (0 m) and the two channel banks with an interval of 10 m for the apex (4u-10d) and inflection region (1ui-3u, 11d-13di) per bend:

$$\overline{\text{Apex Width at ... } m} = \{W_{4u}, W_{5u}, W_{6u}, W_{7ac}, W_{8d}, W_{9d}, W_{10d}\}/n \text{ and}$$

$$\overline{\text{Inflection Width at ... } m} = \{W_{1ui}, W_{2u}, W_{3u}, W_{11d}, W_{12d}, W_{13di}\}/n.$$

The channel height was normalised to compare the apex-inflection width ratio with height between channels since channel height of some submarine channels vary downstream by a few tens of metres (Klaucke *et al.*, 1997), between channels, and between channels from the same system (Straub *et al.*, 2012; Maier *et al.*, 2013). For a normalised height, firstly mean height was calculated for both channel banks per bend:

$$\overline{\text{Height at banks (H1 and H2)}} = \{H_{1ui}, H_{2u}, H_{3u}, H_{4u}, H_{5u}, H_{6u}, H_{7ac}, H_{8d}, H_{9d}, H_{10d}, H_{11d}, H_{12d}, H_{13di}\}/13).$$

Secondly, each height was divided by the maximum height of the banks:

$$\text{Normalised height} = \{H_0, H_{10}, H_{20}, \min(H_1 \text{ or } H_2)\}/\max(H_1 \text{ or } H_2).$$

A normalised height of 0 represented the channel bed, 1 is equivalent to the channel banks, and 0.5 is equivalent to the half-way height between the channel bed and banks. Afterwards, each bend was analysed at 0.1 increments between 0 and 1 of the normalised height to examine if it was wider at the inflection region, equal or wider at the apex region.

Statistical analyses were conducted in Minitab 17. The two-sample t-test was used to test if a significant difference exists between submarine-fan channels and isolated deep-ocean channels in terms of inflection region and apex region width. The two-sample t-test is used for two samples with different sizes, not paired, and which exhibited an underlying a normal distribution. The null hypothesis is ( $H_0$ ): submarine-fan channel and isolated deep-ocean channels have an equal apex-region and



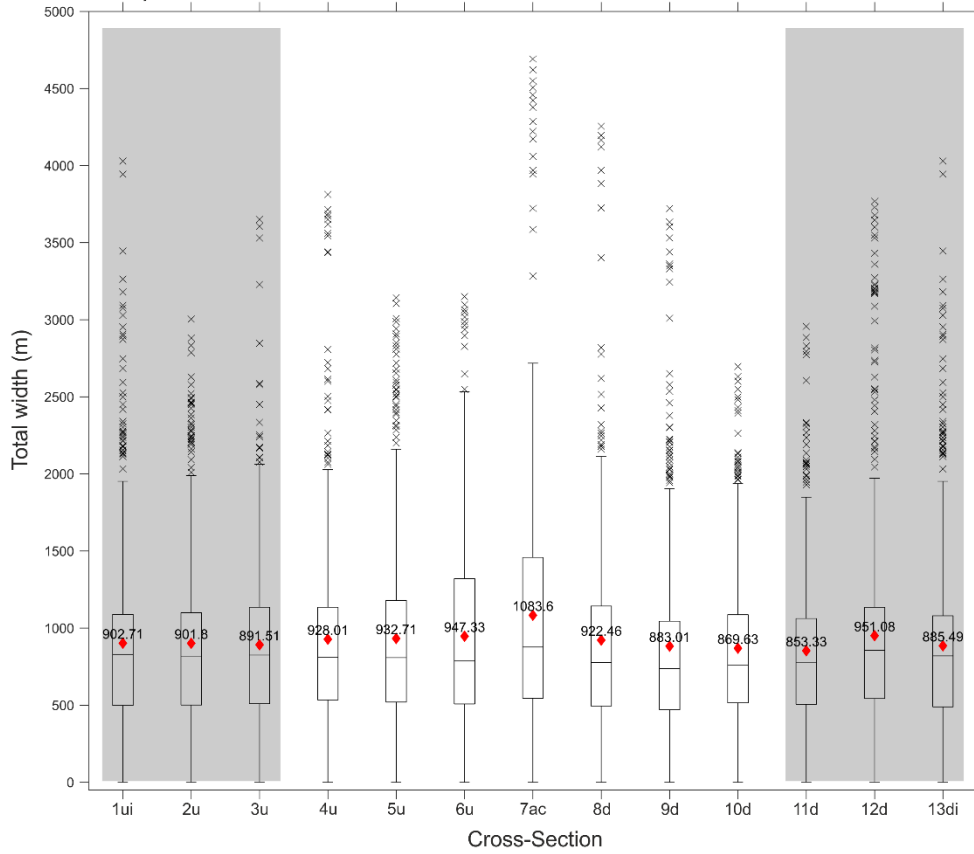
inflection-region width. The alternative hypotheses are: submarine-fan channels inflection-region or apex-region width is smaller compare to isolated deep-ocean channels inflection-region or apex-region width ( $H_{A1}$ ) and submarine-fan channels inflection-region or apex-region width is greater compare to isolated deep-ocean channels inflection-region or apex-region width ( $H_{A2}$ ). The null hypothesis is rejected if the p-value is smaller than 0.05.

## 5.4 Results

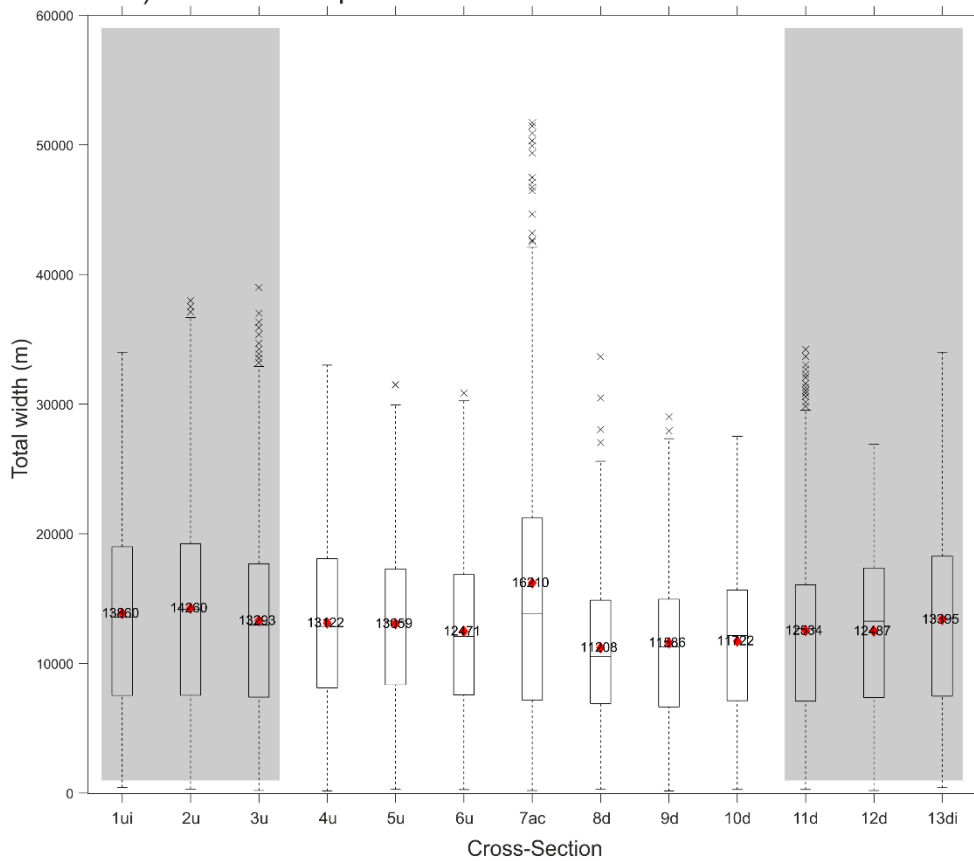
### 5.4.1 Total width around bends

Channel width for submarine-fan channels (Figure 5.6A,C) increased towards the bend apex (1ui-6u) with a peak at the bend apex (7ac) and decreased downstream after the bend apex (8d-13di). By contrast, isolated deep-ocean channels (Figure 5.6B) decreased in channel width upstream of the bend apex from upstream inflection to bend apex region (1ui-6u), had a peak at the bend apex (7ac), decreased afterwards (8d) and then increased again towards the downstream bend inflection (8d-13ui). Non-margin ocean channels were widest at bend apexes, but also exhibited inflections that were widest than the areas between bend apexes and bend inflections (Figure 5.6D).

A) Submarine-fan channels



B) Isolated deep-ocean channels



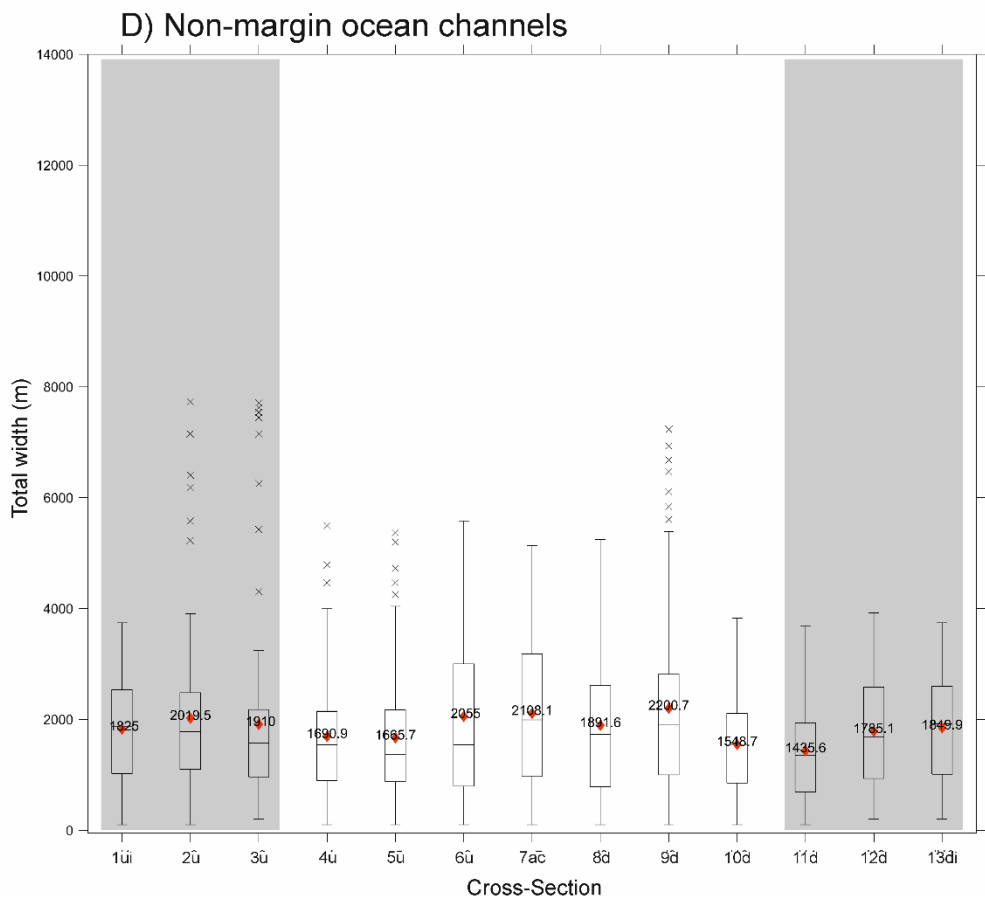
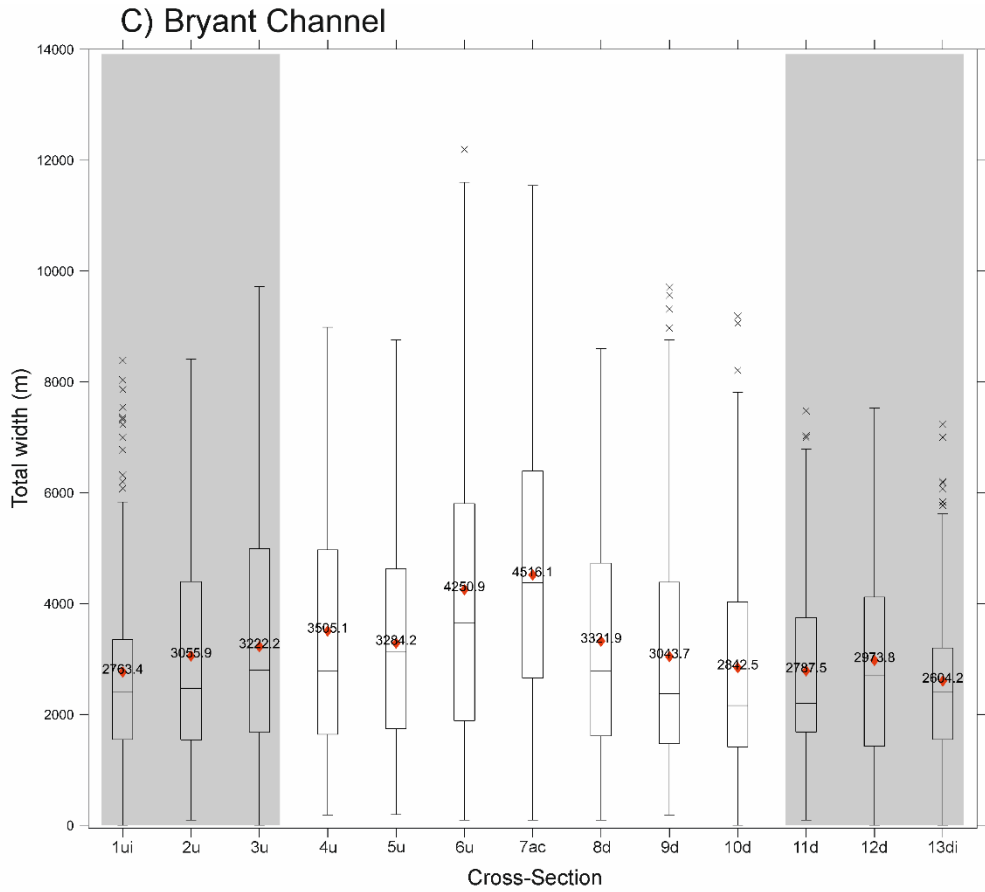


**Figure 5.6** Box and whisker plot of total channel width from each cross-section (averaged channel width from channel bed to channel banks) for A) Submarine-fan, B) Isolated deep-ocean channels, C) Bryant Channel, and D) Non-margin ocean channels. Grey boxes represent inflection region (1ui-3u, 11d-13di) and the white box represents the apex region (4u-10d). Box indicates 25th and 75th percentiles, “red diamond” indicates the mean, “-“ within the box indicates the median, whiskers indicate 99.3% in a normal distribution and “x” indicates outliers.

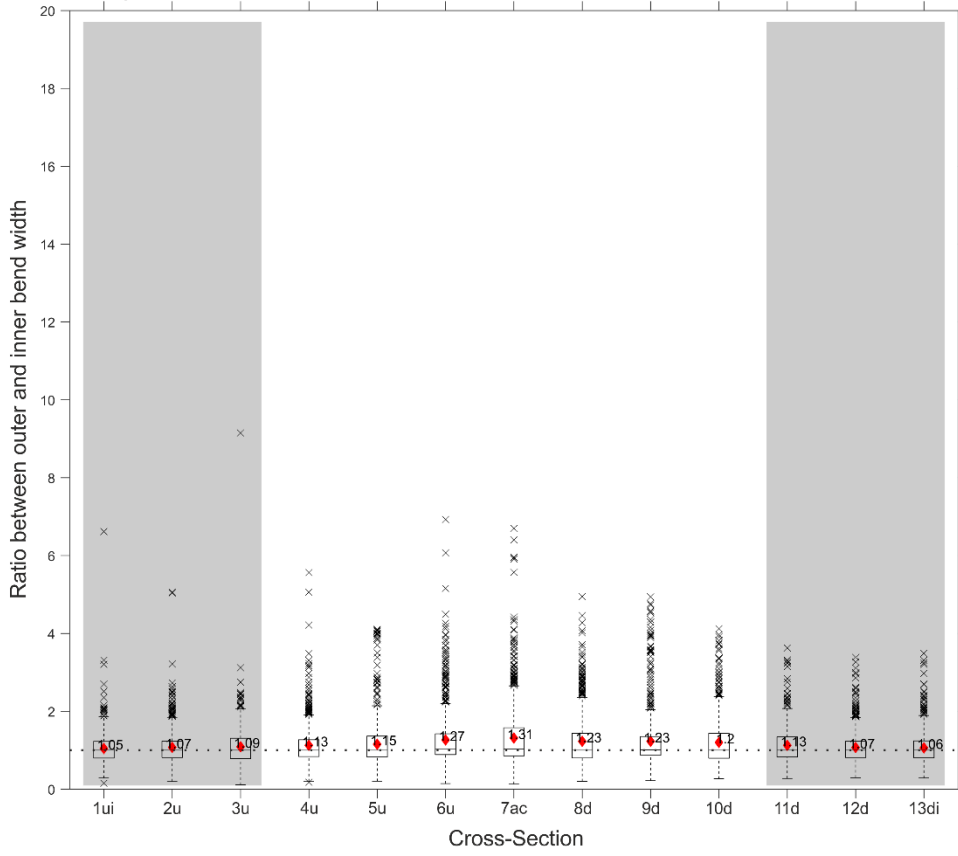
---

#### 5.4.2 Ratio between outer and inner bend width

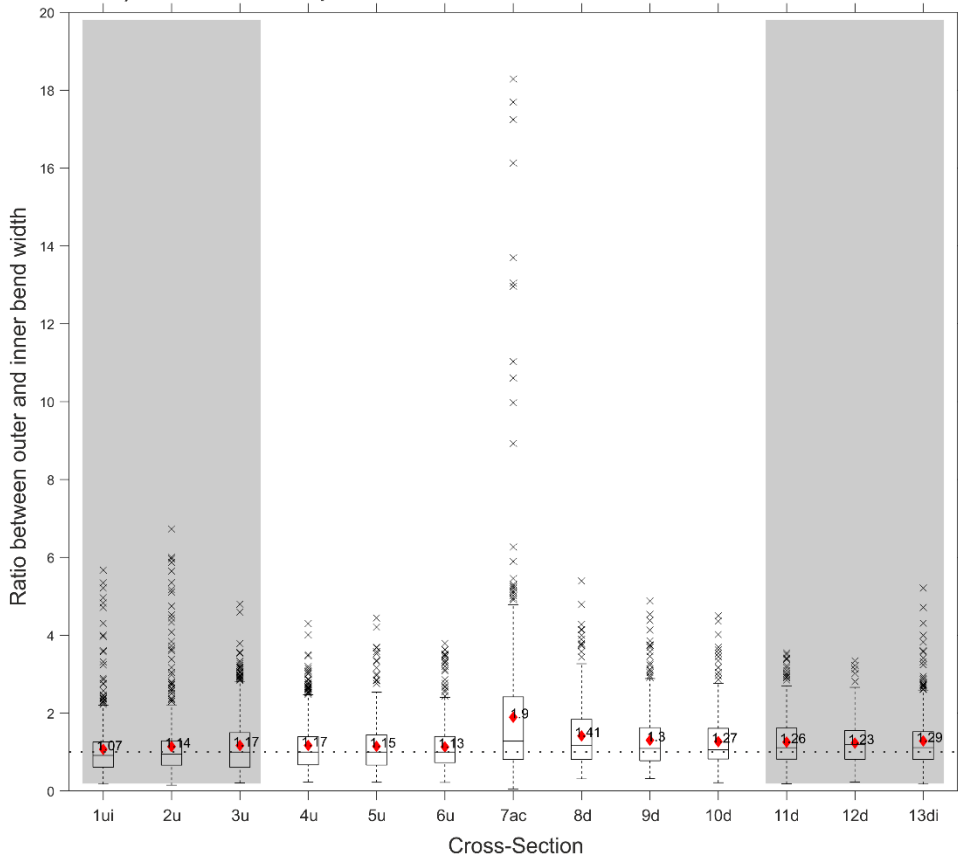
The ratio between the outer and inner bend width was relatively constant for submarine-fan and isolated deep-ocean channels with a peak for the outer bend width at the bend apex (Figure 5.7A,B), whereas the ratio between outer and inner bend width was variable for the Bryant Channel and non-margin ocean channels (Figure 5.7C,D). Submarine-fan and isolated deep-ocean channels had their maximum outer bank width at the bend apex (7ac). Mean outer-inner bend width ratio increased in the upstream part of the bend apex between the bend inflection (1ui) and the bend apex (7u) from 1.05 to 1.31 and decreased downstream after the bend apex (8u) to the bend inflection (13ui) from 1.23 to 1.06 for submarine-fan channels (Figure 5.7A). Mean outer-inner bend width ratio was narrowest at the upstream bend inflection (1ui) with a ratio of 1.07 for isolated-deep ocean channels (Figure 5.7B). Afterwards mean outer-inner bend width ratio was relatively constant between bend inflection and bend apex with a ratio between 1.13 and 1.17. At the bend apex outer-inner bank width ratio was 1.9, but gradually decreased downstream again from 1.41 to 1.23 (Figure 5.7B).

The ratio between outer-inner bank width was variable for the Bryant Channel (Figure 5.7C). In general, outer bank width was greater than inner bend width and outer-inner bend width ratio ranged between 1.12 and 1.5. Additionally, the apex-region (4u-10d) had a greater ratio than the inflection region (1ui-3u, 11d-13di). Non-margin ocean channels (Figure 5.7d) had a variable outer-inner bank width ratio with a relative constant ratio and a general increase towards the apex region (4u-10d) than (1ui-3u, 11d-13di).

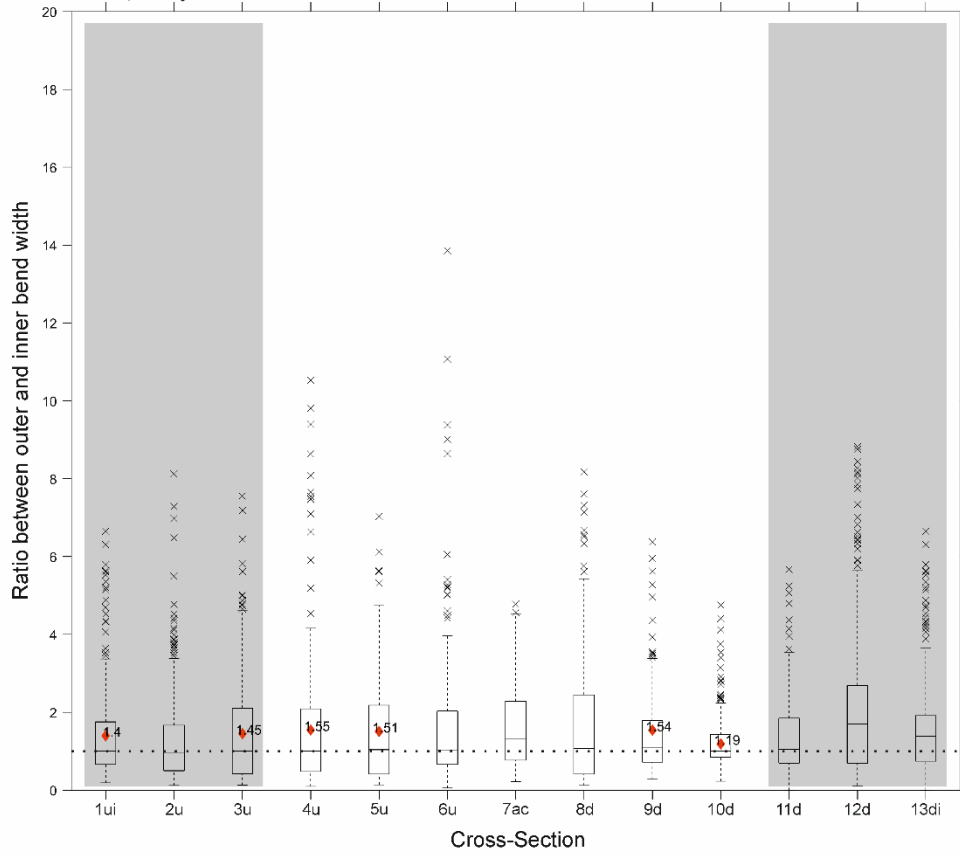
A) Submarine-fan channels



B) Isolated deep-ocean channels



C) Bryant Channel



D) Non-margin ocean channels

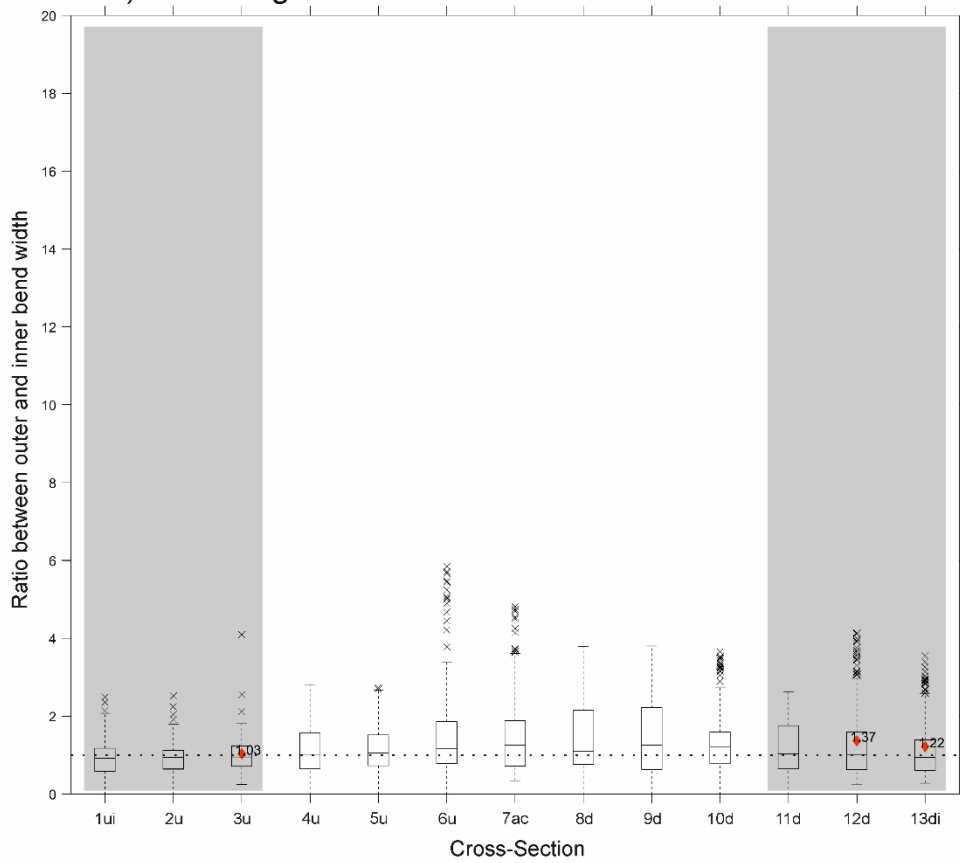


**Figure 5.7** Box and whisker plots of the ratio between outer and inner bank width from each cross-section for A) Submarine-fan, B) Isolated deep-ocean channels, C) Bryant Channel, and D) Non-margin ocean channels. Grey boxes represent the inflection region (1ui-3u, 11d-13di) and the white box represents the apex region (4u-10d). Box indicates 25<sup>th</sup> and 75<sup>th</sup> percentiles, “red diamond” indicates the mean, “-“ within the box indicates the median, whiskers indicate 99.3% in a normal distribution and “x” indicates outliers.

---

### 5.4.3 Width variation between channel base and channel banks

Submarine-fan and non-margin ocean channels have more bends wider at the apex region, whereas more bends are narrower at the apex region for isolated deep-ocean with height (Figure 5.8). Near the channel bed, submarine-fan and isolate deep-ocean channels have more bends wider at the inflection region and non-margin ocean channels and the Bryant Channel have more bends at apex region than at inflection region (Figure 5.8). From 0.2 more bends were wider at apex-region for submarine-fan channels (59%, Figure 5.8A), whereas for isolated-deep ocean channels more bends were still wider at inflection-region (55%, Figure 5.8B). For submarine-fan channels, bends which at wider at the apex-region increased from 59% to 72% between 0.2 to 0.4 of the normalised height and decreased from 71% at 0.5 to 59% at 0.8. Near the channel top, at 0.9 and 1, 53% and 63% of bends were wider at the apex-region (Figure 5.8A). The Bryant Channel was wider at the apex region between 64% and 100% of bends, except for 0.3 were 45% of bends were wider at the apex region (Figure 5.8D).

Isolated-deep ocean channels have more bends narrower at the apex region compared to the inflection region, ranging from 45% at 0.8 to 75% at 0.1 and 0.6 of the normalised height (Figure 5.8B). Bend being wider at apex region ranged from 25% at 0.1, 0.4, 0.5 and 0.6 of the normalised height to 40% at 0.2 and 1 of the normalised height to 45% at 0.8.

All 4 bends from non-margin ocean channel were wider at the apex-region at the channel bed up to 0.6 of the normalised height (Figure 5.8C). Afterwards, no clear pattern is identified. At 0.7 and 0.8 of the normalised height 2 bends were equal width and at 0.9 and 1 of the normalised height 3 bends are wider at inflection region.

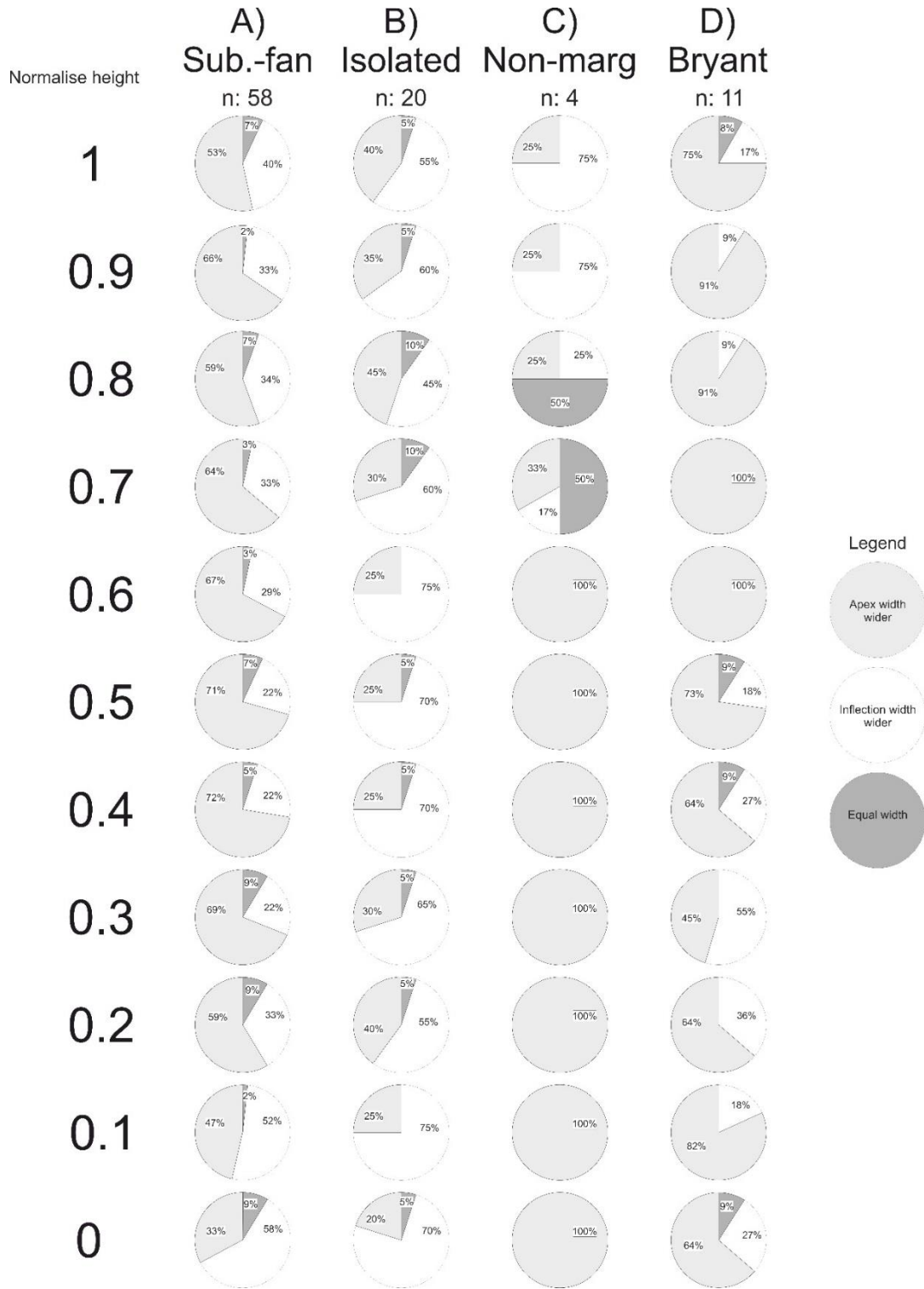


**Figure 5.8** Pie chart of the percentage of bends being wider at bend apex, wider at inflection width or equal with height for all channels. Height is normalised.



#### 5.4.4 Apex-inflection width ratio as a function of sinuosity

Submarine-fan channels (including the Bryant Channel) were wider at the apex-region than at the inflection region (mean ratio: 1.01-1.09), whereas isolated deep-ocean channels were more equi-width (mean ratio 0.95-1.0) for all sinuosity bends (Figure 5.9). Both submarine-fan channels and isolated-deep ocean channels were equiwidth for straight bends ( $1 \leq P \leq 1.2$ ) and were wider at the apex region for low sinuosity bends ( $1.2 < P < 1.5$ ). Most bend were high-sinuosity bends ( $P \geq 1.5$ ) for both submarine-fan and isolated deep-ocean channels, but an equal number of bends were wider at the inflection and apex regions. Maximum values of apex-inflection region (1.3-1.7) were reported for submarine-fan channels were reported for high-sinuosity bends ( $P \geq 1.5$ ).

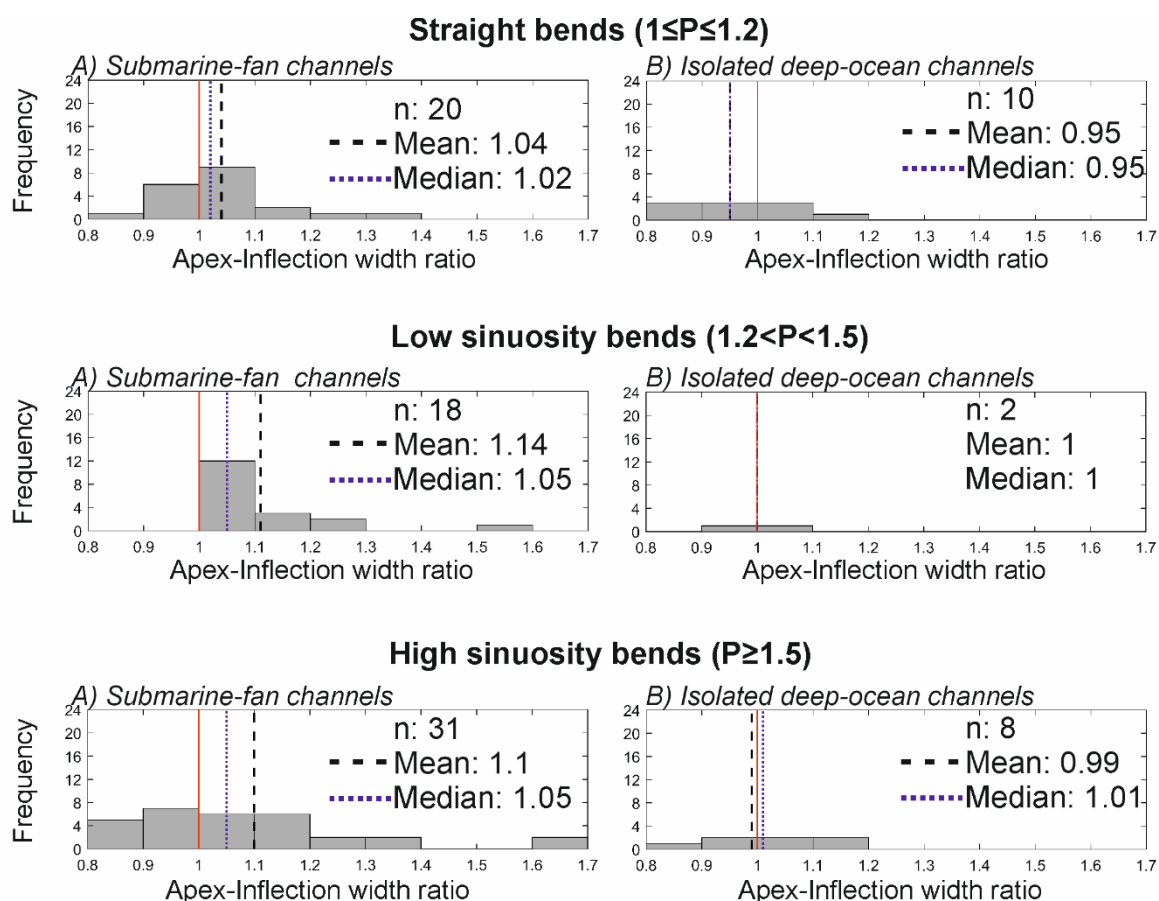


**Figure 5.9** Apex-inflection width ratio distribution based on sinuosity for A) submarine-fan, and B) Isolated deep-ocean channels for straight bends ( $1 \leq P \leq 1.2$ ), low sinuosity bends ( $1.2 < P < 1.5$ ), and high sinuosity bends ( $P \geq 1.5$ ).

### 5.4.5 Overall trend of width around bends

A strong relationship exists between mean apex-region width and mean inflection-region width with an  $R^2$ -value of 0.91 for submarine-fan channels (linear, 69 bends), an  $R^2$ -value of 0.89 for isolated deep-ocean channels (linear), with an overall  $R^2$ -value of 0.98 (linear) for all submarine channel types (Figure 5.10A, B, C) combined. The linear equation for submarine-fan channels showed that for a given apex-region width ( $y=0.82x$ ), inflection-region width is narrower. By contrast, the linear equation for isolated deep-ocean channels showed that mean apex region and mean inflection region width was nearly equal ( $y=1.04x$ ). For non-margin ocean channels 3 out of 4 bends were on average 13.4% wider at inflection region than at apex region. For submarine-fan channels, mean apex-width was on average 14% wider compared to the mean inflection-width for 50 bends from 69 bend with 27 bends from Amazon and 12 bends from Magdalena and all bends from the Bryant Channel. Mean inflection-width was on average 9.5% wider compared to the mean apex width for 19 bends out of 58 bends with 13 bends from Amazon, 6 bends from Magdalena and no bends from Bryant. Isolated deep-ocean channels (Figure 5.10C) had on average a 13.1% wider mean inflection region width compared to the mean apex-region width for 11 out of 20 bends. In detail 2 out of 6 bends for the Surveyor, 4 out of 7 bends for the Horizon and 5 out of 7 bends for the Baranof Channel. Apex-region width was on average only 6.3% wider for 4 out of 6 bends for the Surveyor, 3 out of 7 for the Horizon and 2 out of 7 bends for the Baranof Channel. Non-margin channels were similar to isolated-deep ocean channels on average 13.4% wider at inflection region (3 out 4 bends).

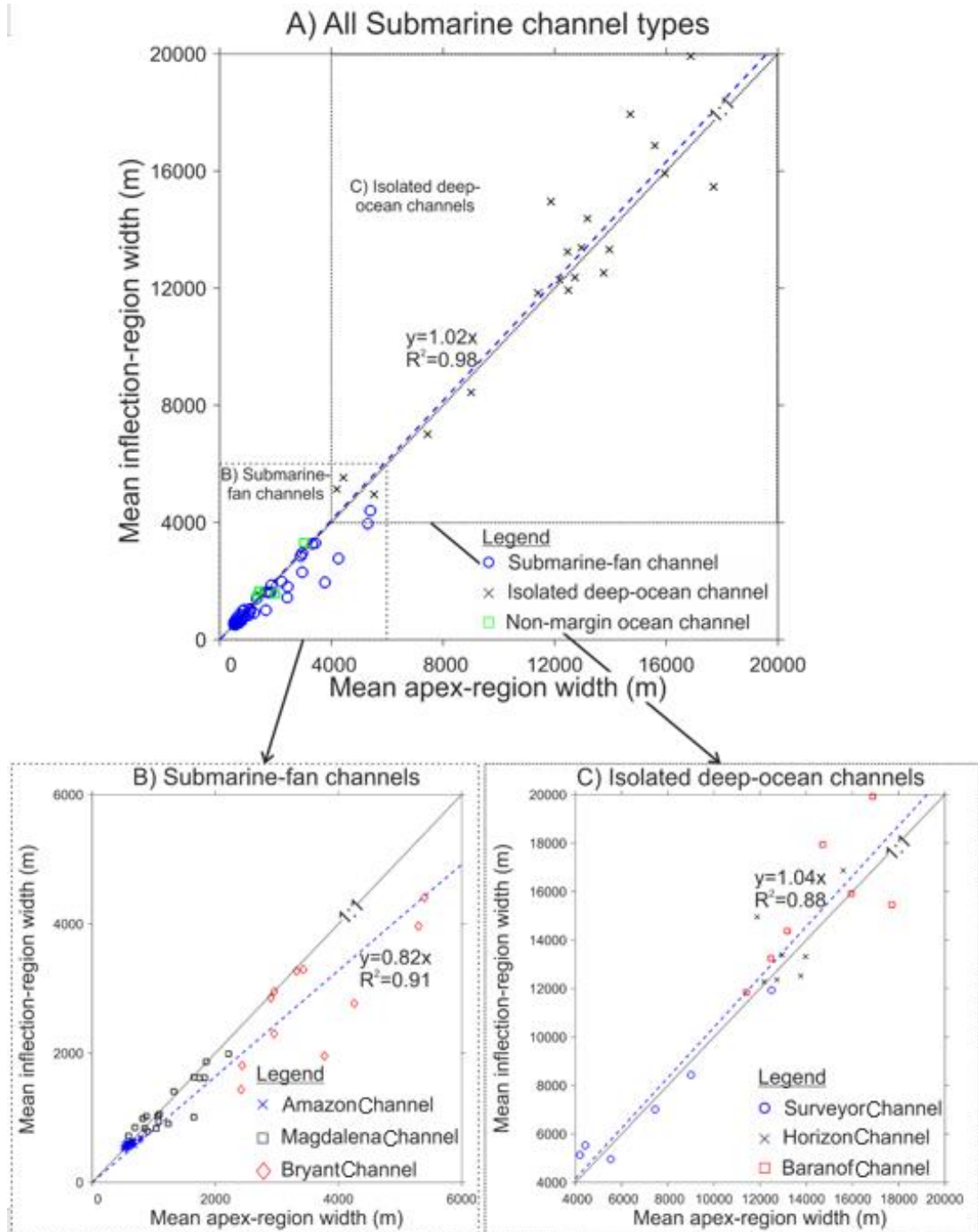


**Figure 5.10** Comparison between mean apex-region and mean inflection-region width for different channel types (A): submarine-fan channel (blue circles, 69 bends), isolated deep-ocean channel (black crosses, 20 bends), and non-margin ocean channels (green squares, 4 bends), and zoomed graphs for B) submarine-fan channels and C) isolated deep-ocean channels. B) High correlation (blue dashed line,  $R^2=0.91$ ) between mean apex-region and mean inflection-region width for submarine-fan channels. Channels were: Amazon channel (blue crosses), Magdalena channel (black squares) and Bryant (red diamonds). C) High correlation (blue dashed line,  $R^2=0.88$ ) between mean apex-region and mean inflection-region width for isolated deep-ocean channels. Channels were: Surveyor Channel (blue circles), Horizon Channel (black crosses) and Baranof

Channel (red squares). For all figures: Each point represents one bend. The mean width for a bend was obtained from six cross-sections for mean inflection-region and seven cross-sections for mean apex-region width. At each cross-section all channel width measurements from channel bed to channel banks were included.

**Table 5.2** Summary of different methodologies for comparing width variations around bends between submarine channels and rivers.

<b>% wider at apex point/region compared to inflection points/region</b>	<b>Rivers Type C from Brice (1975)</b>	<b>Submarine-fan channels</b>	<b>Isolated deep-ocean channels</b>	<b>Non-margin ocean channels</b>
<i>Width at height of the channel banks from the bend apex (cross-section 7) and the inflections (cross-sections 1, 13)</i>	14% (Eke <i>et al.</i> , 2014a)	34.61%	28.27%	12.61%
<i>Depth-averaged width from the channel bed to the height of the channel banks from the bend apex (cross-section 7) and the inflections (cross-sections 1, 13)</i>	x	28.42%	16.21%	4.53%
<i>Width at height of the channel banks from the apex region (cross-sections 4-10) and the inflection region (cross-sections 1-3, 11-13)</i>	x	10.19%	-1.09%	4.11%
<i>Depth-averaged width from the channel bed to the height of the channel banks from the apex region (cross-sections 4-10) and the inflection region (cross-sections 1-3, 11-13)</i>	x	8.57%	-3.00%	-2.14

A statistical test identified a significant difference between submarine-fan and isolated deep-ocean channels in terms of apex-region and inflection region width (Table 5.3). Isolated deep-ocean channels had a mean apex and inflection region width approximately 15-times wider than submarine-fan channels. Apex region width is slightly wider than inflection region width for submarine-fan channels.

**Table 5.3** Statistical results of the two-sampled t-test for submarine-fan channels and isolated deep-ocean channels. Calculation of a significant difference, between mean-apex and mean-inflection region for submarine-fan and isolated deep-ocean channels.

<i>Name</i>	<b>Inflection-region width</b>	<b>Apex-region width</b>
<i>No. of bends for submarine-fan channels</i>	69	69
<i>No. of bends for isolated deep-ocean channels</i>	20	20
<i>Mean width for submarine-fan channels</i>	1101 m	1250 m
<i>Mean width for isolated deep-ocean channels</i>	12370 m	11923 m
<i>Degrees of freedom</i>	19	19
<i>t-value</i>	-11.80	-12.02
<i>p-value</i>	<0.0001	<0.0001
<i>Significant difference between submarine-fan and isolated deep-ocean channels</i>	Yes	Yes

#### **5.4.6 Comparison between upstream and downstream channel section**

Upstream and downstream Amazon Channel region were in general wider at apex region. The fitted trend line was similar between upstream and downstream section with a slope differences of 0.05 with an R<sup>2</sup>-value of 0.61 for mid fan section and 0.4

for low fan section (Figure 5.11). Apex region (4u-10d) and inflection region width (1uic-3u, 11d-13di) decreased downstream from middle fan to lower fan. Mean apex-region width decreased from 635 m to 599 m, so a difference of 36 m and inflection region width decreased from 616 m to 575 m, so a difference of 41 m with no significant difference between channel section in terms apex and inflection region width (Figure 5.11). In details, mid fan section had a peak at apex-region width, which was less profound in the lower fan section (Figure 5.12). Mid-fan section had a mean peak width of 687 m at cross-section 7ac with a mean width between 604 m and 645 m upstream and downstream of 7ac (Figure 5.12a). On the hand, lower fan section has a gradually width variation with a small peak at 7ac with 646 m and a mean channel width between 550 m and 589 m upstream and downstream of 7ac (Figure 5.12b).

Ratio between outer and inner bank width was similar between mid and lower fan section, but a slight increase occurred towards outer than inner bank width from mid and lower fan (Figure 5.13). In the mid fan section outer-inner bank width ratio was between 1.05 and 1.14 (Figure 5.13a) and in the lower fan section between 1.04 and 1.15 (Figure 5.13b). Maximum increase of outer-inner bank width ratio from mid to lower fan occurred at cross-section 6u, just upstream of bend apex from 1.12 at mid-fan section to 1.15 at lower-fan section. Minimum decrease of outer-inner bank width ratio occurred at cross-section at 10d, downstream of bend apex from 1.09 at mid-fan section to 1.04 at lower-fan section.

More bends were wider at apex region than at inflection region with height for mid and lower fan channel section (Figure 5.14). For all channel height 5% to 15% of bends have an equal channel width for mid fan section, whereas 5% to 10% of bend with an equal width were only observed at the bottom up to 0.3 and at the channel top above 0.8 of the normalised height for the lower fan section. An increase of more bend being wider at apex region than at inflection region changed between 0.2 and 0.3 for both sections. At channel bed, 50% of bends of the mid-fan section were wider at inflection region compared to 60% of bend from lower fan section. At 0.1 of the normalised channel heights, percentage of bends being equal and/or wider at inflection region and wider at apex region are the same for both sections.

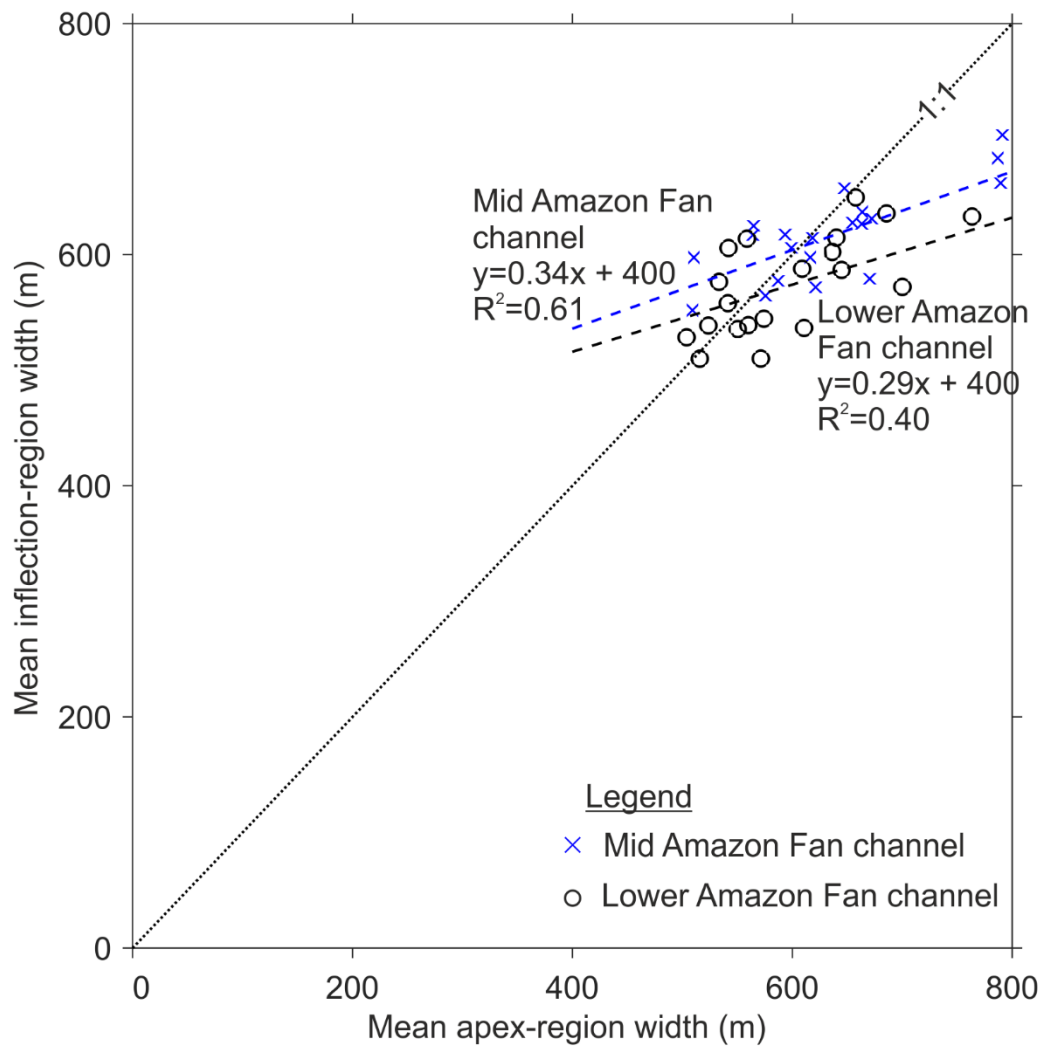


**Figure 5.11** Comparison between mean apex-region and mean inflection-region width for mid (blue cross) and lower fan section (black circle). Each point represents one bend. The mean width for a bend was obtained from six cross-sections for mean inflection-region and seven cross-sections for mean apex-region width. At each cross-sections all channel width measurements from channel bed to channels banks were included.

**Table 5.4** Results of two-sample t-test between apex-region and inflection region with for all channel heights. The null hypotheses ( $H_0$ ) was that apex-region width and inflection-region width were equal. The null hypothesis was tested for each channel.

<i>Name</i>	<b>Apex region</b>	<b>Inflection region</b>
<i>No. of width measurements for Mid-fan</i>	1236	1059
<i>No. of width measurements for Lower fan</i>	826	733
<i>Differences</i>	36.4	41.4
<i>t-value</i>	2.28	2.58
<i>p-value</i>	<0.05	<0.05
<i>Null hypothesis rejected</i>	Yes	Yes



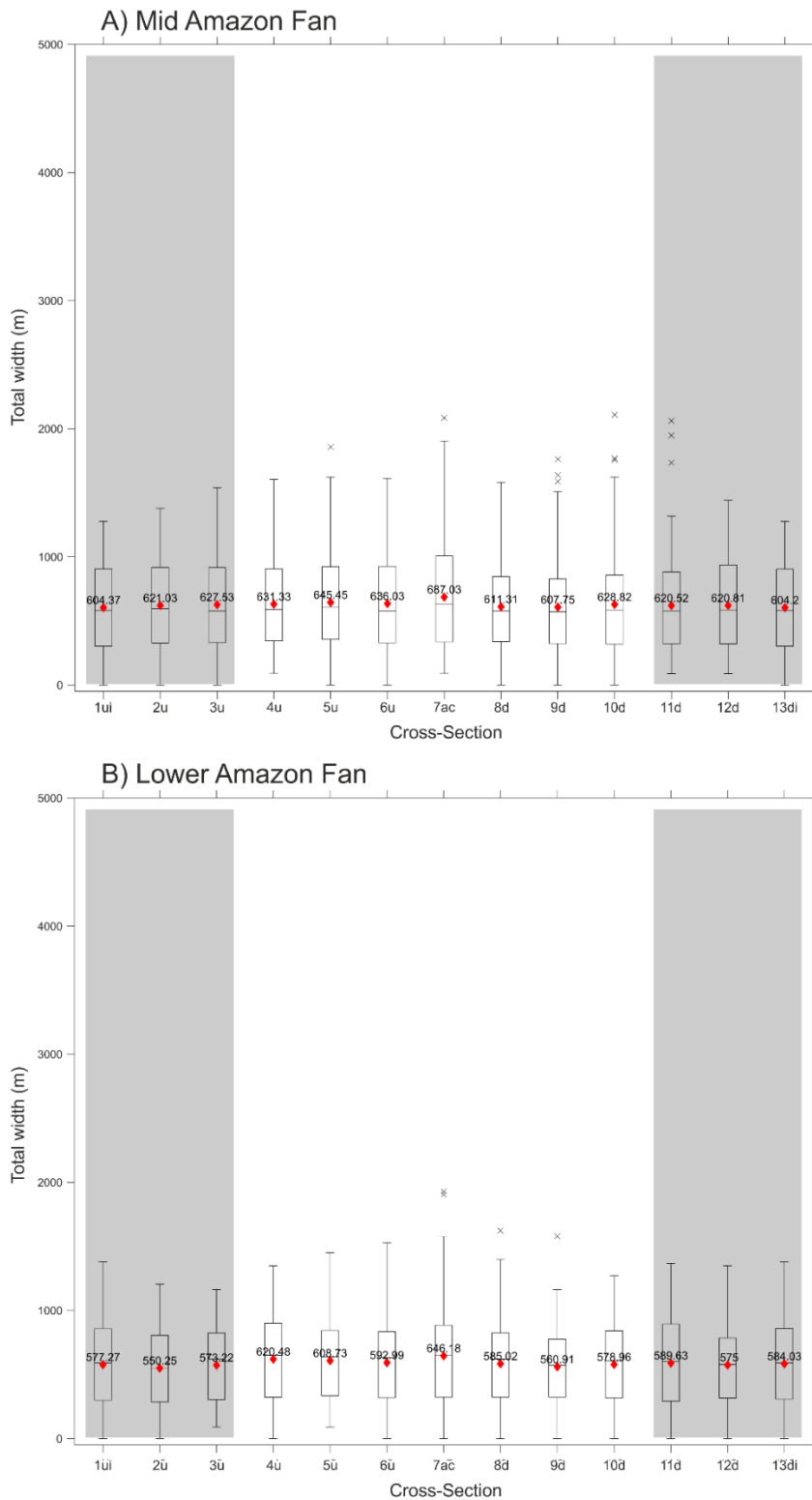


**Figure 5.12** Box and whisker plot of total width from each cross-section for A) Mid Amazon Fan and B) Lower Amazon Fan. Grey box represents inflection region (1ui-3u, 11d-13di) and white box represents apex region (4u-10d). Box indicates 25<sup>th</sup> and 75<sup>th</sup> percentiles, “red diamond” indicates the mean, “-” within the box indicates the median, whiskers indicate 99.3 % in a normal distribution and “x” indicates outliers.

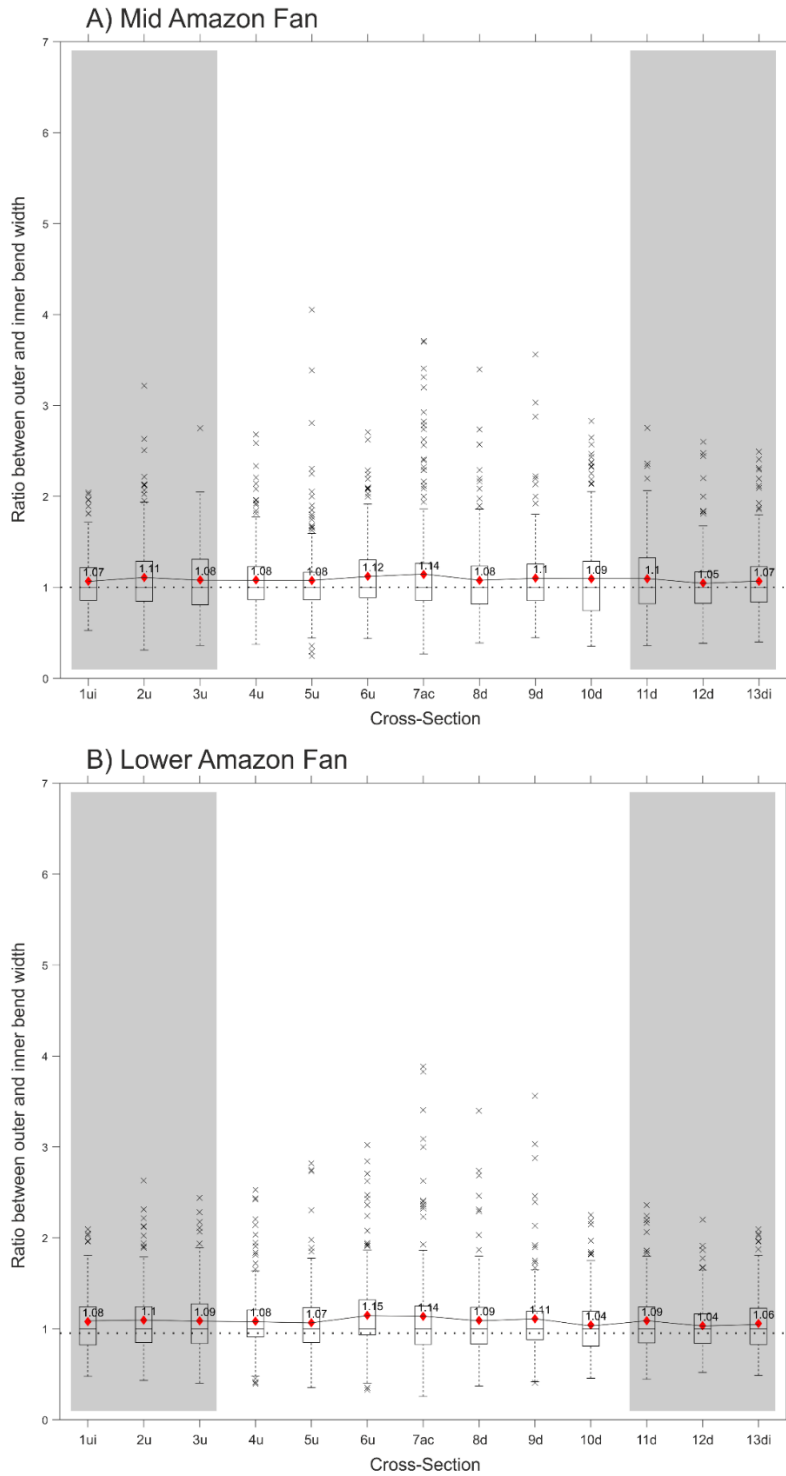


**Figure 5.13** Box and whisker plot of ratio between outer and inner bank width from each cross-section for A) Mid Amazon Fan and B) Lower Amazon Fan. Grey box represents inflection region (1ui-3u, 11d-13di) and white box represents apex region (4u-10d). Box indicates 25<sup>th</sup> and 75<sup>th</sup> percentiles, “red diamond” indicates the mean, “-” within the box indicates the median, whiskers indicate 99.3 % in a normal distribution and “x” indicates outliers.

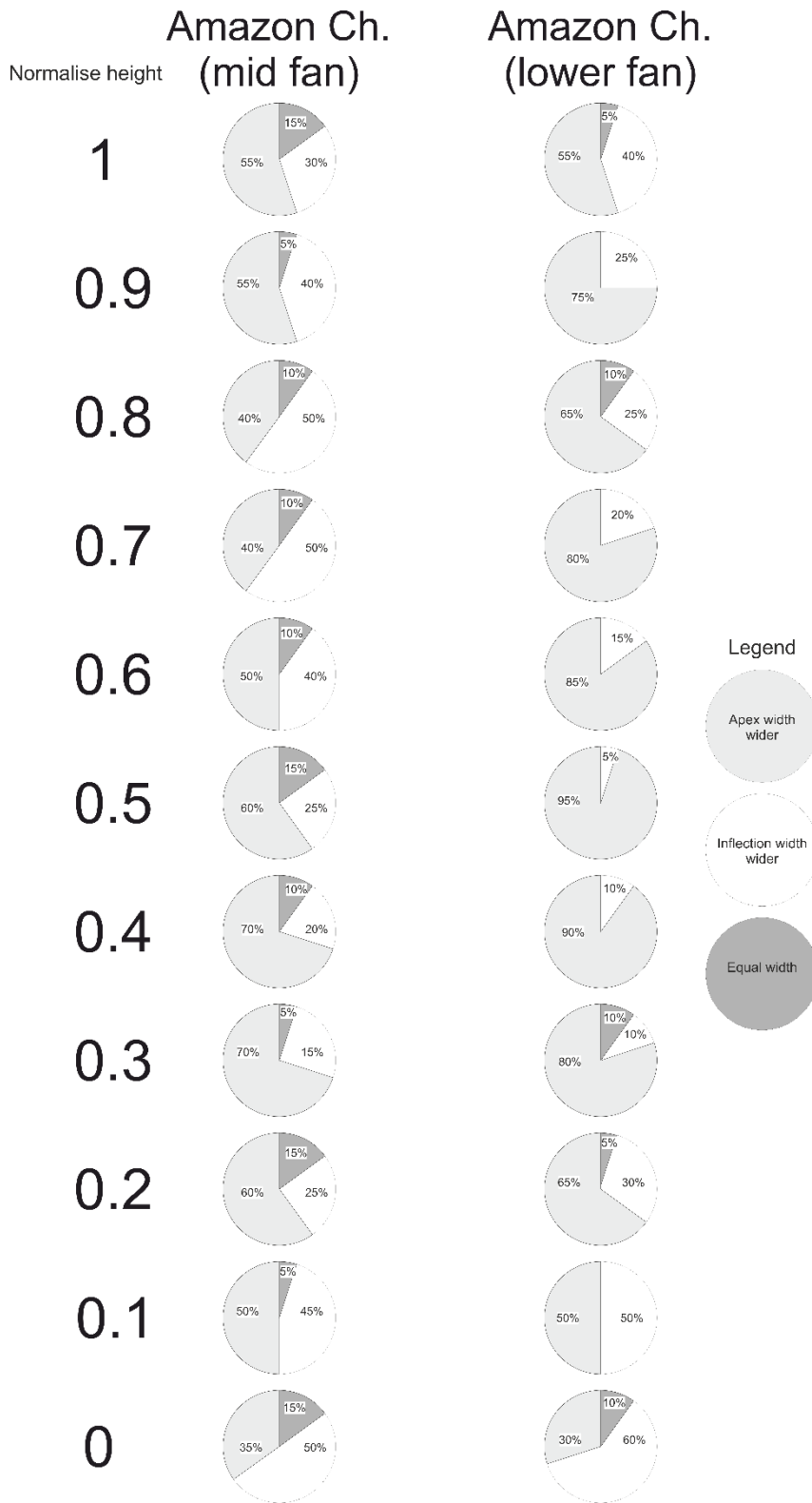


**Figure 5.14** Pie chart of percentage of bends being wider at bend apex (light grey), wider at inflection width (white) or equal (dark grey) with height for all channels. Height is normalised with 0 is equal to channel bed and 1 to channel banks.

## 5.5 Discussion

The analysis of width around bend for different channel types suggest that different channel types have a variable width variation around bends. On average, submarine-fan channels had a wider apex-region width compared to inflection-region width, whereas isolated deep-ocean channels had an equal number of bends being wider at apex and inflection region, hence had an equal width around bends. Non-margin ocean channels were wider at inflection region width than at apex-region width. Both upstream and downstream Amazon channel reach showed a wider at apex region width with no obvious variation identified for upstream to downstream Amazon Channel reach, which may be related to a relative short distance between the two reaches and hence flow variations may not be significant. However, all bends were wider at the outer-bank width than at the inner-bank width suggesting that an increase erosion occur at the outer bank. An increase outer bank width compared to inner bank width may suggest that channel types are controlled by an outer bank erosion, bank pull rather than an inner bend deposition, bar push, similar to rivers (Eke *et al.*, 2014a; Matsubara and Howard, 2014; Van de Lageweg *et al.*, 2014).

### *Width and asymmetry*

A comparison of outer and inner bend width may be used as an indication for cross-sectional asymmetry. A direct comparison of width variation and bend asymmetry around bends for submarine channels and river is complicated because of the variation in cross-sectional geometry and shape with submarine channels being in general deeper and wider than rivers and having lower gradient banks than rivers.

Cross-sectional asymmetry increases in rivers and submarine channels with bend curvature with asymmetrical cross-section near bend apex with maximum curvature and symmetrical cross-section near bed inflections with minimum curvature. (Knighton, 1982; Reimchen *et al.*, 2016). Outer-inner bend width is more equal near inflection points (cross section 1 and 13) and outer bend width is maximum at bend apex (cross-section 7) for all channel types. Outer bend width is wider at bend apex

which may be an indication of the thalweg shift from a central line position near inflection points to a near outer bank position with an enhance erosion near the bend apex (Richards, 1982; Reimchen *et al.*, 2016). In order to directly compare cross-section asymmetry between rivers and submarine channels, a different approach rather than the ratio between the inner and outer bend width is needed. Cross-sectional asymmetry can be calculated as a normalised cross-sectional area:

$$A^* = \frac{A_{outer} - A_{inner}}{A} \text{ (Knighton, 1982),}$$

whereby in this study the inner and outer cross-sectional area rather than the left and right cross-section area is calculated. The area of the inner and outer bend is calculated for each cross-section away from the centre line as the inner and respectively outer width at the channel bed times the width at the top of the channel banks of the inner and respectively outer bank. A positive cross-sectional area would suggest an increased outer-bend area whereas a negative cross-sectional area would suggest an increased inner-bend area, whereby the maximum limits of  $A^*$  represent extreme inner and outer bend asymmetry (Knighton, 1981). A direct comparison with this methodology suggest a symmetrical cross-sectional area at the inflection points and an asymmetrical cross-section with a greater inner bend area at bend apex for both rivers and submarine channels (Knighton, 1982). .....

Width variation around river bends is concentrated on single cross-section (inflection points, cross-section 1 and 13 to apex point, cross-section 7) rather than multiple cross-sections or region as has been proposed in the methodology. In order to directly compare width variation around bends in rivers, the mean width at the channel banks, which is equivalent to the bankfull level in rivers (Clark *et al.*, 1992; Pirmez and Imran, 2003; Konsoer *et al.*, 2013) has to been taken. A direct comparison of inflection points and apex point suggest that submarine-fan channels have a 34.61% wider apex point, isolated deep-ocean channels have a 28.27% wider apex point and non-margin ocean channels have a 12.61% wider apex point compared to a 14% wider apex point for sinuous point bar rivers (type C of the Brice (1975) classification, Eke *et al.*, 2014a), compared to inflection points. On the hand, if the apex region and inflection region at the mean width at the channel banks is taken, submarine-fan channels have a 10.19% and non-margin ocean channels have a 4.11% wider apex region than inflection

region, and isolated deep-ocean have a 1.09% wider inflection region than apex region.

A direct comparison of channel width at the channel banks between inflection points and apex point suggest that the channel width at the apex point is similar between non-margin ocean channels, 2-times wider between isolated deep-ocean and at least 2.5-times wider between submarine-fan channels and sinuous point-bar rivers (Eke *et al.*, 2014a). By contrast, averaged values of submarine channels suggest that submarine-fan channels are similar or wider at apex region compared to rivers, whereas isolated deep-ocean and non-margin ocean channels identify a narrower channel width at bend apex compared to rivers. It is not known, why variations in terms of channel width within submarine channels and between rivers and submarine channels exist, although multiple reason(s) may contribute to a variation within submarine channel types and between rivers and submarine channels.

**Table 5.5** Summary of different methodologies for comparing width variations around bends between submarine channels and rivers.

<b>% wider at apex point/region compared to inflection points/region</b>	<b>River type C from Brice (1975)</b>	<b>Submarine-fan channels (69 bends)</b>	<b>Isolated deep-ocean channels (20 bends)</b>	<b>Non-margin ocean channels (4 bends)</b>
<i>Width at height of the channel banks from the bend apex (cross-section 7) and the inflections (cross-sections 1, 13)</i>	14% (Eke <i>et al.</i> , 2014a)	34.61%	28.27%	12.61%
<i>Depth-averaged width from the channel bed to the height of the channel banks from the bend apex (cross-section 7) and the inflections (cross-sections 1, 13)</i>	x	28.42%	16.21%	4.53%
<i>Width at height of the channel banks from the apex region (cross-sections 4-10) and the inflection region (cross-sections 1-3, 11-13)</i>	x	10.19%	-1.09%	4.11%
<i>Depth-averaged width from the channel bed to the height of the channel banks from the apex region (cross-sections 4-10) and the inflection region (cross-sections 1-3, 11-13)</i>	x	8.57%	-3.00%	-2.14%

### *Variation between channel types*

Isolated deep-ocean channels have a rather constant channel width around bends rather than having a wider channel width at the bend apex compared to submarine fan channels. Channels in the Gulf of Alaska are tectonically controlled, which may suggest that channel width around bends are allogenicly controlled, which may suggest that an allogenic control has an influence on the width around bends and hence channel migration. By contrast, the channel from the Magdalena Fan is also tectonically controlled which is wider at apex region thus suggesting that tectonics is unlikely to be the cause. Additionally, Jobe *et al.* (2016) observed no difference in terms of a reduced channel migration in tectonic or no tectonic setting. Hence allogenic controls such as climate change or tectonic setting in terms of bend migration for different channel types can only explain a minor role.

Channel migration may be related to a change in flow regime or type of sediment load, which may promote a change of sinuosity (Posamentier and Kolla, 2003), but since no significant difference between apex-inflexion width ratio and sinuosity exist, this suggests that the type of sediment may not influence width variation around bends. Flow velocity and concentration may also influence the position of the deposition at either the outer and inner bank. Weak flows may deposit at the outer bank and may develop so called outer bank bars, whereas strong flow may deposit at the inner bank (Kane *et al.*, 2008; Straub *et al.*, 2008; Nakajima *et al.*, 2009), but such processes suggest a universal relationship for all submarine channel types which is not supported by the data.

Super-elevation is around two orders of magnitude greater in submarine channels compared to rivers (Dorrell *et al.*, 2013), and may vary between submarine channels and between channel types. Sandier deposits at the outer bank, forming spillover lobes and sediment waves, can occur due to strong overflows at the outer bank (Nakajima *et al.*, 1998; Wynn and Stow, 2002; Posamentier, 2003; Migeon *et al.*, 2004). These less cohesive sandier deposits may be easily erodible compared to outer bank deposits in rivers leading to a wider-apex point in submarine channels compared to sinuous point bar rivers. Asymmetry in exhumed levees has been reported (Kane and Hodgson, 2011), with outer bank external levees being thicker and having a higher

sand content. The erodibility of external levees would increase in systems prone to avulsion and progradation, such as submarine-fan channels (e.g. Morris *et al.*, 2014b; Picot *et al.*, 2016) and hence may explain variations between submarine channel types.

Dorrell *et al.* (2018) suggested that variations in the orientation of secondary flow cells and how rapidly these switch orientation may lead to variations in channel migration. Channel types are variable in terms of cross-sectional shape. Submarine-fan channels are rather V-shaped with a narrow channel bed and isolated deep-ocean channels are rather box-shaped with a wide channel bed (Carter, 1988, Chapter 3). For a given set of input conditions a trapezoidal channel shape with a narrow channel bed width favours outer-directed near-bed flows rather than a rectangular channel shape with a wider channel bed width (Ezz and Imran, 2014). Hence, submarine-fan channels may have an increased outer-directed near-bed flow compared to isolated deep-ocean channels, which favours bank pull and a wider width at the bend apex region due a greater outer-bank erosion. However, even so the orientation of the secondary flow is important and may contribute to small variation in channel width, channel width is ultimately controlled by the relative rates of erosion at the outer bank and deposition at the inner bank (Eke *et al.*, 2014a, b).

The variation between channel types may be related to the resistance of the channel banks for isolated deep-ocean channels compared to submarine-fan channels, similar to rivers. River with a constant width, which have been referred to canaliform channels are often related to a restricted bank erosion rate due to a resistance of the banks through vegetation or silt/clay or vegetation (Lagasse *et al.*, 2004; Luchi *et al.*, 2011, 2012; Matsubara and Howard, 2014). Isolated deep ocean channels are basement-controlled and form in the early stage of ocean basin formation (Carter, 1988), hence their form through solid bedrock rather than through sand or mud as submarine-fan channels. So, the channel width for isolated deep-ocean channels is limited through the restriction of the channel banks, similar to canaliform rivers. Even so the channel width is restricted through the banks, inner bend deposition with an oblique-accretion deposition at the inner bend can still occur for equiwidth channels (Brice, 1975; Page *et al.*, 2003). Additionally, a constant channel width for isolated deep-ocean channels may be related to a balance between low energy flows



and sedimentation (Nanson, 1980; Matsubara and Howard, 2014), whereby only enough erosion occurs at the outer bank which is balanced by suspended sediment transported onto the inner bend by secondary flow circulation (Nanson, 1980; Matsubara and Howard, 2014). Such observation, may be also important for isolated deep-ocean as an increase outer bank width compared inner bank width suggest that an reduced erosion and deposition. Even so, it sounds like that submarine channel types have contradicting flow and sedimentation processes around bends. Luchi *et al.* (2010, 2012) argues that constant and wider-at-apex width channels, hence different channel types are strongly related but vary in terms of their “hydrodynamic” width, and their “morphologically active” width. The “hydrodynamic” width coincides with the free surface width, whereas the “morphologically active” width is the part of the cross-section where transport occurs during formative flow conditions. In wider-at-bend apex bends, for example submarine-fan channels, the hydrodynamic is not equal to the morphologically active width. By contrast, in canaliform rivers, for example isolated deep-ocean channels, the hydrodynamic and active widths are the same as a high bank resistance in isolated deep-ocean channels through solid bedrock, prevents the formation of a “morphologically active” width at a high flow stage (Luchi *et al.*, 2010, 2012) and hence a further outer bank erosion.

## 5.6 Conclusions

This study analysed width variation around bends from different submarine-channel types. The importance of distinguishing submarine channels based on their environmental setting was highlighted in this study. Submarine channel experience a range of width variation similar to rivers. Submarine-fan channels are wider at bend apex, whereas isolated deep-ocean channels show a relative constant channel width and non-margin ocean channel are wider at inflection region. Submarine-fan channels are controlled by bank pull similar to the channels from the Axial Congo Fan. Isolated deep-ocean channels have a constant width around bends, which looks like a contradiction. However, the width of these channels are mainly controlled by a restriction of the channel banks through a bank resistance. Hence the erosion rate at the outer bank is reduced. Non-margin ocean channels may be also a restricted in

their channel width or channel width at straight section increases at straight section due to a higher slopes, hence a greater flow velocity. The observed diversity of width variation around bends for different channel types has immense implications for the study of submarine channels. as submarine-fan channels act like alluvial meandering rivers and isolated deep-ocean channels act like bedrock or canaliform alluvial rivers.




# Chapter 6 Discussion: Processes and morphology of submarine channels for different channel types, and implications for bend migration

---

## 6.1 Why is it important to distinguish submarine channels?

Deep-marine submarine channels have been classified (Wynn *et al.*, 2007) based on the environmental setting of the channel (Schweller and Kulm, 1977; Carter, 1988; Peakall and Sumner, 2015). These channel types were used as the basis for analysing the morphometrics of submarine channels in the present study. Several previous studies have examined aspects of the morphometrics of submarine channels (e.g. Konsoer *et al.*, 2013; Jobe *et al.*, 2016; Shumaker *et al.*, 2018; Lemay *et al.*, 2020; McArthur and Tek, 2021) but they have not assessed whether different environmental settings and types of submarine channels exhibit different morphometrics. Even so, these previous studies have identified a number of contradictions in terms of the morphometrics between channels (Peakall *et al.*, 2000a, b; Konsoer *et al.*, 2013; Jobe *et al.*, 2016; Pettinga *et al.*, 2018). The question of whether the morphometrics of submarine channels vary by environment and/or type is important, as if they do then it would also suggest that submarine channel types may differ for example in terms of sediment input, flow concentration, flow intensity, development and formation. Submarine channels can be classified into six main types: submarine-fan, isolated deep-ocean, slope, axial, non-margin ocean and confined slope channels (Peakall and Sumner, 2015). The principal morphometric characteristics of the three main studied submarine types (submarine-fan, isolated deep-ocean and axial channels) are summarised in Table 6.1. The morphometric analysis distinguished different properties for each of the three main studied submarine types. Hence, the results of this analysis show that distinguishing between submarine channels is possible based on the morphometrics and environmental setting, and consequently that it is important to consider the type of submarine channel (Mutti and Normark, 1987; Clark and Pickering, 1996a; Lemay *et al.*, 2020).

**Table 6.1** Characteristics of the main studied channel types and their comparison to rivers.

Type	Rivers	Submarine-fan channels	Isolated deep-ocean channels	Axial channels
<b>Definition</b>		- on submarine fans -may develop a complex channel network	- basement controlled - develop in early stage of basin formation	- along axial trenches - parallel to the continental margin
<b>Width (m)</b>	0.5-4800 (mean 275)	161-12195 (mean 2054)	349-51715 (mean 14710)	4196-8259 (mean 6050)
<b>Depth (m)</b>	0.2-47 (mean 5)	10-558 (mean 75)	2-569 (mean 154)	32-197 (mean 82)
<b>Aspect ratio</b>	0.2-2191 (mean 64)	5-193 (mean 33)	6-1059 (mean 117)	34-221 (mean 90)
<b>Channel bed</b>		narrow	wide	wide
<b>Cross-sectional shape (typically)</b>		"V" shape 	convex-upward shape 	Parabolic shape 
<b>Cross-sectional area</b>		on average <0.2 km <sup>2</sup>	on average <1 km <sup>2</sup>	on average between 0.2-1 km <sup>2</sup>

## 6.2 Comparison of the morphometrics between submarine channels and rivers

Both rivers and submarine channels have the main range in aspect ratios between 10:1 and 100:1 with submarine channels typically being wider and deeper than rivers (Figure 6.1). Some of the smaller submarine-fan channels can exhibit similar depths and widths as the largest rivers, whilst in contrast axial channels can be an order of magnitude wider and slightly deeper. Isolated deep-ocean channels are most distinctive relative to rivers, being on average an order of magnitude wider and deeper than the largest rivers (Figure 6.1, Table 6.2). This contrast between different

submarine channel types can explain the contradictions between previous studies (Peakall *et al.*, 2000a, b; Konsoer *et al.*, 2013; Jobe *et al.*, 2016; Pettinga *et al.*, 2018). Direct comparison of the mean width and depth between submarine channels and rivers suggest that submarine channel width is at least 5-times and channel depth at least 10-times greater than rivers.

Width and depth between different submarine channels were also compared in the downstream distance away from the canyon head. Channel width of isolated deep-ocean channels is wider than for submarine fan channels (Figure 6.2), but channel depth is more variable between channel types (Figure 6.3).

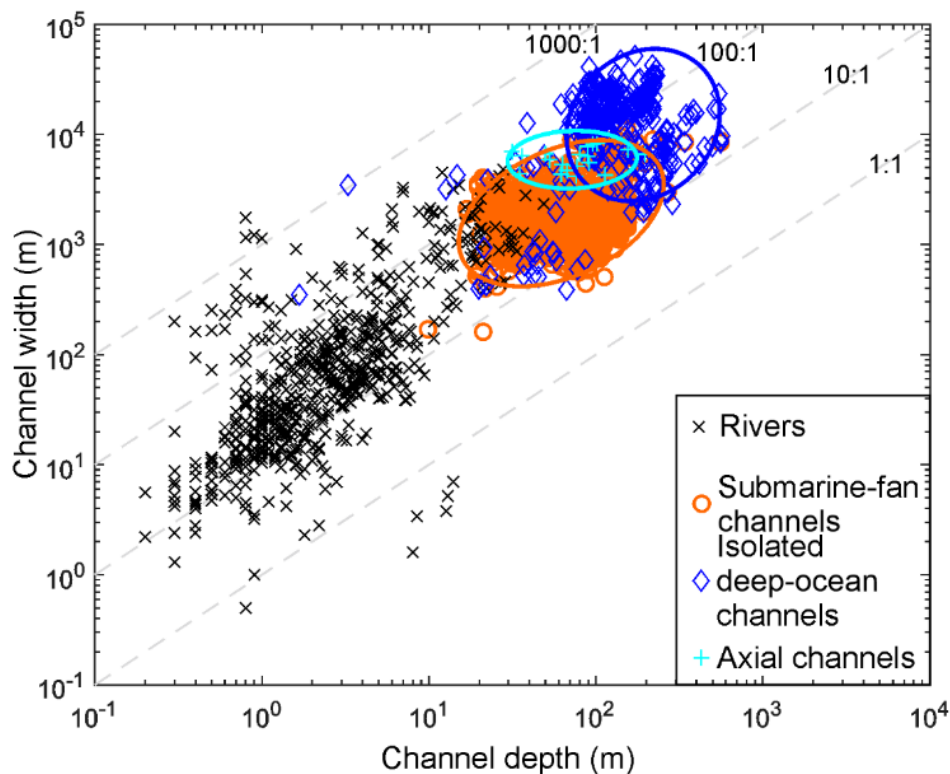
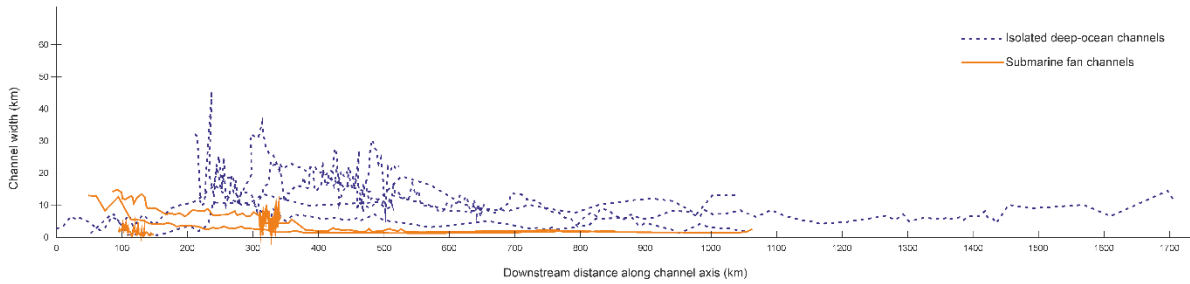


**Figure 6.1** Aspect ratios of different submarine channel types and rivers. Both river and submarine channel widths and depths range between 10:1 and 100:1. Data are composed for rivers (Leeder, 1973; Van den Berg, 1995; Jerolmack and Mohrig, 2007; Whittaker, 2007; Wohl and David, 2008; Yanites *et al.*, 2010; Wilkerson and Parker, 2011) submarine-fan channels (literature-based and studied), isolated deep-ocean channels (literature-based and studied) and axial channels (literature-based).

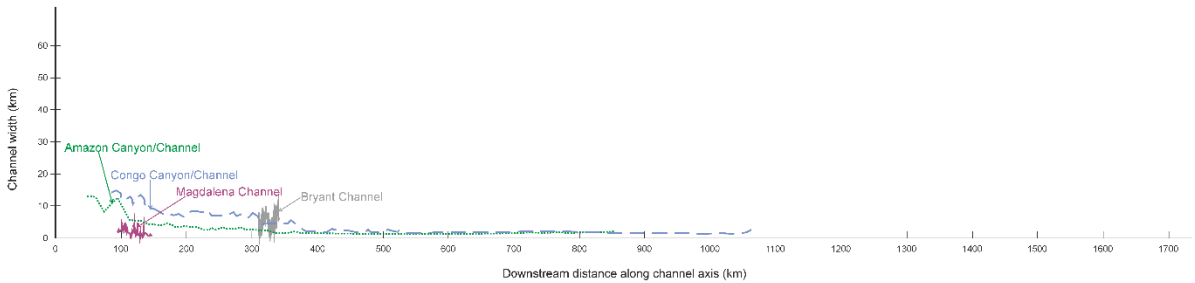
**Table 6.2** Comparison of width, depth and aspect ratio between rivers, submarine fan, isolated deep-ocean and axial channels.

	Width (W) in m				Depth (D) in m				Aspect ratio (W/D)			
	River	Submarine-fan	Isolated deep-ocean	Axial	River	Submarine-fan	Isolated deep-ocean	Axial	River	Submarine-fan	Isolated deep-ocean	Axial
<b>Min</b>	0.5	161	349	4,196	0.2	10	2	32	0.2	5	6	34
<b>Max</b>	4,800	12,195	51,715	8,259	47	558	569	197	2191	193	1,059	221
<b>Mean</b>	275	2,054	14,710	6,050	5	75	154	82	64	33	117	90
<b>Standard deviation</b>	602	1,286	9,005	1,327	6	41	88	41	150	21	91	47
<b>Median</b>	61	1,81	14,516	6,295	2	64	131	77	25	26	112	81

**A)** Channel width for submarine channels



**B)** Channel width for submarine-fan channels



**C)** Channel width for isolated deep-ocean channels

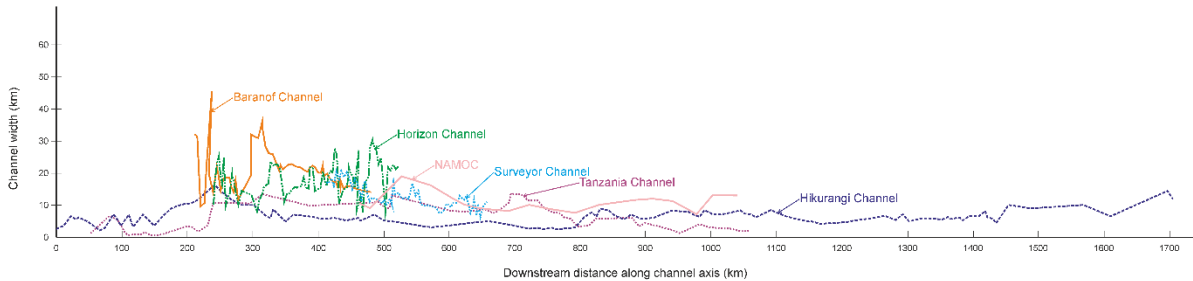


**Figure 6.2** Comparison of channel width between A) submarine fan and isolated deep-ocean channels, B) different submarine fan channels, and C) different isolated deep-ocean channels in the downstream direction. Data are from this study: Bryant, Magdalena, Surveyor, Horizon and Baranof Channel; and from the

literature: NAMOC (Hesse *et al.*, 1987), Hikurangi Channel (Lewis, 1994), Tanzania Channel (Bourget *et al.*, 2008), Amazon Channel (Pirmez and Flood, 1995) and Congo Channel (Babonneau *et al.*, 2002). Distance is based on downstream distance away from the canyon head.

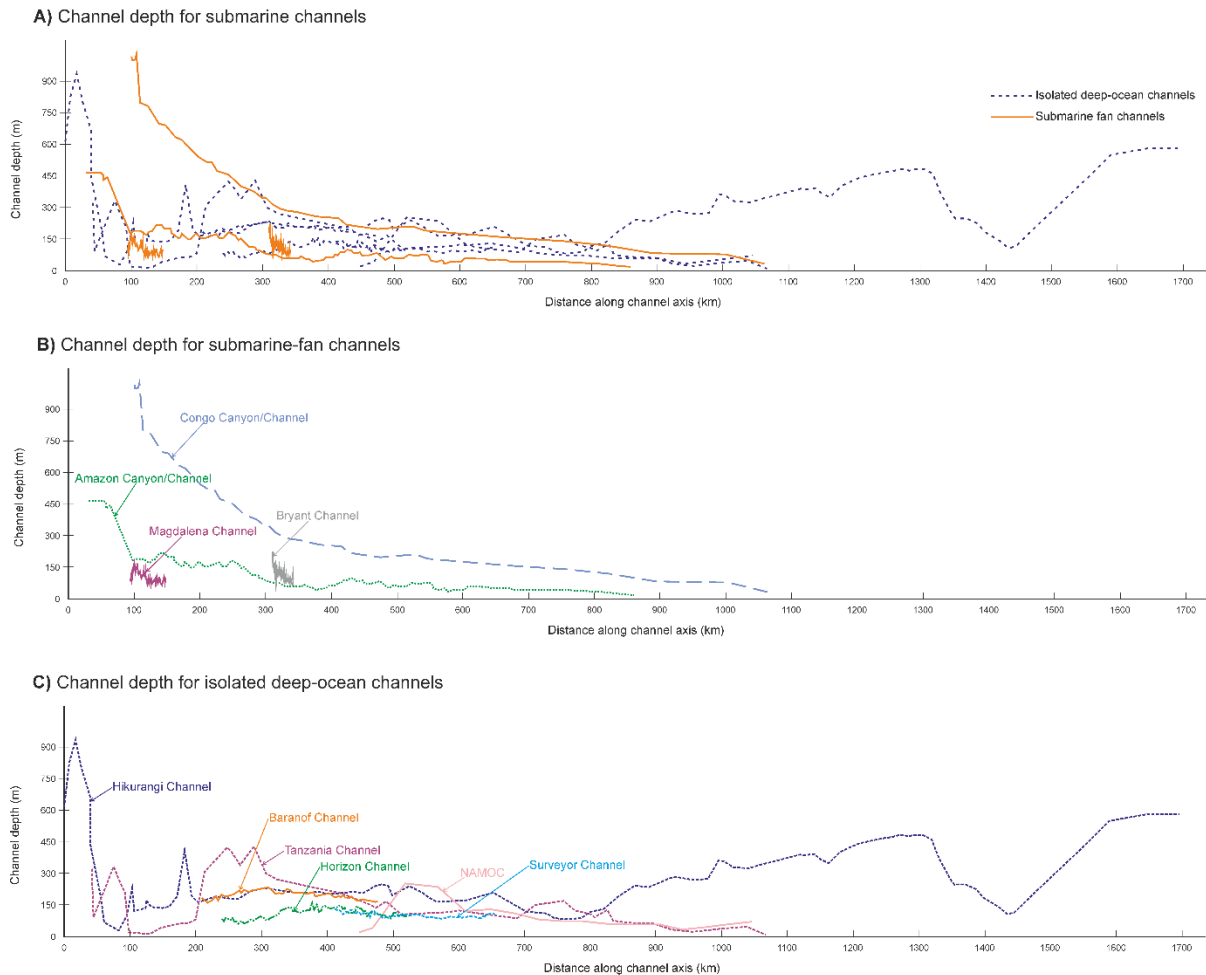


**Figure 6.3** Comparison of channel depth between A) submarine fan and isolated deep-ocean channels, B) different submarine fan channels, and C) different isolated deep-ocean channels in the downstream direction. Data are from this study: Bryant, Magdalena, Surveyor, Horizon and Baranof Channel; and from the literature: NAMOC (Hesse *et al.*, 1987), Hikurangi Channel (Lewis, 1994), Tanzania Channel (Bourget *et al.*, 2008), Amazon Channel (Pirmez and Flood, 1995) and Congo Channel (Babonneau *et al.*, 2002). Distance is based on downstream distance away from the canyon head.

### 6.3 Behaviour of the downstream (primary) directed flow in submarine channels

Flows in submarine channels are fundamentally different compared to flows in rivers. Firstly, the flows in submarine channels are gravity-driven controlled and the main component of the flow is a mixture between water and sediment, rather than mainly water as in rivers (Middleton and Hampton, 1973; Lowe, 1979; Mulder and Alexander, 2001). Secondly, the gravitational driving force between the flow and surrounding fluid is orders of magnitude less in submarine channels than in rivers because the ambient fluid is seawater or freshwater, not air as in rivers (Kneller and Buckee, 2000; Meiburg and Kneller, 2010). These configurations lead to different flow properties in submarine channels and rivers. The maximum downstream flow velocity in the vertical is located near the base of flows in submarine channels rather than near the top of the flow in rivers (Figure 6.4; Hampton, 1972; Kneller and Buckee, 2000; Felix, 2002; Meiburg and Kneller, 2010). Additionally, the density profile is in general relatively constant in rivers as the main component in a river is water, but in submarine channels the density stratification is much greater, with prominent variation from a maximum near the bed, reducing towards the top of the flow (Figure 6.4; Kuenen, 1966; Mulder and Alexander, 2001; Talling *et al.*, 2012; Hansen *et al.*, 2015; Peakall and Sumner, 2015; Azpiroz-Zabala *et al.*, 2017a). Such variations in the flow properties will lead to process differences compared to rivers. For example, since the density stratification is not a clear boundary as in rivers, estimating flow depth is very hard as large-scale, slowly moving, overspill of the banks is common. Hence, the actual height from the channel bed to the maximum height of the channel banks may be an over- or underestimation of the actual flow depth (Figure 6.5).



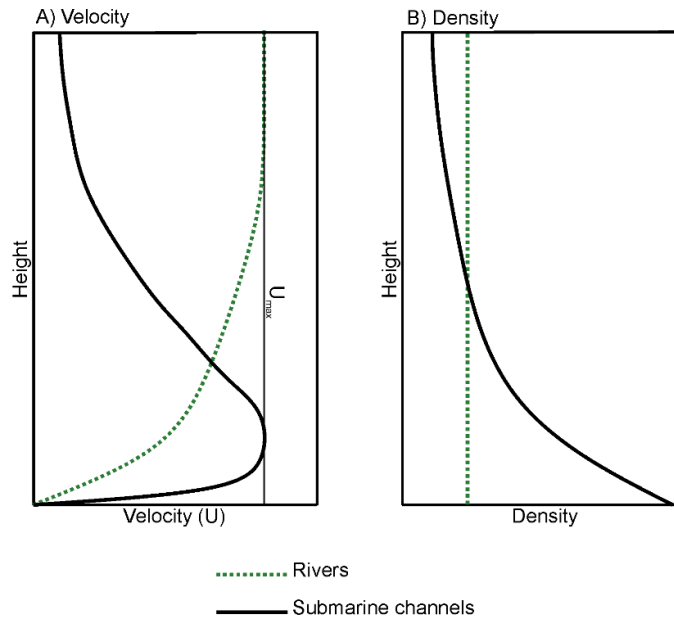


**Figure 6.4** Generalised profiles of A) velocity and B) density for rivers (green dashed line) and submarine channels (black solid line). Maximum velocity ( $U_{max}$ ) in rivers is at the top of the flow and in submarine channels is near the bottom of the flow. Density is relative constant throughout the flow in rivers (shown here schematically, albeit actual profiles will be a function of the Rouse number, related to the sediment grain-size within the flow) but varies to a greater degree in submarine channels with the maximum density close to the bottom. Height of flow in rivers is from the channel bed to the air/water surface (maximum tens of metres for large rivers and a few metres for most rivers). Height of flow for submarine channels is harder to define as it is from the channel bed to the height of the dilute sedimentation/ambient water position (probably a few tens of metres to hundreds of metres depending on the flow). Flow height for submarine channels is usual defined between the channel bed and the banks of the channel.

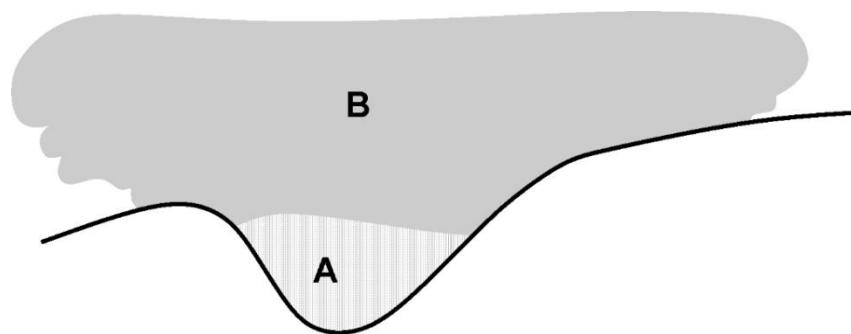


**Figure 6.5** Thickness of turbidity flow changes the type of erosion and deposition. Type A thickness of flow is lower than the channel banks, hence no levee formation. Type B: thickness of flow is higher than the channel banks, hence levee formation. Adapted from Piper and Normark (1983).

## 6.4 Hydraulic power-law scaling relationships

Hydraulic power-law scaling relationships between width, depth, velocity and discharge have been identified for both rivers and submarine channels (Leopold and Maddock, 1953; Pirmez and Imran, 2003; Wohl and David, 2008; Konsoer *et al.*, 2013). Both rivers and submarine channels have similar trends in scaling relationships with increasing hydraulic properties with proportionally increasing discharge (Leopold and Maddock, 1953; Konsoer *et al.*, 2013). This hydraulic power-law scaling relationship is shown with downstream distance in rivers as hydraulic properties (width, depth and velocity) of rivers increase as power-law functions with increasing discharge downstream (Leopold and Maddock, 1953; Wohl and David, 2008). In contrast, submarine channels have been observed to decrease hydraulic properties (width, depth and velocity) with decreasing discharge downstream due to continuous overspill and sediment loss downstream (Babonneau *et al.*, 2002; Pirmez and Imran, 2003; Shumaker *et al.*, 2018). However, there may be exceptions to this relationship in some isolated deep-ocean channels such as the Hikurangi where tectonics controls depth (Figure 6.2 and Figure 6.3). Whilst these trends in hydraulic relationships between rivers and submarine channels are the same with respect to changes in discharge, the absolute scaling relationships are different. The orders of magnitude less driving force in submarine channels, due to the much smaller density difference, means that for a given slope, submarine channels require a much greater cross-sectional area (Figure 6.1; Konsoer *et al.*, 2013).

## 6.5 Influence of the flow on the morphometrics of channels

A detailed analysis of the cross-section characteristics may give an overview of the mechanisms of the flow forming these cross-sections. Submarine-fan channels and slope channels have in general aspect ratios similar to rivers, and a “V”-shaped cross-section with a narrow channel bed. On the other hand,

isolated deep-ocean and axial channels have in general aspect ratios greater than rivers and a “U”-shaped cross-section with a flat channel base (Chapter 3). The cross-sectional shape may be a relic of the flow passing through the channel and the different cross-sectional morphology for the various submarine channel types may suggest different dominant flow mechanisms for the various channel types.

A classification based on the erosional or aggradational characteristics in the cross-section suggested a “U”-shaped profile for depositional and a “V”-shaped profile for an erosional submarine channel, similar to rivers (Mutti and Normark, 1987; Clark and Pickering, 1996b). Consequently, this would suggest a “U”-shaped profile for submarine-fan channels and a “V”-shaped profile for isolated deep-ocean channels, in sharp contrast to the observations. However, isolated deep-ocean channels are long-lived and are often associated with tectonic features. In such cases, a “U”-shaped profile for isolated deep-ocean channels may be created, as the channel base may be cut into bedrock (Carter, 1988), hence it is easier to erode laterally than vertically resulting in the channel widening and hence creating a flat channel base. On the other hand, some submarine fan channels are incisional at their bases in which case a “V”-shaped profile is created (Babonneau *et al.*, 2002; Savoye *et al.*, 2009).

The shape of the profile can also be used in rivers as an identification for the dominant sediment material passing through the channel. In rivers, a wide shallow channel is associated with high bed-load transport, hence a narrow deep channel is associated with a high suspended sediment transport (Schumm, 1963). It is not clear how well such fluvial derived theory can be applied to submarine channels, where turbidity current flows are all primarily suspension driven. However, if this theory was applicable then it would suggest that given isolated deep-ocean channels have a relatively wider basal width due to a “U”-shaped profile, they would exhibit a greater bedload transport. On the other hand, submarine-fan channels have a relative narrow channel width, hence assuming the applicability of this theory to submarine channels, then high suspended sediment transport is predicted.

## 6.6 Equilibrium channel morphometrics

The data suggest that key distinguishing criteria between submarine-fan and isolated deep-ocean channels are channel width and aspect ratio (Table 6.2, Figure 6.2), with much greater similarity in terms of channel depth (Table 6.2, Figure 6.3). The mean channel width and mean aspect ratio are 7-times greater for isolated-deep ocean channels than for submarine-fan channels, but the mean channel depth is only 2-times greater for isolated deep-ocean channels than for submarine-fan channels. Additionally, the actual depth range is very similar for submarine-fan (depth=10-558 m) and isolated deep-ocean channels (depth=2-569 m), but the actual range is very distinctive for channel width (submarine fan channel: 161-12,195 m, isolated deep-ocean channels: 349-51,715 m).

The observations that submarine channel types are distinguishable through aspect ratio and/or channel width, rather than channel depth, supports the early suggestion of Shumaker *et al.* (2018), who mainly analysed submarine-fan channels, and Konsoer *et al.* (2013), that submarine channels adjust their channel depth to a variable flow discharge rather than their channel width, the opposite of rivers (Leopold and Maddock, 1953). Since channel width and aspect ratio are very distinguishable between submarine channel types, it may suggest that channel width and aspect ratio have an environmental control, hence an allogenic control. By contrast, channel depth being more similar between channel types may suggest an autogenic control. Shumaker *et al.* (2018) also suggested that channel width is earlier established than channel depth and speculate that possible control mechanisms for channel width may include the amount of sediment supply, or grain size, and that channel depth is set by levee growth and/or bank erosion. However, Shumaker *et al.* (2018) did not consider these relationships in the light of channel types. Each channel type occurs in a specific environmental setting. As each environmental setting is different, each setting may limit the width. Submarine-fan channels may take a long time until the flow is in equilibrium with the channel form. Once the flow is in equilibrium, estimated as tens to almost 100 km longitudinal distance in some modelling studies

(Traer *et al.*, 2018a, b), the width is established maybe due to a constant grain size supply, and small flow adjustments are achieved by adjusting the channel depth either through bank aggradation and/or bed aggradation/erosion. In contrast, isolated deep-ocean channels develop in the early stages of basin formation and even though they form through poorly consolidated sediment (Carter, 1988), they are restricted by the solid bedrock surrounding the poorly consolidated sediment. Once the channel reaches the bedrock in the early stage of channel formation, the width may be restricted (Figure 6.6) and flow adjustment is achieved through bed aggradation and bank aggradation/erosion.

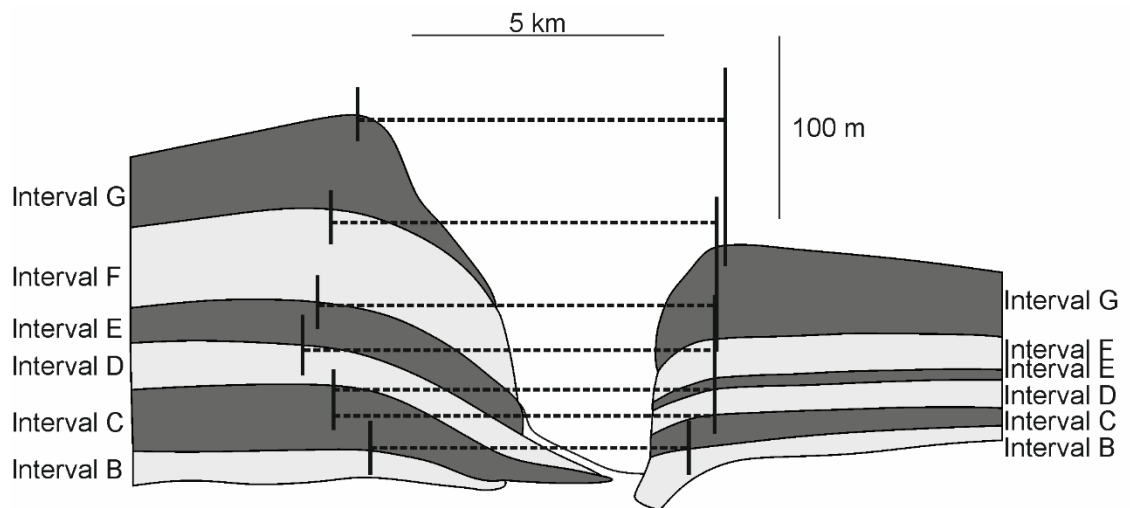


**Figure 6.6** Channel width is established earlier than channel depth. Channel width is relative constant between Interval B and G, but channel depth increases between Interval B and G. Example is from the NAMOC (Adapted from Klauke *et al.*, 1998b).

An equilibrium profile of a submarine channel is, as in rivers, a theoretical profile path along the slope to the lowest point, which adjusts its flow condition to the slope in a way that no net aggradation or erosion occur (Pirmez *et al.*, 2000; Kneller, 2003). The lowest point is often called base level. For submarine channels this local base level is the lowest point to which a turbidity flow can flow whilst remaining confined, that is the channel mouth, where the flow becomes unconfined, which is often at channel-lobe-transition zones. Two end members can be seen if only changing the flow conditions, but

without changing the base level: aggradational and erosional channels. Aggradational channels develop by steepening the gradient through flow density or thickness decrease, or grain size increase. Erosional channels develop by flattening the gradient through flow density or thickness increase, or grain size decrease (Kneller, 2003). Many channels show a variation between these two end members, suggesting that flow properties changed over time. A key question is if any of the identified characteristics can be applied to channels with different environmental settings. Both submarine-fan and isolated deep-ocean channels are controlled by aggradation of the channel bank or bed. An erosional flow may be adjusted for submarine-fan channels by incision (Kneller, 2003), but for isolated deep-ocean channels if there is significant bedrock strength then this may be by channel widening (Figure 6.7).

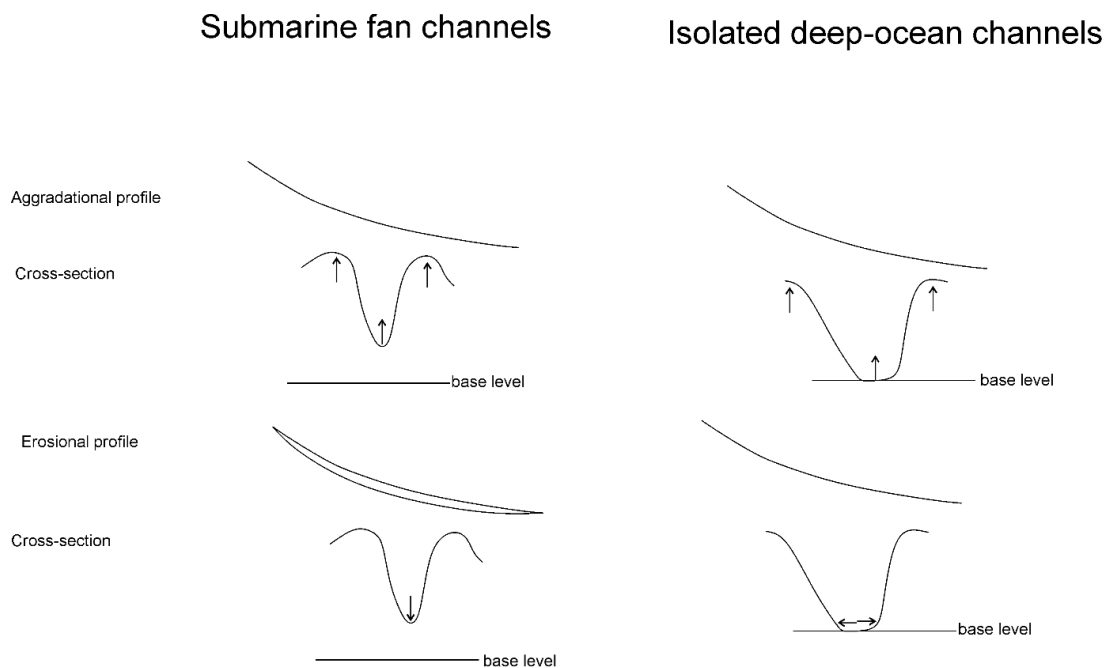


**Figure 6.7** Variations of cross-sections for an aggradational and erosional flow for submarine fan and isolated deep-ocean channels. Arrows indicate the locations where aggradation, erosion or lateral widening occur. Modified from Kneller (2003).

## 6.7 Evolution of channel types

This study has shown that morphometric differences exist between channel types, but as a first order approximation it might be expected that flows within these different submarine channel types are relatively similar. So, is each submarine channel type unique and distinguishable from each other or can they be related to each other in an evolutionary sense?

The channels from the Gulf of Alaska were classified as isolated deep-ocean channels; even so these channels are situated on two submarine-fans (Surveyor and Baranof Fan; Reece *et al.*, 2011; Walton *et al.*, 2014). The Surveyor Channel has a direct connection to the Aleutian Trench, but as it is situated on a submarine fan it may suggest that the channel was originally a submarine fan channel. This would suggest that the Surveyor Channel has been transformed from a submarine-fan channel to an isolated deep ocean channel. How did the transformation occur?

McArthur and Tek (2021) analysed submarine channels connected to axial trenches. Many axial trenches do not contain submarine channels (~64% or 21 trenches out of 33 trenches studied; McArthur and Tek, 2021) and only a few axial channels are known (~22% or 9 axial channels found in 33 trenches; McArthur and Tek, 2021) which follow the path of the axial trench for most its channel length. The observation, that a submarine channel escapes an axial trench is seldom made (Chile, Cascadia, Vidal; 3 escaped channels out of 33 trenches; McArthur and Tek, 2021). However, these channels are not true axial channels as they would be classified herein as isolated deep-ocean channels. The reasons for these three types of interaction between axial trenches and channels are related to the type of trench, sediment supply and subduction rate (McArthur and Tek, 2021). For a true axial channel, where the channel follows the axial trench a medium sediment supply and/or smooth trench and/or medium subduction rate may be needed. The conditions for isolated deep-ocean channels to form may be similar for axial channels. Sediment supply rate is key, it must be enough given that the channel can develop for up to hundreds to kilometres. However, the

sediment supply rate must not be so high that it overwhelms the local morphology and starts to build a sedimentary fan. Despite the sediment supply rate, the path to the base level must exist for isolated-deep ocean channels. Some isolated deep-ocean channels manage to travel to the deepest parts of the ocean, however in contrast some isolated-deep ocean channels are relatively short (e.g. Valencia). Here, 2 submarine fans are connected by a submarine channel. In these conditions, the sediment supply rate can be low, but a downstream gradient between the submarine fan with low rugosity and hence a free channel path is needed, in order that an isolated deep-ocean channel can develop. In summary the key components for an isolated deep-ocean channel to occur are channel bed gradient, sediment supply and a free channel pathway.

## **6.8 Processes around bends**

### **6.8.1 Why is it important to study the width around bends?**

The width around bends in rivers is controlled by the deposition at the inner bend (bar push) and the erosion at the outer bank (bank pull; Nanson and Hickin, 1983; Braudrick *et al.*, 2009; Parker *et al.*, 2011; Eke *et al.*, 2014a, b; Matsubara and Howard, 2014; Van de Lageweg *et al.*, 2014; Wu *et al.*, 2016). Understanding the relative magnitude of width variation around bends, helps to predict the processes of bank control and ultimately bend migration. Quantitative analysis of submarine channels bends (Clark *et al.*, 1992; Pirmez and Imran, 2003; Lemay *et al.*, 2020) and the intra-channel deposition and erosion around bends have been studied (Babonneau *et al.*, 2004, 2010; Nakajima *et al.*, 2009; Peakall and Sumner, 2015). However, a detailed analysis of the variation of the morphology around bends has focused so far on the cross-sectional asymmetry around bends (Reimchen *et al.*, 2016). Cross-sectional asymmetry in submarine channels bends increases with curvature (Reimchen *et al.*, 2016), similar to rivers (Knighton, 1981, 1982), suggesting a connection between flow processes and hence morphology.



Because the width variation around bends in submarine channel bends has previously been unknown, the processes of erosion and deposition around bends and hence bend migration have appeared to be contradictory. Laboratory experiments and numerical modelling have used constant width channels, for simplicity, and because the width variations around submarine bends have been unknown. Such models have predicted a dominantly downstream channel bend migration, but submarine channels on passive margins typically exhibit a lateral expansion rather than a continuous downstream bend migration as has been observed for rivers (Peakall *et al.*, 2000a, b; Reimchen *et al.*, 2016). Hence analysing the width variation around bends, would be powerful tool to understand the positions of erosion and deposition around bends.

### **6.8.2 Summary of width variation around bends for different channel types**

#### *Summary of width variation around bends for submarine fan channels*

All width measurements (depth-averaged and bank-top channel width) for submarine fan channels between points (apex and inflection points) and regions (apex and inflection region) provide a similar result with bend apices being wider than bend inflections (Figure 6.8). The degree of the width variation varied between 1% and 120% depending on the width measurement and the channel reach. The difference between points and regions was greater than the difference of the different width measurement for all studied submarine fans. The width measurement was between 2 to 5 times wider when measured between points than measured between regions for all submarine channel reaches (2 times greater for Congo Ax02; 3 times greater for Congo Ax12, Bryant Channel and Amazon lower fan; 4 times greater for Congo Ax14 and Congo Ax02; and 5 times greater for Amazon upper fan). This could suggest that maximum channel width is closer to the bend apex, and that measuring width around regions may smooth out variations. By

contrast, just focussing on the apex and the inflections may be biased towards the apex as submarine channels bends have a terrace-like inner bend structure, not only due to deposition but also due to margin failure or entrenchments (Hansen *et al.*, 2015).

The different submarine fan channels range in the degree they are wider at apices in contrast to bend inflections. The two tectonic-influenced submarine fan channels, Bryant (Bryant *et al.*, 1990) and Magdalena Fan Channel (Romero-Otero *et al.*, 2015; Idárraga-García *et al.*, 2019) have the greatest difference between bend apex and bend inflections with a wider apex point between 32% and 26% for the Magdalena Channel (6% and 7% wider at the apex region) and 85% and 112% for the Bryant Channel (31% and 45% wider at the apex region). All other submarine fan channels have a width variation less than 25% between apex and inflection points with similar results between bank-top and depth-averaged channel width for all channels, except for the Congo Ax14 (22% and 23% for Congo Ax02, 13% and 15% for Amazon Mid Fan, 7% and 13% for Congo Ax14, 8% and 9% for Congo Ax52 and 9% for Amazon Lower Fan). The variation between apex and inflection regions for the other submarine-fan channels was also less than 25% with similar results between bank-top and depth-averaged channel width for all channels (9% and 11% for Congo Ax02, 3% for Amazon Mid Fan, 3% and 4% for Amazon Lower Fan, 1% and 4% for Congo Ax14 and 1% and 3% for Congo Ax52).

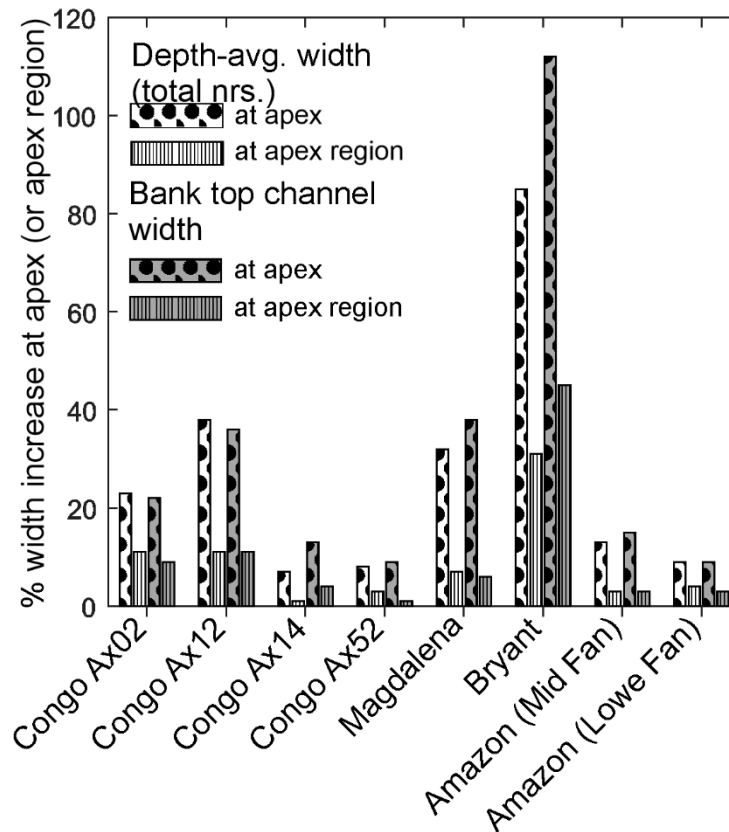


**Figure 6.8** Bar chart showing the percentage width increase at apices compared to bend inflections (symbol: dots), or at apex compared to inflections regions (symbol: vertical lines) at different width measurements (depth-avg. width (symbol: white box) or bank-top channel width (symbol: grey box)) for all studied submarine-fan channels.

*Summary of width variation around bends for isolated deep-ocean channels in the Gulf of Alaska*

The width measurements (depth-averaged and bank-top channel width) for isolated deep-ocean channels (Gulf of Alaska) between points (apex and inflection points) and regions (apex and inflection region) identified two different cases: 1) the Surveyor Channel is narrower at the bend apex point than at the inflection points and 2) the Horizon and the Baranof Channel are wider at the apex point than at the inflection points (Figure 6.9). The variation between points and regions was in general greater than the difference of the different width measurements, with the majority of width measurements being wider at the apex than at the inflection points. In contrast, the majority of width measurements were wider at the inflection than at the apex regions. This could suggest that maximum channel width is closer to the bend apex for the majority of isolated deep-ocean channels and that measuring width around regions may smooth out variations, but the contradictory results for regions that channel width is widest near the inflections suggest that width is only wider close to the apex. The width variation between apex and inflection points is at least 3-times greater for the Horizon Channel than for Baranof Channel with a wider depth-averaged and bank-top channel width between 12% and 72% wider at the apex points than at the inflection points. The Surveyor Channel is between 2% and 11% wider at the inflection points and regions than at the apex points and regions, irrespective of the choice of width measurement, except for the bank top channel width at the apex region (2% wider apex region).

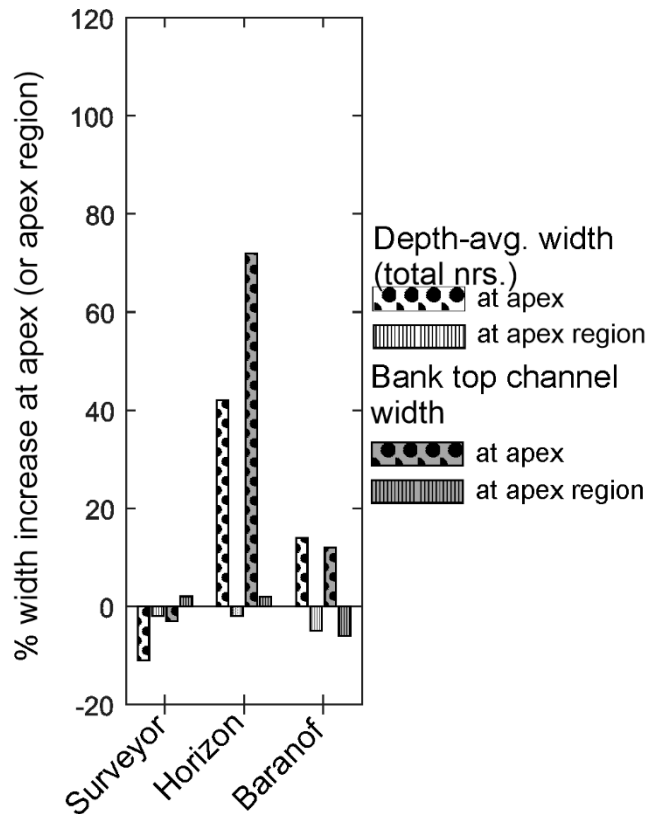


**Figure 6.9** Bar chart showing the percentage width increase at apices compared to bend inflections (symbol: dots), or at apex compared to inflections regions (symbol: vertical lines) at different width measurements (depth-avg. width (symbol: white box) or bank-top channel width (symbol: grey box)) for isolated deep-ocean channels in the Gulf of Alaska.

*Comparison of width variation around bends between submarine fan channel and isolated deep-ocean channels*

Submarine fan channels are wider at bend apices than bend inflections irrespective of the choice of width measurements (depth-averaged and bank-top channel width) between points (apex and inflection points) and regions (apex and inflection regions). By contrast, isolated deep-ocean channels are typically wider at bend apex than bend inflection points and narrower at apex regions than inflection regions irrespective of the choice of width measurements (depth-averaged and bank-top channel width).

Submarine-fan channels are 2-times wider at the apex point than isolated deep-ocean channels if using the depth-averaged channel width but

are similar in width if using the bank-top channel width. This implies that maximum channel width is close to the bank-top channel width in isolated-deep ocean channels and that the depth-averaged channel width and the width measurement around regions may smooth out the variation of a wider bank-top channel width at apex points for isolated deep-ocean channels. However, just looking at the bank-top channel width for submarine channels would be oversimplified since submarine channels have their maximum channel velocity and sediment concentration near the bottom (Hampton, 1972; Kneller and Buckee, 2000; Meiburg and Kneller, 2010; Talling *et al.*, 2012; Hansen *et al.*, 2015; Peakall and Sumner, 2015; Azpiroz-Zabala *et al.*, 2017a).

#### *Comparison of submarine channel bends to river bends*

The simplest way to compare submarine channels to rivers is to look at the percentage of bends being wider at the apex point/region (Table 6.3). Slightly more bends are wider at the apex point/region for submarine fan channels (69%-75%) and slightly less bends are wider for isolated deep-ocean channels (46%-55%) than sinuous point-bar rivers (60% of bends wider at the apex point, type C of the Brice (1975) classification; Lagasse *et al.*, 2004; Eke *et al.*, 2014a). The summary of submarine-fan and isolated deep-ocean channels shows that submarine channels (60-63%) have on average the same number of bends being wider at the apex point/region than rivers (60%). The differences between bends being wider at the depth-averaged or the bank-top channel width and region or points was small for each channel type (maximum 6%). The differences between each category were smoothed out for both submarine-fan and isolated deep-ocean channels as variations were often between individual channels. Such individual variations between channels may be true also for rivers. It must be noted that here only comparison is made to the type C of the Brice (1975) classification (sinuous point-bar rivers), which are rivers with the maximum migration rate (Lagasse

*et al.*, 2004). Other types of the classification, such as constant-width river channels have not been used as a comparison.

**Table 6.3** Percentage of bends being wider

Width	Depth-averaged width		Bank-top channel width	
	Apex point	Apex region	Apex point	Apex region
<i>Rivers</i>			60	
<i>Submarine-fan</i>	73	75	72	69
<i>Isolate deep-ocean</i>	49	46	55	51
<i>Submarine channels</i>	61	61	63	60

Another way to compare submarine channel bends to river bends is to look at the percentage of average width that bends are wider at the apex point/region relative to inflection points/regions (Table 6.4). A direct comparison is made at the bank-top channel width (mean width at the channel banks) between apex point and inflection points, which is equivalent to bankfull level in rivers (Clark *et al.*, 1992; Pirmez and Imran, 2003; Konsoer *et al.*, 2013). Here, submarine channels, both submarine-fan and isolated deep-ocean channels (27% and 32% wider bank-top channel width at the apex point), have an average increase in width that is approximately twice that of sinuous point-bar rivers (14% wider width at the apex point, Eke *et al.* (2014a). This two-times greater bank-top channel width variation at the apex point for submarine channels may potentially be explained by an average two-orders of magnitude greater super-elevation in submarine channels compared to rivers (Dorrell *et al.*, 2013), but this may vary between submarine channel types. Such super-elevation reflects the reduced gravity in these submarine channel systems which enables much deeper channels, and in turn deeper and wider channels. The measurement at the bank-top channel width may be an overestimation, relative to the overall cross-section, for submarine channels as they have lower gradient banks than rivers (rather V-shaped cross-sections; Islam *et al.*,

2008), but this is only true for submarine-fan channels in contrast to isolated deep-ocean channels (rather U-shaped cross-sections). The depth-averaged width increase at the apex point is also two-times greater compared to rivers for submarine-fan channels, but is similar to rivers for isolated deep-ocean channels. This variation between bank top width differences between bend apices and inflections, and depth-averaged ones, between different submarine channel types suggests variations in geomorphological processes. These geomorphological differences between channel types may suggest that super-elevation in submarine channels may be different between types and that super-elevation for isolated deep-ocean channels may preferentially erode the bank-top channel.

Analysis of the apex and inflection points rather than the regions may lead to ambiguity for both rivers and submarine channels, but especially for rivers as the maximum migration rate is not happening at the bend apex point but further downstream (Ikeda *et al.*, 1981; Sylvester *et al.*, 2019), hence a comparison between regions might be a better approach as it also acts to smooth out outliers at the points. Unfortunately, these data are not available for rivers. The data for submarine channels varied between channel types: submarine-fan channels are on average 10% wider (both depth-averaged and bank-top channel width) at the apex region and isolated deep-ocean channels are slightly narrower (both depth-averaged and bank-top channel width) at the apex region. In summary, these data indicate that the enhanced width variations in isolated deep-ocean channels are comparatively tightly focused at bend apices, and are more pronounced at bank-tops, in contrast to submarine fan channels which have broader enhanced width variations, that are consistent with height. Furthermore, these increases in width at bend apices in isolated deep-ocean channels are only seen in around 50% of bends.



**Table 6.4** Percentage of average width that bend apices are wider than inflections.

Width	Depth-averaged width		Bank-top channel width	
	Apex point	Apex region	Apex point	Apex region
<i>Rivers</i>			14	
<i>Submarine-fan</i>	27	9	32	10
<i>Isolate deep-ocean</i>	15	-3	27	-1
<i>Submarine channels</i>	21	3	29	5

### 6.8.3 Bend evolution

A key question in the studies of bend evolution is how bends initiate, whereby two diverse theories exist: bar theory (Gorycki, 1973) and bend theory (Ikeda *et al.*, 1981). Even so, flow and sedimentation processes are interrelated, both theories argue that one controls the other. Bend theory argues that bend evolution is initiated through natural variations within the flow, hence the flow controls bend evolution which alters the sedimentation. By contrast, bar theory argues that altering deposition along the bank, hence a variation of the sedimentation, causes a variation of the flow. Both theories have their limitations (see Section 2.3) as bend evolution is a dynamic process with an interaction of flow instability, sedimentation and bank processes. Additionally, many factors, such as channel width, curvature, bed topography, cross-sectional shape, secondary flow circulation due to the curvature, density stratification, and the Coriolis Force may all influence the initiation and processes of bend evolution (Parker *et al.*, 1982; Luchi *et al.*, 2011; Cossu and Wells, 2013; Dorrell *et al.*, 2013; Ezz and Imran, 2014; Palm *et al.*, 2021). Some of the aspects of bend and bar theory can be applied to understand the evolution of submarine channel bends. An argument for bend theory is the alteration of the flow, which alters the secondary flow and then alters the sedimentation and triggers bend evolution through bank pull or bar push. By contrast, an argument for bar theory is that variations of the banks, through erosion or deposition, may cause variation of the flows around bends and

hence trigger bend evolution. The controlling factors for each theory are considered for submarine channels in subsequent sections in order to examine what combination of factors may influence bend migration in submarine channels.

#### 6.8.4 Behaviour of flow around bends

Submarine channels exhibit a 3D-helical flow structure due to a curved flow stream, in a broadly similar way to rivers, albeit as explained below important differences are often observed. The 3D-helical flow structure is composed of the main primary downstream flow and a secondary lateral flow component (Leopold and Wolman, 1960; Thompson, 1986; Kasvi *et al.*, 2015; Peakall and Sumner, 2015). The maximum flow of the primary flow component in rivers, called the high velocity core (HVC), shifts from an inner/central position prior to the bend apex to an outward position at the bend apex (Figure 6.10A; Leopold and Wolman, 1960; Dietrich and Smith, 1983; Dietrich, 1987). The secondary flow component is a snapshot of the lateral flows around bends and is composed of a locally imbalance between the centrifugal (from Latin centri “centre” + fugere “to flee”) and the pressure gradient force (Rozovskii, 1957; Engelund, 1974; Thorne *et al.*, 1985). Secondary flows are created by the curvature of the bend due to an increase of pressure and the centrifugal force ( $F = \frac{mv^2}{r}$ , where  $m$  is mass of the object,  $v$  is velocity and  $r$  is the radius of a circle) at the outer bend and a decrease of pressure and centrifugal force at the inner bend.

If a river cross-section is taken at a bend apex, an outward-directed flow can be observed near the surface due to a maximum centrifugal force (Figure 6.11A; Leopold and Wolman, 1960; Thompson, 1986; Kasvi *et al.*, 2015). Towards the channel bed, the centrifugal force is decreasing due to a decrease in velocity. In contrast, the pressure gradient force is assumed to be constant with depth. The pressure gradient force is a force going from high pressure (outer bend) to lower pressure (inner bend). Near the channel bed

at the boundary layer, as the velocity goes to zero, centrifugal force is zero ( $F = \frac{mv^2}{r} = 0$ ), hence the pressure gradient force is dominant, and the secondary flow is moving from the outer to the inner bend. For continuity of the flow and due to the imbalance of the forces a spiral-like flow structure is created with an outer-directed flow near the top and an inward-directed flow near the bottom of the flow (“basal-inward” or “river-like” flow direction). The spiral-like flow structure of the secondary flow is reduced at the beginning of the bend apex, increased at the bend apex and reduced after the maximum bend curvature (Figure 6.10A).

Generally, the primary downstream flow component (HVC) shifts around submarine channels bends similar to rivers from an inner/central position prior to the bend apex to an outward position at the bend apex (Figure 6.10B; Giorgio Serchi *et al.*, 2011; Peakall and Sumner, 2015; Reimchen *et al.*, 2016), but the vertical position of the HVC is located in contrast to rivers near the base rather than near the top of the flow (Figure 6.10B; Hampton, 1972; Kneller and Buckee, 2000; Felix, 2002; Meiburg and Kneller, 2010). It must be noted that an inward position of the HVC at the bend apex is also possible due to a switch of the secondary flow direction from an outward-directed to an inner-directed near-bed secondary flow, but may be infrequent (Giorgio Serchi *et al.*, 2011). As the HVC shifts to an outer bend position at the bend apex, outflows may increase as superelevation can be up to two orders of magnitude greater in submarine channels than in rivers due to a reduced density difference between the flow and the surrounding ambient water (Pirmez and Imran, 2003; Dorrell *et al.*, 2013). The secondary flow in submarine channels is also created by an increase of the centrifugal and the pressure force at the outer bend and a decrease of the centrifugal and the pressure force at the inner bend. This imbalance creates an outward-directed centrifugal force and an inward-directed pressure gradient force. Multiple observations and interpretations from laboratory experiments, numerical simulations, direct flow measurements and outcrop studies have been identified for the direction of the secondary flow for submarine channels at bend apices:

- a) “basal-inward” or “river-like” flow direction (Kassem and Imran, 2004; Imran *et al.*, 2007; Islam and Imran, 2008; Islam *et al.*, 2008),
- b) two secondary flow cells stacked on top of each other (Figure 6.11B ; Imran *et al.*, 2007; Islam *et al.*, 2008; Dorrell *et al.*, 2013; Arnott *et al.*, 2021) and,
- c) a “basal-outward” or “reversed” flow direction (Figure 6.11C; Keevil *et al.*, 2006, 2007; Peakall *et al.*, 2007; Amos *et al.*, 2010; Parsons *et al.*, 2010; Wei *et al.*, 2013; Sumner *et al.*, 2014; Davarpanah Jazi *et al.*, 2020) whereby the most common one appears to be the “basal-outward” or “reversed” spiral-like flow structure.

Considering just the centrifugal and pressure gradient forces in a submarine channel bend, and balancing the forces across a given cross-section in the same way as considered for rivers, then prior to the bend apex (upstream) and at the bend apex, the centrifugal force is dominant in the vertical just above the bed, where the maximum downstream velocity occurs. At the channel bed as the velocity goes to zero, the centrifugal force is zero. Additionally, the centrifugal force decreases towards the top of the flow, as the downstream velocity decreases. The pressure gradient force is typically assumed to be constant with height (e.g., Dorrell *et al.*, 2013) and thus dominates at the top where centrifugal forces are weak, and might also be expected to dominate at the base where centrifugal force goes to zero. This would give twin flow cells, stacked in the vertical, the basal one inward directed and the upper one outward directed (Figure 6.11B; e.g., Dorrell *et al.*, 2013). Towards the bend apex, as the super-elevation is increasing the position of the maximum flow velocity increases vertically and the high velocity core shifts towards an outer-bend position. Past the bend apex (downstream), the pressure gradient-force start to dominate the centrifugal force near the channel bed hence an inward-directed near bed flow due to the pressure gradient force and an outward-directed top flow due to the centrifugal force

occur. However, this analysis misses the importance of the radial fluid flux which gives rise to the superelevation (Dorrell *et al.*, 2013).

The radial fluid flux is the horizontal flow due the density stratification giving rise to superelevation and potential overspill. As the superelevation is small in rivers (Leopold, 1982), the radial fluid flux is very small and thus is ignored, but the up to two orders of magnitude difference in superelevation in submarine channels means that radial fluxes are important. Radial fluxes in the upstream part of the bend (as superelevation grows) enhance outward directed flow at all levels, and are thought in many cases to dominate the basal pressure gradient leading to outwards directed basal flow and the formation of a single flow cell with reversed secondary circulation (Figure 6.11C; Dorrell *et al.*, 2013; Peakall and Sumner, 2015). Downstream of the bend apex, the radial fluxes will at some point turn inwards, as superelevation declines, enhancing the inward directed basal flow (Figure 6.10; Dorrell *et al.*, 2013). As discussed in part, above, and considered in more detail below, the variations between secondary flow structures are likely caused by a range of factors, such as the height of the maximum flow velocity above the bed (Corney *et al.*, 2006, 2008), the material transported radially (radial flux) which can vary depending on the flow superelevation and overspill (Dorrell *et al.*, 2013), density stratification, and a number of additional factors (Peakall and Sumner, 2015).

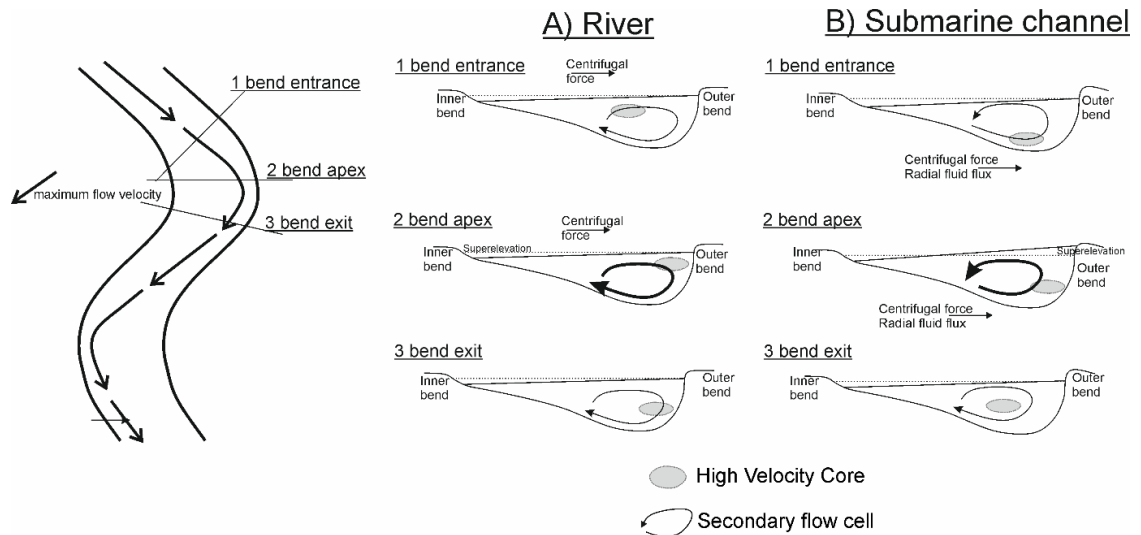


**Figure 6.10** Comparison of flow processes around bends for A) rivers and B) submarine channels. HVC moves from an inner bend position at the bend entrance to an outer bend position at the bend exit. At the bend entrance (cross-section 1) maximum centrifugal force is near the bed in submarine channels and near the top in rivers. Superelevation starts to occur. At the bend apex (cross-section 2), superelevation is greater in submarine channels than in rivers, due to dominant radial fluid fluxes, which leads to outer-directed basal flow in submarine channels with HVC is situated at the outer bend position. Past the bend apex (cross-section 3) as the high velocity core shifts inward in submarine channels, the pressure gradient force towards the inner bend starts to be dominant near the bed and the secondary flow cell is directed towards the inner bend near the bed. Adapted from Leopold and Wolman (1960), Kasvi *et al.* (2015) and Peakall and Sumner (2015).

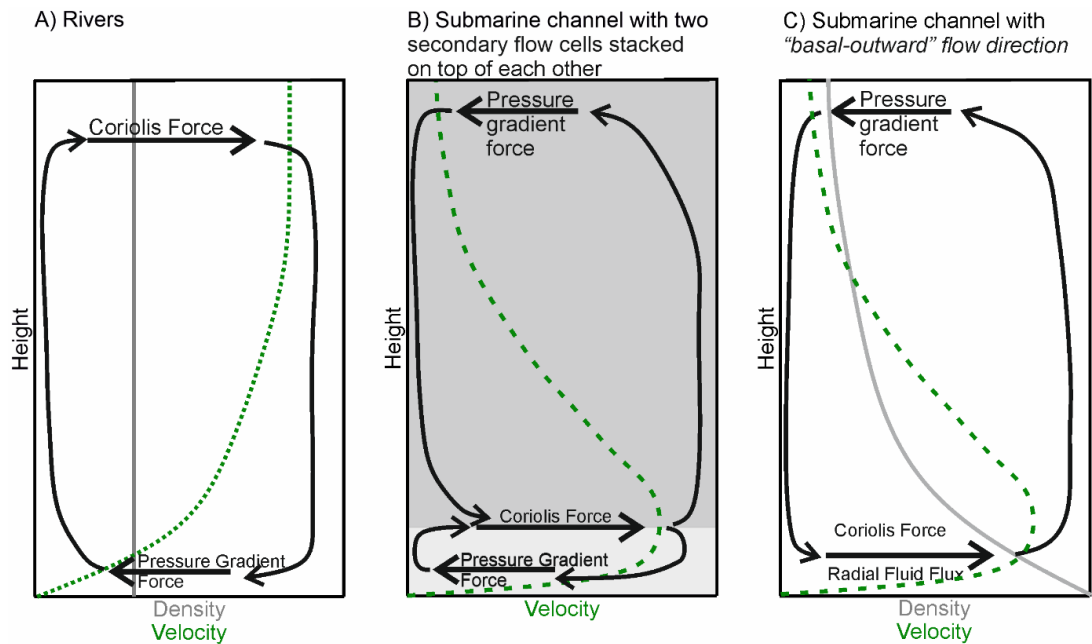


**Figure 6.11** Snapshot of the secondary flow at the bend apex for A) Rivers, B) Submarine channels with two flow cells stacked on top of each other, and C) Submarine channels with a reversed secondary flow cell. A) In rivers, centrifugal force is dominated at the top of the flow due to the maximum flow velocity near the top of the flow. The pressure gradient force is dominated near the channel bed due to a reduction of the centrifugal force. Radial fluid fluxes are not important as density stratification is in general small in rivers. B) Submarine channels with two flow cells stacked on top of each other occur when just considering the velocity and not the radial fluid flux due to the density stratification. Coriolis Force is dominated where the maximum flow velocity occur and pressure gradient force with an inward-directed flow exceeds the centrifugal force near the channel bed and on top of the flow. Hence two cells stacked on top of each other are created. C) A “basal-outward” flow direction in submarine channels is created by considering the radial fluid flux due to the density stratification giving rise to the superelevation. The combination of the radial fluid flux and the centrifugal force exceeds the pressure gradient force near the channel bed, hence only one basal-outward directed flow cell is created. For further explanation see Dorrell *et al.* (2013) and Peakall and Sumner (2015). Note: The height of the secondary flow cells is not for scale.

*“basal-inward” or “river-like” flow direction*

A “basal-inward” or river-like flow direction for secondary flow has been observed in the first laboratory experiments for submarine channels (Kassem and Imran, 2004; Imran *et al.*, 2007; Islam and Imran, 2008; Islam *et al.*, 2008).

The secondary flow direction would be the same as in rivers with an outer bend directed top flow and an inner bend directed bottom flow. Such secondary flow direction is suggested to occur for submarine channels, but it is often suggested as a later stage for channel aggradation in submarine channels, or at the ends of submarine channels, where the downstream velocity maximum is much higher in the flow, and superelevation and thus radial fluxes are small (Dorrell *et al.*, 2013; Peakall and Sumner, 2015). All of this previous work has looked at individual time-slices, or time-averaged flow fields. However, repeated changes of orientation of the secondary flow cells has been shown to occur at a given point with time (Dorrell *et al.*, 2018). These temporal changes in orientation are suggested to be caused by vortex shedding due to the interaction of the sediment flow and surrounding fluids at separation zones (Dorrell *et al.*, 2018).

*“basal-outward” or “reversed” flow direction*

A “basal-outward” or “reversed” flow direction have been observed in laboratory experiments (Peakall *et al.*, 2007; Amos *et al.*, 2010; Cossu and Wells, 2013) and from direct field measurements (Parsons *et al.*, 2010; Wei *et al.*, 2013; Sumner *et al.*, 2014). It is caused due to the highest flow velocities and thus largest centrifugal forces occurring near to the bed, and the pressure gradient force dominating towards the top of the flow. As discussed earlier, the radial fluxes related to growth in superelevation (plus overspill if present) lead to the basal flow overcoming the pressure gradient and being outward directed (Dorrell *et al.*, 2013; Peakall and Sumner, 2015). The reversed secondary flow direction leads to the high velocity core shifting from an inner bend to an outer bend position (Giorgio Serchi *et al.*, 2011; Peakall and Sumner, 2015; Reimchen *et al.*, 2016).



*Does the secondary flow change with the cross-sectional shape (“U” vs “V”-shaped cross-section)?*

Numerical simulations with saline-density flows have identified variations of the secondary flow with a change of the cross-sectional shape (Ezz and Imran, 2014). These simulations were conducted with a constant channel width around bends, and were for pre-formed channels that could not adjust to the imposed flow conditions. From these experiments, it suggests that for confined channels, trapezoidal cross-sections favoured reversed flows when compared to rectangular cross-sections (Ezz and Imran, 2014; Peakall and Sumner, 2015). Thus, dominantly “V”-shaped cross-sections with a narrow channel bed width, hence submarine-fan channels, may favour a “basal-outward” or “reversed” secondary flow around bends. In contrast, a “U”-shaped cross-section with a wider channel bed width, hence isolated deep-ocean channels, may be more likely to have a “basal-inward” or “river-like” secondary flow around bends. For these confined flows, the specific processes involved in these secondary flow changes as a function of cross-sectional geometry were not highlighted in Ezz and Imran (2014). However, Ezz and Imran (2014) did note the complexity of the flow dynamics, including the influence of run-up in the trapezoidal cases, and width changes between sections; both rectangular and trapezoidal channels had the same 0.3 m wide flat basal floor, with the trapezoidal channel wings extending from this. Unconfined channels that enabled overspill were only examined for trapezoidal channels, where it was observed that overspill aided the prevalence of reversed secondary flow relative to confined channels (Ezz and Imran, 2014), as predicted by Dorrell *et al.* (2013).

It must be noted that in reality, the “U”-shaped cross-sections have a wider channel bed width compared to a “V”-shaped cross-sections (Chapter 3). This would mean that the radius of curvature is slightly decreased for “V”-shaped cross-sections compared to “U”-shaped cross-sections near the channel bed (Figure 6.12). As the radius of curvature for “U”-shaped cross-sections is slightly increased relative to “V”-shaped cross-sections, the

centrifugal force is decreased assuming a constant channel velocity ( $F_c = \frac{mv^2}{r}$ ). Depending on the reduction of the centrifugal force, the pressure-gradient force may be already dominated near the channel bed and hence a near-bed inward-directed bed flow may be dominated at the bend apex. However, as superelevation due to the radial fluid flux enhances outer-directed near bed flow and increases at the bend apex (Dorrell *et al.*, 2013) the influence of the width at the channel bed may be minimal.

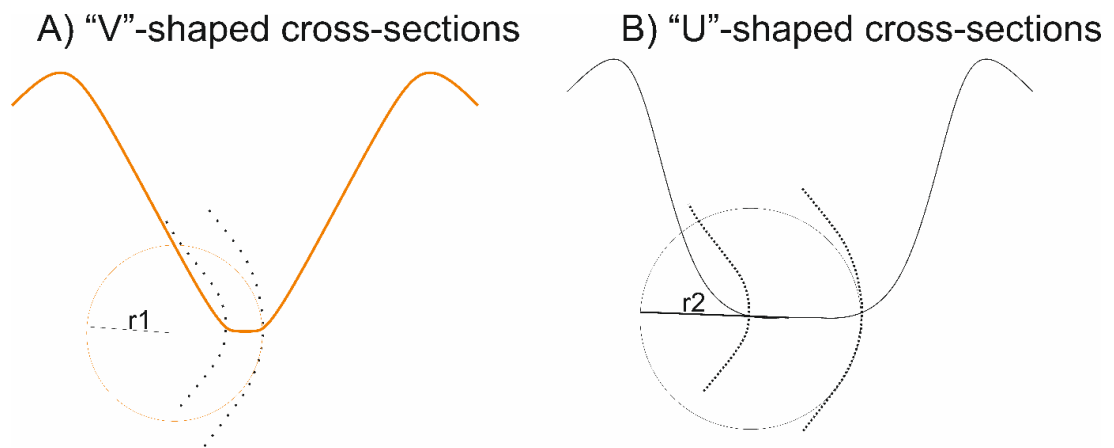


**Figure 6.12** Comparison of the radius of curvature near the channel bed. The radius of curvature for “V”-shaped cross-section ( $r_1$ ) is smaller than for the “U”-shaped cross-section.

Direct observations of secondary flows have so far only been taken for submarine channels from a submarine-fan channel (Congo), which showed two-stacked secondary flow cells with a “basal-outward” directed near bed flow (Azpiroz-Zabala *et al.*, 2017b). It must be noted however that the measurements to study the secondary flow was taken very near to the bend inflection, where secondary flows are weakened rather than near a bend apex. Additionally, the work is taken at a single point in the vertical, rather than across a cross-section, and assumes that the cross-section balances and thus exclude radial fluxes related to superelevation. Additionally, “basal-outward” or “reversed” secondary flows have also been observed from repeat cross-sections at multiple points around bends at a saline outflow into the Black Sea with a wide channel bed width (Parsons *et al.*, 2010; Sumner *et al.*, 2014), and

for particulate flows in a reservoir Wei *et al.* (2013). Hence, an increase in super-elevation around submarine channel bends may still be the dominant factor for an outer-directed bed flow and the dominant cross-sectional shape may be a small factor.

### **6.8.5 Bend migration**

Bend evolution in aggradational submarine channels is primarily controlled by expansion (swing), rather than downstream (sweep) migration as in rivers. A downstream (sweep) migration in rivers occurs due to a phase lag between sediment deposition and flow dynamics. This phase lag causes sedimentation at the inner bend, and erosion at the outer bend, to reach a maximum slightly downstream of the bend apex (Ikeda *et al.*, 1981; Sylvester *et al.*, 2019). Even so, secondary flows shift sediment towards the inner bend, and the ultimate stability of inner bend deposition is caused by the shoaling across point bars and by gravity induced sediment sorting across the bar slope (Nelson and Smith, 1989). A reversed secondary flow in submarine channels laboratory experiments and numerical simulations has been observed to create deposition at the inner bend and erosion at the outer bend, but this occurs further downstream than in equivalent river systems (Peakall *et al.*, 2007; Amos *et al.*, 2010; Darby and Peakall, 2012; Cossu and Wells, 2013; Wells and Cossu, 2013; Cossu *et al.*, 2015), which would lead to a strong downstream (sweep) bend migration. However, a continuous downstream bend migration as has been observed for rivers, has not been observed for aggradational submarine channels in passive margin settings (Peakall *et al.*, 2000a,b; Reimchen *et al.*, 2016). This downstream bend deposition as observed in laboratory experiments and numerical simulations may be due to the phase lag (Ezz and Imran, 2014) between sedimentation and flow processes as has been observed in rivers (Palm *et al.*, 2021); in turn channel width has an influence on the phase lag and thus secondary flow (Ezz and Imran, 2014).

*Influence of channel bend width variations on flow dynamics*

Channel widening at the bend apex relative to bend inflections in submarine fan channels has profound implications for sedimentation. The occurrence of reversed secondary flow, with an outer-directed near bed flow, will still occur despite a wider channel width (Ezz and Imran, 2014), however it will affect the distribution of centrifugal and pressure gradient forces around the bend. A wider width at the bend apex will reduce the centrifugal force in the upstream part of the bend, reduces radial fluid fluxes hence superelevation (Figure 6.13). After the bend apex, a narrowing of width will lead to enhanced maintenance of superelevation and the pressure gradient, which counteracts the centrifugal force, leading to stronger basal-inward directed bed-flow relative to a fixed width channel. Consequently, the convergence of sediment and fluid is further upstream relative to constant width channels as the wider width at the bend apex reduces the strength of the helical flow. As noted above, the helical flow is flipped towards a basal-inward directed bed-flow just after the bend apex as the helical flow cannot remain outward-directed at the channel bed forever due to continuity of the flow (Peakall and Sumner, 2015); the high velocity core is already near the outer bend position and will move towards a central channel position at the inflection point with accompanying reduction in the strength of the helical flow cell.

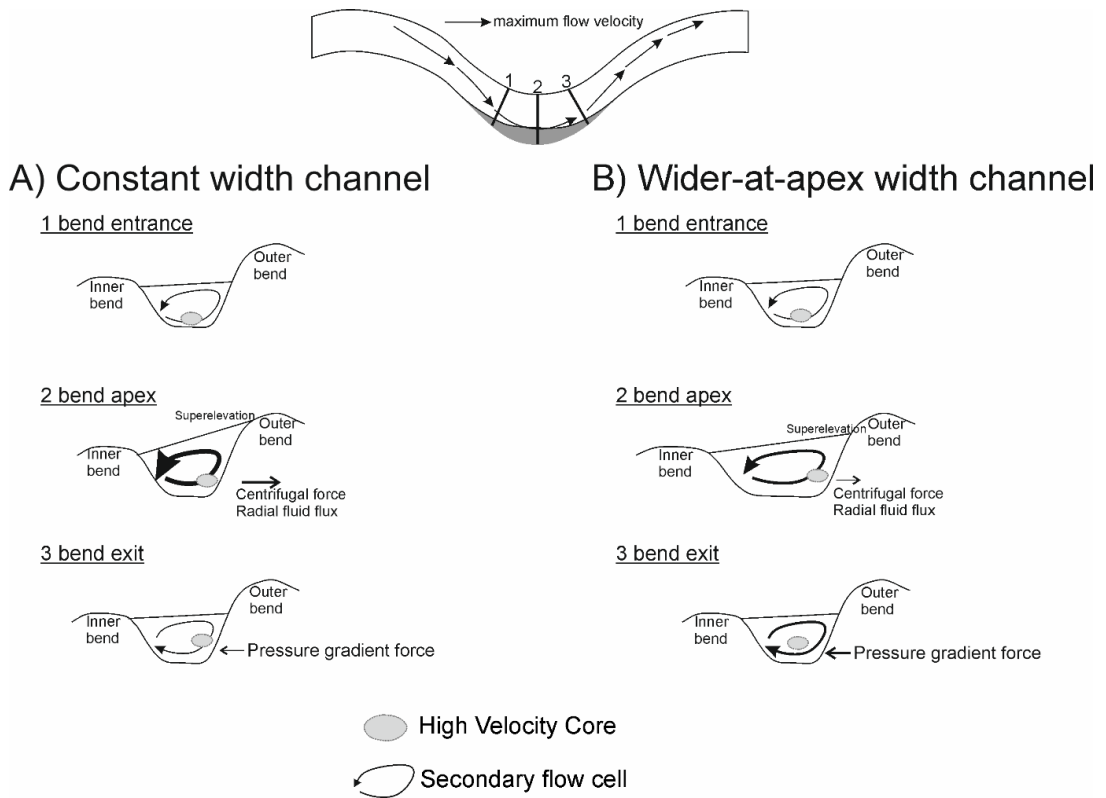


**Figure 6.13** Comparison of the flow field with a constant and wider-at-bend apex width. At the bend entrance (Cross-section 1), centrifugal force and radial fluid flux is dominated near the bottom. The secondary flow cell increases due to increase of the radial fluid flux hence superelevation towards the bend apex. At the bend apex (cross section 2), outer-directed bed flow is dominated due to an increase in the radial fluid flux hence superelevation, but is reduced in wider-width cross-section relative to constant-width cross-section. At the bend exit (cross-section 3), the pressure gradient force is maintained for longer around the bend and therefore near the bed is dominant, relative to the centrifugal force, in wider-at-apex width than at constant width channels, hence this causes a quicker switch of the secondary flow cell.

### *Bank pull or bar push?*

The differences in channel width variation for submarine-fan channels and isolated deep-ocean channels could suggest that submarine channels may be dominated by different bend processes through bank pull or bar push (Figure 6.14). Here, bend processes are first discussed for submarine fan channels and then for isolated deep-ocean channels in the Gulf of Alaska.

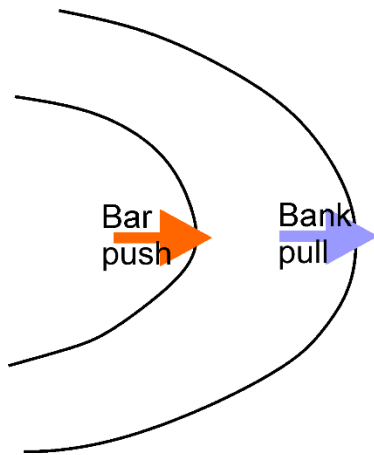


**Figure 6.14** Bend processes are either controlled by bar push, inner bend deposition, or bank pull, outer bend erosion.

All studied submarine-fan channels (Congo, Amazon, Magdalena, Bryant) have consistent wider bend apices relative to inflections for all width measurements, similar to sinuous point-bar rivers (type C of the Brice (1975) classification; Lagasse *et al.*, 2004; Eke *et al.*, 2014a). A wider width at bend apices might be explained by channel expansion over time driven by outer bank erosion that exceeds inner bend deposition (Eke *et al.*, 2014b). Alternatively, it could also suggest that bar push (inner bend deposition) due to a point bar developing at the inner bend occurs, leading to forcing of the high velocity flow towards the outer bank, increasing shear stress and erosion at the outer bank, widening the channel (Dietrich and Smith, 1983). A key difference between bank pull and bar push in rivers is the sediment supply rate to a specific system (Constantine *et al.*, 2014; Donovan *et al.*, 2021). For a system with mobile banks, if the sediment supply rate is low the bend is controlled by bank pull and if the sediment supply rate is high the bend is controlled by bar push. The sediment supply rates, particularly in terms of traction load, to submarine-fan channels are not known, so the sediment deposition is used as an interpretation for the sediment supply rate. Point bars are not commonly observed in submarine channels (Peakall and Sumner, 2015), but if present they form high amplitude deposits in seismic data, and are much smaller than the flow depth, opposite to rivers (Nakajima *et al.*, 2009; Babonneau *et al.*, 2010; Darby and Peakall, 2012). On top of the point bars are vertically accreting, low-angle inclined finer-grained deposits analogous to

oblique accretion deposits in mixed load rivers (Page *et al.*, 2003), which are suggested to have formed after the point bar development (Babonneau *et al.*, 2010; Peakall and Sumner, 2015). So, the only mechanism for bend migration through bar push is by the relative thin point bar deposits, which are probably not big enough to push the movement of high velocity toward the outer bend to increase shear, leading to outer bank erosion and consequently creating a wider channel width. Hence, since submarine-fan channels have a consistently wider width at bend apices (this study) and point bars are often non-existent (Peakall and Sumner, 2015), it is likely that submarine-fan channels are controlled by bank pull, outer bank erosion, rather than bar push. However, since inner bend deposition for submarine channels is often composed of low-angle inclined finer-grained deposits similar to oblique accretion deposits in rivers, it could be that the oblique accretion deposits will increase with a greater outer bend erosion similar to rivers, since an increase in outer bank erosion will enhance inner bend deposition (Van de Lageweg *et al.*, 2014). An increase in outer bank erosion might additionally be enhanced by knickpoints (Heijnen *et al.*, 2020), or salt basins (instability of the substrate, Covault *et al.*, 2019; 2021), where bend migration is often increased.

The studied isolated deep-ocean channels from the Gulf of Alaska seem to show, in contrast to submarine-fan channels and sinuous point-bar rivers, a greater diversity of results in terms of width measurements. Isolated deep-ocean channels are typically wider at bend apices than bend inflections, but narrower at apex regions than inflection regions. Additionally, only 50% of bends are wider at bend apices despite irrespective of the methodology used. Hence, for isolated deep-ocean channels in the Gulf of Alaska multiple bank processes for deposition and erosion are possible based on the obtained width results:

- a) a wider width at the apex than at inflection points, suggesting a width expansion controlled by either bank pull or bar push similar to submarine fan channels,

- b) a narrower width at the apex than at inflection points, suggesting a faster inner-bank deposition than outer-bank erosion, hence a control by bar push
- c) the width is similar between apex and inflection, suggesting an equilibrium of erosion at the outer bank and deposition at the inner bank;
- d) or banks are restricted and hence no erosion or deposition occur.

Channel width between bend apices and bend inflections was close to equal for the Horizon Channel (between regions) and the Surveyor Channel (all width measurements, depth-averaged width between points), which would suggest an equilibrium of deposition and erosion between inner and outer bank or a restriction of bank movement due to bank stability. Isolated deep-ocean channels are long-lasting features, which may suggest that the banks are in equilibrium with the flow but a constant width channel in submarine channels would suggest that inner-bend deposition would occur past the bend apex (Peakall *et al.*, 2007; Amos *et al.*, 2010; Keevil *et al.*, 2010). However, a downstream bend migration is not normally observed for isolated deep-ocean channels. Hence, a relatively constant width channel may not necessarily mean an equilibrium between erosion at the outer bank and deposition at the inner bank. Another explanation is that the banks are comparatively stable, and sediment is unable to erode or deposit sediment on either side of the banks, similar to rivers where banks are restricted due to vegetation or bedrock (Luchi *et al.*, 2010). Isolated deep-ocean channels are often incised into bedrock as they are basement controlled, hence are restricted in their free flow and form during early ocean basin formation (Carter, 1988). Other mechanisms for a reduction in outer bend erosion are speculative. Dorrell *et al.* (2018) suggested that flow shedding leads to a change in orientations of the secondary flow, which reduces bend growth and increases aggradation. Such a process is unique to submarine channels and not applicable to rivers. The experiments were carried out with a rectangular channel cross-section and a constant channel width around bends. The question is whether such a process varies if the apex width is wider at the bend apex and therefore if it



would still lead to a reduction in outer bend erosion for submarine fan channels. Given that the process of flow shedding is thought to be primarily related to flow separation at inner bends (Dorrell *et al.*, 2018) and that such separation will likely be enhanced by increased channel width at bend apices, the process of flow shedding and hence variation of secondary flow orientation is plausible and logical for most aggradational submarine channels.

#### *The influence of bank pull and bar push on cross-section morphology*

The influence of the banks on the cross-sectional morphology can be both analysed at a small scale (local cross-sectional variation), medium scale (around bends) and on a larger scale (variation between channel types). On a small scale, cross-sections can change locally through margin failure or bank collapse, bend cut-offs, channel incision or entrenchment and topographic variation such as presence of faults, knickpoints and terraces (Chapter 3 and 4; Heiniö *et al.*, 2007; Hansen *et al.*, 2015; Jolly *et al.*, 2017; Babonneau *et al.*, 2002; Palm *et al.*, 2021). On a small scale, cross-sections may get either wider or deeper through the above processes, so changing from an often 'V'- to 'U'-shaped or from an 'U'-to a 'box'-shaped cross-section.

On a bend scale, depositional and erosional processes are coupled to the fluid flow (primary and secondary) fields. Such coupling is two-way, with flow and sedimentation both influencing each other. In rivers, a numerical simulation (Eke *et al.*, 2014b) with a constant vertical erosion and deposition have shown that multiple schemes of bank erosion and deposition are possible: 1. both banks erode, 2. both banks deposit, 3. both banks migrate outward, but with a faster inner bank deposition (bar push), and/or 4. both banks migrate outward, but with a faster outer bank erosion (bank pull).

For submarine fan channels, it has been argued that channel bends are primarily driven by bank pull, outer bank erosion. Experimental and numerical studies of bend flow in submarine channels have not examined the nature of applied shear stresses on channel banks. However, it is known in

rivers that migration rate (reflecting applied shear stresses) reaches a maximum at a point slightly downstream of the bend apex (Ikeda *et al.*, 1981; Sylvester *et al.*, 2019). For submarine channels, reversed secondary flow is typically expected (Dorrell *et al.*, 2013; Peakall and Sumner, 2015), and this is known to move the high velocity core towards the outer bank (Giorgio-Serchi *et al.*, 2011; Peakall and Sumner, 2015). Consequently, it might be expected that this would further enhance outer bank erosion relative to rivers, and may account for the increased variation in the width of channel apices relative to inflections. These width variations in turn alter the growth and decay of the secondary flow cells, which as argued herein act to move the locus of deposition on the inner bank upstream relative to predictions from previous studies on constant width channels. As a consequence, this may act to maintain the presence of the high velocity zone close to the outer bank of the channel. Isolated ocean-margin channels show a far more complex relationship in the nature of width variations around bends, with only around half of all bends showing an enhancement of width at the bend apex. Nonetheless, there was still an overall increase in channel width at bend apices relative to inflections, so some of the same processes identified in the submarine fan channels may still operate in these systems. There must, however, be additional processes in these systems, and this may be related to their association with bedrock features, and tectonic controls, as discussed earlier.

As discussed above, channel width is maximum at bend apices, submarine-fan channels are expected to have the greatest migration rate at bend apices. Since migration rate, which reflects applied shear stresses is further downstream of the bend apex in rivers due to the phase lag (Ikeda *et al.*, 1981; Sylvester *et al.*, 2019), applied shear stresses are expected to be highest at bend apices for submarine-fan channels. If the cross-sectional shape around bends is controlled by the banks, a variation of the cross-sectional shape between apex point and inflection points or between apex region and inflection region might be expected assuming increased applied shear stress at the bend apex. Here, cross-sectional analyses were conducted using the General Power Law Program (Chapter 3;  ${}^{\text{G}}\text{P}_L$ ; Pattyn *et al.*, 1998).

The results suggest that the cross-sectional shape is consistent at apices and inflections for isolated deep-ocean channels and submarine-fan channels (Table 6.5). Hence, it is expected that for isolated deep-ocean and submarine-fan channels, secondary flow processes do not play a significant role, and instead downstream-flow processes, and their interaction with sedimentation and erosion are key for the cross-sectional shape.

At a larger scale (beyond the bend scale dynamics), there are major differences in cross-sectional shape between channel types, with more V-shaped and U-shaped profiles. This broad cross-sectional shape of the channel is universal through the whole channel hence likely related as discussed earlier, primarily to the style of erosion, deposition/aggradation, and the nature of the substrate.

**Table 6.5** Results of cross-section shape analysis for submarine-fan channels (orange) and isolated deep-ocean channels (blue). A value of  $1 > b \geq 0$  represents a convex-upward shaped cross-section, a value of  $b = 1$  represents a “V”-shaped cross-section, a value of  $2 \geq b > 1$  represents a “U” or parabolic-shaped cross-section and a value of  $b > 2$  represents a box-shaped cross-section. Cross-sectional shape did not change substantially between points and regions. Note the channel bed width was not considered in this analysis.

	Apex point (Cross-section 7a)	Inflection points (1ui, 13di)	Apex region (4u-10d)	Inflection region (1ui-3u, 11d-13di)
<b>Congo Channel Ax52</b>	0.4 convex- upward shaped (n=41)	0.5 convex- upward shaped (n=72)	0.4 convex- upward shaped (n=230)	0.5 convex- upward shaped (n=199)
<b>Magdalena Channel</b>	2.3 “box”-shaped (n=10)	2.0 “U”-shaped (n=13)	2.3 “box”-shaped (n=51)	1.8 “U”-shaped (n=29)
<b>Bryant Channel</b>	1.5 “U”-shaped (n=11)	1.2 “U”-shaped (n=2)	1.4 “U”-shaped (n=49)	1.8 “U”-shaped (n=11)
<b>Surveyor Channel</b>	0.9 convex-upward shape (n=6)	0.5 convex-upward shape (n=7)	0.6 convex-upward shape (n=42)	0.6 convex-upward shape (n=36)
<b>Horizon Channel</b>	1.3 “U”-shaped (n=6)	1.1 “U”-shaped (n=3)	1.1 “U”-shaped (n=14)	1.1 “U”-shaped (n=8)
<b>Baranof Channel</b>	1.8 “U”-shaped (n=7)	1.6 “U”-shaped (n=11)	1.5 “U”-shaped (n=37)	1.5 “U”-shaped (n=32)

## 6.9 Conclusions

This study has analysed the morphometrics and the processes around bends of 8 submarine-fans and 3 isolated deep-ocean channels, and examined these in the context and through incorporation of relevant literature. Distinguishing criteria between submarine channel types were identified in terms of the analysed general morphometrics and on width variations around bends, which have wider implications for downstream flow processes and bend migration. Submarine channels are on average 5-times wider and 10-times deeper than rivers with different channel types clearly distinguishable.

The main submarine channel types, submarine-fan channels and isolated deep-ocean channels can be distinguished based on their morphometrics with isolated deep-ocean channels having mean channel width and mean aspect ratio 7-times greater and mean channel depth 2-times greater than submarine-fan channels. The data also suggest that channel width is established early on, and is related to the environmental setting, and variations in flow are adjusted for in submarine channels through an adjustment of the channel depth. Additionally, a variable cross-section profile between submarine-fan and isolated deep-ocean channels may suggest different erosional and aggradational characteristics and hence potentially different dominant sediment transport mechanisms. Variations between channel types were also identified based on the morphometrics around bends, with submarine-fan channels having a wider width variation around bends interpreted as being dominated by bank pull (outer bank erosion). In comparison, isolated-deep ocean channels are probably also mainly dominated by bank pull (outer bank erosion) but with a restriction of the banks through solid bedrock. Bend evolution in submarine channels supports the bend theory as the flow is controlled by the overall cross-sectional shape of the channel, but the overall direction of the secondary flow cell do not change by a wider-width at bend apex. The wider width at the apex rather reduces the phase lag between sediment deposition and flow dynamics as the convergence of sediment and fluid is upstream relative to constant width channels.

## Chapter 7 Thesis summary

---

In this chapter, the research questions posed in Chapter 1 are addressed, with reference to the results presented in Chapters 3-5 and concludes with recommendation for future research arising from this PhD research.

### **7.1 Is channel width constant around submarine channel bends? How does width vary around a bend in submarine channels?**

Laboratory experiments and numerical simulation have used, so far a constant width around bend as it was not known how the width varied around bends (Peakall *et al.*, 2007; Straub *et al.*, 2008; Amos *et al.*, 2010; Darby and Peakall, 2012; Janocko *et al.*, 2013; Basani *et al.*, 2014). Here, width around bends has been analysed for different submarine channel types (Chapter 4, 5 and 6). Submarine channels show a wide diversity of width variation around bends, for example for submarine-fan channels are wider at bend apex relative to inflections, in contrast isolated deep-ocean channels on many measurement methods have a more constant channel width around bends. Additionally, the channel width may be controlled by allogenic controls, such as climatic condition which controls the magnitude of the width variation around bends.

## **7.2 Are there morphometric variations between different types of submarine channels and how do the morphometrics of different types compare to rivers?**

Previous authors (Flood and Damuth, 1987; Clark *et al.*, 1992; Peakall *et al.*, 2000a; Konsoer *et al.*, 2013; Jobe *et al.*, 2016) have classified submarine channels as one group when comparing to rivers, and came to contradictory results in term of for example aspect ratio. Even though various studies have highlighted the diversity of submarine channels (Schweller and Kulm, 1977; Carter, 1988; Klauke *et al.*, 1998a; Peakall and Sumner, 2015), a detailed analysis of different morphometric variations has not been conducted to date. In chapter 3, a detailed analysis of the morphometrics for different submarine channel types has been conducted. In general, single-thread deep-marine submarine channels beyond the shelf break can be divided depended in the environmental setting into submarine-fan, isolated deep-ocean, axial, non-margin and slope channels. Submarine-fan channels occur as a network of channels on deep-sea fans; isolated deep-ocean channels are basement-controlled and develop in the early stage of basin formation, axial channels occur along axial trenches, non-margin ocean channels occur far from any terrestrial channel and slope channels are restricted to the continental slope. The contradiction in terms of aspect ratio between rivers and submarine channels can be explained by the chosen channel type of each study. Channel width varied by 2 orders of magnitude between channel types, and channel depth by an order of magnitude. Slope, submarine-fan, and non-margin channels are shown to have aspect ratios similar to rivers, whereas isolated deep-ocean and axial channels have aspect ratios much greater than rivers. In terms of cross-sectional shape, submarine-fan, slope and non-margin ocean channels exhibit a more “V”-shaped cross-section and axial and isolated deep-ocean channels a more “U”-shaped cross-section.

### **7.3 What can the width variation around bends tell us about the flow and sediment processes and hence the evolution of submarine channel bends?**

Width around bends in rivers and submarine channels is controlled by erosion of the outer bank and deposition at the inner bank (Luchi *et al.*, 2012; Eke *et al.*, 2014a, b). In rivers, it is known that bend migration in rivers occurs either through inner bend deposition, bar push, or outer bend erosion, bank pull (Eke *et al.*, 2014a; Matsubara and Howard, 2014; Van de Lageweg *et al.*, 2014).

Laboratory experiments and numerical models with a constant width around bends predicted an inner bend deposition, further downstream of the bend apex due to a reversed secondary flow at the bend apex (Peakall *et al.*, 2007; Straub *et al.*, 2008; Amos *et al.*, 2010; Darby and Peakall, 2012; Janocko *et al.*, 2013; Basani *et al.*, 2014) since the point at which flow and sediment flux converge, in turn driving sedimentation deposition at the inner bend (Nelson and Smith, 1989), is beyond the bend apex. Even though the delay in the convergence of flux as a result of a reversed secondary flows at bend apex will still occur in submarine channels (Corney *et al.*, 2006, 2008; Keevil *et al.*, 2007; Darby and Peakall, 2012; Sumner *et al.*, 2014), a wider width at bend apexes as a result of bank pull, will lead to deposition much closer to the bend apex. Hence, this will lead to reduced downstream bend migration (sweep) relative to previous flow-process models, instead of favouring lateral bend migration (Peakall *et al.*, 2000a, b; Jobe *et al.*, 2016). The process of bank pull is likely the common process for submarine-fan channels. Isolated deep-ocean channels show a more constant channel width, but also here no downstream bend migration is observed. Here, a higher bank resistance through solid banks for isolated deep-ocean channels is postulated to reduce outer bank erosion, and hence inner bend deposition, since they are also controlled by bank pull. However, submarine-fan channels and isolated deep-ocean channels may at some point undergo a near cessation of movement (Peakall *et al.*, 2000a, b). At the point of near



cessation, the “hydrodynamic” width (Luchi *et al.*, 2010, 2012), which is only wider for wider-at bend apex channels, hence submarine-fan channels than for constant channel width, hence isolated deep-ocean channels, may get narrower and only the morphological active width (Luchi *et al.*, 2010, 2012) is active for both submarine-fan and isolated deep-ocean channels. The cessation of movement is a late development stage for aggradational channels and often occur through outer bank bars formation, which reduces bend sinuosity over time (Kane *et al.*, 2008; Nakajima *et al.*, 2009; Straub *et al.*, 2011). However, the reduction of the width at the outer bank is part of the morphological active width and not part of the wider “hydrodynamic” width at the inner bend.

## **7.4 Recommendations for future research**

The variation of morphometrics between submarine channels types and around bends have been investigated for single-thread submarine channels on the modern sea floor. Variations of the morphometrics have been identified to occur between submarine channel types (Chapter 3, 5 and 6) and around bends (Chapter 4-6). The research conducted could be further extended to enhance our understanding of the morphometrics around submarine channels in particular around bends. The dataset would benefit from further expansion particularly for those channel types such as axial and non-ocean channels where data were very scarce. Alongside this, a comparison between the morphometrics from the modern seafloor to outcrop and seismic dataset would be interesting, as such analysis would then enable an understanding of the preserved infill, which is largely missing from modern studies . However, distinguishing between different channel types based on the aspect ratio may be challenging, in such analysis, due to compaction. In combination with the cross-sectional shape analysis, a more accurate analysis of the cross-section may be possible. Width analysis around bends has been used to address the contradiction between laboratory experiments or numerical simulations, and

observations of bend migration from natural systems. However, neither a numerical model nor a laboratory experiments have been set-up to test the models developed herein for how flow, sedimentation, and bend development are coupled. Such simulations/experiments are a logical next step in order to examine these processes in more detail, and to directly assess the variations between these and existing process studies based on fixed width channels. In turn, such studies will help disentangle the key fluid dynamics, and sedimentation processes of submarine channel bends, and the external and internal controls on these, which remain relatively poorly understood.

## List of References

Abreu, V., Sullivan, M., Pirmez, C., Mohrig, D., 2003. Lateral accretion packages (LAPs): an important reservoir element in deep water sinuous channels. *Marine and Petroleum Geology*. **20**, 631–648.

Allen, J.R.L., 1965. A review of the origin and characteristics of recent alluvial sediments. *Sedimentology*. **5**, 89–191.

Allen, J.R.L., 1982. *Developments in Sedimentology 30: Sedimentary Structures-Their Character and Physical Basis Volume I*. Elsevier Science Publishers, p. 612.

Alonso, B., Canals, M., Palanques, A., Rehault, J.-P., 1995. A deep-sea channel in the northwestern Mediterranean Sea: morphology and seismic structure of the Valencia Channel and its surroundings. *Marine Geophysical Researches*. **17**, 469–484.

Amos, K.J., Peakall, J., Bradbury, P.W., Roberts, M., Keevil, G., Gupta, S., 2010. The influence of bend amplitude and planform morphology on flow and sedimentation in submarine channels. *Marine and Petroleum Geology*. **27**, 1431–1447.

Arnott, R.W.C., Tilston, M., Fraino, P., Navarro, L., Dumouchel, G., Miklovich, N., 2021. Laterally accreting sinuous channels and their deposits: the Goldilocks of deep-water slope systems. *Journal of Sedimentary Research*. **91**, 451–463.

Azpiroz-Zabala, M., Cartigny, M.J.B., Talling, P.J., Parsons, D.R., Sumner, E.J., Clare, M.A., Simmons, S.M., Cooper, C., Pope, E.L., 2017a. Newly recognized turbidity current structure can explain prolonged flushing of submarine canyons. *Science Advances*. **3**, e170020.

Azpiroz-Zabala, M., Cartigny, M.J.B., Sumner, E.J., Clare, M.A., Talling, P.J., Parsons, D.R., Cooper, C., 2017b. A general model for the helical structure of geophysical flows in channel bends. *Geophysical Research Letters*. **44**, 11932–11941.

Babonneau, N., Savoye, B., Cremer, M., Klein, B., 2002. Morphology and architecture of the present canyon and channel system of the Zaire deep-sea fan. *Marine and Petroleum Geology*. **19**, 445–467.

Babonneau, N., Savoye, B., Cremer, M., Bez, M., 2004. Multiple terraces within the deep incised Zaire Valley (ZaiAngo Project): are they confined levees? In: Lomas, S.A., Joseph, P. (Eds.), *Confined Turbidite Systems*. Geological Society, London, pp. 91–114.

- Babonneau, N., Savoye, B., Cremer, M., Bez, M., 2010. Sedimentary architecture in meanders channel: detailed study of the present Congo Turbidite Channel (ZaiAngo Project). *Journal of Sedimentary Research*. **80**, 852–866.
- Basani, R., Janocko, M.J., Cartigny, M.J.B., Hansen, E.W.M., Eggenhuisen, J.T., 2014. MassFLOW-3DTM as a simulation tool for turbidity currents: some preliminary results. In: *Martinius, A.W., Ravnås, R., Howell, J.A., Steel, R.J., Wonham, J.P. (Eds.), From Depositional Systems to Sedimentary Successions on the Norwegian Continental Margin, Special Publication No. 46.* Wiley-Blackwell, pp. 587–608.
- Belderson, R.H., Kenyon, N.H., Stride, A.H., Pelton, C.D., 1984. A “braided” distributary system on the Orinoco deep-sea fan. *Marine Geology*. **56**, 195–206.
- Bourget, J., Zaragosi, S., Garlan, T., Gabelotaud, I., Guyomard, P., Dennielou, B., 2008. Discovery of a giant deep-sea valley in the Indian Ocean, off eastern Africa: the Tanzania Channel. *Marine Geology*. **255**, 179–185.
- Braudrick, C.A., Dietrich, W.E., Leverich, G.T., Sklar, L.S., 2009. Experimental evidence for the conditions necessary to sustain meandering in coarse-bedded rivers. *Proceedings of the National Academy of Sciences of the United States of America*. **106**, 16936–16941.
- Brice, J.C., 1973. Meandering pattern of the White River in Indiana: an analysis. In: *Morisawa, M. (Ed.), Fluvial Geomorphology.* Binghamton State University of New York, Binghamton, pp. 178–200.
- Brice, J.C., 1974. Evolution of meander loops. *Geological Society of America Bulletin*. **85**, 581–586.
- Brice, J.C., 1975. Airphoto Interpretation of the Form and Behavior of Alluvial Rivers ( No. Final report to the U.S Army Research Office-Durham). Washington University, St. Louis, p.10.
- Brice, J.C., 1982. Stream Channel Stability Assessment (No. No.FHWA/RD-82-021). Federal Highway Administration, Office of Research and Development, p.43.
- Brice, J.C., 1984. Planform properties of meandering rivers. In: *Elliott, C.M. (Ed.), River Meandering.* American Society of Civil Engineers, pp. 1–15.
- Bryant, W.R., Bryant, J.R., Feeley, M.H., Simmons, G.R., 1990. Physiographic and bathymetric characteristics of the continental slope, northwest Gulf of Mexico. *Geo-Marine Letters*. **10**, 182–199.

- Burgess, P.M., Hovius, N., 1998. Rates of delta progradation during highstands: Consequences for timing of deposition in deep-marine systems. *Journal of the Geological Society*. **155**, 217–222.
- Calder, B., 2006. On the uncertainty of archive hydrographic data sets. *IEEE Journal of Oceanic Engineering*. **31**, 249–265.
- Calder, B., 2007. Multi-algorithm swath consistency detection for multibeam echosounder data. *International Hydrographic Review*. **8**, 9–25.
- Caley, T., Malaizé, B., Revel, M., Ducassou, E., Wainer, K., Ibrahim, M., Shoeaib, D., Migeon, S., Marieu, V., 2011. Orbital timing of the Indian, East Asian and African boreal monsoons and the concept of a “global monsoon”. *Quaternary Science Reviews*. **30**, 3705–3715.
- Carling, P.A., 1991. An appraisal of the velocity-reversal hypothesis for stable pool-riffle sequences in the river Severn, England. *Earth Surface Processes and Landforms*. **16**, 19–31.
- Carter, L., Burnett, D., Drew, S., Marle, G., Hagadorn, L., Bartlett-McNeil, D., Irvine, N., 2009. Submarine cables. *Wire Journal International*. **49**, 44–46.
- Carter, R.M., 1988. The nature and evolution of deep-sea channel systems. *Basin Research*. **1**, 41–54.
- Carter, R.M., Carter, L., 1996. The abyssal Bounty fan and lower Bounty channel: evolution of a rifted-margin sedimentary system. *Marine Geology*. **130**, 181–202.
- Clark, J., Kenyon, N., Pickering, K., 1992. Quantitative analysis of the geometry of submarine levees. *Geology*. **60**, 877–910.
- Clark, J.D., Pickering, K.T., 1996a. Submarine Channels- Processes and Architecture. Vallis Press, London, p.231.
- Clark, J.D., Pickering, K.T., 1996b. Architectural elements and growth patterns of submarine channels: application to hydrocarbon exploration. *AAPG Bulletin*. **80**, 194–221.
- Constantine, J.A., Dunne, T., Ahmed, J., Legleiter, C., Lazarus, E.D., 2014. Sediment supply as a driver of river meandering and floodplain evolution in the Amazon Basin. *Nature Geoscience*. **7**, 899–903.
- Conway, K.W., Barrie, J.V., Picard, K., Bornhold, B.D., 2012. Submarine channel evolution: Active channels in fjords, British Columbia, Canada. *Geo-Marine Letters*. **32**, 301–312.

Copeland, R.R., Biedenharn, D.S., Fischenich, J.C., 2000. Channel-forming discharge and hydraulic geometry width predictors in meandering sand-bed rivers. *World Water and Environmental Resources Congress*. 1–12.

Corney, R.K.T., Peakall, J., Parsons, D.R., Elliott, L., Amos, K.J., Best, J.L., Keevil, G.M., Ingham, D.B., 2006. The orientation of helical flow in curved channels. *Sedimentology*. **53**, 249–257.

Cossu, R., Wells, M.G., 2010. Coriolis Forces influence the secondary circulation of gravity currents flowing in large-scale sinuous submarine channel systems. *Geophysical Research Letters*. **37**, 1–6.

Cossu, R., Wells, M.G., 2013. The evolution of submarine channels under the influence of Coriolis Forces: experimental observations of flow structures. *Terra Nova*. **25**, 65–71.

Cossu, R., Wells, M.G., Peakall, J., 2015. Latitudinal variations in submarine channel sedimentation patterns: the role of Coriolis Forces. *Journal of the Geological Society*. **172**, 161–174.

Covault, J.A., Fildani, A., Romans, B.W., McHargue, T., 2011. The natural range of submarine canyon-and-channel longitudinal profiles. *Geosphere*. **7**, 313–332.

Covault, J.A., Graham, S.A., 2010. Submarine fans at all sea-level stands: Tectono-morphologic and climatic controls on terrigenous sediment delivery to the deep sea. *Geology*. **38**, 939–942.

Covault, J.A., Sylvester, Z., Hudec, M.R., Ceyhan, C., Dunlap, D., 2020. Submarine channels “swept” downstream after bend cutoff in salt basins. *The Depositional Record*. **6**, 259–272.

Cullis, S., Patacci, M., Colombera, L., Bührig, L., McCaffrey, W.D., 2019. A database solution for the quantitative characterisation and comparison of deep-marine siliciclastic depositional systems. *Marine and Petroleum Geology*. **102**, 321–339.

Curry, J.R., Emmel, F.J., Moore, D.G., 2003. The Bengal Fan: morphology, geometry, stratigraphy, history and processes. *Marine and Petroleum Geology*. **19**, 1191–1223.

Czuba, J.A., Best, J.L., Oberg, K.A., Parsons, D.R., Jackson, P.R., Garcia, M.H., Ashmore, P., 2011. Bed morphology, flow structure and sediment transport at the outlet of Lake Huron and in the upper St. Clair River. *Journal of Great Lakes Research*. **37**, 480–493.

Damuth, J.E., Flood, R.D., 1984. Morphology, sedimentation processes, and growth pattern of the Amazon deep-sea Fan. *Geo-Marine Letters*. **3**, 109–117.

Damuth, J.E., Flood, R.D., Kowsmann, R.O., Belderson, R.H., Gorinf, M.A., 1988. Anatomy and Growth Pattern of Amazon Deep-Sea Fan as revealed by long-range side-scan sonar (GLORIA) and high-resolution seismic studies. *AAPG Bulletin*. **8**, 885–911.

Darby, S.E., Peakall, J., 2012. Modelling the equilibrium bed topography of submarine meanders that exhibit reversed secondary flows. *Geomorphology*. **163–164**, 99–109.

Das, H.S., 2004. Numerical modeling of flow and bed evolution in meandering submarine channels. *Journal of Geophysical Research*. **109**, C10009.

Davarpanah Jazi, S., Wells, M.G., Peakall, J., Dorrell, R.M., Thomas, R.E., Keevil, G.M., Darby, J., Sommeria, S., Viboud, T.V., 2020. Influence of Coriolis Force upon bottom boundary layers in a large-scale gravity current experiment: implications for evolution of sinuous deep-water channel systems. *Journal of Geophysical Research*. **125**, e2019JC015284.

de Leo, F.C.D., Smith, C.R., Rowden, A.A., Bowden, D.A., Clark, M.R., 2010. Submarine canyons: hotspots of benthic biomass and productivity in the deep sea. *Proceedings of the Royal Society*. **277**, 2783–2792.

de Ruig, M.J., 2003. Deep marine sedimentation and gas reservoir distribution in upper Austria. *Oil Gas European Magazine*. **29**, 64–73.

Deptuck, M.E., Steffens, G.S., Barton, M., Pirmez, C., 2003. Architecture and evolution of upper fan channel-belts on the Niger Delta slope and in the Arabian Sea. *Marine and Petroleum Geology*. **20**, 649–676.

Deptuck, M.E., Sylvester, Z., Pirmez, C., O'Byrne, C., 2007. Migration–aggradation history and 3-D seismic geomorphology of submarine channels in the Pleistocene Benin-major Canyon, western Niger Delta slope. *Marine and Petroleum Geology*. **24**, 406–433.

Dietrich, W.E., 1987. Mechanics of flow and sediment transport in river bends. In: Richards, K.S. (Ed.), *River Channels*. Basil Blackwell, Oxford, pp. 179–227.

Dietrich, W.E., Smith, J.D., 1983. Influence of the point bar on flow through curved channels. *Water Resources Research*. **19**, 1173–1192.

Donovan, M., Belmont, P., Sylvester, Z., 2021. Evaluating the relationship between meander-bend curvature, sediment supply, and migration rates. *Journal of Geophysical Research*. **126**, e2020JF006058.

Dorrell, R.M., Darby, S.E., Peakall, J., Sumner, E.J., Parsons, D.R., Wynn, R.B., 2013. Superelevation and overspill control secondary flow dynamics in submarine channels. *Journal of Geophysical Research*. **118**, 3895–3915.

- Dorrell, R.M., Peakall, J., Burns, C., Keevil, G.M., 2018. A novel mixing mechanism in sinuous seafloor channels: implications for submarine channel evolution. *Geomorphology*. **303**, 1–12.
- Dowdeswell, J.A., Vásquez, M., 2013. Submarine landforms in the fjords of southern Chile: Implications for glacial-marine processes and sedimentation in a mild glacier-influenced environment. *Quaternary Science Reviews*. **64**, 1–19.
- Droz, L., Marsset, T., Ondréas, H., Lopez, M., Savoye, B., Spy-Anderson, F.L., 2003. Architecture of an active mud-rich turbidite system: the Zaire Fan (Congo-Angola margin southeast Atlantic): results from ZaiAngo 1 and 2 cruises. *AAPG Bulletin*. **87**, 1145–1168.
- Droz, L., Mougénot, D., 1987. Mozambique Upper Fan: origin of depositional units. *AAPG Bulletin*. **71**, 1355–1365.
- Droz, L., Rigaut, F., Cochonat, P., Tofani, R., 1996. Morphology and recent evolution of the Zaire turbidite system (Gulf of Guinea). *Geological Society of America Bulletin*. **108**, 253–269.
- Duró, G., Crosato, A., Tassi, P., 2016. Numerical study on river bar response to spatial variations of channel width. *Advances in Water Resources*. **93**, 21–38.
- Eke, E., Czapiga, M.J., Viparelli, E., Shimizu, Y., Imran, J., Sun, T., Parker, G., 2014a. Coevolution of width and sinuosity in meandering rivers. *Journal of Fluid Mechanics*. **760**, 127–174.
- Eke, E., Parker, G., Shimizu, Y., 2014b. Numerical modeling of erosional and depositional bank processes in migrating river bends with self-formed width: Morphodynamics of bar push and bank pull. *Journal of Geophysical Research*. **119**, 1455–1483.
- Embley, R.W., Ewing, J.I., Ewing, M., 1970. The Vidal deep-sea Channel and its relationship to the Demerara and Barracuda Abyssal plains. *Deep Sea Research and Oceanographic Abstracts*. **17**, 539–552.
- Engelund, F., 1974. Flow and bed topography in channel bends. *Journal of Hydraulic Engineering*. **100**, 1631–1648.
- Ercilla, G., Alonso, B., Baraza, J., Casas, D., Chiocci, F.L., Estrada, F., Farrán, M., Gonthier, E., Pérez-Belzuz, F., Pirmez, C., Reeder, M., Torres, J., Urgeles, R., 1998. New high-resolution acoustic data from the 'braided system' of the Orinoco deep-sea fan. *Marine Geology*. **146**, 243–250.
- Ercilla, G., Alonso, B., Estrada, F., Chiocci, F.L., Baraza, J., Farran, M., 2002. The Magdalena Turbidite System (Caribbean Sea): present-day morphology and architecture model. *Marine Geology*. **185**, 303–318.



- Ezz, H., Imran, J., 2014. Curvature-induced secondary flow in submarine channels. *Environmental Fluid Mechanics*. **14**, 343–370.
- Felix, M., 2002. Flow structure of turbidity currents. *Sedimentology*. **49**, 397–419.
- Felix, M., Peakall, J., 2006. Transformation of debris flows into turbidity currents: mechanisms inferred from laboratory experiments. *Sedimentology*. **53**, 107–123.
- Field, M.E., Gardner, J.V., Prior, D.B., 1999. Geometry and significance of stacked gullies on the northern California slope. *Marine Geology*. **154**, 271–286.
- Fierens, R., Droz, L., Toucanne, S., Raison, F., Jouet, G., Babonneau, N., Miramontes, E., Landurain, S., Jorry, S.J., 2019. Geomorphology Late Quaternary geomorphology and sedimentary processes in the Zambezi turbidite system (Mozambique Channel). *Geomorphology*. **334**, 1–28.
- Finnegan, N.J., Dietrich, W.E., 2011. Episodic bedrock strath terrace formation due to meander migration and cutoff. *Geology*. **39**, 143–146.
- Flood, R.D., Manley, P.L., Kowsmann, R.O., Appi, C.J., Pirmez, C., 1991. Seismic facies and late quaternary growth of Amazon Submarine Fan. In: Weimer, P., Link, M.H. (Eds.), *Seismic Facies and Sedimentary Processes of Submarine Fans and Turbidite Systems*. Springer, New York, pp. 415–433.
- Fonnesu, F., 2003. 3D seismic images of a low-sinuosity slope channel and related depositional lobe (West Africa deep-offshore). *Marine and Petroleum Geology*. **20**, 615–629.
- Foreman, B.Z., Lai, S.Y.J., Komatsu, Y., Paola, C., 2015. Braiding of submarine channels controlled by aspect ratio similar to rivers. *Nature Geoscience*. **8**, 700–703.
- Forwick, M., Laberg, J.S., Hass, H.C., Osti, G., 2015. The Kongsfjorden Channel System offshore NW Svalbard: downslope sedimentary processes in a contour-current-dominated setting. *Arktos*. **1**, 17.
- Fournier, I., 2016. Rôle des facteurs de contrôle sur l'architecture et le fonctionnement sédimentaire des systèmes turbiditiques de l'océan Indien au cours du Cénozoïque: exemple des systèmes Rovuma-Rufiji et Gange-Brahmapoutre. Sciences de la Terre. (PhD thesis). Université de Bordeaux.
- Frederici, B., Seminara, G., 2003. On the convective nature of bar instability. *Journal of Fluid Mechanics*. **487**, 125–145.

- Gales, J.A., Larter, R.D., Mitchell, N.C., Dowdeswell, J.A., 2013. Geomorphic signature of Antarctic submarine gullies: implications for continental slope processes. *Marine Geology*. **337**, 112–124.
- Gales, J.A., Larter, R.D., Mitchell, N.C., Hillenbrand, C., Østerhus, S., Shoosmith, D.R., 2012. Southern Weddell Sea shelf edge geomorphology: implications for gully formation by the overflow of high-salinity water. *Journal of Geophysical Research*. **117**, F04021.
- Gales, J.A., Talling, P.J., Cartigny, M.J.B., Hughes Clarke, J., Lintern, G., Stacey, C., Clare, M.A., 2018. What controls submarine channel development and the morphology of deltas entering deep-water fjords? *Earth Surface Processes and Landforms*. **44**, 535–551.
- Gardner, J.V., 2010. The West Mariana Ridge, western Pacific Ocean: Geomorphology and processes from new multibeam data. *Geological Society of America Bulletin*. **122**, 1378–1388.
- Gardner, J.V., Mayer, L.A., 2005. U.S. Law of the Sea Cruise to Map the Foot of the Slope and 2500-m Isobath of the Gulf of Alaska Continental Margin. Cruise Report. University of New Hampshire (UNH), Center for Coastal and Ocean Mapping (CCOM)/Joint Hydrographic Center (JHC), p.111.
- Ghazi, S., Mountney, N.P., 2009. Facies and architectural element analysis of a meandering fluvial succession: The Permian Warchha Sandstone, Salt Range, Pakistan. *Sedimentary Geology*. **221**, 99–126.
- Gibson, S., Osorio, A., Creech, C., Amorim, R., Dirksen, M., Dahl, T., Koohafkan, M., 2019. Two pool-to-pool spacing periods on large sand-bed rivers: Mega-pools on the Madeira and Mississippi. *Geomorphology*. **328**, 196–210.
- Giorgio Serchi, F., Peakall, J., Ingham, D.B., Burns, A.D., 2011. A unifying computational fluid dynamics investigation on the river-like to river-reversed secondary circulation in submarine channel bends. *Journal of Geophysical Research*. **116**, C06012.
- Gorycki, M.A., 1973. Hydraulic drag: a meander-initiating mechanism. *Geological Society of America Bulletin*. **84**, 175–186.
- Griggs, G.B., Kulm, L.D., 1973. Origin and development of Cascadia deepsea channel. *Journal of Geophysical Research*. **78**, 6325–6339.
- Guiastrenec-Faugas, L., Gillet, H., Peakall, J., Dennielou, B., Gaillot, A., Silva Jacinto, R., 2021. Initiation and evolution of knickpoints and their role in cut-and-fill processes in active submarine channels. *Geology*. **49**, 314–319.
- Guiastrenec-Faugas, L., Gillet, H., Silva Jacinto, R., Dennielou, B., Hanquiez, V., Schmidt, S., Simplet, L., Rousset, A., 2020. Upstream migrating

knickpoints and related sedimentary processes in a submarine canyon from a rare 20-year morphobathymetric time-lapse (Capbreton submarine canyon, Bay of Biscay, France). *Marine Geology*. **423**, 106143.

Gulick, S.P.S., Lowe, L.A., Pavlis, T.L., Gardner, J.V., Mayer, L.A., 2007. Geophysical insights into the Transition fault debate: Propagating strike slip in response to stalling Yakutat block subduction in the Gulf of Alaska. *Geology*. **35**, 763–766.

Hampton, M.A., 1972. The role of subaqueous debris flow in generating turbidity currents. *Journal of Sedimentary Petrology*. **42**, 775–793.

Hansen, L., Janocko, M., Kane, I., Kneller, B., 2017. Submarine channel evolution, terrace development, and preservation of intra-channel thin-bedded turbidites: Mahin and Avon channels, offshore Nigeria. *Marine Geology*. **383**, 146–167.

Hansen, L.A.S., Callow, R.H.T., Kane, I.A., Gamberi, F., Rovere, M., Cronin, B.T., Kneller, B.C., 2015. Genesis and character of thin-bedded turbidites associated with submarine channels. *Marine and Petroleum Geology*. **67**, 852–879.

Harbor, J.M., Wheeler, D.A., 1992. On the mathematical description of glaciated valley cross sections. *Earth Surface Processes and Landforms*. **17**, 477–485.

Harris, P.T., Whiteway, T., 2011. Global distribution of large submarine canyons: Geomorphic differences between active and passive continental margins. *Marine Geology*. **285**, 69–86.

Heezen, B.C., Menzies, R.J., Schneider, E.D., Ewing, W.M., Granelli, N.C.I., 1964. Congo submarine canyon. *AAPG Bulletin*. **48**, 1126–1149.

Heijnen, M.S., Clare, M.A., Cartigny, M.J.B., Talling, P.J., Hage, S., Lintern, D.G., Stacey, C., Parsons, D.R., Simmons, S.M., Chen, Y., Sumner, E.J., Dix, J.K., Hughes Clarke, J.E., 2020. Rapidly-migrating and internally-generated knickpoints can control submarine channel evolution. *Nature Communications*. **11**, 3129.

Heiniö, P., Davies, R.J., 2007. Knickpoint migration in submarine channels in response to fold growth, western Niger Delta. *Marine and Petroleum Geology*. **24**, 434–449.

Hernández-Molina, F.J., Llave, E., Stow, D.A.V., García, M., Somoza, L., Vázquez, J.T., Lobo, F.J., Maestro, A., Díaz del Río, V., León, R., Medialdea, T., Gardner, J., 2006. The contourite depositional system of the Gulf of Cádiz: A sedimentary model related to the bottom current activity of the Mediterranean outflow water and its interaction with the continental margin. *Deep-Sea Research Part II*. **53**, 1420–1463.

- Hesse, R., Chough, S.K., 1980. The Northwest Atlantic Mid-Ocean Channel of the Labrador Sea: II. Deposition of parallel laminated levee-muds from the viscous sublayer of low density turbidity currents. *Sedimentology*. **27**, 697–711.
- Hesse, R., Chough, S.K., Rakofsky, A., 1987. The Northwest Atlantic Mid-Ocean Channel of the Labrador Sea. V. Sedimentology of a giant deep-sea channel. *Canadian Journal of Earth Sciences*. **24**, 1595–1624.
- Hey, R.D., Thorne, C.R., 1986. Stable channels with mobile gravel beds. *Journal of Hydraulic Engineering*. **112**, 671–689.
- Hiscott, R.N., 1994. Loss of capacity, not competence, as the fundamental process governing deposition from turbidity currents. *Journal of Sedimentary Research*. **64**, 209–214.
- Hodgson, D.M., Di Celma, C.N., Brunt, R.L., Flint, S.S., 2011. Submarine slope degradation and aggradation and the stratigraphic evolution of channel-levee systems. *Journal of the Geological Society*. **168**, 625–628.
- Hooke, J.M., 2004. Cutoffs Galore!: Occurrence and Causes of multiple Cutoffs on a Meandering River. *Geomorphology*. **61**, 225–238.
- Hooke, J.M., 2007. Spatial variability, mechanisms and propagation of change in an active meandering river. *Geomorphology*. **84**, 277–296.
- Hubbard, S.M., Covault, J. a., Fildani, A., Romans, B.W., 2014. Sediment transfer and deposition in slope channels: Deciphering the record of enigmatic deep-sea processes from outcrop. *Geological Society of America Bulletin*. **126**, 857–871.
- Hudson, P.F., 2002. Pool-Riffle morphology in an actively migrating alluvial channel: the Lower Mississippi River. *Physical Geography*. **23**, 154–169.
- Hughes Clarke, J.E., 2016. First wide-angle view of channelized turbidity currents links migrating cyclic steps to flow characteristics. *Nature Communications*. **7**, 11896.
- Idárraga-García, J., Douglas G. Masson, Jacqueline García, Hermann León, 2019. Architecture and development of the Magdalena Submarine Fan (southwestern Caribbean). *Marine Geology*. **414**, 18–33.
- Ikeda, S., Parker, G., Sawai, K., 1981. Bend theory of river meanders: part I, linear development.. *Journal of Fluid Mechanics*. **112**, 363–377.
- Imran, J., Islam, M.A., Huang, H., Kassem, A., Dickerson, J., Pirmez, C., Parker, G., 2007. Helical flow couplets in submarine gravity underflows. *Geology*. **35**, 659–662.

- Imran, J., Parker, G., Pirmez, C., 1999. A nonlinear model of flow in meandering submarine and subaerial channels. *Journal of Fluid Mechanics*. **400**, 295–331.
- Islam, M., Imran, J., 2008. Experimental modeling of gravity underflow in a sinuous submerged channel. *Journal of Geophysical Research*. **113**, C07041.
- Islam, M.A., Imran, J., Pirmez, C., Cantelli, A., 2008. Flow splitting modifies the helical motion in submarine channels. *Geophysical Research Letters*. **35**, L22603.
- Janocko, M., Nemec, W., Henriksen, S., Warchoř, M., 2013. The diversity of deep-water sinuous channel belts and slope valley-fill complexes. *Marine and Petroleum Geology*. **41**, 7–34.
- Jansen, J.H.F., Giresse, P., Moguedet, G., 1984. Structural and sedimentary geology of the Congo and Southern Gabon continental shelf; a seismic and acoustic reflection survey. *Netherlands Journal of Sea Research*. **17**, 364–384.
- Jegou, I., Savoye, B., Pirmez, C., Droz, L., 2008. Channel-mouth lobe complex of the recent Amazon Fan: the missing piece. *Marine Geology*. **252**, 62–77.
- Jerolmack, D.J., Mohrig, D., 2007. Conditions for branching in depositional rivers. *Geology*. **35**, 463–466.
- Jobe, Z.R., Howes, N.C., Auchter, N.C., 2016. Comparing submarine and fluvial channel kinematics: Implications for stratigraphic architecture. *Geology*. **44**, 931–934.
- Jobe, Z.R., Howes, N.C., Straub, K.M., Cai, D., Deng, H., Laugier, F.J., Pettinga, L.A., Shumaker, L.E., 2020. Comparing aggradation, superelevation, and avulsion frequency of submarine and fluvial channels. *Frontier Earth Science*. **8**, 53.
- Johnson, G.L., Vogt, P.R., Schneider, E.D., 1971. Morphology of the Northeastern Atlantic and Labrador Sea. *Deutsche Hydrographische Zeitschrift*. **24**, 49–73.
- Johnson, T.M., Heil, P.A., 1996. Uncertainty in estimating bankfull conditions. *Journal of The American Water Resources Association*. **32** 1283-, 1283–1291.
- Jolly, B.A., Whittaker, A.C., Lonergan, L., 2017. Quantifying the geomorphic response of modern submarine channels to actively growing folds and thrusts, deep-water Niger Delta. *Geological Society of America Bulletin*. **129**, 1123–1139.

- Kane, I.A., Hodgson, D.M., 2011. Sedimentological criteria to differentiate submarine channel levee subenvironments: exhumed examples from the Rosario Fm. (Upper Cretaceous) of Baja California, Mexico, and the Fort Brown Fm. (Permian), Karoo Basin, S. Africa. *Marine and Petroleum Geology*. **28**, 807–823.
- Kane, I.A., McCaffrey, W.D., Peakall, J., 2008. Controls on sinuosity evolution within submarine channels. *Geology*. **36**, 287.
- Kassem, A., Imran, J., 2004. Three-dimensional modeling of density current. II. Flow in sinuous confined and unconfined channels. *Journal of Hydraulic Research*. **42**, 591–602.
- Kasvi, E., Vaaja, M., Kaartinen, H., Kukko, A., Jaakkola, A., Flener, C., Hyyppä, H., Hyyppä, J., Alho, P., 2015. Sub-bend scale flow-sediment interaction of meander bends—a combined approach of field observations, close-range remote sensing and computational modelling. *Geomorphology*. **238**, 119–134.
- Keevil, G.M., Peakall, J., Best, J.L., 2007. The influence of scale, slope and channel geometry on the flow dynamics of submarine channels. *Marine and Petroleum Geology*. **24**, 487–503.
- Keevil, G.M., Peakall, J., Best, J.L., Amos, K.J., 2006. Flow structure in sinuous submarine channels: Velocity and turbulence structure of an experimental submarine channel. *Marine Geology*. **229**, 241–257.
- Keller, E.A., Melhorn, W.N., 1978. Rhythmic spacing and origin of pools and riffles: discussion. *Geological Society of America Bulletin*. **89**, 723–730.
- Kenyon, N.H., Amir, A., Cramp, A., 1995. Geometry of the younger sediment bodies of the Indus Fan. In: Pickering, K.T., Hiscott, R.N., Kenyon, N.H., Ricci Lucchi, F., Smith, R.D.A. (Eds.), *Atlas of Deep-Water Environments: Architectural Styles in Turbidite Systems*, Springer, pp. 89–93.
- Khripounoff, A., Vangriesheim, A., Babonneau, N., Crassous, P., Dennielou, B., Savoye, B., 2003. Direct observation of intense turbidity current activity in the Zaire submarine valley at 400 m water depth. *Marine Geology*. **194**, 151–158.
- Klaucke, I., Hesse, R., 1996. Fluvial features in the deep-sea: new insights from the glacial submarine drainage system of the Northwest Atlantic Mid-Ocean Channel in the Labrador Sea. *Sedimentary Geology*. **106**, 223–234.
- Klaucke, I., Hesse, R., Ryan, W.B.F., 1997. Flow parameters of turbidity currents in a low-sinuosity giant deep-sea channel. *Sedimentology*. **44**, 1093–1102.

- Klaucke, I., Hesse, R., Ryan, W.B.F., 1998a. Morphology and structure of a distal submarine trunk channel: The Northwest Atlantic Mid-Ocean Channel between lat 53°N and 44°30'N. *Geological Society of America Bulletin*. **110**, 22–34.
- Klaucke, I., Hesse, R., Ryan, W.B.F., 1998b. Seismic stratigraphy of the Northwest Atlantic Mid-Ocean Channel: growth pattern of a mid-ocean channel-levee complex. *Marine and Petroleum Geology*. **15**, 575–585.
- Kneller, B., 2003. The influence of flow parameters on turbidite slope channel architecture. *Marine and Petroleum Geology*. **20**, 901–910.
- Kneller, B., Buckee, C., 2000. The structure and fluid mechanics of turbidity currents: a review of some recent studies and their geological implications. *Sedimentology*. **47**, 62–94.
- Knighton, A.D., 1981. Asymmetry of river channel cross-sections: part I. quantitative indices. *Earth Surface Processes and Landforms*. **6**, 581–588.
- Knighton, A.D., 1982. Asymmetry of river channel cross-sections: part II. mode of development and local variation. *Earth Surface Processes and Landforms*. **7**, 117–131.
- Kolla, V., 2007. A review of sinuous channel avulsion patterns in some major deep-sea fans and factors controlling them. *Marine and Petroleum Geology*. **24**, 450–469.
- Kolla, V., A. Bandyopadhyay, P. Gupta, B. Mukherjee, D. Ramana, 2012. Morphology and internal structure of a recent upper Bengal Fan-Valley Complex. In: Prather, B.E., Deptuck, M.E., Mohrig, D., van Hoorn, B., Wynn, R.B. (Eds.), *Application of the Principles of Seismic Geomorphology to Continental-Slope and Base-of-Slope Systems: Case Studies from Seafloor and Near-Seafloor Analogues*, Special Publication No. 99. SEPM Society for Sedimentary Geology, pp. 347–369.
- Kolla, V., Bourges, P., Urruty, J.-M., Safa, P., 2001. Evolution of deep-water Tertiary sinuous channels offshore Angola (west Africa) and implications for reservoir architecture. *AAPG Bulletin*. **85**, 1373–1405.
- Kolla, V., Buffier, R.T., 1984. Morphologic, acoustic, and sedimentologic characteristics of the Magdalena Fan. *Geo-Marine Letters*. **3**, 85–91.
- Kolla, V., Coumes, F., 1987. Morphology, internal structure, seismic stratigraphy, and sedimentation of Indus Fan. *AAPG Bulletin*. **71**, 34.
- Kolla, V., Posamentier, H.W., Wood, L.J., 2007. Deep-water and fluvial sinuous channels-Characteristics, similarities and dissimilarities, and modes of formation. *Marine and Petroleum Geology*. **24**, 388–405.

- Konsoer, K., Zinger, J., Parker, G., 2013. Bankfull hydraulic geometry of submarine channels created by turbidity currents: Relations between bankfull channel characteristics and formative flow discharge. *Journal of Geophysical Research*. **118**, 216–228.
- Kostaschuk, R.A., Luternauer, J. L., McKenna, G.T., Moslow, T.F., 1992. Sediment transport in a submarine channel system; Fraser River delta, Canada. *Journal of Sedimentary Research*. **62**, 273–282.
- Kristoffersen, Y., Sorokin, M.Y., Jokat, W., Svensson, O., 2004. A submarine fan in the Amundsen Basin, Arctic Ocean. *Marine Geology*. **204**, 317–324.
- Kudrass, H.R., Michels, K.H., Wiedicke, M., Suckow, A., 1998. Cyclones and tides as feeders of a submarine canyon off Bangladesh. *Geology*. **26**, 715–718.
- Kuenen, P.H., 1966. Matrix of turbidites: experimental approach. *Sedimentology*. **7**, 267–297.
- Lagasse, P.F., Spitz, W.J., Zevenberger, L.W., Zachmann, D.W., 2004. Handbook for predicting stream meander migration (No. 533). National Cooperative Highway Research Program, p.328.
- Lastras, G., Arzola, R.G., Masson, D.G., Wynn, R.B., Huvenne, V.A.I., Hühnerbach, V., Canals, M., 2009. Geomorphology and sedimentary features in the Central Portuguese submarine canyons, Western Iberian margin. *Geomorphology*. **103**, 310–329.
- Lee, G.H., Watkins, J.S., Bryant, W.R., 1996. Bryant Canyon fan system: An unconfined, large river-sourced system in the northwestern Gulf of Mexico. *AAPG Bulletin*. **80**, 340–358.
- Leeder, M.R., 1973. Fluvial fining-upwards cycles and the magnitude of palaeochannels. *Geological Magazine*. **110**, 265–276.
- Lemay, M., Jean-Louis Grimaud, Isabelle Cojan, Jacques Rivoirard, Fabien Ors, 2020. Geomorphic variability of submarine channelized systems along continental margins: Comparison with fluvial meandering channels. *Marine and Petroleum Geology*. **115**, 104295.
- Leopold, L.B., 1982. Water surface topography in river channels and implications for meander development. John Wiley, Gravel-Bed Rivers, pp. 359–383. In: Hey, R.D., Bathurst, J.C., Wiley, T. (Eds.), *Gravel-Bed Rivers*. John Wiley, pp. 359–383.
- Leopold, L.B., 1994. A view of the river. Harvard University Press, p. 289.



- Leopold, L.B., Maddock, T., 1953. The Hydraulic Geometry of Stream Channels and Some Physiographic Implications. *U.S. Government Printing Office*. **252**, 57.
- Leopold, L.B., Wolman, M.G., 1960. River meanders. *Geological Society of America Bulletin*. **71**, 769–794.
- Lewis, K.B., 1994. The 1500-km-long Hikurangi Channel: Trench-axis channel that escapes its trench, crosses a plateau, and feeds a fan drift. *Geo-Marine Letters*. **14**, 19.
- Lewis, K.B., Collot, J.-Y., Lallemand, S.E., 1998. The dammed Hikurangi Trough: a channel-fed trench blocked by subduction seamounts and their wake avalanches (New Zealand-France GeodyNZ Project). *Basin Research*. **10**, 441–468.
- Lewis, K.B., Pantin, H.M., 2002. Channel-axis, overbank and drift sediment waves in the southern Hikurangi Trough, New Zealand. *Marine Geology*. **192**, 123–151.
- Lowe, D.R., 1979. Sediment gravity flows: their classification and some problems of application to natural flows and deposits. In: Doyle, L.J., Pilkey Jr., O.H. (Eds.), *Geology of Continental Slopes, Special Publication No. 27*. SEPM Society for Sedimentary Geology, pp. 75–82.
- Luchi, R., Bolla Pittaluga, M., Seminara, G., 2012. Spatial width oscillations in meandering rivers at equilibrium. *Water Resources Research*. **48**, W05551.
- Luchi, R., Hooke, J.M., Zolezzi, G., Bertoldi, W., 2010. Width variations and mid-channel bar inception in meanders: River Bollin (UK). *Geomorphology*. **119**, 1–8.
- Luchi, R., Zolezzi, G., Tubino, M., 2011. Bend theory of river meanders with spatial width variations. *Journal of Fluid Mechanics*. **681**, 311–339.
- Maier, K.L., Fildani, A., McHargue, T.R., Paull, C.K., Graham, S.A., Caress, D.W., 2012. Punctuated deep-water channel migration: high resolution subsurface data from the LUCIA Chica Channel System, offshore California, U.S.A.. *Journal of Sedimentary Research*. **82**, 1–8.
- Maier, K.L., Fildani, A., Paull, C.K., McHargue, T.R., Graham, S.A., Caress, D.W., 2013. Deep-sea channel evolution and stratigraphic architecture from inception to abandonment from high-resolution Autonomous Underwater Vehicle surveys offshore central California. *Sedimentology*. **60**, 935–960.
- Markham, A.J., Thorne, C.R., 1992. Geomorphology of gravel-bed river bends. In: Billi, P., Hey, R.D., Thorne, C.R., Tacconi, P. (Eds.), *Dynamics of Gravel-Bed Rivers*. John Wiley & Sons, Chichester, pp. 433–456.

- Marsset, T., Droz, L., Dennielou, B., Pichon, E., 2009. Cycles in the architecture of the Quaternary Zaire Turbidite System: a possible link with climate. In: Kneller, B., Martinsen, O.J., McCaffrey, B. (Eds.), *External Controls on Deep-Water Depositional Systems, Special Publication No. 92*. SEPM Society for Sedimentary Geology, Tulsa, pp. 89–106.
- Matsubara, Y., Howard, A.D., 2014. Modeling planform evolution of a mud-dominated meandering river: Quinn River, Nevada, USA. *Earth Surface Processes and Landforms*. **39**, 1365–1377.
- Mayall, M., Jones, E., Casey, M., 2006. Turbidite channel reservoirs-Key elements in facies prediction and effective development. *Marine and Petroleum Geology*. **23**, 821–841.
- McArthur, A.D., Tek, D.E., 2021. Controls on the origin and evolution of deep-ocean trench-axial channels. *Geology*. **49**, 883–888.
- Meiburg, E., Kneller, B., 2010. Turbidity Currents and Their Deposits. *Annual Review of Fluid Mechanics*. **42**, 135–156.
- Menard, H.W., 1955. Deep-Sea channels, topography, and sedimentation. *AAPG Bulletin*. **39**, 236–255.
- Micallef, A., Mountjoy, J.J., 2011. A topographic signature of a hydrodynamic origin for submarine gullies. *Geology*. **39**, 115–118.
- Micheli, E.R., Larse, E.W., 2010. River channel cutoff dynamics, Sacramento River, California, USA. *River Research Application*. **27**, 328–344.
- Middleton, G.V., Hampton, M.A., 1973. Part I. Sediment gravity flows: mechanics of flow and deposition. In: Middleton, G.V., Bouma, A.H. (Eds.), *Turbidity and Deep Water Sedimentation, Pacific Section, Short Course Lecture Notes*. SEPM, Anaheim, California, pp. 1–38.
- Migeon, S., Savoye, B., Babonneau, N., Spy-Andersson, F.-L., 2004. Processes of sediment-wave construction along the present Zaire deep-sea meandering channel: Role of meanders and flow stripping. *Journal of Sedimentary Research*. **74**, 580–598.
- Milliman, J.D., Meade, R.H., 1983. World-Wide Delivery of River Sediment to the Oceans. *The Journal of Geology*. **91**, 1–21.
- Mishra, R., Pandey, D.K., Ramesh, P., Clift, P.D., 2016. Identification of new deep sea sinuous channels in the eastern Arabian Sea. *Springer Plus*. **5**, 1–18.
- Mohrig, D., Buttles, J., 2007. Deep turbidity currents in shallow channels. *Geology*. **35**, 155–158.

- Montgomery, D.R., 1995. Pool spacing in forest channels. *Water Resources Research*. **31**, 1097–1105.
- Montgomery, D.R., Gran, K.B., 2001. Downstream variations in the width of bedrock channels. *Water Resources Research*. **37**, 1841–1846.
- Morris, E.A., Hodgson, D.M., Brunt, R.L., Flint, S.S., 2014a. Origin, evolution and anatomy of silt-prone submarine external levées. *Sedimentology*. **61**, 1734–1763.
- Morris, E.A., Hodgson, D.M., Flint, S.S., Brunt, R.L., Butterworth, P.J., Verhaeghe, J., 2014b. Sedimentology, stratigraphic architecture, and depositional context of submarine frontal-lobe complexes. *Journal of Sedimentary Research*. **84**, 763–780.
- Mulder, T., Alexander, J., 2001. The physical character of subaqueous sedimentary density flows and their deposits. *Sedimentology*. **48**, 269–299.
- Murray, A.B., Paola, C., 1994. A cellular model of braided rivers. *Nature*. **371**, 54–57.
- Mutti, E., Normark, W.R., 1987. Comparing examples of modern and ancient turbidite systems: problems and concepts. In: Leggett, J.K., Zuffa, G.G. (Eds.), *Marine Clastic Sedimentology*. Springer, Dordrecht, pp. 1–38.
- Nakajima, T., Kneller, B.C., 2013. Quantitative analysis of the geometry of submarine external levées. *Sedimentology*. **60**, 877–910.
- Nakajima, T., Peakall, J., McCaffrey, W.D., Paton, D.A., Thompson, P.J.P., 2009. Outer-bank bars: a new intra-channel architectural element within sinuous submarine slope channels. *Journal of Sedimentary Research*. **79**, 872–886.
- Nakajima, T., Satoh, M., 2001. The formation of large mudwaves by turbidity currents on the levees of the Toyama Deep-Sea Channel, Japan Sea. *Sedimentology*. **48**, 435–463.
- Nakajima, T., Satoh, M., Okamura, Y., 1998. Channel-levee complexes , terminal deep-sea fan and sediment wave fields associated with the Toyama Deep-Sea Channel system in the Japan Sea. *Marine Geology*. **147**, 25–41.
- Nanson, G.C., 1980. Point bar and floodplain formation of the meandering Beaton River, northeastern British Columbia, Canada. *Sedimentology*. **27**, 3–29.
- Nanson, G.C., Hickin, E.J., 1983. Channel migration and incision on the Beaton River. *Journal of Hydraulic Engineering*. **109**, 327–337.

- Navratil, O., Albert, M.-B., Hérouin, E., Gresillon, J.M., 2006. Determination of bankfull discharge magnitude and frequency: comparison of methods on 16 gravel-bed. *Earth Surface Processes and Landforms*. **31**, 1345–1363.
- Nelson, H., 1976. Late Pleistocene and Holocene depositional trends, processes, and history of Astoria deep-sea fan, Northeast Pacific. *Marine Geology*. **20**, 129–173.
- Nelson, J.M., Smith, J.D., 1989. Evolution and stability of erodible channel beds. In: Ikeda, S., Parker, G. (Eds.), *River Meandering, Water Resources Monograph*. American Geophysical Union, pp. 321–377.
- Nelson, P.A., Brew, A.K., Morgan, J.A., 2015. Changes in Sediment Supply. *Water Resources Research*. **51**, 5717–5734.
- Ness, G.E., Kulm, L.D., 1973. Origin and Development of Surveyor Deep-Sea Channel. *Geological Society of America Bulletin*. **84**, 3339–3354.
- Ó Cofaigh, C., Dowdeswell, J.A., Kenyon, N.H., 2006. Geophysical investigations of a high-latitude submarine channel system and associated channel-mouth lobe in the Lofoten Basin, Polar North Atlantic. *Marine Geology*. **226**, 41–50.
- O’Connell, S., Alonso, B., Kastens, K.A., Maldonado, A., Malinverno, A., Nelson, C.H., Palanques, A., Ryan, W.B.F., 1985. Morphology and downslope sediment displacement in a deep-sea valley, the Valencia Valley (Northwestern Mediterranean). *Geo-Marine Letters*. **5**, 149–156.
- Okino, K., Kasuga, S., Ohara, Y., 1998. A new scenario of the Parece Vela Basin genesis. *Marine Geophysical Researches*. **20**, 21–40.
- Ortiz-Karpf, A., Hodgson, D.M., McCaffrey, W.D., 2015. The role of mass-transport complexes in controlling channel avulsion and the subsequent sediment dispersal patterns on an active margin: the Magdalena Fan, offshore Colombia. *Marine and Petroleum Geology*. **64**, 58–75.
- Osterkamp, W.R., Hedman, E.R., 1977. Variation of width and discharge for natural high-gradient stream channels. *Water Resources Research*. **13**, 256–258.
- Page, K.J., Nanson, G.C., Frazier, P.S., 2003. Floodplain formation and sediment stratigraphy resulting from oblique accretion on the Murrumbidgee River, Australia. *Journal of Sedimentary Research*. **73**, 5–14.
- Palm, F.A., Peakall, J., Hodgson, D.M., Marsset, T., Silva Jacinto, R., Dennielou, B., Babonneau, N., Wright, T.J., 2021. Width variation around submarine channel bends: Implications for sedimentation and channel evolution. *Marine Geology*. **437**, 106504.

- Parker, G., Sawai, K., Ikeda, S., 1982. Bend theory of river meanders. Part 2. nonlinear deformation of finite-amplitude bends. *Journal of Fluid Mechanics*. **115**, 303–314.
- Parker, G., Shimizu, Y., Wilkerson, G.V., Eke, E.C., Abad, J.D., Lauer, J.W., Paola, C., Dietrich, W.E., Voller, V.R., 2011. A new framework for modeling the migration of meandering rivers. *Earth Surface Processes and Landforms*. **36**, 70–86.
- Parsons, D.R., Peakall, J., Aksu, A.E., Flood, R.D., Hiscott, R.N., Beşiktepe, Ş., Moulard, D., 2010. Gravity-driven flow in a submarine channel bend: direct field evidence of helical flow reversal. *Geology*. **38**, 1063–1066.
- Pattyn, F., Van Huele, W., 1998. Power Law or Power Flaw? *Earth Surface Processes and Landforms*. **23**, 761–767.
- Paull, C.K., Caress, D.W., Lundsten, E., Gwiazda, R., Anderson, K., McGann, M., Conrad, J., Edwards, B., Sumner, E.J., 2013. Anatomy of the La Jolla Submarine Canyon system; offshore southern California. *Marine Geology*. **335**, 16–34.
- Peakall, J., Amos, K.J., Keevil, G.M., Bradbury, P.W., Gupta, S., 2007. Flow processes and sedimentation in submarine channel bends. *Marine and Petroleum Geology*. **24**, 470–486.
- Peakall, J., McCaffrey, B., Kneller, B., 2000a. A process model for the evolution, morphology, and architecture of sinuous submarine channels. *Journal of Sedimentary Research*. **70**, 434–448.
- Peakall, J., McCaffrey, W.D., Kneller, B.C., Stelting, C.E., McHargue, T.R., Schweller, W.J., 2000b. A process model for the evolution of submarine fan channels: implications for sedimentary architecture. In: *Bouma, A.H., Stone, C.G. (Eds.), Fine-Grained Turbidite Systems, AAPG Memoir 72*. American Association of Petroleum Geologists, pp. 73–87.
- Peakall, J., Sumner, E.J., 2015. Submarine channel flow processes and deposits: a process-product perspective. *Geomorphology*. **244**, 95–120.
- Peakall, J., Wells, M.G., Cossu, R., Kane, I.A., Masson, D.G., Keevil, G.M., Mccaffrey, W., Corney, R., 2012. Global (latitudinal) variation in submarine channel sinuosity. *Geology*. **40**, 11–14.
- Peakall, J., Wells, M.G., Cossu, R., Kane, I.A., Masson, D.G., Keevil, G.M., Mccaffrey, W., Corney, R., 2013. Global (latitudinal) variation in submarine channel sinuosity: REPLY. *Geology*. **41**, e288.
- Peters, H., Johns, W.E., Bower, A.S., Fratantoni, D.M., 2005. Mixing and entrainment in the Red Sea outflow plume. Part I: plume structure. *Journal of Physical Oceanography*. **35**, 569–583.

Pettinga, L., Jobe, Z., Shumaker, L., Howes, N., 2018. Morphometric scaling relationships in submarine channel-lobe systems. *Geology*. **46**, 819–822.

Pickering, K.T., Hiscott, R.N., 2015. Deep Marine Systems: Processes, Deposits, Environments, Tectonics and Sedimentation. American Geophysical Union, Chichester, p. 672.

Pickering, K.T., Underwood, M.B., Saito, S., Naruse, H., Kutterolf, S., Scudder, R., Park, J.-O., Moore, G.F., Slagle, A., 2013. Depositional architecture, provenance, and tectonic/eustatic modulation of Miocene submarine fans in the Shikoku Basin: Results from Nankai Trough Seismogenic Zone experiment. *Geochemistry, Geophysics, Geosystems*. **14**, 1722–1739.

Pickup, G., Warner, R.F., 1976. Effects of hydrologic regime on magnitude and frequency of dominant discharge. *Journal of Hydrology*. **29**, 51–75.

Picot, M., Droz, L., Marsset, T., Dennielou, B., Bez, M., 2016. Controls on turbidite sedimentation: Insights from a quantitative approach of submarine channel and lobe architecture (Late Quaternary Congo Fan). *Marine and Petroleum Geology*. **72**, 423–446.

Picot, M., Marsset, T., Droz, L., Dennielou, B., Baudin, F., Hermoso, M., de Rafelis, M., Sionneau, T., Cremer, M., Laurent, D., Bez, M., 2019. Monsoon control on channel avulsions in the Late Quaternary Congo Fan. *Quaternary Science Reviews*. **204**, 149–171.

Piper, D.J.W., Deptuck, M., 1997. Fine-grained turbidites of the Amazon Fan: facies characterization and interpretation. In: Flood, R.D., Piper, D.J.W., Klaus, A., Peterson, L.C. (Eds.), *Proceeding of the Ocean Drilling Program, Initial Reports 155*. Ocean Drilling Program, College Station, Texas, pp. 79–108.

Piper, D.J.W., Kontopoulos, N., Anagnostou, C., Chronis, G., Panagos, A.G., 1990. Modern Fan Deltas in the Western Gulf of Corinth, Greece. *Geo-Marine Letters*. **10**, 5–12.

Piper, D.J.W., Normark, W.R., 1983. Turbidite depositional patterns and flow characteristics, Navy Submarine Fan, California Borderland. *Sedimentology*. **30**, 681–694.

Piper, D.J.W., Normark, W.R., 2001. Sandy fans-from Amazon to Hueneme and beyond. *AAPG Bulletin*. **85**, 1407–1438.

Piper, D.J.W., Normark, W.R., 2009. Processes that initiate turbidity currents and their influence on turbidites: a marine geology perspective. *Journal of Sedimentary Research*. **79**, 347–362.

Pirmez, C., Beaubouef, R.T., Friedmann, S.J., Mohrig, D.C., 2000. Equilibrium profile and baselevel in submarine channels: examples from late Pleistocene systems and implications for the architecture of deepwater reservoirs. In: Weimer, P. (Ed.), *Deep Water Reservoirs of the World, Special Publication No. 20*. SEPM Society for Sedimentary Geology, pp. 782–805.

Pirmez, C., Flood, R.D., 1995. Morphology and structure of Amazon Channel. In: Flood, R.D., Piper, D.J.W., Klaus, A., Peterson, L.C. (Eds.), *Proceeding of the Ocean Drilling Program, Initial Reports 155*. Ocean Drilling Program, College Station, Texas, pp. 23–45.

Pirmez, C., Imran, J., 2003. Reconstruction of turbidity currents in Amazon Channel. *Marine and Petroleum Geology*. **20**, 823–849.

Pope, E.L., Normandeau, A., Ó Cofaigh, C., Stokes, C.R., Talling, P.J., 2019. Controls on the formation of turbidity current channels associated with marine-terminating glaciers and ice sheets. *Marine Geology*. **415**, 105951.

Pope, E.L., Talling, P., Carter, L., 2017. Which earthquakes trigger damaging submarine mass movements: insights from a global record of submarine cable breaks? *Marine Geology*. **384**, 131–146.

Posamentier, H.W., 2003. Depositional elements associated with a basin floor channel-levee system: case study from the Gulf of Mexico. *Marine and Petroleum Geology*. **20**, 677–690.

Posamentier, H.W., Kolla, V., 2003. Seismic geomorphology and stratigraphy of depositional elements in deep-water settings. *Journal of Sedimentary Research*. **73**, 367–388.

Prélat, A., Covault, J.A., Hodgson, D.M., Fildani, A., Flint, S.S., 2010. Intrinsic controls on the range of volumes, morphologies and dimensions of submarine lobes. *Sedimentary Geology*. **232**, 66–76.

Pyles, D.R., Tomasso, M., Jennette, David C., 2012. Flow processes and sedimentation associated with erosion and filling of sinuous submarine channels. *Geology*. **40**, 143–146.

Reading, H.G., Richards, M., 1994. Turbidite systems in deep-water basin margins classified by grain size and feeder system 1. *AAPG Bulletin*. **78**, 792–822.

Rebesco, M., Hernández-Molina, F.J., Van Rooij, D., Wåhlin, A., 2014. Contourites and associated sediments controlled by deep-water circulation processes: state-of-the-art and future considerations. *Marine Geology*. **352**, 111–154.

Reece, R.S., Gulick, S.P.S., Christeson, G.L., Horton, B.K., Avendonk, H.V., Barth, G., 2013. The role of far field tectonic stress in oceanic intraplate

deformation, Gulf of Alaska. *Journal of Geophysical Research*. **118**, 1862–1872.

Reece, R.S., Gulick, S.P.S., Horton, B.K., Christeson, G.L., Worthington, L.L., 2011. Tectonic and climatic influence on the evolution of the Surveyor Fan and Channel system, Gulf of Alaska. *Geosphere*. **7**, 830–844.

Reimchen, A.P., Hubbard, S.M., Stright, L., Romans, B.W., 2016. Using sea-floor morphometrics to constrain stratigraphic models of sinuous submarine channel systems. *Marine and Petroleum Geology*. **77**, 92–115.

Richards, K.S., 1976. The morphology of riffle-pool sequences. *Earth Surface Processes*. **1**, 71–88.

Richards, K.S., 1982. Rivers: Form and Process in Alluvial Channels. *Methuen, London*. p. 358.

Richards, K.S., Bowman, M., Reading, H.G., 1998. Submarine-fan systems I: characterization and stratigraphic prediction. *Marine and Petroleum Geology*. **15**, 689–717.

Romero-Otero, G.A., Slatt, R.M., Pirmez, C., 2015. Evolution of the Magdalena Deepwater Fan in a tectonically active setting, Offshore Colombia. In: Bartolini, C., Mann, P. (Eds.), *Petroleum Geology and Potential of the Colombian Caribbean Margin, AAPG Memoir 108*. American Association of Petroleum Geologists, pp. 675–707.

Rossi, C.E., 2012. Developing hydraulic relationships at the riffle crest thalweg in gravel bed streams (Master of Science). Humboldt State University.

Rozovskii, I.L., 1957. Flow of Water in Bends of Open Channels. Acad. of Sci. of the Ukrainian SSR, Israel Prog. Sci. Translations, Jerusalem.

Russell, C.E., 2017. Prediction of sedimentary architecture and lithological heterogeneity in fluvial point-bar deposits (PhD thesis). University of Leeds.

Russell, C.E., Mountney, N.P., Hodgson, D.M., Colombera, L., 2019. A novel approach for prediction of lithological heterogeneity in fluvial point-bar deposits from analysis of meander morphology and scroll-bar pattern.. In: Ghinassi, M., Colombera, L., Mountney, N.P., Reesink, A.J.H., Bateman, M. (Eds.), *Fluvial Meanders and Their Sedimentary Products in the Rock Record*. John Wiley & Sons Ltd., Chichester, UK, pp. 385–417.

Savoye, B., Babonneau, N., Dennielou, B., Bez, M., 2009. Geological overview of the Angola–Congo margin, the Congo deep-sea fan and its submarine valleys. *Deep Sea Research Part II*. **56**, 2169–2182.

Schumm, S.A., 1963. Sinuosity of alluvial rivers on the Great Plains. *Geological Society of America Bulletin*. **74**, 1089–1100.



- Schweller, W.J., Kulm, L.D., 1977. Depositional pattern and channelized sedimentation in active Eastern Pacific trenches. *In: Stanley, D.J., Kelling, G. (Eds.), Sedimentation in Submarine Canyons, Fans, and Trenches*. Dowden, Hutchinson & Ross, Stroudsburg, pp. 311–324.
- Schwenk, T., Spieß, V., Breitzke, M., Hübscher, C., 2005. The architecture and evolution of the Middle Bengal Fan in vicinity of the active channel-levee system imaged by high-resolution seismic data. *Marine and Petroleum Geology*. **22**, 637–656.
- Schwenk, T., Spieß, V., Hübscher, C., Breitzke, M., 2003. Frequent channel avulsions within the active channel-levee system of the middle Bengal Fan: an exceptional channel-levee development derived from Parasound and Hydrosweep data. *Deep-Sea Research Part II*. **50**, 1023–1045.
- Seminara, G., Tubino, M., 1989. Alternate bars and meandering: free, forced and mixed interactions. *Water Resource Management*. **12**, 267–320.
- Shepard, F.P., 1973. *Submarine Geology*. Harper & Row, New York, p.517.
- Shepard, F.P., Emery, K.O., 1973. Congo Submarine Canyon and Fan Valley. *AAPG Bulletin*. **57**, 1679–1691.
- Shimamura, K., 1989. Topography and sedimentary facies of the Nankai Deep Sea Channel. *In: Taira, A., Masuda, F. (Eds.), Sedimentary Facies in the Active Plate Margin*. pp. 529–556.
- Showers, W.J., Bevis, M., 1988. Amazon cone isotopic stratigraphy: evidence for the source of the tropical freshwater spike.. *Palaeogeography, Palaeoclimatology, Palaeoecology*. **64**, 189–199.
- Shumaker, L.E., Jobe, Z.R., Johnstone, S.A., Pettinga, L.A., Cai, D., Moody, J.D., 2018. Controls on submarine channel-modifying processes identified through morphometric scaling relationships. *Geosphere*. **14**, 2171–2187.
- Snyder, N.P., Whipple, K.X., Tucker, G.E., Merritts, D.J., 2003. Channel response to tectonic forcing: Field analysis of stream morphology and hydrology in the Mendocino triple junction region, northern California. *Geomorphology*. **53**, 97–127.
- Stern, R.J., 2010. The anatomy and ontogeny of modern intra-oceanic arc systems. *In: Pankhurst, B. (Ed.), The Evolving Continents: Understanding Processes of Continental Growth, Special Publications No. 338*. Geological Society, London, pp. 7–34.
- Stevenson, C.J., Feldens, P., Georgiopoulou, A., Schönke, M., Krastel, S., Piper, D.J.W., Lindhorst, K., Mosher, D., 2018. Reconstructing the sediment concentration of a giant submarine gravity flow. *Nature Communications*. **9**, 2616.

Stevenson, C.J., Talling, P.J., Wynn, R.B., Masson, D.G., Hunt, J.E., Frenz, M., Akhmetzhanov, A., Cronin, B.T., 2013. The flows that left no trace: very large-volume turbidity currents that bypassed sediment through submarine channels without eroding the sea floor. *Marine and Petroleum Geology*. **41**, 186–205.

Stow, D.A.V., Hernández-Molina, F.J., Llave, E., Bruno, M., García, M., Díaz del Rio, V., Somoza, L., Brackenridge, R.E., 2013. The Cadiz Contourite Channel: sandy contourites, bedforms and dynamic current interaction. *Marine Geology*. **343**, 99–114.

Straub, K.M., Mohrig, D., Buttles, J., McElroy, B., Pirmez, C., 2011. Quantifying the influence of channel sinuosity on the depositional mechanics of channelized turbidity currents: a laboratory study. *Marine and Petroleum Geology*. **28**, 744–760.

Straub, K.M., Mohrig, D., McElroy, B., Buttles, J., Pirmez, C., 2008. Interactions between turbidity currents and topography in aggrading sinuous submarine channels: a laboratory study. *Geological Society of America Bulletin*. **120**, 368–385.

Straub, K.M., Mohrig, D., Pirmez, C., 2012. Architecture of an aggradational tributary submarine-channel network on the continental slope offshore Brunei Darussalam.. In: Prather, P.E., Deptuck, M.E., Mohrig, D., van Hoorn, B., Wynn, R.B. (Eds.), *Application of the Principles of Aeismic Geomorphology to Continental-Slope and Base-of-Slope Systems: Case Studies from Seafloor and Near-Seafloor Analogues*, Special Publication No. 98. SEPM Society for Sedimentary Geology, pp. 13–30.

Sumner, E.J., Peakall, J., Dorrell, R.M., Parsons, D.R., Darby, S.E., Wynn, R.B., McPhail, S.D., Perrett, J., Webb, A., White, D., 2014. Driven around the bend: Spatial evolution and controls on the orientation of helical bend flow in a natural submarine gravity current. *Journal of Geophysical Research*. **119**, 898–913.

Suter, J.R., Berryhill, H.L., 1985. Late Quaternary shelf-margin deltas, northwest Gulf of Mexico. *AAPG Bulletin*. **69**, 77–91.

Svensson, H., 1959. Is the cross-section of a glacial valley a parabola? *Journal of Glaciology*. **3**, 362–363.

Swartz, J.M., Gullick, S.P.S., Goff, J.A., 2015. Gulf of Alaska continental slope morphology: Evidence for recent trough mouth fan formation. *Geochemistry, Geophysics, Geosystems*. **16**, 165–177.

Sylvester, Z., Covault, J.A., 2016. Development of cutoff-related knickpoints during early evolution of submarine channels. *Geology*. **44**, 835–838.

Sylvester, Z., Deptuck, M.E., Prather, B.E., Pirmez, C., O'Byrne, C., 2012. Seismic stratigraphy of a shelf-edge delta and linked submarine channels in the northeastern Gulf of Mexico. In: Prather, P.E., Deptuck, M.E., Mohrig, D., Van Hoorn, B., Wynn, R.B. (Eds.), *Application of the Principles of Seismic Geomorphology to Continental Slope and Base-of-Slope Systems: Case Studies from SeaFloor and Near-Sea Floor Analogues*, Special Publication No. 99. SEPM Society for Sedimentary Geology, pp. 31–59.

Sylvester, Z., Durkin, P., Covault, J.A., 2019. High curvatures drive river meandering. *Geology*. **47**, 263–266.

Sylvester, Z., Pirmez, C., Cantelli, A., 2011. A model of submarine channel-levee evolution based on channel trajectories: Implications for stratigraphic architecture. *Marine and Petroleum Geology*. **28**, 716–727.

Talling, P.J., Masson, D.G., Sumner, E.J., Malgesini, G., 2012. Subaqueous sediment density flows: depositional processes and deposit types. *Sedimentology*. **59**, 1937–2003.

Thompson, A., 1986. Secondary flows and the riffle-pool unit: a case study of the processes of meander development. *Earth Surface Processes and Landforms*. **11**, 631–641.

Thornburg, T.M., Kulm, L.D., 1987. Sedimentation in the Chile Trench: Depositional morphologies, lithofacies, and stratigraphy. *Geological Society of America Bulletin*. **98**, 33–52.

Thorne, C., Zevenbergen, L., Pitlick, J., Rais, S., Bradley, J.B., Julien, P.Y., 1985. Direct measurements of secondary currents in a meandering sand-bed river. *Nature*. **315**, 746–747.

Tinkler, K.J., 1970. Pools, riffles, and meanders. *Geological Society of America Bulletin*. **81**, 547–552.

Traer, M.M., Fildani, A., Fringer, O., McHargue, T., Hilley, G.E., 2018a. Turbidity current dynamics: 1. Model formulation and identification of flow equilibrium conditions resulting from flow stripping and overspill. *Journal of Geophysical Research*. **123**, 501–519.

Traer, M.M., Fildani, A., Fringer, O., McHargue, T., Hilley, G.E., 2018b. Turbidity current dynamics: 2. Simulating flow evolution toward equilibrium in idealized channels. *Journal of Geophysical Research*. **123**, 520–534.

Tripsanas, E.K., Bryant, W.R., Slowey, N.C., Bouma, A.H., Karageorgis, A.P., Berti, D., 2007. Sedimentological history of Bryant Canyon area, northwest Gulf of Mexico, during the last 135 kyr (Marine Isotope Stages 1–6): A proxy record of Mississippi River discharge. *Palaeogeography, Palaeoclimatology, Palaeoecology*. **246**, 137–161.

- Trush, W.J., McBain, S.M., Leopold, L.B., 2000. Attributes of an alluvial river and their relation to water policy and management. *Proceedings of the National Academy of Sciences of the United States of America*. **97**, 11858–11863.
- Twichell, D.C., H. Nelson, John E. Damuth, 2000. Late-stage development of the Bryant Canyon turbidite pathway on the Louisiana Continental Slope. *In: GCSSEPM Foundation 20th Annual Research Conference*. Curran, Red Hook, NY, pp. 1032–1044.
- Van de Lageweg, W.I., Van Dijk, W.M., Baar, A.W., Rutten, J., Kleinhans, M.G., 2014. Bank pull or bar push: What drives scroll-bar formation in meandering rivers? *Geology*. **42**, 319–322.
- Van den Berg, J.H., 1995. Prediction of alluvial channel pattern of perennial rivers. *Geomorphology*. **12**, 259–279.
- Van Weering, T.C.E., van Iperen, J., 1984. Fine-grained sediments of the Zaire deep-sea fan, southern Atlantic Ocean. *In: Stow, D.A.V., Piper, D.J.W. (Eds.), Fine-Grained Sediments: Deep-Water Processes and Facies, Special Publications No. 15.* Geological Society, London, pp. 95–113.
- Vangriesheim, A., Khripounoff, A., Crassous, P., 2009. Deep-Sea Research II Turbidity events observed in situ along the Congo submarine channel. *Deep-Sea Research Part II*. **56**, 2208–2222.
- Vendettuoli, D., Clare, M.A., Hughes Clarke, J.E., Vellinga, A., Hizzet, J., Hage, S., Cartigny, M.J.B., Talling, P.J., Waltham, D., Hubbard, S.M., Stacey, C., Lintern, D.G., 2019. Daily bathymetric surveys document how stratigraphy is built and its extreme incompleteness in submarine channels. *Earth and Planetary Science Letters*. **515**, 231–247.
- Von Huene, R., Arthur, M.A., 1982. Sedimentation across the Japan Trench off northern Honshu Island. *In: Leggett, J.K. (Ed.), Trench-Forearc Geology: Sedimentation and Tectonics on Modern and Ancient Active Plate Margins, Special Publications No. 10.* Geological Society, London, pp. 27–48.
- Wahl, D., 1984. Evolution of the use of channel cross-section properties for estimating streamflow characteristics. *United States Geological Survey Water Supply Paper*. **2262**, 53–66.
- Walton, M.A.L., Gulick, S.P.S., Reece, R.S., Barth, G.A., Christeson, G.L., Van Avendonk, H.J.A., 2014. Dynamic response to strike-slip tectonic control on the deposition and evolution of the Baranof Fan, Gulf of Alaska. *Geosphere*. **2**, 680–691.
- Wei, T., Peakall, J., Parsons, D.R., Chen, Z., Zhao, Best, J., 2013. Three-dimensional gravity-current flow within a subaqueous bend: spatial evolution and force balance variations. *Sedimentology*. **60**, 1668–1680.

- Weisstein, E.W., 2021. Square Point Picking. From *MathWorld - A Wolfram web resource*. URL <https://mathworld.wolfram.com/SquarePointPicking.html>
- Wells, M., Cossu, R., 2013. The possible role of Coriolis forces in structuring large-scale sinuous patterns of submarine channel–levee systems. *Philosophical Transactions of the Royal Society A: Mathematical, Physical and Engineering Sciences*. **371**, 1–20.
- Wells, M.G., Dorrell, R.M., 2021. Turbulence processes within turbidity currents. *Annual Review of Fluid Mechanics*. **53**, 59–83.
- Wetzel, A., 1993. The transfer of river load to deep-sea fans: a quantitative approach. *AAPG Bulletin*. **77**, 1679–1692.
- Whiting, P.J., Dietrich, W.E., 1993. Experimental constraints on bar migration through bends: Implications for meander wavelength selection. *Water Resources Research*. **29**, 1091–1102.
- Whittaker, A.C., 2007. Investigating Controls on Bedrock River Incision Using Natural and Laboratory Experiments (PhD thesis). University of Edinburgh.
- Wilkerson, G.V., Parker, G., 2011. Physical basis for quasi-universal relationships describing bankfull hydraulic geometry of sand-bed rivers. *Journal of Hydraulic Engineering*. **137**, 739–753.
- Williams, G.P., 1978. Bank-full discharge of rivers. *Water Resources Research*. **14**, 1141–1154.
- Wohl, E., David, G.C.L., 2008. Consistency of scaling relations among bedrock and alluvial channels. *Journal of Geophysical Research*. **113**, 1–16.
- Wohl, E., Merritt, D.M., 2008. Reach-scale channel geometry of mountain streams. *Geomorphology*. **93**, 168–185.
- Wu, C., Ullah, M.S., Lu, J., Bhattacharya, J.P., 2016. Formation of point bars through rising and falling flood stages: evidence from bar morphology, sediment transport and bed shear stress. *Sedimentology*. **63**, 1458–1473.
- Wynn, R.B., Cronin, B.T., Peakall, J., 2007. Sinuous deep-water channels: genesis, geometry and architecture. *Marine and Petroleum Geology*. **24**, 341–387.
- Wynn, R.B., Stow, D.A.V., 2002. Classification and characterisation of deep-water sediment waves. *Marine Geology*. **192**, 7–22.
- Xu, J.P., Noble, M., Eittreim, S.L., Rosenfeld, L.K., Schwing, F.B., Pilskalns, C.H., 2002. Distribution and transport of suspended particulate matter in Monterey Canyon, California. *Marine Geology*. **181**, 215–234.

Yanites, B.J., Tucker, G.E., Mueller, K.J., Chen, Y.-G., Wilcox, T., Huang, S.-Y., Shi, K.-W., 2010. Incision and channel morphology across active structures along the Peikang River, central Taiwan: Implications for the importance of channel width. *Geological Society of America Bulletin*. **122**, 1192–1208.

Zhang, J., Gulick, S.P.S., 2019. Sequence stratigraphy and depositional history of the Baranof Fan: Insights for Cordilleran Ice Sheet outflow to the Gulf of Alaska. *Geological Society of America Bulletin*. **132**, 353-372.

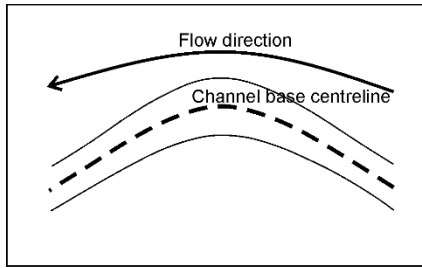
Zhou, J., Chang, H.H., Stow, D., 1993. A model for phase lag of secondary flow in river meanders. *Journal of Hydrology*. **146**, 73–88.

Zinger, J.A., Rhoads, B.L., Best, J.L., 2011. Extreme sediment pulses generated by bend cutoffs along a large meandering river. *Nature Geoscience*. **4**, 675–678.

Zolezzi, G., Luchi, R., Tubino, M., 2012. Modeling morphodynamic processes in meandering rivers with spatial width variations. *Reviews of Geophysics*. **50**, 1–24.

## **Appendix A: Methodology guide for measuring the width and depth of cross-sections around bends**

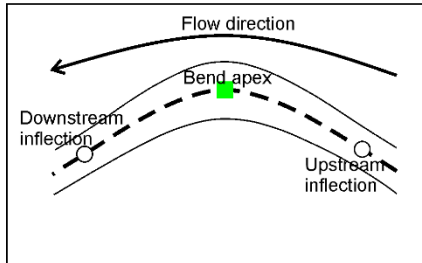
This guide is a visual step by step summary of the methodology used in Chapter 3, 4 and 5. More details of each step are explained in the chapters, particularly in Chapter 4.



**Step 1. Identify channel base centreline**

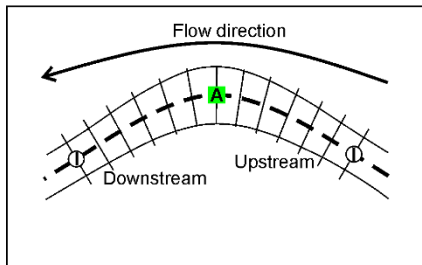
Channel base centreline is the midpoint of the channel base where the slope approximated to zero, between the points where the lateral gradient abruptly increases.

Channel base centreline is identified manually using the bathymetry map, in combination with the slope map of the bathymetric data, and cross-sections.



**Step 2. Identify bend apices and inflections along channel base centreline**

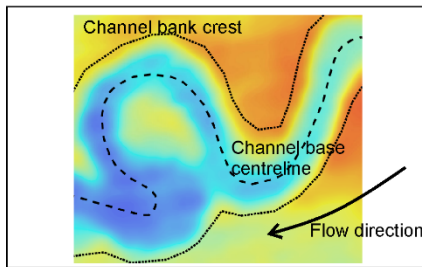
Bend apices: points of maximum curvature  
Bend inflections: points of minimum curvature



**Step 3. Make cross-sections perpendicular to the channel base centreline**

Here, 13 cross-sections for each bend were taken at the bend apex, inflection points, and 5 equally spaced cross-sections between the upstream inflection point and the bend apex, and 5 equally spaced cross-sections between the bend apex and downstream inflection point. The equal spacing was achieved using the split tool in the editor of ArcMap.

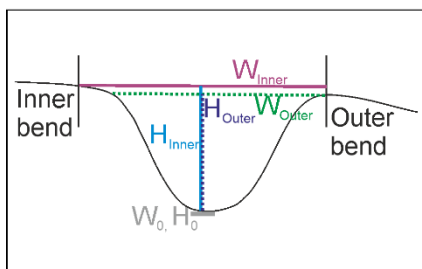
The 13 cross-sections were taken perpendicular to the channel base centreline using the right angle tool in the editor of ArcMap.



**Step 4. Identify the channel bank crests**

Channel bank crests are identified between the external levee crests (Kane and Hodgson, 2011; Hansen *et al.*, 2015), or if the crest line is poorly observed due to a gentle rise of the banks bathymetric mapping is used as a second tool.

Channel bank crest lines are identified manually using a combination of bathymetric data, the slope map, and cross-sections.

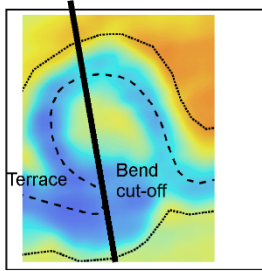


**Step 5A. Take measurements of width and height for a cross-section between channel banks (simple topography)**

Channel width ( $W$ ) was measured at the channel base ( $W_0$ ) centreline, and at a vertical increment (on the channel base centreline) of 10 m up to the outer ( $W_{Outer}$ ) and inner channel bank crests ( $W_{Inner}$ )

Channel height ( $H$ ) was measured from the channel base ( $H_0$ ) centreline up to the outer ( $H_{Outer}$ ) and inner channel bank crests ( $H_{Inner}$ ).

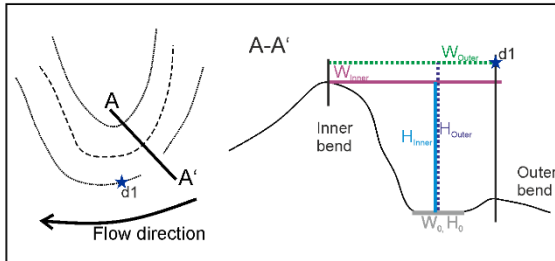




**Step 5B-1. Take measurements of width and height for a cross-section in a complex topography**

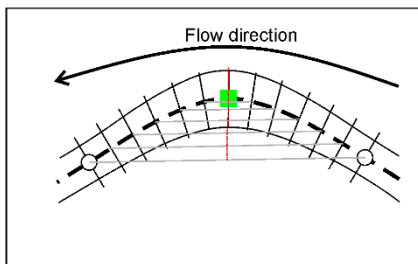
Example of a complex topography for submarine channels:

- The presence of terraces or bend cut-off at the inner bend (causing the topography to be lower than channel bank crest) would cause for example an overestimation of the width
- Channel bank failure could cause the bank crest to have a lower topography than it would have otherwise had, thus leading to an underestimation of channel depth



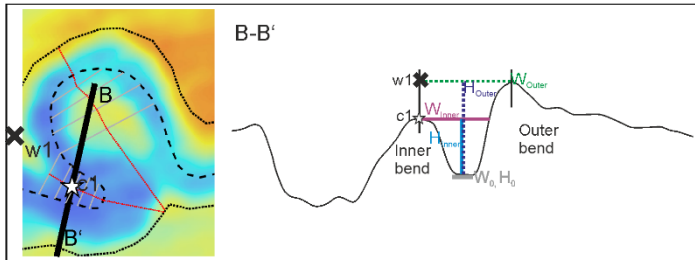
**Step 5B-2. Take measurements of width and height for a cross-section with a bank failure at the outer bend**

Channel width was measured between the primary position of the channel bank prior to bank failure at the outer bend and at the inner bank crest line. Channel height was measured at the outer bend up to the nearest position where no channel bank failure occurred ( $d_1$ ).



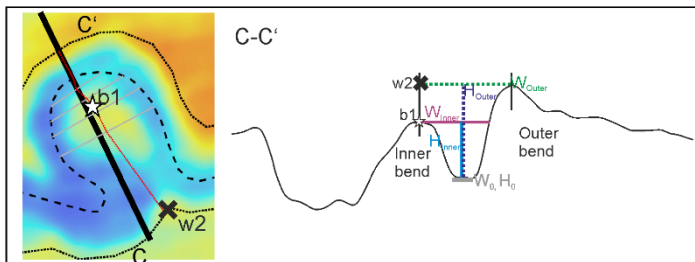
**Step 5B-2. Present of inner bend terraces Draw the trajectory line for each bend**

Draw the trajectory line for each bend. The trajectory line (red dashed line) is an imaginary bank line to compensate for the missing topography due to the presence of terraces or bend cut-offs. The trajectory line is drawn by connecting the midpoints of opposite cross-sections (grey line) to the bend apex and linking it to the channel bank crestline.



**Step 5B-3. Example of a cross-section in a complex topography (A-A')**

At the outer bend, width and height were measured normally. At the inner bend, width was measured up to the intersection of the trajectory line (position  $c_1$ ), and channel height was measured up to the point where the trajectory line intersects with the bank crest



**Step 5B-3. Example of a cross-section in a complex topography (B-B')**

In rare cases, where there was no intersection of the cross-section with the trajectory line, width was measured up to the maximum elevation of the inner bend along the cross-section ( $c_2$ ), and channel height was measured up to the point where the trajectory line intersects with the bank crest.

## Appendix B: References used for the literature-based channel dataset in Section 3.4.4

23 submarine channels were used for the compiled dataset from four submarine channel types: submarine-fan (red, ■), isolated deep-ocean (grey, ▲), slope (orange, ▲), and axial channels (yellow, ◆)

Name of channel	Number of cross-section	Reference and Figures
Amazon ■	3	(Flood and Damuth, 1987 Figure 4)
Bengal ■	6	(Schwenk <i>et al.</i> , 2003 Figure 3, 4, 5 downslope, upslope, 6, 8 PSD2g)
Congo ■	6	(Babonneau <i>et al.</i> , 2004 Figure 6b, 6c Z2-42, 6c ZSAR-37) (Babonneau <i>et al.</i> , 2010 Figure 5 G2Z-07, G2Z-04)
Indus ■	19	(Mishra <i>et al.</i> , 2016 Figure 7a P1-3, 7b P4, 5, 7-11, 8 P14, 9 P24-25, 10A P32, 10B P35-37, 11 P41 P44)
Magdalena ■	3	(Estrada <i>et al.</i> , 2005 Figure 6 b, c, d)
Toyama ▲	9	Figure 4b,d,f,g,h (Nakajima <i>et al.</i> , 1998); Figure 6a, 10a, b, c (Nakajima and Satoh, 2001)
Tanzania ▲	2	(Bourget <i>et al.</i> , 2008 Figure 2c 3a, b)
Lofoten ▲	3	(Laberg and Vorren, 2003 Figure 2a, b, 5a; Ó Cofaigh <i>et al.</i> , 2006)
Cascadia ▲	9	(Griggs and Kulm, 1973 Figure 4, 5, 7, 8, 9, 10, 11, 12, 13)
Surveyor ▲	11	(Ness and Kulm, 1973 Figure 2a-k)
Bounty ▲	12	(Carter and Carter, 1996 Figure 4a, 4b, 7a-j)
Hikurangi ▲	3	(Lewis and Pantin, 2002 Figure 7c, 11b, 11c)

North Atlantic Mid-Ocean Channel (NAMOC) ▲	16	Figure 3a-k, 4, 5, 7, 8 (Klaucke <i>et al.</i> , 1998); Figure 3 (Skene <i>et al.</i> , 2002)
Kongsfjorden Channel System ▲	6	Figures 5d, 5e, 5g, 6h, 6a, 6b (Forwick <i>et al.</i> , 2015)
Vidal ▲	23	Figures 5.6A, 5.6G, 6.1-6.21 (Embley <i>et al.</i> , 1970)
Valencia ▲	4	Figures 3c, 4b.1, 4b.2, 4c (O'Connell <i>et al.</i> , 1985)
Zambezi ▲	7	Figure 4 (Droz and Mougnot, 1987)
North Pole Submarine Channel (NPSC) ▲	4	Figure 2, 4.1-4.3 (Kristoffersen <i>et al.</i> , 2004)
Brunei ▲	17	Figure 9, 13 (Straub <i>et al.</i> , 2012)
Lucia Chica channel system (LUCIA) ▲	10	Figure 2b, d, e (Maier <i>et al.</i> , 2012)
Einstein ▲	13	analysed data from Bureau of Ocean Energy Management
Chile♦	2	Figure 8a, b (Thornburg and Kulm, 1987)
Nankai♦	17	Figure 19 Cross 1-17 (Shimamura, 1988)

## References

Babonneau, N., Savoye, B., Cremer, M., Bez, M., 2004. Multiple terraces within the deep incised Zaire Valley (ZaiAngo Project): are they confined levees? *In: Lomas, S.A., Joseph, P. (Eds.), Confined Turbidite Systems*. Geological Society, London, pp. 91–114.

Babonneau, N., Savoye, B., Cremer, M., Bez, M., 2010. Sedimentary architecture in meanders channel: detailed study of the present Congo

Turbidite Channel (ZaiAngo Project). *Journal of Sedimentary Research*. **80**, 852–866.

Bourget, J., Zaragosi, S., Garlan, T., Gabelotaud, I., Guyomard, P., Dennielou, B., 2008. Discovery of a giant deep-sea valley in the Indian Ocean, off eastern Africa: the Tanzania Channel. *Marine Geology*. **255**, 179–185.

Carter, R.M., Carter, L., 1996. The abyssal Bounty Fan and lower Bounty Channel: evolution of a rifted-margin sedimentary system. *Marine Geology*. **130**, 181–202.

Droz, L., Mougnot, D., 1987. Mozambique Upper Fan: origin of depositional units. *AAPG Bulletin*. **71**, 1355–1365.

Embley, R.W., Ewing, J.I., Ewing, M., 1970. The Vidal Deep-Sea Channel and its relationship to the Demerara and Barracuda Abyssal plains. *Deep Sea Research and Oceanographic Abstracts*. **17**, 539–552.

Ercilla, G., Alonso, B., Estrada, F., Chiocci, F.L., Baraza, J., Farran, M., 2002. The Magdalena Turbidite System (Caribbean Sea): present-day morphology and architecture model. *Marine Geology*. **185**, 303–318.

Flood, R.D., Damuth, J.E., 1987. Quantitative characteristics of sinuous distributary channels on the Amazon Deep-Sea Fan. *Geological Society of America Bulletin*. **98**, 728–738.

Forwick, M., Laberg, J.S., Hass, H.C., Osti, G., 2015. The Kongsfjorden Channel System offshore NW Svalbard: downslope sedimentary processes in a contour-current-dominated setting. *Arktos*. **1**, 17.

Griggs, G.B., Kulm, L.D., 1973. Origin and development of Cascadia Deepsea Channel. *Journal of Geophysical Research*. **78**, 6325–6339.

Klaucke, I., Hesse, R., Ryan, W.B.F., 1998. Morphology and structure of a distal submarine trunk channel: the Northwest Atlantic Mid-Ocean Channel between lat 53°N and 44°30'N. *Geological Society of America Bulletin*. **110**, 22–34.

Kristoffersen, Y., Sorokin, M.Y., Jokat, W., Svensson, O., 2004. A submarine fan in the Amundsen Basin, Arctic Ocean. *Marine Geology*. **204**, 317–324.

Laberg, J.S., Vorren, T.O., 2003. Morphology of the Lofoten Basin Channel. In: Mienert, J., Weaver, P. (Eds.), *European Margin Sediment Dynamics*. Springer, Berlin, Heidelberg, pp. 99–101.

Lewis, K.B., Pantin, H.M., 2002. Channel-axis, overbank and drift sediment waves in the southern Hikurangi Trough, New Zealand. *Marine Geology*. **192**, 123–151.

- Maier, K.L., Fildani, A., McHargue, T.R., Paull, C.K., Graham, S.A., Caress, D.W., 2012. Punctuated deep-water channel migration: high resolution subsurface data from the LUCIA Chica Channel System, offshore California, USA. *Journal of Sedimentary Research*. **82**, 1–8.
- Mishra, R., Pandey, D.K., Ramesh, P., Clift, P.D., 2016. Identification of new deep sea sinuous channels in the eastern Arabian Sea. *Springer Plus*. **5**, 1–18.
- Nakajima, T., Satoh, M., 2001. The formation of large mudwaves by turbidity currents on the levees of the Toyama Deep-Sea Channel, Japan Sea. *Sedimentology*. **48**, 435–463.
- Nakajima, T., Satoh, M., Okamura, Y., 1998. Channel-levee complexes, terminal deep-sea fan and sediment wave fields associated with the Toyama Deep-Sea Channel system in the Japan Sea. *Marine Geology*. **147**, 25–41.
- Ness, G.E., Kulm, L.D., 1973. Origin and development of Surveyor Deep-Sea Channel. *Geological Society of America Bulletin*. **84**, 3339–3354.
- Ó Cofaigh, C., Dowdeswell, J.A., Kenyon, N.H., 2006. Geophysical investigations of a high-latitude submarine channel system and associated channel-mouth lobe in the Lofoten Basin, Polar North Atlantic. *Marine Geology*. **226**, 41–50.
- O’Connell, S., Alonso, B., Kastens, K.A., Maldonado, A., Malinverno, A., Nelson, C.H., Palanques, A., Ryan, W.B.F., 1985. Morphology and downslope sediment displacement in a deep-sea valley, the Valencia Valley (Northwestern Mediterranean). *Geo-Marine Letters*. **5**, 149–156.
- Schwenk, T., Spieß, V., Hübscher, C., Breitzke, M., 2003. Frequent channel avulsions within the active channel-levee system of the middle Bengal Fan—an exceptional channel-levee development derived from Parasound and Hydrosweep data. *Deep-Sea Research Part II*. **50**, 1023–1045.
- Shimamura, K., 1988. Sedimentation and tectonics of Zenisu Ridge, Eastern Nankai Trough and Suruga Trough Regin. *Science Report, Tohoku University, 2nd series (Geology)*. **58**, 107–167.
- Skene, K.I., Piper, D.J.W., Hill, P.S., 2002. Quantitative analysis of variations in depositional sequence thickness from submarine channel levees. *Sedimentology*. **49**, 1411–1430.
- Straub, K.M., Mohrig, D., Pirmez, C., 2012. Architecture of an aggradational tributary submarine-channel network on the continental slope offshore Brunei Darussalam. In: Prather, P.E., Deptuck, M.E., Mohrig, D., van Hoorn, B., Wynn, R.B. (Eds.), *SEPM Special Publication 98: Application of the Principles of Seismic Geomorphology to Continental-Slope and Base-of-Slope Systems: Case Studies from Seafloor and near-Seafloor Analogues*. pp. 13–30.

Thornburg, T.M., Kulm, L.D., 1987. Sedimentation in the Chile Trench: depositional morphologies, lithofacies, and stratigraphy. *Geological Society of America Bulletin*. **98**, 33–52.

## Appendix C: Width measurement results for Chapter 4

*Downstream bank-top channel width variations per region in individual channel reaches*

The mean bank-top channel width was wider at the apex region compared to the inflection region (Figure S1) for the majority of bends in all channel reaches, with 17 of 19 bends (90%) for Ax02 (Fig. S1A), 18 of 27 (67%) for Ax12 (Figure S1B), 10 of 13 (77%) bends for Ax14 (Fig. S1C), and 26 of 49 (53%) bends for Ax52 (Fig. S1D) wider at the apex region. Most bends (12 of 19 bends) for Ax02 were at least 5% wider at the apex region compared to the inflection region with 7 bends (Figure S1A) more than 25% wider at the apex region and 2 bends greater than 30% wider. Similarly, most bends (16 of 27 bends) for Ax12 were at least 5% wider at the apex region, with 9 bends (Figure S1B) 20% wider at the apex region. In contrast, 10 of 13 bends in Ax14 were less than 10% wider at the bend apex region, with 2 bends >15% wider (Figure S1C). For Ax52 there were 18 bends more than 5% wider, and 3 bends more than 20% wider.

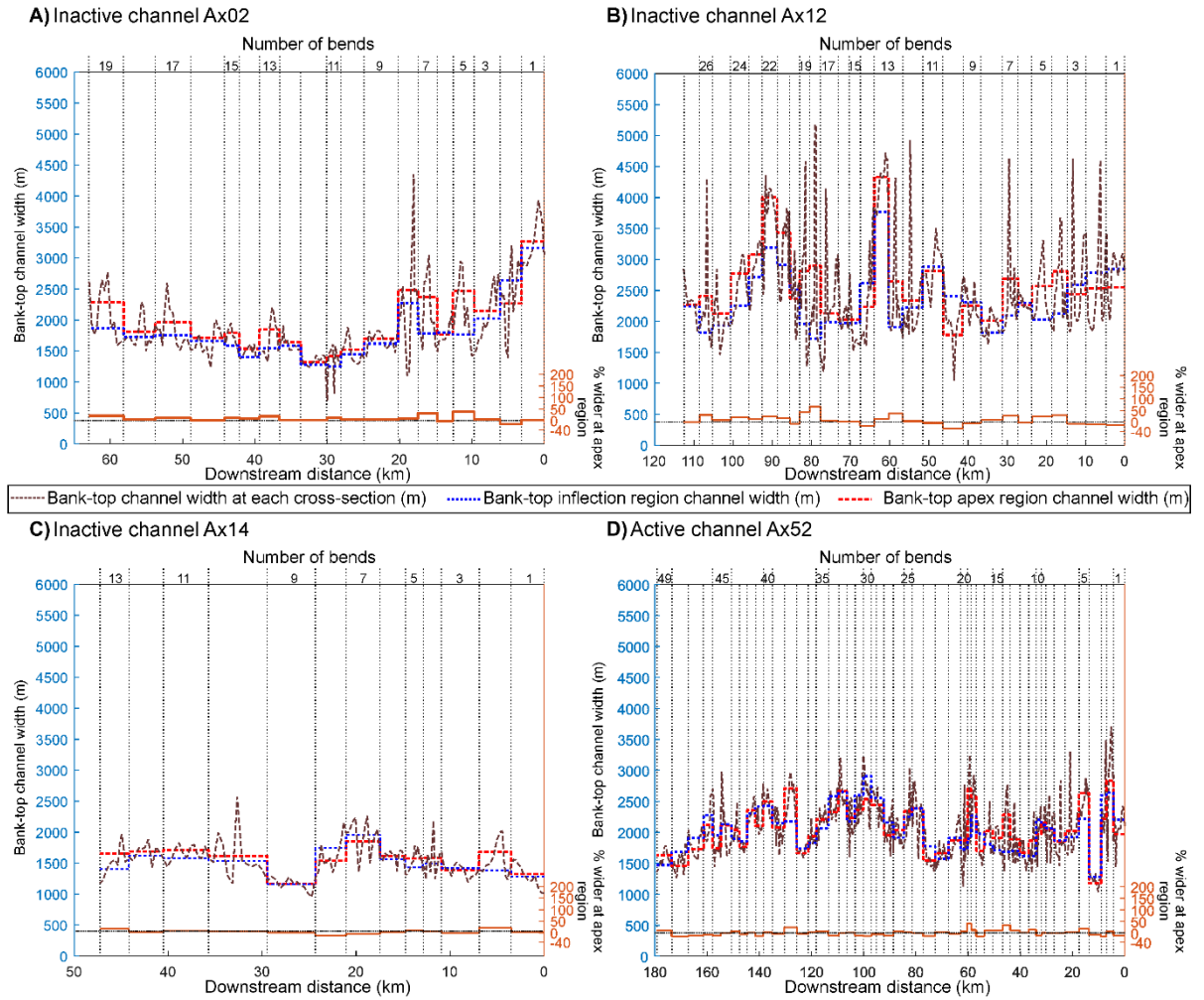


**Figure S1.** Bank-top channel width at individual cross-sections (brown dashed-pointed line), at mean bank inflection region (blue dotted line), at mean bank apex region per bend (red solid line), and % wider at apex region, against downstream distance (km) and bend number for individual channel reaches A) Ax02, B) Ax12, C) Ax14 and D) Ax52. Flow direction is from right to left.